

DISSERTATION ZUR ERLANGUNG DES DOKTORGRADES
DER FAKULTÄT FÜR CHEMIE UND PHARMAZIE
DER LUDWIG-MAXIMILIANS-UNIVERSITÄT MÜNCHEN

IDENTIFICATION AND CHARACTERIZATION OF
NOVEL CANDIDATE MOLECULES FOR
POSTTRAUMATIC STRESS DISORDER

LEONIE HERRMANN GEB. CHRISTIAN

AUS

BONN, DEUTSCHLAND

2012

Erklärung

Diese Dissertation wurde im Sinne von § 7 der Promotionsordnung vom 28. November 2011 von Herrn Prof. Dr. med. Dr. rer. nat. Dr. h.c. F. Holsboer betreut und von Herrn Prof. Dr. rer. nat. C. Turck von der Fakultät für Chemie und Pharmazie vertreten.

Eidesstattliche Versicherung

Diese Dissertation wurde eigenständig und ohne unerlaubte Hilfe erarbeitet.

München,

(Leonie Herrmann)

Dissertation eingereicht am 05.07.2012

1. Gutachter: Prof. Dr. rer. nat. C. Turck

2. Gutachter: Prof. Dr. med. Dr. rer. nat. Dr. h.c. F. Holsboer

Mündliche Prüfung am 31.10.2012

To Stefan

Abstract

Posttraumatic stress disorder (PTSD) is an anxiety disorder that can develop after exposure to a life or health threatening event and is mainly characterized by re-experiencing of the traumatic incident, nervous hyperarousal, and avoidance of trauma-related cues. Clinical and animal studies already identified PTSD-related alterations inter alia in the stress hormone-, the neurotransmitter-, and the immune system, but despite these efforts the distinct pathomechanisms of PTSD still remain elusive. Furthermore, the molecular underpinnings of the hippocampal volume loss that has been found both in PTSD patients and the mouse model of PTSD employed in the thesis at hand are so far not completely understood.

This thesis aimed to further elucidate the pathomechanisms of PTSD by two different approaches: first, by characterization of an already known candidate molecule for anxiety disorders, i.e. transmembrane protein 132 D (TMEM132D), and, second, by a screen for novel candidate molecules for PTSD pathogenesis in a mouse model of PTSD.

In the first part of this thesis, a previously identified anxiety disorder candidate gene of yet unknown function, i.e. TMEM132D, was further characterized in view of its regulatory mechanisms. Due to the previously reported association of TMEM132D with mature oligodendrocytes, an extensive characterization of the TMEM132D promoter was performed in the oligodendrocytic MO3.13 cell line. This promoter analysis identified a number of transcription factors inhibiting TMEM132D gene expression, namely HES1, MYT1, ZNF219, GCM1, MTF1, NFKB1, MZF1, and SP1. Increased expression of TMEM132D mRNA in differentiated versus non-differentiated MO3.13 cells was paralleled by a reduced expression of four of these transcription factors, namely ZNF219 and three regulatory factors already known to be involved in oligodendrocyte differentiation, i.e. MYT1, HES1, and SP1.

In the second part of this thesis, brain region specific expression level differences of selected marker proteins were assessed in mice subjected to a traumatic electric footshock and a single stressful re-exposure to trauma-related environmental cues 28 days after shock application or

in control mice subjected to mock treatment. This analysis revealed an enduring hippocampal downregulation of the synaptic proteins synapsin Ia-b/IIa, synaptophysin, and homer 1b/c to accompany the PTSD-like behavior and the hippocampal volume loss in traumatized mice. In contrast to synaptic proteins, the expression of the dendritic protein MAP-2 and the astroglial protein GFAP was found to be unaltered in the hippocampus of traumatized mice. This trauma stress-induced synaptic protein loss might, at least in part, be caused by increased extracellular glutamate levels as alluded by the here observed decreased expression levels of hippocampal glutamate transporter proteins, i.e. GLT1 and EAAC1, in traumatized mice. Treatment with the SSRI antidepressant fluoxetine alleviated the PTSD-like symptoms and, moreover, counteracted the reduction of synaptic protein and GLT1 expression. Finally, by serendipity, a trauma stress-induced delayed-onset increase of immunoglobulin G (IgG) was identified in the hippocampus, where IgG was found to be associated with microglial cells. Furthermore, decreased expression of the microglial marker Iba1 points at a stress-induced reduction of microglial cell numbers accompanying the increased IgG expression in traumatized mice. Alterations in IgG expression were also detected in another mouse model, namely in the HAB/LAB trait anxiety mouse model, as well as in an *in silico* analysis of publicly available peripheral blood mononuclear cell (PBMC) gene expression data of PTSD patients.

In conclusion, this thesis comprises the first characterization of the TMEM132D promoter and revealed several transcription factors to inhibit the expression of the anxiety disorder candidate gene TMEM132D in an oligodendrocyte cell culture model. The second part of this thesis demonstrates PTSD-like symptoms in mice to be accompanied by hippocampal synaptic protein loss. The fact that fluoxetine was found to effectively counteract both behavioral symptoms and the alterations in synaptic protein expression levels further highlights the importance of hippocampal synaptic protein loss in the murine PTSD-like syndrome and the associated hippocampal shrinkage. In addition, reduced levels of distinct glutamate transporters and alterations of protein levels associated with the immune system were identified to occur in the aftermath of the traumatic footshock. However, clinical studies are clearly needed to analyze the importance of the findings presented here in patients suffering from PTSD and other anxiety disorders.

Contents

Abstract	iii
Abbreviations	ix
1. Introduction	1
1.1. History, epidemiology, and symptomatology of PTSD	1
1.2. Neurobiology of PTSD	3
1.2.1. The neuroendocrine stress response and its alterations in PTSD	3
1.2.2. Neurotransmitter systems in PTSD	7
1.2.3. Genetic and epigenetic risk factors for PTSD	9
1.2.4. Pathoanatomical alterations associated with PTSD	11
1.2.4.1. Hippocampus	12
1.2.4.2. Prefrontal cortex	13
1.2.4.3. Amygdala	14
1.3. PTSD Biomarkers	15
1.4. Pharmacotherapy of PTSD	17
1.5. Animal models of anxiety disorders	18
1.5.1. The PTSD mouse model	19
1.5.2. The HAB/LAB mouse model	21
1.6. Transmembrane protein 132D - a candidate gene for anxiety phenotypes	21
1.7. Aim of the thesis	23
2. Materials and Methods	25
2.1. Animals	26
2.1.1. Combined restraint and forced swim stress experiments	26
2.1.2. PTSD mouse model	27
2.1.2.1. Fluoxetine treatment	30
2.1.3. HAB/LAB mouse model	30
2.2. Immunoassays	31
2.2.1. Western blot	31
2.2.1.1. Bicinchoninic acid (BCA) assay	31
2.2.1.2. Sodium dodecyl sulfate polyacrylamid gel electrophoresis (SDS-PAGE)	32
2.2.1.3. Western blot transfer	33
2.2.1.4. Densitometry	35
2.2.2. Immunohistochemistry (IHC)	35
2.3. Molecular biological methods	37
2.3.1. Cultivation of <i>E. coli</i> bacteria	37
2.3.1.1. Preparation of competent cells	37
2.3.1.2. Transformation of <i>E. coli</i> bacteria	38
2.3.2. Isolation of plasmid DNA	38

2.3.3.	Cloning of reporter plasmids and transcription factor expression plasmids	40
2.3.3.1.	RNA isolation	40
2.3.3.2.	Concentration measurements of nucleic acids	41
2.3.3.3.	Reverse transcription (RT)	41
2.3.3.4.	Polymerase chain reaction (PCR)	41
2.3.3.5.	Gel electrophoresis	43
2.3.3.6.	DNA purification from agarose gels	43
2.3.3.7.	Restriction digest of DNA	43
2.3.3.8.	Ligation	44
2.3.3.9.	Site-directed mutagenesis	44
2.3.4.	RT-PCR for semi-quantitative detection of gene expression	45
2.4.	Cell culture	47
2.4.1.	Cell line subcultivation	47
2.4.1.1.	Freezing and thawing of cells	47
2.4.1.2.	Mycoplasma test	48
2.4.1.3.	Cell counting	48
2.4.2.	TMEM132D overexpression	48
2.4.3.	Reporter gene assay	49
2.4.4.	MO3.13 differentiation assay	51
2.4.5.	siRNA mediated knock-down of TMEM132D	51
2.5.	Bioinformatical methods	52
2.5.1.	Analysis of phylogenetic conservation of TMEM132D proteins	53
2.5.2.	Identification of homologous protein domains of TMEM132D	54
2.5.3.	TMEM132D <i>in silico</i> promoter analysis	54
2.5.4.	NCBI GEO DataSet analyses	55
2.6.	Statistics	55
2.6.1.	Pearson correlation	56
3.	Results I: Transcriptional regulation of the human TMEM132D gene	57
3.1.	Analysis of TMEM132D gene structure and prediction of possible protein functions	57
3.2.	<i>In silico</i> analysis of the TMEM132D promoter	64
3.3.	Analysis of TMEM132D promoter activity in the oligodendrocytic MO3.13 cell line	70
3.4.	Transcriptional regulation of TMEM132D during oligodendrocyte differentiation	81
3.5.	Summary of Results I	85
4.	Results II: Identification of PTSD candidate proteins in a mouse model of PTSD	87
4.1.	Behavioral analyses (PTSD mouse model)	87
4.2.	Screening for PTSD candidate molecules	89
4.2.1.	Neurostructural proteins	90
4.2.1.1.	Synapsin and synaptophysin protein expression is differentially regulated in mice exposed to repetitive acute stress	90
4.2.1.2.	Traumatic footshock stress reduces hippocampal synaptic protein expression	94
4.2.1.3.	Hippocampal expression of neurofilament H, but not MAP-2, is reduced in mice subjected to a single electric footshock	98

4.2.1.4.	Hippocampal synaptic protein expression correlates with the conditioned and generalized fear response but not with the acoustic startle response	100
4.2.1.5.	Chronic fluoxetine treatment increases synaptic vesicle protein expression in mice subjected to a single electric footshock . . .	102
4.2.2.	Glutamate transporters	106
4.2.2.1.	Hippocampal glutamate transporter expression is reduced in mice subjected to a single electric footshock	106
4.2.2.2.	GFAP protein expression remains unchanged in footshocked mice	108
4.2.2.3.	Fluoxetine treatment increases GLT1 but not EAAC1 and GFAP protein expression	109
4.2.3.	Immune system proteins	111
4.2.3.1.	An immunoglobulin G immunoreactive band is detected in the C57BL/6 mouse brain	111
4.2.3.2.	IgG expression is increased in mice subjected to a single electric footshock	115
4.2.3.3.	IgG expression is reduced in HAB compared to LAB mice . . .	119
4.2.3.4.	Analysis of microglial and endothelial marker protein expression levels in the PTSD and the HAB/LAB mouse model	122
4.2.3.5.	<i>In silico</i> analysis of immunoglobulin expression in PTSD patients	122
4.3.	Summary of Results II	129
5.	Discussion	131
5.1.	Identification of transcription factors targeting TMEM132D	131
5.2.	Identification of novel PTSD candidate proteins	137
5.2.1.	Traumatic stress induces a long-lasting hippocampal synaptic protein loss	137
5.2.2.	Traumatic stress induces a reduction of glutamate transporter expression	144
5.2.3.	The expression of immune system associated molecules is altered both in mice exhibiting a PTSD-like syndrome and in PTSD patients	146
5.2.4.	Model conception of the speculated trauma stress-induced synapse loss .	151
5.2.5.	Conclusions	151
A.	Appendix	155
	Bibliography	165
	Acknowledgments	193
	Curriculum vitae	195
	Publications	197

Abbreviations

ACTH	adrenocorticotropin
ANOVA	analysis of variance
BBB	blood-brain barrier
BCA	bicinchoninic acid
BDNF	brain-derived neurotrophic factor
BLAST	basic local alignment search tool
BSA	bovine serum albumine
CA1	cornu ammonis area 1
CA3	cornu ammonis area 3
CD31	cluster of differentiation 31
CD68	cluster of differentiation 68
CER	cerebellum
CNS	central nervous system
CREB	cAMP response element-binding protein
CRH	corticotropin-releasing hormone
DG	dentate gyrus
DMEM	Dulbecco's modified Eagle's medium
DNA	desoxyribonucleic acid
dNTP	desoxynucleotide-triphosphate
DSM-IV	Diagnostic and Statistical Manual of Mental Disorders IV
E. coli	Escherichia coli
EAAC1	excitatory amino acid carrier 1
EAAT	excitatory amino acid transporter
ERK	extracellular signal-regulated kinase
FCS	fetal calf serum
FDA	U.S. Food and Drug Administration
FKBP5	FK506 binding protein 5
fMRI	functional magnetic resonance imaging
FSS	forced swim stress
GABA	γ -aminobutyric acid
GAPDH	glyceraldehyd-3-phosphat-dehydrogenase
GFAP	glial fibrillary acidic protein
GLAST	glutamate/aspartate transporter
GLT1	glutamate transporter 1
GO	gene ontology
GR	glucocorticoid receptor
GWAS	genome-wide association studies
HAB	high anxiety-related behavior
HC	hippocampus
HPA axis	hypothalamic-pituitary-adrenal axis
HRP	horseradish-peroxidase
Iba1	ionized calcium-binding adaptor molecule 1
IgG	immunoglobulin G

Contents

IHC	immunohistochemistry
kb	kilobases
kD	kilo Dalton
LAB	low anxiety-related behavior
LTP	long-term potentiation
MAP-2	microtubule-associated protein 2
MAPK	mitogen-activated protein kinases
NMDA	N-methyl-D-aspartate
NPY	neuropeptide Y
PBMC	peripheral blood mononuclear cells
PBS	phosphate-buffered saline
PET	positron emission tomography
PFA	paraformaldehyde
PFC	prefrontal cortex
PMA	phorbol 12-myristate 13-acetate
PTSD	posttraumatic stress disorder
PVN	paraventricular nucleus
RNA	ribonucleic acid
RPMI	Roswell Park Memorial Institute
SAM axis	sympathetic-adrenal-medullary axis
SDS-PAGE	sodium dodecyl sulfate polyacrylamid gel electrophoresis
SNP	single nucleotide polymorphism
SSRI	serotonin reuptake inhibitor
TBS/T	Tris-buffered saline supplemented with Tween-20
TF	transcription factor
TFBS	transcription factor binding site
TMEM132D	transmembrane protein 132 D
TSS	transcription start site
WB	Western blot

1. Introduction

In 1936, stress was defined by Hans Selye as the unspecific response to noxious events including physical trauma, infection, and other adverse life conditions that the organism typically encounters throughout life (Selye, 1936). Thus, the stress response constitutes a physiological adaptation process enabling the individual to cope with a constantly changing environment. Perception of fear and anxiety is essential for the adaptation to threatening situations: while the fear reaction enables the organism to escape from a life-threatening situation, the emotion of anxiety is thought to be longer lasting and future-focused, and thus prepares the individual to adapt to a potential future threat (Barlow, 2000). Whether the organism can handle a stressful challenge or fails to adapt is determined by a variety of factors including its genetic and epigenetic predisposition (Cornelis et al., 2010; Schmidt et al., 2011) as well as the experienced cumulative lifetime stress, i.e. the allostatic load (McEwen and Stellar, 1993). It is well accepted that pathological alterations of the stress response as well as fear and anxiety reactions are associated with psychiatric disorders like major depression, panic disorder, and posttraumatic stress disorder (PTSD) (De Kloet et al., 2005; McEwen, 2007).

1.1. History, epidemiology, and symptomatology of PTSD

In 1980, the term ‘posttraumatic stress disorder’ was first officially noted in the Diagnostic and Statistical Manual of Mental Disorders III (DSM-III), the classification system of the American Psychiatric Association (American Psychiatric Association, 1980). However, psychic symptoms following trauma have been described much earlier: Herodotus (490 B.C.) described an Athenian soldier who was not physically wounded during the Battle of Marathon but nevertheless became permanently blind after witnessing the death of a fellow soldier (Schiraldi, 1999). Different terms including ‘traumatic neurosis’, ‘fright neurosis’, ‘shell shock’, ‘combat fatigue’, and ‘survival syndrome’ were used to describe a PTSD-equivalent syndrome

1. Introduction

(Shorter, 2005; Bronisch, 2010). In the current edition of the DSM, the DSM-IV, PTSD is assigned to the group of anxiety disorders which also include generalized anxiety disorder, panic disorder, obsessive-compulsive disorder, acute stress disorder as well as agoraphobia, social and specific phobia (American Psychiatric Association, 2000).

The life-time prevalence of PTSD was described by the National Comorbidity Survey (NCS) to be 10.4 % in females and 5.0 % in males of the U.S. population (Kessler et al., 1995), while in Germany the prevalence rate was reported to be 2.2 % in females and less than 1 % in males (Perkonig et al., 2000). The risk of developing PTSD is inter alia dependent on the type of trauma, i.e. the stress dose experienced by the affected individual, as it can be deduced from the fact that PTSD occurs much more frequently after rape and combat than for instance after accidents (Foa et al., 2006). Additionally, biological vulnerability factors as well as gender, the socioeconomic background, and secondary posttraumatic stressors have been described to modulate the probability of PTSD onset (Yehuda et al., 2011; Foa et al., 2006).

To date, as every psychiatric diagnosis, also the diagnosis of PTSD relies on self reports, clinical expert interviews, and clinical behavioral monitoring. According to the DSM-IV, PTSD diagnosis requires the respective individual to have been either directly exposed to a life or health threatening traumatic event or to have instantaneously witnessed another person being exposed to such an incident. PTSD core symptoms can be classified into three clusters: first, the re-experiencing symptoms which include recurrent intrusive memories of the event in form of intrusions and flashbacks as well as distressing dreams. Environmental cues reminding patients of the traumatic experience usually trigger those re-experiencing symptoms. The second symptom cluster comprises avoidance and numbing symptoms: affected patients avoid thoughts, feelings, activities, places, or people associated with the traumatic event. Furthermore, loss of memory of important aspects of the event and emotional numbing might occur in PTSD patients. Hyperarousal symptoms constitute the third PTSD symptom cluster comprising inter alia sleep difficulties and an exaggerated startle response. PTSD symptoms have to last for at least one month to justify a diagnosis of PTSD (North et al., 2009; Foa et al., 2006; American Psychiatric Association, 2000).

1.2. Neurobiology of PTSD

1.2.1. The neuroendocrine stress response and its alterations in PTSD

It is well accepted that glucocorticoids and catecholamines play a major role in regulating the stress response of human beings and other mammals. This stress response implies changes in brain metabolism and behavior. Secretion of the two major stress hormones, i.e. cortisol and epinephrine, is regulated by the hypothalamic-pituitary-adrenal (HPA) axis and the sympathetic-adrenal-medullary (SAM) axis, respectively. While catecholamines induce an immediate response to the stressor, activation of the HPA axis, occurring with a time delay, rather effects long-term adaption processes.

The hypothalamus, the anterior pituitary, and the cortex of the adrenal gland constitute the effector organs of the HPA axis (Figure 1.1). Additionally, limbic structures processing the emotional response to stressors are known to modulate HPA axis activation: while the hippocampus and the prefrontal cortex inhibit the HPA axis, the amygdala activates it (Herman et al., 2005). Stress induces the release of corticotropin-releasing hormone (CRH) from parvocellular secretory neurons which project from the hypothalamic paraventricular nucleus (PVN) to the median eminence of the hypothalamic-hypophyseal portal circulation (Figure 1.1). CRH is transported via the blood to the anterior pituitary where it stimulates the release of adrenocorticotropin (ACTH) (Figure 1.1). Subsequently, ACTH is transported via the blood circulation to the adrenal cortex where it induces the release of glucocorticoids (Papadimitriou and Priftis, 2009), that is cortisol in humans and corticosterone in rodents, as well as the mineralocorticoid aldosterone (Funder, 2010). Glucocorticoids support the body to cope with the stressor by increasing the energy metabolism and the vascular tone as well as by inhibiting immune and reproductive functions (Haddy and Clover, 2001; Herman et al., 2003). HPA axis activation is regulated via a negative feedback inhibition loop, i.e. cortisol exerts an inhibitory effect on the ACTH-secreting neurons in the pituitary and the CRH-secreting neurons in the hypothalamus. Under physiological conditions, this negative feedback-loop results in a temporary well defined upregulation of glucocorticoids in response to stressors (Herman et al., 2003).

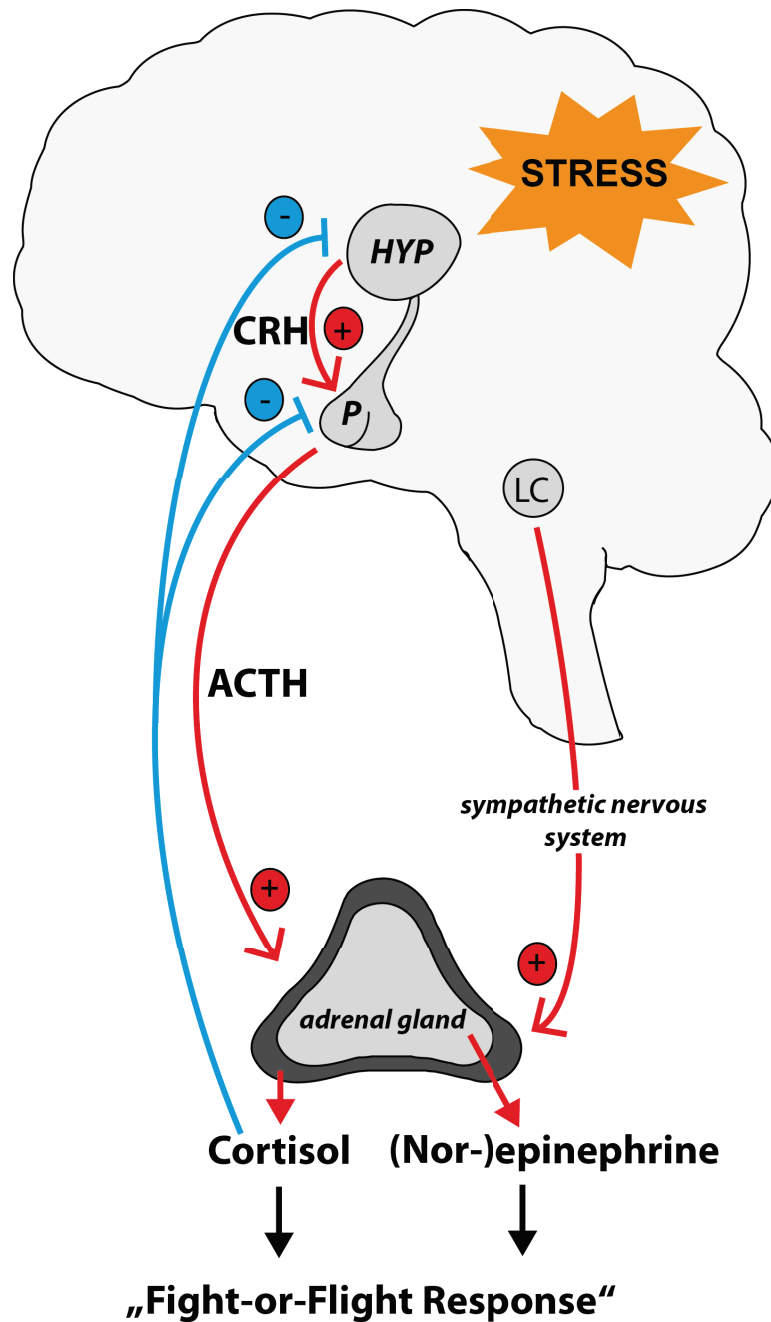


Figure 1.1.: **Scheme of the neuroendocrine stress response.** HPA axis: stress-induced cortisol secretion from the adrenal cortex is stimulated by ACTH secreted from the anterior pituitary (P) which is in turn stimulated by CRH secreted from the parvocellular secretory neurons of the hypothalamus (HYP). Via a negative feedback loop, cortisol inhibits both CRH and ACTH secretion. SAM axis: via the locus coeruleus (LC)-noradrenergic system, stress activates the sympathetic nervous system and induces the release of epinephrine from the adrenal medulla.

Besides the HPA axis, stressors activate the release of norepinephrine from locus coeruleus neurons and immediately activate the sympathetic-adrenal-medullary (SAM) axis, i.e. an increased activation of sympathetic neurons projecting from the spinal cord to the adrenal medulla stimulating inter alia the production and release of the catecholamines epinephrine and norepinephrine (Figure 1.1). Increased catecholamine levels immediately evoke a physical stress response (the ‘fight-or-flight response’) by increasing blood pressure and heart rate as well as by inhibiting appetite, digestion, and reproductive functions (Carrasco and Van de Kar, 2003). During this short-term catecholamine mediated stress response the immune system is activated (Wong et al., 2011) to enable the organism to cope with immune challenges that often accompany the stressor (Sorrells and Sapolsky, 2007). In contrast, upregulation of glucocorticoids, which have been repeatedly reported to mediate the long-term adaptation to the stressor, are known to have anti-inflammatory effects whereby they attenuate the stress-induced immune activation (Sorrells and Sapolsky, 2007).

There are multiple evidences for a dysregulation of both the HPA and the SAM axis in PTSD (De Kloet et al., 2006; Bowirrat et al., 2010). HPA axis alterations in PTSD are controversially discussed in scientific literature: most studies have reported peripheral cortisol levels measured in urine, saliva, or plasma to be decreased, while others found unchanged cortisol levels in PTSD patients (Yehuda, 2009). In contrast, major depression and anxiety disorders have been found to go along with increased peripheral cortisol levels (Parker et al., 2003; Lightman, 2008). The discordance of cortisol measurements in PTSD may, at least in part, be explained by the high comorbidity of PTSD with major depression and other HPA axis influencing disorders. Further support for a hypoactivation of the HPA axis in PTSD pathophysiology is provided by studies reporting PTSD patients to exhibit an increased suppression of cortisol secretion in the dexamethasone suppression test, i.e. the administration of the glucocorticoid derivate dexamethasone followed by a measurement of cortisol levels. The increased suppression of cortisol secretion in this test indicates an enhanced negative feedback inhibition in PTSD patients which is probably due to an increased glucocorticoid receptor (GR) sensitivity (Yehuda, 2009). Furthermore, an enhanced feedback inhibition is also supported by reduced ACTH levels measured upon cortisol injections (Yehuda, 2009; Pace

1. Introduction

and Heim, 2011). The importance of the GR in mediating the pathogenic effects of stress is *inter alia* highlighted by a study reporting that antagonism of GR prior to stress exposure prevents potentiation of fear conditioning in a rat model of PTSD (Kohda et al., 2007).

In contrast to glucocorticoids, central and peripheral catecholamine levels have been found to be increased in PTSD patients (Dikanović et al., 2011). Additionally, PTSD patients have been reported to exhibit an increased heart rate, increased blood pressure, and tremor responses at rest as well as upon trauma reminders (Bedi and Arora, 2007); these symptoms are well known to be provoked by increased SAM activity. Low cortisol and high plasma catecholamine levels shortly after the trauma have been recently proposed to serve as predictors for PTSD development (Pace and Heim, 2011; Yehuda, 2009).

Several behavioral and biological alterations in psychiatric disorders like PTSD have been attributed to changes in stress hormone levels. It is well known that elevated glucocorticoid levels can exert toxic effects, and therefore, glucocorticoids are discussed to be involved in the development of hippocampal shrinkage, which has been associated with PTSD and other stress-associated psychiatric disorders (McEwen, 1997). This hippocampal volume loss, described in greater detail in section 1.2.4.1, might at least partially underlie cognitive deficits found in a majority of PTSD patients (Brewin, 2011; McEwen, 1997). Moreover, both glucocorticoids and catecholamines have been reported to enhance memory consolidation, *i.e.* the stabilization of a memory trace leading to the formation of long-term memory (Quervain et al., 2009; Roozendaal et al., 2009). Thus, increased stress hormone levels during and shortly after the trauma might lead to an overrepresentation of emotionally arousing memories. Furthermore, glucocorticoids also inhibit the retrieval of stored memories, and thus, low cortisol levels in PTSD patients might facilitate pathological excessive retrieval of aversive memories (Quervain et al., 2009). Additionally, diminished cortisol levels can reduce the consolidation of fear extinction memory, *i.e.* the reduction of the conditioned fear response following the presentation of a traumatic cue in absence of the aversive stimulus (Quervain et al., 2009). Impaired fear extinction has been proposed to be responsible for the persistence of traumatic memories in PTSD patients (Wessa and Flor, 2007). A possible molecular mechanism of the glucocorticoid enhanced memory (re)consolidation has been

recently investigated in the hippocampus of rats in a predator scent based model of PTSD: trauma stress-induced increase in corticosterone secretion and enhanced GR translocation to the nucleus were found to induce an increased expression of the immediate early gene *Zif/268* shortly after stress exposure (Kozlovsky et al., 2009). *Zif/268* is a critical factor for synaptic modifications and the formation of long-term memory (Guzowski, 2002; Abraham et al., 1991). Furthermore, the molecular underpinnings of fear extinction have been addressed in a recent study showing that inhibition of hippocampal cyclin dependent kinase 5 (CDK5) activity facilitates fear extinction in mice (Sananbenesi et al., 2007).

1.2.2. Neurotransmitter systems in PTSD

Processing of information in neuronal networks of the brain depends on neuron-to-neuron signaling which is transduced via neurotransmitter release in chemical synapses. As described below in section 1.2.4, traumatic experiences activate certain neuronal circuits and can also induce long-lasting changes in neurotransmitter systems. Furthermore, single nucleotide polymorphisms (SNP), i.e. a DNA sequence variation in a single nucleotide, in genes associated with neurotransmitter systems have been shown to be associated with the individuals predisposition to develop PTSD (see also section 1.2.3). Several monoaminergic transmitters including norepinephrine (see section 1.2.1), dopamine, and serotonin have been implicated in PTSD pathogenesis: clinical studies identified increased urinary dopamine levels in PTSD patients (Glover et al., 2003) as well as an association of SNPs in the dopamine transporter 1 (DAT1) gene (Valente et al., 2011; Segman et al., 2002; Drury et al., 2009), the dopamine receptor 2 (DRD2) gene (Comings et al., 1996; Young et al., 2002; Voisey et al., 2009), and the dopamine receptor 4 (DRD4) gene (Dragan and Oniszczenko, 2009) with PTSD. In addition, a polymorphism in the catecholamine catabolizing enzyme Catechol-O-methyltransferase (COMT) has been proposed as a risk factor for PTSD development (Kolassa et al., 2010b). Furthermore, dysregulation of the serotonin signaling pathway has been suggested to contribute to PTSD pathophysiology: in PTSD patients decreased platelet concentrations of serotonin (Mück-Seler et al., 2003; Spivak et al., 1999; Kovacic et al., 2008) as well as an association of SNPs in the serotonin transporter (SLC6A4)

1. Introduction

gene (Lee et al., 2005; Kolassa et al., 2010a; Kilpatrick et al., 2007; Koenen et al., 2009) and the serotonin receptor 2A (5-HTR2A) gene with PTSD (Lee et al., 2007) have been reported. Besides these alterations in monoaminergic pathways, also alterations in amino acid neurotransmitter pathways have been identified in PTSD: decreased plasma levels of γ -aminobutyric acid (GABA), the major inhibitory neurotransmitter of the CNS, have been found in PTSD patients (Vaiva et al., 2004). Furthermore, genetic variations of GABA receptor A2 (GABARA2) have been associated with human PTSD (Nelson et al., 2009). Dysregulation of the GABAergic neurotransmitter system has also been reported in a rat model of PTSD: a downregulation of the GABAA receptor has been detected in the amygdala (Ponomarev et al., 2010). Moreover, dysfunction of glutamatergic neurotransmission is known to play a major role in the stress response and in stress-related disorders (Popoli et al., 2012). Animal studies have found that acute stress induces a glucocorticoid-dependent increase in glutamate release that may at least in part be mediated via a cannabinoid receptor dependent pathway (Popoli et al., 2012). Interestingly, a single nucleotide polymorphism (SNP) in the cannabinoid receptor 1 (CNR1) gene has recently been associated with PTSD (Lu et al., 2008). Stress-induced elevation of glutamate release facilitates memory formation by inducing long-term potentiation (Anwyl, 2009). Excessive glutamate levels, however, can result in excitotoxicity, i.e. cellular damage (Wang and Qin, 2010). Besides this finding and the fact that anti-glutamatergic drugs like lamotrigine have been proven to be effective in pharmacotherapy of PTSD patients (Berger et al., 2009), there are so far no human studies showing altered glutamatergic neurotransmission in PTSD patients. However, evidence for a role of the glutamatergic system in PTSD pathogenesis is provided by rodent studies in which blocking N-methyl-D-aspartate (NMDA) receptors prior to exposure to a predator scent stress prevented anxiety-like behavior (Adamec et al., 1999; Blundell et al., 2005). Independent from that, hypoactivity of the hippocampal inhibitory glycinergic system has been recently linked to impaired fear extinction in a rat model of PTSD (Yamamoto et al., 2010).

Finally, also altered neuropeptide levels have been found associated with PTSD: besides the alterations in CRH, described in section 1.2.1, decreased expression of neuropeptide Y (NPY) has been reported both in PTSD patients (Rasmusson et al., 2000) and in rats exhibiting

PTSD-like symptoms (Ponomarev et al., 2010; Cohen et al., 2012). NPY is known to stimulate the secretion of CRH in the hypothalamus (Haas and George, 1989). In addition, increased secretion of the neuropeptide PACAP, which inter alia also increases CRH secretion in the hypothalamus (Grinevich et al., 1997), have been associated with PTSD in female patients (Ressler et al., 2011). In the same study also a SNP in the PACAP receptor PAC1 has been associated with PTSD in female patients, and furthermore, the identified risk genotyp was linked to decreased PAC1 receptor mRNA expression in cortex samples of healthy females (Ressler et al., 2011)

1.2.3. Genetic and epigenetic risk factors for PTSD

Only a subset of trauma victims develops PTSD. A recent study in a U.S. patient cohort has determined that less than 10 % of individuals exposed to any traumatic event develop PTSD (Breslau, 2009). However, depending on the type and intensity of the traumatic event the proportion of individuals developing PTSD patients can be substantially higher. Thus, additional factors, including environmental, genetic, and epigenetic risk factors are thought to contribute to the individuals predisposition to develop PTSD. Twin studies can contribute to differentiate the influence of environmental and genetic factors on behavior. Studying trauma-exposed twin pairs it has been estimated that approximately 30 % of the PTSD symptoms rely on a heritable component (Afifi et al., 2010; Skelton et al., 2012). The identification of specific genes involved in PTSD pathogenesis has been mainly addressed in candidate gene association studies, while so far no genome-wide association study (GWAS) has been performed with PTSD patients (Cornelis et al., 2010). In contrast to GWAS, which investigate genetic variations in the whole genome, the candidate gene association approach selectively searches for association of single SNPs with certain symptoms or syndromes aiming to identify genetic regions involved in certain diseases like PTSD (Cornelis et al., 2010). These candidate gene association studies have so far mainly searched for genetic variations in genes associated with the HPA axis (summarized in Table 1.1): the PTSD syndrome was found to be associated with SNPs inter alia in the CRH receptor 1 (CRHR1) gene (Amstadter et al., 2011), and in the FK506 bindin protein 5 (FKBP5) gene (Binder et al., 2008; Xie

1. Introduction

et al., 2010) which regulates the cortisol-binding affinity of the glucocorticoid receptor. It is hypothesized that these genetic variations in the CRHR1 and FKBP5 genes contribute to the dysregulation of the HPA axis in individuals developing PTSD. Furthermore, a polymorphism in the anxiety-associated gene regulator of G-protein signaling 2 (RSG2) has been reported to be associated with PTSD symptom severity after trauma exposure (Amstadter et al., 2009). Finally, SNPs in a variety of neurotransmitter system associated genes have been linked to PTSD, as described in section 1.2.2 and summarized in Table 1.1.

Besides genetic variations, the risk to develop PTSD is also influenced by environmental factors like early-life stress but also trauma type or severity which can modify gene activity *inter alia* via epigenetic mechanisms. Epigenetic modifications are heritable functional changes of the genetic activities that are not accompanied by alterations of the DNA sequence, e.g. acetylation of histone proteins or methylation of cytosine residues residing in CpG dinucleotides that are often found to be enriched in promoter regions (Schmidt et al., 2011). The transgenerational transmission of potential trauma stress-induced epigenetic modifications is alluded by a study showing that maternal PTSD increases the risk of Holocaust survivors offspring to develop PTSD (Yehuda et al., 2008). This assumption is further supported by a study reporting decreased salivary cortisol levels in both babies and their mothers, who developed PTSD after experiencing the World Trade Center attacks during pregnancy (Yehuda et al., 2005). Epigenetic regulation of HPA axis activity has been also addressed in a study using human *post-mortem* hippocampus samples from suicide victims showing reduced GR expression levels and increased GR promoter methylation in those individuals that had experienced early-life traumatic stress (McGowan et al., 2009). Furthermore, a recent study in mice reported early-life stress to decrease methylation of a regulatory region in the vasopressin gene, which was accompanied by increased vasopressin expression and HPA axis hyperactivation (Murgatroyd et al., 2009). Importantly, in the same study neuronal activity was reported to regulate vasopressin transcription by increasing methyl CpG-binding protein 2 (MeCP2) phosphorylation and thereby preventing the MeCP2-mediated upregulation of vasopressin expression. Recently, also the methylation of the stress-related PAC1 receptor gene, measured in blood samples of PTSD patients,

has been associated with PTSD symptom severity (Ressler et al., 2011). Binding of the neuropeptide PACAP to the PAC1 receptor is involved in the stress response inter alia by stimulating CRH gene expression (Grinevich et al., 1997). Furthermore, epigenetic variations in PTSD patients have been assessed using methylation microarrays with blood samples of PTSD-affected and PTSD-unaffected individuals revealing a reduced methylation of immune function associated genes in PTSD-affected individuals (Uddin et al., 2010). A second study using the same patient samples also identified an interaction between methylation of the gene encoding mannosidase alpha class2C member 1 (MAN2C1) and the number of potentially traumatic events; thus, high MAN2C1 methylation rates and a high number of potentially traumatic events increase the risk of developing PTSD (Uddin et al., 2011). Finally, distinct alterations in global hippocampal DNA methylation patterns have been identified in a rat model of PTSD (Chertkow-Deutsher et al., 2010). In the same PTSD animal model increased methylation of the Disks Large-Associated Protein (Dlgap2) encoding gene was associated with decreased Dlgap2 gene expression, which, in turn, was found to be correlated with the behavioral stress response (Chertkow-Deutsher et al., 2010).

Altogether, environmental and genetic factors as well as gene x environment interactions, that are inter alia mediated via epigenetic mechanisms, modulate the individuals vulnerability to PTSD (Mehta and Binder, 2011). In particular, the findings on genetic and epigenetic variations of HPA axis associated genes underline the importance of this neuroendocrine stress response system for PTSD susceptibility and pathogenesis. Furthermore, evidence from genetic and epigenetic studies propose an involvement of both neurotransmitter system and immune function related genes to contribute to PTSD pathogenesis.

1.2.4. Pathoanatomical alterations associated with PTSD

Structural and functional alterations of several brain regions including the amygdala, the hippocampus (HC), and the prefrontal cortex (PFC) have been identified in PTSD patients. These brain regions form a functional neurocircuit activated during both the stress response and fear conditioning (Heim and Nemeroff, 2009). Several neuroimaging studies using mostly positron emission tomography (PET) and functional magnetic resonance imaging

(fMRI) found a hyperresponsivity of the amygdala in PTSD patients which was correlated with symptom severity, while hippocampal and prefronto-cortical regions were found to be hypo-responsive (Shin and Liberzon, 2010).

1.2.4.1. Hippocampus

The hippocampus, which is *inter alia* involved in the formation and the maintenance of declarative and spatial memory as well as in memory consolidation processes generating long-term memory (Elzinga and Bremner, 2002), was found to be hypoactive in PTSD patients. This hypoactivation inversely correlated with symptom severity (Shin and Liberzon, 2010). Furthermore, a reduction of hippocampal volume has been repeatedly associated with PTSD (Shin and Liberzon, 2010). Additionally, decreased levels of hippocampal N-acetylaspartate (NAA), a marker for neuronal integrity, have been associated with traumatic stress and argue for dysfunctional hippocampal neuronal networks in PTSD patients (Schuff et al., 2006). Moreover, in the PTSD mouse model used also in the thesis at hand, hippocampal NAA measurements in mice have been reported to predict the development of PTSD-like symptoms (Siegmund et al., 2009). Accordingly, findings of twin studies suggest hippocampal volume to represent a predisposition factor rather than a consequence of PTSD pathogenesis (Gilbertson et al., 2002).

Despite several alterations proposed to underlie trauma stress-induced hippocampal shrinkage comprising decreased neurogenesis and gliogenesis, apoptosis, and reduction in glial cell numbers as well as morphological changes of neurons like dendritic retraction (Czeh and Lucassen, 2007), the exact cellular and molecular correlates of the PTSD associated hippocampal volume loss still remain elusive. Glucocorticoids and brain-derived neurotrophic factor (BDNF) are discussed to be involved in the development of hippocampal shrinkage: it is well known that persistently elevated levels of glucocorticoids have neurotoxic effects (You et al., 2009; Uno et al., 1994) which are, at least in part, mediated by a glucocorticoid-induced increase in hippocampal glutamate levels and subsequent excitotoxic effects (McEwen, 1997). Animal studies further suggest that stress-induced alterations in hippocampal expression levels of glucocorticoid receptors (Kohda et al., 2007) and NMDA receptors (Yamamoto et al., 2008)

might further aggravate the toxic effects of increased glucocorticoid and glutamate levels. Furthermore, clinical studies showing an inverse correlation of cortisol levels with hippocampal volume (Knoops et al., 2010; Tessner et al., 2007) support the hypothesis of glucocorticoids playing a major role in stress-associated hippocampal shrinkage. In contrast to glucocorticoids, BDNF represents an important factor in hippocampal plasticity since it promotes neuronal growth and survival (Numakawa et al., 2010). Reduced BDNF gene expression has been found both in plasma of PTSD patients (Dell'osso et al., 2009) as well as in the hippocampus of rats showing a PTSD-like syndrome (Kozlovsky et al., 2007). An epigenetic mechanism of BDNF downregulation has been recently reported in a study showing reduced BDNF expression to be associated with increased BDNF DNA methylation rates in rats exhibiting PTSD-like symptoms (Roth et al., 2011). BDNF-induced long-term potentiation (LTP) has been shown to include the activation of the extracellular signal-regulated kinase (ERK) and p38 mitogen-activated protein kinases (MAPK) which both induce phosphorylation of cAMP response element-binding (CREB) protein (Ying et al., 2002). Phosphorylated CREB, in turn, is able to induce the immediate early genes activity-regulated cytoskeleton-associated protein (Arc) and Zif/268, thereby possibly contributing to changes in synaptic structure (Ying et al., 2002). Both Arc and Zif/268 have been found to exhibit increased expression in different PTSD rat models (Kozlovsky et al., 2008; Kozlovsky et al., 2009). Despite these efforts, however, the molecular correlates of the PTSD associated hippocampal shrinkage are not completely understood.

1.2.4.2. Prefrontal cortex

The prefrontal cortex integrates sensory information received from numerous brain regions with inter alia emotional memory from the limbic system (Gray et al., 2002). Based on these information, the prefrontal cortex plans and initiates goal-directed behavior (Miller et al., 2002). Decreased activation of the medial prefrontal cortex (mPFC) was found in PTSD patients in response to both trauma-related and trauma-unrelated stimuli, and moreover, it was inversely correlated with PTSD symptom severity (Shin and Liberzon, 2010). Furthermore, a reduction of the PFC volume was found in PTSD patients (Shin and Liberzon,

2010). The cellular and molecular correlates of this PFC volume loss, however, are poorly understood. In accordance with these clinical studies, a study that subjected rats to chronic restraint stress reported reductions in prefronto-cortical dendrite lengths (Radley et al., 2004). The latter might contribute to the PFC volume loss and cognitive impairments, however, this still awaits experimental confirmation. On the molecular level, so far only a single study employing a PTSD rat model showed a prefronto-cortical reduction of phosphorylated ERK1/2 which is *inter alia* involved in the formation of BDNF-induced LTP (Wang et al., 2010a).

1.2.4.3. Amygdala

The third brain region involved in the neurocircuitry of PTSD is the amygdala which has been repeatedly shown to be hyperactive in PTSD patients. As HC and PFC exert inhibitory actions on the amygdala, hypoactivity of these two regions might further enhance the hyperresponsivity of the amygdala, which is *inter alia* involved in the emotional processing of stress (Rauch et al., 2006). Several studies reported that the amygdala volume is reduced in PTSD patients (Karl et al., 2006; Rogers et al., 2009). Findings of animal studies suggest that apoptosis contributes largely to this volume loss (Xiao et al., 2011b; Liu et al., 2011; Ding et al., 2010). On the cellular level, the hyperactivation of the amygdala might be reflected by increased dendritic arborization and increased spine density found in animal models of PTSD (Mitra et al., 2005; Adamec et al., 2012; Cui et al., 2008). These alterations in dendritic spine density are thought to affect the storage of fear memories, which is disturbed in PTSD (Mitra et al., 2005). Interestingly, expression of phosphorylated ERK (pERK) was increased in the hyperresponsive amygdala (Xiao et al., 2011a), while, as mentioned in the previous section, pERK expression was decreased in the hyporesponsive prefrontal cortex (Wang et al., 2010a).

Altogether, studies on animal models of PTSD are starting to address the cellular and molecular correlates of structural and functional neuroanatomical alterations that have been found in PTSD patients, however, the distinct molecular mechanisms underlying the trauma stress-induced shrinkage of these brain regions still remain elusive.

1.3. PTSD Biomarkers

The term biological marker or biomarker was defined by the Biomarker Definitions Working Group as ‘a characteristic that is objectively measured and evaluated as an indicator of normal biological processes, pathogenic processes, or pharmacologic responses to a therapeutic intervention’ (Biomarkers Definitions Working Group, 2001). In addition to providing a tool for measuring processes in the clinical setting, the search for new biomarkers aims at contributing to further elucidation of (patho-)mechanisms underlying the respective pathogenic processes. A wide variety of indicators can serve as biomarkers: genomic alterations like single nucleotide polymorphisms (SNPs) have been proposed to predict disease vulnerability and treatment responsiveness of individuals, e.g. a SNP in the FKBP5 gene has been associated with the response to antidepressant treatment (Binder et al., 2004). Additionally, alterations in gene or protein expression can serve as measurable tools in normal biological as well as pathogenic processes and therapeutic treatment responses (Hampel et al., 2010). Besides genomic, transcriptomic, and proteomic markers, also altered brain activities determined by PET or fMRI imaging and any physiological parameter like blood pressure, electrocardiogram (ECG), and heart rate can serve as biomarker (Hampel et al., 2010; Zhang et al., 2009).

To date, several potential PTSD biomarkers have been proposed, e.g. the startle response, which positively correlates with the state of nervous hyperarousal (Skelton et al., 2012). However, so far no PTSD biomarker has been licensed for use in the clinical practice. Table 1.1 summarizes genomic alterations as well as gene and protein expression changes that have been found to be associated with human PTSD and were proposed to serve as potential PTSD biomarkers. Several of these potential biomarkers are HPA axis associated factors and are described in greater detail in chapters 1.2.1 and 1.2.3. In addition, high dexamethasone binding capacity in peripheral blood mononuclear cells (PBMCs), reflecting a measurement of GR numbers, have been proposed as a vulnerability factor for PTSD development (van Zuiden et al., 2011). Besides the HPA axis, several genes encoding neurotransmitter system associated proteins, as described in section 1.2.2, have been associated with PTSD. Additionally,

Table 1.1.: **Potential biomarkers for PTSD.** Unless indicated otherwise the cited studies used blood samples of PTSD patients and control individuals. This list is not intended to be exhaustive.

Biomarker	Type	References
HPA-Axis		
Glucocorticoid receptor (GR)	protein	(Gotovac et al., 2003; van Zuiden et al., 2011)
CRHR1	SNP	(Amstadter et al., 2011)
FKBP5	SNP, mRNA	(Binder et al., 2008; Xie et al., 2010; Yehuda et al., 2009)
circulating cortisol levels		reviewed in (Yehuda, 2009)
Neurotransmitter Systems		
NPY expression	protein	(Rasmusson et al., 2000; Yehuda et al., 2006)
PACAP and PAC1	SNP, mRNA, methylation	(Ressler et al., 2011)
Dopamine transporter (DAT1)	SNP	(Valente et al., 2011; Segman et al., 2002; Drury et al., 2009)
Dopamine receptor (DRD2)	SNP	(Comings et al., 1996; Young et al., 2002; Voisey et al., 2009)
Dopamine receptor (DRD4)	SNP	(Dragan and Oniszczenko, 2009)
urinary dopamine increase		(Glover et al., 2003)
Serotonin transporter (SLC6A4)	SNP	(Lee et al., 2005; Kolassa et al., 2010a; Kilpatrick et al., 2007; Koenen et al., 2009)
Serotonin receptor (5-HTR2A)	SNP	(Lee et al., 2007)
Platelet serotonin concentration		(Mück-Seler et al., 2003; Spivak et al., 1999; Kovacic et al., 2008)
GABA receptor (GABARA2)	SNP	(Nelson et al., 2009)
GABA plasma levels decreased		(Vaiva et al., 2004)
Catechol-O-methyltransferase (COMT)	SNP	(Kolassa et al., 2010b)
Cannabinoid receptor (CNR1)	SNP	(Lu et al., 2008)
p11 (S100-A10)	mRNA	(Su et al., 2009)
Immunological Factors		
IL-6 and IL-6R	protein	(Maes et al., 1999; Baker et al., 2001; von Känel et al., 2010)
IL-2 and IL-8	protein	(Song et al., 2007)
CRP and serum amyloid A	protein	(Söndergaard et al., 2004; von Känel et al., 2010)
Neopterin reduction		(Atmaca et al., 2002)
increased inflammatory immune activities	mRNA, protein, cells	reviewed in (Gill et al., 2009; Vidovic et al., 2011)
Other Factors		
BDNF	mRNA	(Dell'osso et al., 2009)
MAN2C1	methylation	(Uddin et al., 2011)
RGS2	SNP	(Amstadter et al., 2009)

decreased gene expression of p11, which has been linked to neurotransmitter transport, in blood of PTSD patients has been proposed as a potential biomarker that can distinguish PTSD from other psychiatric disorders (Su et al., 2009). Moreover, low GABA plasma levels have been suggested to serve as a predictive factor for PTSD development (Vaiva et al., 2004). On the protein level, however, so far almost only immunological factors like the cytokines IL-2, IL-6, and IL-8 have been found to be increased in PTSD patients (Maes et al., 1999; Baker et al., 2001; von Känel et al., 2010; Song et al., 2007). In contrast, the immunological factors C-reactive protein (CRP), serum amyloid A (SAA), and neopterin were found to be reduced in PTSD patients (Söndergaard et al., 2004; von Känel et al., 2010; Atmaca et al., 2002). The lack of protein expression changes associated with PTSD not related to the immune system might be at least partially be due to the lack of efficient high-throughput protein array techniques. Additionally, studies using human material are in most cases limited to blood samples. Studying expression changes in the blood is especially interesting with regard to the HPA axis and immunological factors. Besides sporadic studies with human *post-mortem* brain samples (McGowan et al., 2009), studies addressing brain specific expression changes, however, are so far mainly restricted to the analysis of animal models.

1.4. Pharmacotherapy of PTSD

A combination of trauma-psychotherapy and pharmacotherapy, mainly employing antidepressants of the serotonin reuptake inhibitor (SSRI) type, is currently considered as the gold standard in PTSD treatment (Berger et al., 2009). Due to the complex symptomatology of PTSD, however, there is no medication addressing all of the symptom clusters mentioned in chapter 1.1, and moreover, there is no drug specifically acting against re-experiencing and hyperarousal symptoms which are pathognomonic for this anxiety disorder. The rationale for treating PTSD patients with SSRIs, which are widely prescribed in depressive and anxiety disorders, is a presumed dysregulation of the serotonergic neurotransmission (section 1.2.2). Although their mode of action is so far not completely understood, SSRIs increase the serotonin concentration in the synaptic cleft by inhibiting its uptake into the presynapse. Currently, only

the SSRIs sertraline and paroxetine have been officially approved by the U.S. Food and Drug Administration (FDA) for treatment of PTSD (Ravindran and Stein, 2009). Besides SSRIs, other antidepressants, mood stabilizers, and even neuroleptics are employed for symptomatic treatment of PTSD (Steckler and Risbrough, 2012).

Interestingly, clinical pilot studies demonstrate that anti-adrenergic drugs are suitable for the treatment of PTSD associated hyperarousal symptoms, especially for the treatment of sleep disturbances and nightmares: the α_2 -adrenoreceptor agonist clonidine, the α_1 -adrenoreceptor antagonist prazosin, and the β -adrenoreceptor antagonist propranolol, all widely used in treatment of hypertension, have been proven to effectively counteract PTSD associated hyperarousal symptoms (Ravindran and Stein, 2009).

As introduced in section 1.2.1, dysregulation of the HPA axis plays an important role in PTSD and most studies found an HPA axis hypoactivity in PTSD patients. Glucocorticoids are known to impair memory retrieval and to enhance the consolidation of extinction memory (Quervain et al., 2009), implicating a possible beneficial effect of glucocorticoids in the treatment of PTSD. Indeed, first pilot studies allude that low-dose cortisol treatment improves re-experiencing and avoidance symptoms (Aerni et al., 2004).

Taken together, the fact that less than 20-30 % of PTSD patients achieve full remission with the current first-line treatment, the SSRI antidepressants, (Berger et al., 2009) accentuates the need for the discovery of novel PTSD-specific drugs and hence for further elucidation of PTSD etiopathology.

1.5. Animal models of anxiety disorders

Modeling psychiatric disorders is challenging since most parameters of the human psyche are not objectively measurable but only assessable by talking to the patient. Thus, animal models of psychiatric disorders are limited to the interspecies measurable parameters like fear or arousal, while symptoms like intrusive thoughts and dreams of course can not be assessed. A valid animal model has to fulfill several criteria: the face validity of an animal model describes to what extent the animal model reflects the human symptomatology, the etiological

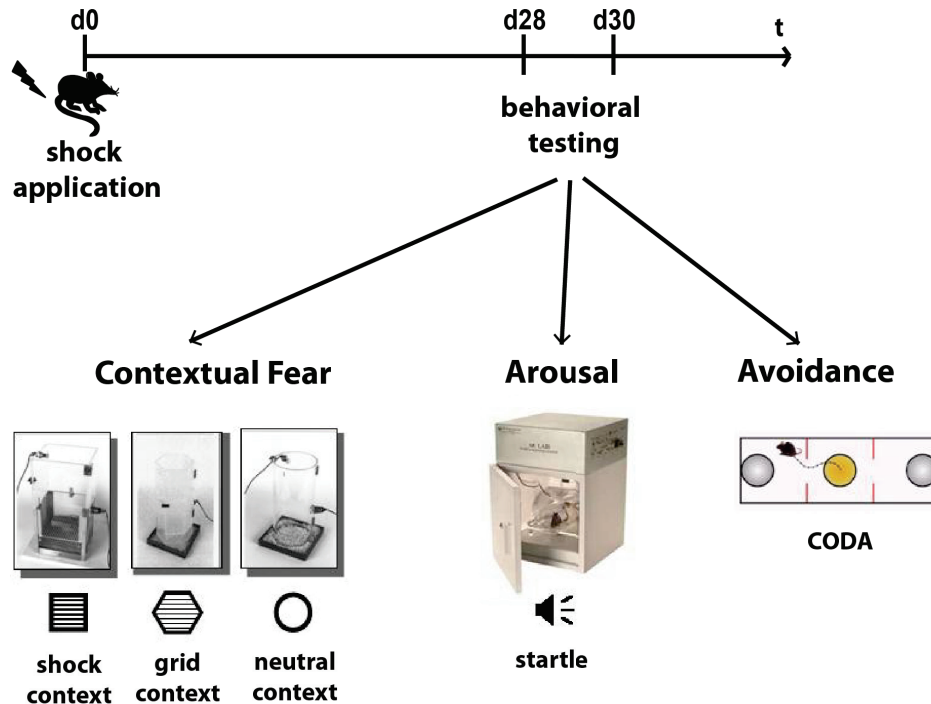


Figure 1.2.: **The PTSD mouse model.** On day 0 C57BL/6NCrI receive a 1.5 mA footshock applied for 2 s via a metal grid. After 28 days PTSD-like behavior is tested: contextual fear is assessed by measuring the freezing response in the shock context, the grid context, and the neutral context. Arousal is assessed by measuring the acoustic startle response to a neutral tone. Avoidance behavior can be tested in a CODA chamber with three compartments: the nest compartment, a compartment with a smell reminding of the shock context and a neutrally smelling compartment.

validity results from the comparison of factors that trigger the disease pathogenesis in animals and humans, the construct validity represents the similarity of etiopathological correlates in humans and the model organisms employed, and the predictive validity represents the similarity of successful treatment options between model organisms and humans (Chadman et al., 2009; Siegmund and Wotjak, 2006).

1.5.1. The PTSD mouse model

The PTSD mouse model used in this study meets many of the criteria mentioned above (Siegmund and Wotjak, 2007). In this PTSD mouse model, a 2 s long 1.5 mA footshock that cannot be anticipated by the mouse represents the traumatic event. 28 days after application of the traumatic footshock a set of behavioral tests is performed to assess PTSD-like symptoms

(Figure 1.2). Both the conditioned fear response and the generalized fear response are increased in footshocked mice. The conditioned fear response is rated by observation of the freezing response in the shock context, and the generalized fear response is assessed by measuring the freezing response in a context resembling the shock context in its dominant feature (i.e. the metal grid) as well as in a completely neutral context (Siegmund and Wotjak, 2007). Furthermore, footshocked mice show an hyperarousal phenotype. The latter is evaluated by assessing the intensity of the acoustic startle response to a neutral tone of different intensities (Siegmund and Wotjak, 2007). The avoidance behavior can be analyzed in a CODA chamber consisting of three compartments: the nest compartment, one compartment smelling like the shock context (ethanol), and one compartment with a different, but also intense smell representing the neutral stimulus (acetic acid). Due to their inquisitive nature, mice usually spend approximately the same amount of time in each compartment. Mice having received a footshock avoid the compartment smelling like the shock context and spend an increased amount of time in the nest compartment (Pamplona et al., 2011). Taken together, the etiologic validity (traumatic event $\hat{=}$ traumatic footshock) and the face validity (increased contextual fear, hyperarousal phenotype and avoidance of the trauma context) are met.

As introduced in section 1.4, so far no PTSD specific pharmacotherapy exists, and SSRIs like for instance fluoxetine currently represent the treatment of choice. Chronic fluoxetine treatment of traumatized mice has been shown to ameliorate PTSD-like symptoms (Siegmund and Wotjak, 2007) pointing at a high predictive validity of this PTSD mouse model.

As so far the distinct biological mechanisms of PTSD are elusive, the construct validity criterion is difficult to fulfill. One biological correlate found in PTSD patients but also in patients with other affective disorders like major depression is the hippocampal volume loss (section 1.2.4). Indeed, in the PTSD mouse model used here, traumatized mice also exhibit a reduced hippocampal volume (Golub et al., 2011). However, the pathomechanisms underlying this trauma stress-induced hippocampal shrinkage still remain elusive.

1.5.2. The HAB/LAB mouse model

In contrast to the PTSD mouse model in which the anxiety phenotype is caused by an external factor, i.e. the electric footshock, the HAB/LAB mouse model represents a model for trait anxiety. In contrast to the state anxiety paradigm, trait anxiety reflects the permanent disposition for enhanced anxiety responses. High anxiety (HAB) and low anxiety (LAB) mouse strains were generated by selective breeding of CD1 outbred mice showing high or low anxiety-like behavior on the elevated plus maze, that is a plus-shaped apparatus with two open and two closed arms (Krömer et al., 2005). As mice typically avoid open space, low anxiety-like behavior is represented by an increased time spent on the open arms. The maximum of behavioral divergence between HAB and LAB mice was reached after 9 generations with the HAB mice spending less than 10 % of the test period on the open arms and the LAB mice spending more than 50 % of the test period on the open arms (Krömer et al., 2005). Furthermore, isolated HAB pups showed an increased ultrasonic vocalization that is used as an index of anxiety, while prior diazepam treatment was able to reduce the ultrasonic vocalization. In the tail-suspension test and in the forced swim test, both well-accepted tests for the assessment of depression-like behavior in rodents, HAB mice showed more immobility than LAB mice (Krömer et al., 2005; Landgraf et al., 2007).

Several molecular alterations, e.g. glyoxalase-I and vasopressin expression changes (Krömer et al., 2005; Kessler et al., 2007), have been reported in the HAB/LAB mouse model. Of importance for the thesis at hand is in particular the increased expression of the potential anxiety disorder biomarker transmembrane protein 132 D (TMEM132D) (see section 1.6) in the cingulate cortex of HAB mice (Erhardt et al., 2011).

1.6. Transmembrane protein 132D - a candidate gene for anxiety phenotypes

TMEM132D was recently identified as a new candidate gene for anxiety phenotypes (Erhardt et al., 2011): in detail, in a clinical study with 909 cases and 915 controls, the SNPs rs7309727 and rs11060369 located in intron 3 of the TMEM132D gene were identified to be associated

1. Introduction

with panic disorder, and in addition, the SNPs rs900256, rs879560, and rs10847832 located in intron 4 of the TMEM132D gene were found to be associated with symptom severity of anxiety in both panic disorder and major depression. Furthermore, in the same study it was shown that mice exhibiting a high anxiety phenotype (HAB) express higher levels of TMEM132D in the cingulate cortex than mice exhibiting a low anxiety phenotype (LAB). Accordingly, humans expressing the panic disorder associated genotype at SNP rs11060369 exhibited increased TMEM132D mRNA expression in the frontal cortex (Erhardt et al., 2011). The precise functions of TMEM132D and its paralogs TMEM132A, TMEM132B, TMEM132C, and TMEM132E have not been identified so far. The function of TMEM132A, a transmembrane protein also known as glucose regulated protein 78 (GRP78) binding protein, was investigated in a few studies proposing it to be involved in the embryonic and postnatal development of the rat brain (Oh-hashii et al., 2003). In addition, TMEM132A was reported to inhibit the expression of the astrocytic cytoskeleton protein glial fibrillary acidic protein (GFAP) in an astrocytic cell line (Oh-hashii et al., 2006) and to affect neurite outgrowth and serum-starvation induced cell death in a neuronal cell line (Oh-hashii et al., 2010). Thus, TMEM132A probably plays a critical role in cell survival during development of the brain.

A potential role of TMEM132D in psychiatric disorders as postulated by the findings of Erhardt et al. (2010) is further supported by a recent report identifying TMEM132D as a possible candidate gene for attention deficit hyperactivity disorder (ADHD) (Mick et al., 2011). The function of TMEM132D has so far only been investigated in one single study which demonstrates mature oligodendrocytes to express higher TMEM132D mRNA levels than oligodendrocytic precursor cells (Nomoto et al., 2003). Although the contribution of myelinating oligodendrocytes to the pathogenesis of anxiety disorders is not completely understood, increased expression of myelin proteins and lipids in the amygdala and the hippocampus have been linked with early weaning induced anxiety-like behavior in rodents (Ono et al., 2008; Kodama et al., 2008). In addition, a lack of myelin in galectin-3 knockout mice was found to be associated with decreased anxiety-like behavior (Pasquini et al., 2011). Finally, immunization of mice with a myelin-related peptide reduced trauma stress-induced anxiety (Lewitus et al., 2008). These studies show that oligodendrocytes might be involved in

the development of anxiety-like behavior. Moreover, it can be hypothesized that TMEM132D might be crucial for oligodendrocyte function as well as their involvement in anxiety disorder pathogenesis. Altogether, the candidate gene TMEM132D as well as a potential TMEM132D dependent oligodendrocyte differentiation might contribute to the pathogenesis of anxiety disorders including PTSD.

1.7. Aim of the thesis

The thesis at hand aimed to contribute to the elucidation of the still unknown molecular mechanisms of PTSD pathogenesis:

1. by promoter analysis of TMEM132D, an already identified anxiety disorder candidate molecule, with the aim to identify regulatory mechanisms of TMEM132D gene expression (chapter 3).
2. by screening for novel PTSD candidate proteins in a mouse model of PTSD (chapter 4).
 - A secondary goal of this screen was to identify the molecular underpinnings of the PTSD associated hippocampal shrinkage by analyzing a set of neurostructural and glutamate system associated proteins in the hippocampus, and additionally also in the prefrontal cortex and in the cerebellum (chapter 4.2.1 and 4.2.2).
 - Motivated by the serendipitous finding of a trauma stress-induced increase in immunoglobulin G expression, another aim of this thesis was to further elucidate the immune system's contribution to PTSD pathogenesis (chapter 4.2.3).

2. Materials and Methods

If not indicated otherwise, chemicals were purchased from Carl Roth (Karlsruhe, Germany) and plastic disposables were obtained from Peske GmbH & Co KG (Aindlingen-Arnhofen, Germany). General lab equipment is listed in Table 2.1. Specific materials and buffer compositions are given in the sections of the respective methods.

Table 2.1.: **General lab equipment.** Listed are names and manufacturers of equipment used in the experiments of this thesis.

Equipment	Manufacturer
Eppendorf Research pipette 100-1000 μl	Eppendorf (Hamburg, Germany)
Eppendorf Research pipette 20-200 μl	Eppendorf (Hamburg, Germany)
Eppendorf Research pipette 10-100 μl	Eppendorf (Hamburg, Germany)
Eppendorf Research pipette 2-20 μl	Eppendorf (Hamburg, Germany)
Eppendorf Research pipette 0.5-10 μl	Eppendorf (Hamburg, Germany)
Eppendorf Research pipette 0.1-2.5 μl	Eppendorf (Hamburg, Germany)
Multichannel pipette Transferpette-12 10-100 μl	Brand (Wertheim, Germany)
Multichannel pipette Transferpette-8 5-50 μl	Brand (Wertheim, Germany)
Multichannel pipette ExactaCruz 50-300 μl	Santa Cruz Biotechnology Inc. (Santa Cruz, CA, USA)
Pipettor pipetus for 0.1 ml to 200 ml pipettes	Hirschmann Laborgeräte GmbH & Co. KG (Eberstadt, Germany)
Vortex REAXtop	Heidolph (Schwabach, Germany)
Mini-centrifuge for PCR-tubes	Fisherbrand (Schwerte, Germany)
Centrifuge 5415R, refrigerated microcentrifuge	Eppendorf (Hamburg, Germany)
Centrifuge Sigma 2-6	Sigma Zentrifugen (Osterode am Harz, Germany)
Beckman Coulter Allegra X-22R centrifuge	Beckman Coulter (Krefeld, Germany)
Beckman Coulter J2-MC	Beckman Coulter (Krefeld, Germany)
Beckman Coulter XL-90 ultracentrifuge	Beckman Coulter (Krefeld, Germany)
Thermoshaker TS-100	Peqlab (Erlangen, Germany)
Thermoshaker HLC 13	MS-L GmbH Laborgeräte (Dielheim, Germany)
Balance Pioneer Serie PA4102C	Ohaus (Pine Brook, NJ, USA)
Balance Voyager 50228	Ohaus (Pine Brook, NJ, USA)
Magnetic stirrer with heater VMS-A	VWR (Darmstadt, Germany)

2.1. Animals

All animal experiments were carried out with the approval of local authorities and conducted according to current regulations for animal experimentation in Germany and the European Union (European Communities Council Directive 86/609/EEC). An overview of all mouse batches employed in this thesis is provided in Table 2.2.

Table 2.2.: **Overview of employed mouse batches.** Abbreviations: WB = Western blot , IHC = immunohistochemistry

Batch name	Molecular analyses	Batch size (n = number of mice per group)
Acute Restraint Stress (RS0)	WB	n = 9
Repetitive Acute Stress (RSI/RSII)	WB	n = 6
PTSD I (d2, d28, d60)	WB (neurostructural and glutamate transporter proteins)	n = 6
PTSD II (d60)	WB (neurostructural proteins), IHC (synapsin)	n = 6
PTSD III (d60)	WB (immune system proteins)	n = 6
PTSD IV (d2, d28, d60)	WB (immune system proteins)	n = 7
PTSD V	behavior only	n = 16
Fluoxetine in PTSD	WB	n = 16 (ctrl), n = 14 (fluoxetine) for behavior; n = 6 for WB
HAB/LAB	WB	n = 4 (HAB), n = 7 (LAB)

2.1.1. Combined restraint and forced swim stress experiments

The combined restraint and forced swim stress animal experiments were performed in collaboration with the research group of Chadi Touma from the Max Planck Institute of Psychiatry. Here, 10-16 weeks old male 129SvJ/C57BL/6 mice from the FKBP5 knockout breeding line (Touma et al., 2011) homozygote for the FKBP5 WT allele were obtained from the animal facility at the Max Planck Institute of Psychiatry and single housed two weeks prior to the experiments under standard laboratory conditions (light-dark cycle 12:12 h, lights on: 08:00 a.m.) with food and water *ad libitum*.

In a first experiment short-term effects of acute restraint stress were analyzed. For this

purpose, mice were subjected to a 15-min restraint stressor by confining the mice in cylindrical plastic tubes. The mice were sacrificed by cervical dislocation 24 h later (RS0 paradigm, $n = 9$). To study long-term effects of acute repetitive stress, in a second experiment two different stress paradigms were applied (RSI/RSII paradigm). In the RSI paradigm, mice ($n = 6$) were either subjected to a 15-min restraint stressor which was, after a 15-min interval in the home cage, followed by a 6-min forced swim stressor (FSS) accomplished in a glass beaker filled with 23 °C warm water. Then, after 24 h in the home cage, the mice were subjected to a second 6-min forced swim stressor. For the RSII paradigm, mice ($n = 6$) were subjected to a 60-min restraint stressor followed by a 6-min forced swim stressor 24 h later. Mice of the RSI and RSII paradigm were sacrificed 8 days after application of the last stressor. Subsequently, bilateral hippocampus (HC), prefrontal cortex (PFC), and cerebellum (CER) were dissected from all mice, shock-frozen in methyl butane on dry ice, and stored at -80 °C before subjection to immunoblot analyses.

2.1.2. PTSD mouse model

All behavioral experiments with the PTSD mouse model were performed in collaboration with the research group of Carsten Wotjak from the Max Planck Institute of Psychiatry. The PTSD mouse model was established by Siegmund and Wotjak (2007) and fulfills the criteria for face and predictive validity as explained in section 1.5.1. For this thesis, male C57BL/6NCrl mice aged 4-5 weeks (see Table 2.2 for overview of employed mouse batches) were purchased from Charles River Germany GmbH (Sulzfeld, Germany). Animals were housed in groups of 4 animals for 6 weeks under an inverse 12:12 h light-dark cycle (lights off: 09:00 a.m.) with food and water *ad libitum* before starting the experiments. All experiments were performed during the activity phase of the animals (9:30 a.m. to 6:00 p.m.).

The traumatic stress was induced by applying an inescapable footshock: after a 198 s acclimatization interval in the shock chamber, that is a cubic-shaped transparent box with a metal grid for shock application, mice received a single scrambled electric footshock (2 s, 1.5 mA) which was administered via the metal grid. Animals remained in the shock chamber for another 60 s before they were returned to their home cages. Control mice were placed

2. *Materials and Methods*

into the shock chamber for the total of 260 s, but no electric footshock was administered (Kamprath and Wotjak, 2004).

Behavioral experiments were performed on days 28-30 after footshock (batch PTSD I, II, III) or on days 59-61 after footshock (batch PTSD V); batch PTSD IV was not subjected to the behavioral test battery. The details of the behavioral protocols are displayed in Figure 2.1. First, hyperarousal was tested by measuring the acoustic startle response of mice in startle chambers (SR-LAB, San Diego Instruments SDI, San Diego, CA, USA). Mice were exposed to 20 ms long white noise burst stimuli of different intensities (75 dB, 90 dB, 105 dB, and 115 dB) presented against the background of continuous white noise of 50 dB. After 5 min of acclimatization, 16 control trials in which only background noise was presented and 30 white noise burst stimuli of each intensity were presented in a pseudorandom order with an average interstimulus interval of 15 s. Startle chambers were cleaned thoroughly after each session.

Then, fear generalization was tested by measuring the freezing behavior during a 3-min exposure to the neutral context (a cylindrical-shaped transparent box without a metal grid) or the grid context (a hexagonal-shaped non-transparent box with a metal grid floor as a dominant reminder of the shock context). Finally, conditioned fear was assessed by measuring the freezing behavior during a 3-min exposure to the shock chamber. After each experiment, all boxes were cleaned thoroughly with neutrally smelling detergents.

Mice were sacrificed at least 10 days after terminating the last behavioral experiment. To obtain hippocampus, prefrontal cortex, and cerebellum, mice were sacrificed by cervical dislocation on days 2, 28, or 60 after footshock. First, total brains were isolated, and then, hippocampus, prefrontal cortex and cerebellum were dissected on ice. The tissue was shock frozen in methyl butane on dry ice and stored at -80 °C for subsequent analyses. In addition, trunk blood was collected for the analysis of immune system proteins. For immunohistochemical analysis mice were perfused transcardially with PBS followed by 15 min perfusion with 4 % paraformaldehyde (PFA). Finally, total brains were dissected and processed as described in section 2.2.2.

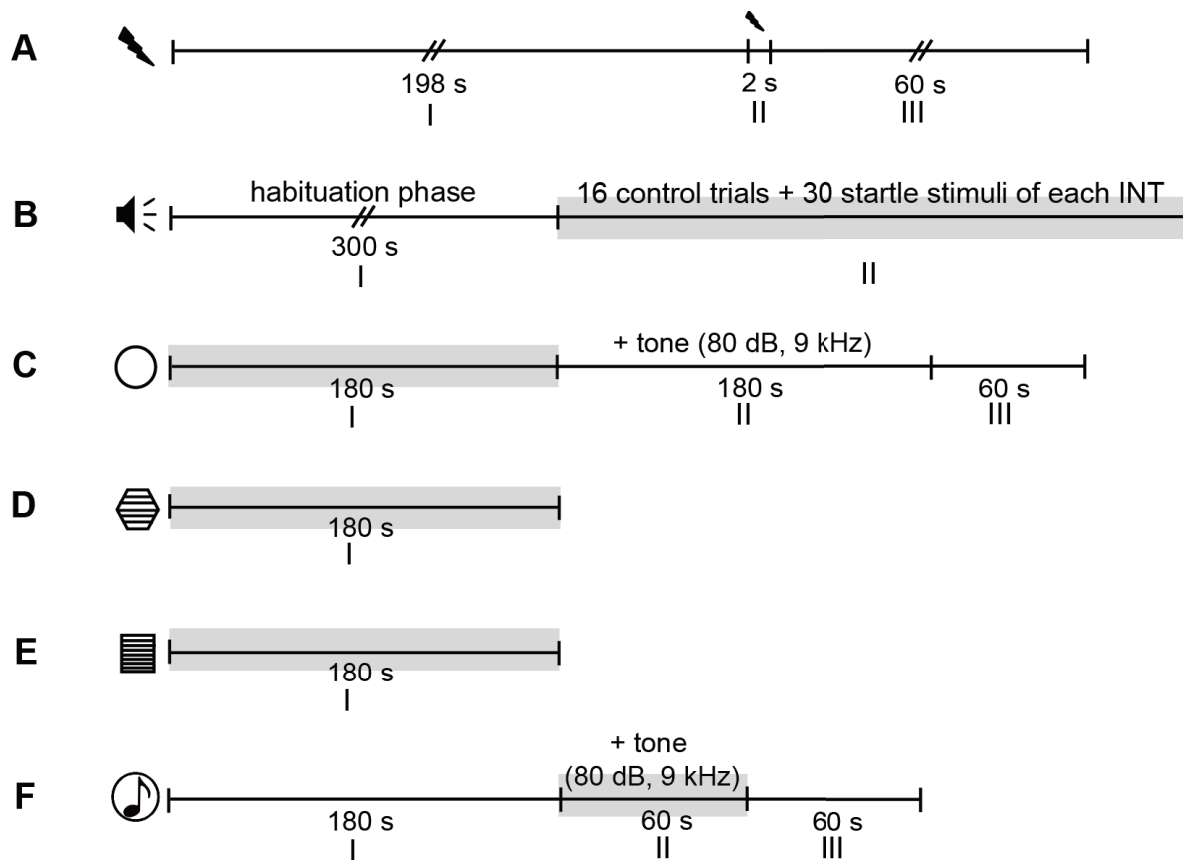


Figure 2.1.: **Protocols of behavioral tests (PTSD mouse model).** The different phases of the behavioral test protocols are indicated in Roman numerals. Mouse behavior was scored in the phase highlighted in gray. On day 0 a 1.5 mA single electric footshock was applied (A). After 198 s in the shock chamber, the footshock was administered for 2 s, followed by additional 60 s in the shock chamber. Control mice remained in the shock chamber for 260 s without administration of the electric shock. The acoustic startle response (B) was assessed in startle chambers. Briefly, after 300 s of habituation, 16 control trials and 30 startle stimuli of 20 ms duration of each intensity (INT), 75, 90, 105, and 115 dB, were presented in a pseudorandom order with an interstimulus interval of 15 s. For analysis of generalized fear (C), mice were exposed to a neutral context for 180s. Then a neutral tone (80 dB, 9 kHz) was presented for 180 s and mice remained for additional 60 s in the neutral context before returning to their home cage. Generalized fear was further tested in a context with the grid as a dominant reminder of the shock context (D) and conditioned fear (E) was assessed by scoring the freezing response for 180 s in the shock context. To test for treatment efficacy of the fluoxetine treatment, after 180 s in the neutral context, the freezing response was assessed during a 60 s presentation of a neutral tone in a neutral context (F). After additional 60 s in the neutral context, mice returned to their home cage. Figure adopted from (Herrmann et al., 2012)

2.1.2.1. Fluoxetine treatment

A group of 30 male C57BL/6NCrl mice aged 10 weeks (batch 'Fluoxetine in PTSD', Table 2.2) was exposed to a single inescapable footshock as described above. On day 1 after the footshock, the treatment group (n = 14) was subjected to chronic fluoxetine (Ratiopharm, Ulm, Germany) treatment which was administered in a dose of 20 mg/kg body weight per day for 4 weeks via drinking water, while the control group (n = 16) received drug-free drinking water. On day 28 after shock, fluoxetine efficacy was assessed by evaluating the generalized fear response for 60 s during the presentation of a neutral tone (80 dB, 9 kHz) in the neutral context. This was followed by 10 mg/kg fluoxetine per day for 3 days and a 4 week washout period, where mice received pure drinking water. On days 59 to 61, animals were tested for PTSD-like symptoms as described above. On day 74, mice were sacrificed by cervical dislocation and the hippocampus was dissected as described above and stored at -80 °C for subsequent immunoblot analyses (section 2.2.1).

2.1.3. HAB/LAB mouse model

Female HAB and LAB mice aged 19 weeks (section 1.5.2, batch 'HAB/LAB' Table 2.2) were obtained from the animal facility at the Max Planck Institute of Psychiatry. Mice were single housed under a 12:12 h light-dark cycle with food and water *ad libitum*. Without further behavioral testing, HAB (n = 4) and LAB (n = 7) mice were sacrificed by cervical dislocation. Subsequently, hippocampus and cerebellum were dissected, immediately shock frozen in methyl butane and stored at -80 °C for subsequent molecular analyses. In addition, trunk blood was collected in EDTA-supplemented tubes, centrifuged at 6000 x g for 10 min at 4 °C and supernatants were stored at -20 °C for further molecular analyses.

2.2. Immunoassays

2.2.1. Western blot

Homogenization buffer

50 mM Tris-HCl pH 7.6
150 mM NaCl
5 mM EDTA
4 x proteinase inhibitor

4 x Extraction buffer

50 mM Tris-HCl pH 7.6
150 mM NaCl
2 % NP40
2 % deoxycholate

For western blot analysis hippocampal and prefronto-cortical tissues were homogenized in 150 μ l homogenization buffer using a Turrax disperser (Turrax homogenizer VDI12, VWR, Darmstadt, Germany); for cerebellar tissue samples 300 μ l homogenization buffer was used. Then, proteins were extracted by mixing the homogenate with 50 μ l extraction buffer (100 μ l for cerebellar samples). Subsequently, the lysates were sonicated and centrifuged for 30 min at 16000 x g at 4 °C. Finally, supernatants were transferred to new reaction tubes and protein concentration was determined using a BCA assay.

2.2.1.1. Bicinchoninic acid (BCA) assay

To determine the protein concentration of tissue lysates a commercially available BCA protein assay kit (Thermo scientific, Waltham, MA, USA) was employed according to the manufacturer's instructions. Briefly, 10 μ l of bovine serum albumine (BSA) standards ranging from 2 mg/ml to 0.025 mg/ml as well as tissue lysate samples diluted 1:10 with H₂O were pipetted into wells of a 96 well plate. Then, 200 μ l of a 1:50 mix of solution B and solution A of the BCA assay kit were added to the 96 well plate which was then incubated for 30 min at 37 °C for color development. The purple color was then measured at 562 nm using the Dynatech MR5000 plate reader (Dynatech Laboratories, Denkendorf, Germany).

2.2.1.2. Sodium dodecyl sulfate polyacrylamid gel electrophoresis (SDS-PAGE)

5 x Lämmli sample buffer

5 % SDS
 40 % glycin
 160 mM Tris pH 6.8
 5 % β -mercaptoethanol
 0.04 % bromphenol blue
 in H₂O

4 x Lämmli upper Tris

0.5 M Tris pH 6.8
 in H₂O

10 x Lämmli running buffer

25 mM Tris
 192 mM glycin
 0.5% SDS
 in H₂O

4x Lämmli lower Tris

1.5 M Tris pH 8.8
 in H₂O

Electrophoretic separation of proteins was performed using the Mini-PROTEAN Electrophoresis System (Bio-Rad, München, Germany). SDS-polyacrylamid gels (1 mm x 8.6 cm x 6.8 cm) were casted with the following composition:

Table 2.3.: Composition of SDS-polyacrylamid gels

	10 % separation gel (4x)	4 % stacking gel (4x)
H ₂ O	10.5 ml	6.5 ml
30 % Acrylamid-Bis solution	8.5 ml	1.3 ml
4 x Lämmli lower Tris	6.25 ml	2.3 ml (Lämmli upper Tris)
20 % SDS	0.25 ml	0.1 ml
10 % APS	65 μ l	35 μ l
TEMED	65 μ l	35 μ l

To cast a SDS-polyacrylamid gel H₂O, acrylamid-bisacrylamid solution, Tris buffer, and SDS were mixed. Then, for initiation of the polymerization reaction ammonium persulfate (APS) and N, N, N', N'-tetramethylethylenediamine (TEMED) were added to the mix just before casting the gels. The separation gel was casted first and overlaid with isopropanol to inhibit evaporation. In a second step, after polymerization of the separation gel and removal of isopropanol the stacking gel was casted and a 15 well comb was inserted. For final polymerization gels were wrapped in a moist tissue and stored in a plastic bag at 4 °C. To run the SDS-polyacrylamid gels, protein lysates were mixed with Lämmli sample buffer and boiled for 5 min at 95 °C. Equal amounts of protein (10 μ g, for proteins with low expression levels 20 μ g) were loaded on to the gels using a 50 μ l Hamilton syringe (Hamilton Bonaduz AG, Bonaduz, Switzerland). 5 μ l of peqGOLD prestained protein marker VI (Peqlab

Biotechnologie GMBH, Erlangen, Germany) was loaded on each gel for monitoring protein separation during electrophoresis and subsequent size determination of the protein bands. The electrophoresis was performed in Lämmli running buffer at 120 V (Power-Pac 400, Bio-Rad, München, Germany).

2.2.1.3. Western blot transfer

10 x TBS

100 mM Tris
1.5 mM NaCl
pH 7.6
in H₂O

1 x TBS/T

1 l 10x TBS + 10 ml Tween-20 (0.1 %)
add H₂O to a final volume of 10 l

10 x Wet-blot buffer

250 mM Tris
1900 mM glycine
in H₂O

1 x Wet-blot buffer

100 ml 10 x Wet-blot buffer
700 ml H₂O
200 ml methanol

After separating the protein lysates by SDS-PAGE, the proteins were electrotransferred to nitrocellulose membranes (Carl Roth GmbH + Co. KG, Karlsruhe) using the Mini Trans-Blot System (Bio-Rad, München, Germany). For this purpose, a 'sandwich' was assembled in a blotting cassette composed of a sponge, two layers of filter paper, the nitrocellulose membrane, the gel, again two layers of filter paper, and a sponge. Everything was equilibrated in 1 x Wet-blot buffer. The transfer was then conducted in 1 x Wet-blot buffer for 2 h at 400 mA. A subsequent Ponceau staining of the nitrocellulose membrane confirmed the effectiveness of the transfer. For this, the nitrocellulose membrane was incubated in a 0.2 % solution of Ponceau S in 1 % acetic acid. The membrane was then rinsed with water until protein bands appeared.

For immunodetection the membranes were then incubated for 1 h in 5 % non-fat dried milk in Tris-buffered saline supplemented with Tween-20 (TBS/T) on an orbital shaker (Shaker Gyro-rocker SSL3, Stuart, Staffordshire, UK) to block unspecific antibody binding. Then, the membranes were incubated overnight at 4 °C with the primary antibody diluted in 2.5 % non-fat dried milk in TBS/T supplemented with 0.01 % NaN₃ on an overhead-shaker (Roto shake genie, Scientific Industries, Bohemia, NY, USA). Primary antibodies used in this thesis and the respective dilutions are indicated in Table 2.4. Subsequently, the membranes were

2. Materials and Methods

Table 2.4.: **Primary antibodies.** Abbreviations: WB = Western blot, IHC = immunohistochemistry

Antibody	Manufacturer	Species	Application	Dilution
CD31	Santa Cruz Biotechnology (Santa Cruz, CA, USA)	rabbit	IHC, WB	1:500
CD68	Santa Cruz Biotechnology	rabbit	WB	1:500
EAAC1 (EAAT3)	Santa Cruz Biotechnology	rabbit	WB	1:500
Fc γ RI (CD64)	Santa Cruz Biotechnology	rabbit	WB	1:500
GAPDH	Santa Cruz Biotechnology	mouse	WB	1:2000
GFAP	DAKO (Hamburg, Germany)	rabbit	IHC, WB	1:1000 (IHC) 1:2000 (WB)
GLT1 (EAAT2)	Santa Cruz Biotechnology	goat	WB	1:1000
homer 1b/c	Santa Cruz Biotechnology	rabbit	WB	1:1000
Iba1	WAKO Pure Chemical Industries, Ltd. (Osaka, Japan)	rabbit	IHC, WB	1:500
Ig κ light chain	Jackson ImmunoResearch Laboratories (Newmarket, Suffolk, UK)	goat	IHC, WB	1:500
Ig λ light chain	Santa Cruz Biotechnology	rabbit	WB	1:500
IgG Fc	Jackson ImmunoResearch Laboratories	goat	IHC, WB	1:2000
neurofilament	Abcam (Cambridge, UK)	mouse	WB	1:1000
MAP-2	Sigma-Aldrich (St. Louis, MO, USA)	mouse	WB	1:1000
synapsin I/II	Synaptic Systems (Göttingen, Germany)	rabbit	IHC, WB	1:1000
synaptophysin	Santa Cruz Biotechnology	rabbit	WB	1:2000

washed in TBS/T 5 times for at least 5 minutes on an orbital shaker. Next, the membranes were incubated with an appropriate horseradish-peroxidase (HRP) conjugated secondary antibody diluted in 2.5 % non-fat dried milk in TBS/T (see Table 2.5) for 1 h at room temperature, followed by 5 washing steps for 5 min with TBS/T. Finally, the membranes were incubated with a chemoluminescence substrate solution (Immobilon HRP Substrat Luminol Reagenz, Millipore) for 5 minutes, and the chemoluminescence of the immunoreactive complexes was detected on X-ray films (FujiFilm X-Ray 18x24 100NF, Bender). 2-3 technical replicates of each western blot experiment were performed.

Table 2.5.: **Secondary antibodies.** Abbreviations: WB = Western blot, IHC = immunohistochemistry

Antibody	Manufacturer	Species	Application	Dilution
HRP conjugated anti-goat	Santa Cruz Biotechnology	donkey	WB	1:10000
anti-goat AlexaFluor594	Invitrogen (Grand Island, NY, USA)	donkey	IHC	1:300
HRP conjugated anti-mouse	Sigma-Aldrich	goat	IHC, WB	1:1000 (IHC) 1:50000 (WB)
anti-mouse AlexaFluor488	Invitrogen	donkey	IHC	1:300
HRP conjugated anti-rabbit	Sigma-Aldrich	goat	WB	1:30000
anti-rabbit AlexaFluor488	Invitrogen	donkey	IHC	1:300
anti-rabbit AlexaFluor594	Invitrogen	goat	IHC	1:300

2.2.1.4. Densitometry

For quantification of immunoreactive bands, the X-ray films were digitalized, and the pixel density was measured using the ImageJ software (Rasband, W.S., ImageJ, U.S. National Institutes of Health Bethesda, Maryland, USA, <http://rsb.info.nih.gov/ij/>, 1997-2009).

2.2.2. Immunohistochemistry (IHC)

Phosphate-buffered saline (PBS)

140 mM NaCl
 10 mM Na₂HPO₄
 1.75 mM KH₂PO₄
 2.5 mM KCl
 adjust to pH 7.4

Isoflurane-anesthetized mice were perfused transcardially on day 60 after footshock with phosphate-buffered saline (PBS) followed by 4 % paraformaldehyde (PFA) in PBS for 15 min using a peristaltic pump (n = 6 per group). For post-fixation total brains were dissected and kept in 4 % PFA overnight and one week in 30 % sucrose in PBS at 4 °C. Then, the brains were shock frozen in methyl butane on dry ice and stored at -80 °C. 40 μm coronal sections were cut, and sections were kept in storage medium (25 % glycerol and 25 % ethylenglycol in PBS) at -20°C.

2. *Materials and Methods*

For immunohistochemistry, sections were washed with PBS and blocked with a 10 % bovine serum albumin (BSA) solution containing 1 % Triton X-100 in PBS. Then, sections were incubated overnight at room temperature with primary antibodies (see Table 2.4) which were diluted in a BSA buffer solution containing 1 % BSA and 0.3 % Triton X-100 in PBS. The next day, sections were washed with PBS and incubated for 2 h at room temperature with a fluorophore-conjugated secondary antibody (see Table 2.5), diluted 1:300 in BSA buffer solution containing 1 % BSA and 0.3 % Triton X-100 in PBS. Subsequently, sections were washed with PBS, including 0.2 mg/ml of the nuclear stain DAPI (4',6-diamidino-2-phenylindole) in one washing step. Finally, sections were mounted on slides and covered with embedding medium (ImmuMount, Thermo Scientific, Waltham, MA, USA). Images were obtained using an Olympus IX81 confocal microscope (Olympus, Hamburg, Germany).

2.3. Molecular biological methods

2.3.1. Cultivation of *E. coli* bacteria

LB medium

20 g LB Broth Base
in 1 l dH₂O
autoclave

LB-Agar plates

20 g LB-Broth
15 g Agar-Agar (1.5 %)
in 1 l dH₂O, autoclave
cool down to approximately 50 °C
add antibiotics (100 µg/ml ampicillin; 50 µg/ml
kanamycin)
cast plates

Escherichia coli (*E. coli*) DH5 α bacteria were cultivated in LB medium supplemented with the appropriate antibiotic (100 µg/ml ampicillin or 50 µg/ml kanamycin) at 37 °C. To sub-culture a single colony, bacteria were streaked onto LB-Agar plates containing the appropriate antibiotic. Then, LB-medium was inoculated with a single colony from the LB-Agar plate using a sterile pipette tip and cultured at 37 °C shaking at 200 rpm. For long-term storage, glycerolstocks were prepared by adding 20 % glycerol to the bacterial culture which was then stored at -80 °C.

2.3.1.1. Preparation of competent cells

TFBI buffer

30 mM kaliumacetate
50 mM MgCl₂
100 mM KCl
10 mM CaCl₂
adjust to pH 5.8 with 0.2 M acetic acid
filter sterile

TFBII buffer

10 mM Na-MOPS pH 7.0
75 mM CaCl₂
10 mM KCl
20 % glycerol
add H₂O to a volume of 100 ml
filter sterile

E. coli have to be in a 'competent state' to incorporate plasmid DNA efficiently during transformation. To prepare competent cells, 5 ml LB medium was inoculated with 10 µl *E. coli* DH5 α bacteria and cultured overnight at 37 °C shaking at 200 rpm. The next day, 400 ml LB medium was added and bacteria were cultured at 37 °C shaking at 200 rpm until the OD₅₅₀ was 0.480. Then, bacteria were centrifuged at 1000 x g for 10 min at 4 °C, and

2. Materials and Methods

the pellet was resuspended in 80 ml TFBI buffer. After 5 min incubation on ice, bacteria were centrifuged at 1000 x g for 5 min at 4 °C. Finally, the pellet containing the bacteria was resuspended in 16 ml TFBII buffer and incubated on ice for 15 min. Aliquots of competent *E. coli* DH5 α bacteria were stored at -80 °C.

2.3.1.2. Transformation of *E. coli* bacteria

Transformation was performed by exposing *E. coli* DH5 α bacteria in presence of plasmid DNA to a 42 °C heatshock. For this purpose, 100 μ l competent DH5 α cells were incubated with the respective plasmid DNA for 30 min on ice. The heatshock was then performed for 45 s at 42 °C. Subsequently, the cells were cooled down on ice for 2 min. Then, 900 μ l LB-medium was added and the bacteria were incubated for 60 min at 37 °C to develop their specific antibiotic resistance encoded on the transformed plasmid DNA. The bacteria were plated on an agar plate containing the respective antibiotic and incubated overnight at 37 °C. The next day, single colonies were picked using a sterile pipette tip and incubated in 3 ml of antibiotic-containing LB-medium for 8 h at 37 °C. Finally, the plasmid DNA was either isolated using a Mini-preparation kit (section 2.3.2) or for large scale preparation bacteria were cultured in 100 ml LB-medium which was subsequently subjected to Midi-preparation for plasmid DNA isolation (section 2.3.2).

2.3.2. Isolation of plasmid DNA

Depending on the required amount of plasmid DNA either Mini or Midi cultures (3 ml or 100 ml LB-Medium) were prepared as described above. Mini cultures were mainly used during cloning, while Midi cultures were used to produce larger amounts of plasmid DNA for subsequent transfection into eukaryotic cells. From the Mini or Midi bacteria cultures plasmid DNA was isolated using a Mini Prep Kit or Midi Prep Kit (Promega, Madison, WI, USA) according to the manufacturer's specifications. The isolated plasmid DNA was then analyzed by restriction digest or sequencing (GATC Biotech AG, Konstanz, Germany) and was stored at -20 °C.

Table 2.6.: Overview of generated plasmid constructs. Plasmids were generated as described in section 2.3.3.

Name	Description	Primer	Vector
pGL3SV40	constitutive active gaussia luciferase construct	SV40_for + SV40_rev	pGL3 basic
pGL3T5066	TMEM132D promoter 5066 bp upstream of ATG	TMEM-5066 (BgIII) + TMEM-1 (HindIII)	pGL3 basic
pGL3T3090	TMEM132D promoter 3090 bp upstream of ATG	TMEM-3090 (BgIII) + TMEM-1 (HindIII)	pGL3 basic
pGL3T2493	TMEM132D promoter 2493 bp upstream of ATG	TMEM-2493 (BgIII) + TMEM-1 (HindIII)	pGL3 basic
pGL3T1498	TMEM132D promoter 1498 bp upstream of ATG	TMEM-1498 (BgIII) + TMEM-1 (HindIII)	pGL3 basic
pGL3T829	TMEM132D promoter 829 bp upstream of ATG	TMEM-829 (BgIII) + TMEM-1 (HindIII)	pGL3 basic
pGL3T604	TMEM132D promoter 604 bp upstream of ATG	TMEM-604 (BgIII) + TMEM-1 (HindIII)	pGL3 basic
pGL3T300	TMEM132D promoter 300 bp upstream of ATG	TMEM-300 (BgIII) + TMEM-1 (HindIII)	pGL3 basic
pGL3T210	TMEM132D promoter 210 bp upstream of ATG	TMEM-210 (BgIII) + TMEM-1 (HindIII)	pGL3 basic
pGL3T150	TMEM132D promoter 150 bp upstream of ATG	TMEM-150 (BgIII) + TMEM-1 (HindIII)	pGL3 basic
pGL3T604GCMFdel	pGL3T604 with GCMF binding site deletion	GCMFdel_for + GCMFdel_rev	pGL3 basic
pGL3T604MTFdel	pGL3T604 with MTF1 binding site deletion	MTFdel_for + MTFdel_rev	pGL3 basic
pGL3T604HESFdel	pGL3T604 with HESF binding site deletion	HESFdel_for + HESFdel_rev	pGL3 basic
pGL3T604MYTdel	pGL3T604 with MYT1 binding site deletion	MYTdel_for + MYTdel_rev	pGL3 basic
pGL3T604NRF1.2del	pGL3T604 with proximal NRF1 binding site deletion	NRF1.2del_for + NRF1.2del_rev	pGL3 basic
pGL3T604ZFXdel	pGL3T604 with ZFX binding site deletion	ZFXdel_for + ZFXdel_rev	pGL3 basic
pGL3T604NRF1mut	pGL3T604 with mutated distal NRF binding site	NRF1mut_for + NRF1mut_rev	pGL3 basic
pGL3T604HESFmut	pGL3T604 with mutated HESF binding site	HESFmut_for + HESFmut_rev	pGL3 basic
pGL3T604ZF5Fmut	pGL3T604 with mutated ZF5F binding site	ZF5Fmut_for + ZF5Fmut_rev	pGL3 basic
pGL3T829EGRFmut	pGL3T829 with mutated EGRF binding site	EGRFmut_for + EGRFmut_rev	pGL3 basic
pGL3T829NFKBmut	pGL3T829 with mutated NFKB1 binding site	NFKBmut_for + NFKBmut_rev	pGL3 basic
pGL3T829SP1mut	pGL3T829 with mutated SP1 binding site	SP1mut_for + SP1mut_rev	pGL3 basic
pGL3T300HAMLmut	pGL3T300 with mutated HAML binding site	HAMLmut_for + HAMLmut_rev	pGL3 basic
pcDNA3.1HES1	HES1 expression plasmid	HES1_cl_for + HES1_cl_rev	pcDNA3.1(-)
pcDNA3.1ZNF219	ZNF219 expression plasmid	ZNF219_cl_for + ZNF219_cl_rev	pcDNA3.1(-)
pcDNA3.1ZFP161	ZFP161 expression plasmid	ZFP161_cl_for + ZFP161_cl_rev	pcDNA3.1(-)
pcDNA3.1ZFX	ZFX expression plasmid	ZFX_cl_for + ZFX_cl_rev	pcDNA3.1(-)
pcDNA3.1MTF1	MTF1 expression plasmid	MTF1_cl_for + MTF1_cl_rev	pcDNA3.1(-)
pcDNA3.1NRF1	NRF1 expression plasmid	NRF1_cl_for + NRF1_cl_rev	pcDNA3.1(-)

2.3.3. Cloning of reporter plasmids and transcription factor expression plasmids

For the generation of TMEM132D promoter constructs, the region 5066 bp upstream of the start codon was amplified from human genomic DNA by polymerase chain reaction (PCR) and cloned into the commercially available pGL3 basic vector (Promega, Madison, WI, USA). The other 5' deletion mutants were generated using the primers indicated in Table 2.7 and the pGL3T5066 plasmid as a template for PCR. Amplified fragments were cloned into the pGL3 basic vector via restriction digest of vector and insert followed by sticky end ligation. Sequence identities were verified by sequencing (GATC Biotech, Konstanz, Germany). All generated constructs are listed in Table 2.6.

Expression plasmids of the transcription factors HAML (PlasmID CloneID: HsCD00342124), SP1 (PlasmID CloneID: HsCD00338893), WT1 (PlasmID CloneID: HsCD00333689), MZF1 (PlasmID CloneID: HsCD00330552), MYT1L (PlasmID CloneID: HsCD00342588), GCM1 (PlasmID CloneID: HsCD00346282), and NFkB1 (PlasmID CloneID: HsCD00340105) were purchased from PlasmID (Boston, MA, USA). The transcription factor expression plasmids of HES1, NRF1, ZFP161, ZNF219, MTF1, and ZFX were generated (Table 2.6) by amplification of the coding sequence from the reverse transcribed mRNA isolated from human MO3.13 cells using the primers indicated in Table 2.8. Subsequently, the amplified fragments were inserted into the pcDNA3.1(-) vector (Invitrogen) via restriction digest of vector and insert followed by sticky end ligation. Sequence identities were confirmed by sequencing.

2.3.3.1. RNA isolation

Before starting the work with RNA, instruments were cleaned with ethanol. Filtered pipette tips were used to minimize contamination. Total RNA isolation from eukaryotic cells was performed using the NucleoSpin RNA II kit (Macherey-Nagel, Düren, Germany) according to the manufacturer's instructions. The concentration of the isolated RNA was subsequently measured at a spectrophotometer (Nanophotometer Implen, München, Germany). The isolated RNA was stored at -80 °C.

2.3.3.2. Concentration measurements of nucleic acids

The concentration of nucleic acids was measured spectrophotometrically using an Implen Nanophotometer (Implen, München, Germany). 3 μl of nucleic acid solution was subjected to the spectrophotometrical measurement at 260 nm. Additionally, the extinction at 280 nm was measured and the $\text{OD}_{260}/\text{OD}_{280}$ ratio was calculated. This ratio indicates possible contamination with proteins and should ideally be 1.8 for pure DNA and 2.0 for pure RNA. Based on the fact that the OD_{260} is 1 at a concentration of 50 $\mu\text{g}/\text{ml}$ DNA or 40 $\mu\text{g}/\text{ml}$ RNA the concentrations can be calculated by multiplying the OD_{260} with the dilution factor and either 50 $\mu\text{g}/\text{ml}$ for DNA or 40 $\mu\text{g}/\text{ml}$ for RNA.

2.3.3.3. Reverse transcription (RT)

RNA was reverse transcribed to cDNA employing the Omniscript RT kit (Qiagen, Hilden, Germany) according to the manufacturer's instructions. In general, 2 μg of total RNA were reverse transcribed using oligo-dT primer (Promega, Madison, WI, USA) which anneal to the poly-A tail of mRNAs and thus exclude the reverse transcription of other non-coding RNAs. The reverse transcription was performed for 1 h at 37 °C in a thermocycler (Thermocycler Tprofessional Standard, Biometra, Göttingen, Germany). The cDNA was then stored at -20 °C.

2.3.3.4. Polymerase chain reaction (PCR)

Regions of interest for cloning were amplified in a polymerase chain reaction (PCR) using the Herculase II DNA polymerase (Agilent Technologies, Santa Clara, CA, USA). Herculase II DNA polymerase is a Pfu-based polymerase optimized for the amplification of long GC-rich targets. The primers were designed to specifically bind to the flanking sites of the regions of interest, and for further processing restriction sites were attached to the primer sequence (primers and restriction sites indicated in Table 2.7 and 2.8). For amplification, 200 ng of template DNA was added to the reaction mix containing 1 x Herculase reaction buffer, 10 pmol of each forward and reverse primer, 500 μM of each desoxynucleotide-triphosphate (dNTP), 8 % dimethyl sulfoxide (DMSO), 1 μl Herculase, and H_2O in a total volume of 50 μl .

2. Materials and Methods

The thermal cycling comprised a 5 min interval at 98 °C for initial denaturation, followed by 40 cycles consisting of a 30 s denaturation step at 98 °C, a 1 min annealing step at 60 °C and an elongation step at 68 °C for 1 min per kilo-bases of template DNA. This was followed by a final 3 min elongation interval at 68 °C. Finally, the amplicon was analyzed by agarose gel electrophoresis.

Table 2.7.: **Cloning primers for reporter plasmid generation.** Restriction sites are indicated in brackets behind the primer name.

Name	Sequence 5' → 3'
SV40_for (BglII)	cga ata gat ctt gtg tgt cag tta ggg tgt gg
SV40_rev (HindIII)	cta gta agc ttg gaa tag ctc aga ggc cga g
TMEM-5066 (BglII)	cga ata gat ctg ctt ctg ttg gca gtg atg a
TMEM-3060 (BglII)	cga ata gat ctc gct caa agt tgc cat ttc t
TMEM-2493 (BglII)	cga ata gat ctc ttc tgc aat ggc aaa aag a
TMEM-1498 (BglII)	cga ata gat ctt aca gga cgg tgc tta ggg a
TMEM-829 (BglII)	cga ata gat ctc ttg cgg agc gga gc
TMEM-604 (BglII)	cga ata gat ctc gca ccc gcc aaa ct
TMEM-300 (BglII)	cga ata gat ctg gaa ata ccc cct gtg gat ta
TMEM-210 (BglII)	cga ata gat ctg gag agc aac tca gga gcc
TMEM-150 (BglII)	cga ata gat cta aga ggg agc agg gcg
TMEM-1 (HindIII)	cta gta agc ttc ctg gag acc cgg agc

Table 2.8.: **Cloning primers for generation of transcription factor expression plasmids.** Restriction sites are indicated in brackets behind the primer name. for = forward primer, rev = reverse primer

Name	Sequence 5' → 3'
HES1_cl_for (EcoRI)	cgc gaa ttc tat gcc agc tga tat aat gga gaa
HES1_cl_rev (BamHI)	gat gga tcc tca gtt ccg cca cgg c
ZNF219_cl_for (EcoRI)	cgc gaa ttc tat gga ggg ctc acg tcc c
ZNF219_cl_rev (BamHI)	gat gga tcc cta ccg ttc ttg ccc ccc
ZFP161_cl_for (EcoRI)	cgc gaa ttc tat gga gtt ttt cat cag tat gtc tg
ZFP161_cl_rev (BamHI)	gat gga tcc cta gct aca ggc tat cgt ctc ca
ZFX_cl_for (EcoRI)	cgc gaa ttc tat gga tga aga tgg gct tga
ZFX_cl_rev (NheI)	cta ggc taa gct tag ggc agg cca act tct
MTF1_cl_for (EcoRI)	cgc gaa ttc tat ggg gga aca cag tcc a
MTF1_cl_rev (NheI)	cta ggc tag ctc act tgg aga agc tgc tgg
NRF1_cl_for (XhoI)	tcg act cga gta tgg agg aac acg gag tga c
NRF1_cl_rev (BamHI)	gat gga tcc tca ctg ttc caa tgt cac cac

2.3.3.5. Gel electrophoresis

1 x TBE buffer

90 mM Tris 8.3
90 mM boric acid
2.5 mM EDTA pH 8
adjust to pH 8.3

5 x sample loading buffer

60 % glycerol
50 mM Tris-HCl pH 7.6
50 mM EDTA
0.025 % bromphenol blue
0.0025 % xylene cyanol

For separation of DNA by gel electrophoresis, 0.7 - 2 % agarose (Agarose Universal peqgold, peqlab, Erlangen, Germany) was dissolved in TBE buffer by heating it in a microwave oven. After cooling the dissolved agarose down to approximately 65 °C, 0.5 µg/ml ethidiumbromide was added, and the gel was casted. For subsequent gel electrophoresis the Bio-Rad DNA Subcell System was employed (Bio-Rad, München, Germany). The DNA samples were first mixed with 5 x sample loading buffer and then loaded on to the gel. Electrophoretic separation was accomplished by running the gel in TBE buffer at 100 - 150 V for approximately 30 min. Finally, the gel was analyzed and documented using the Protean GelDoc2000 System (Bio-Rad, München, Germany).

2.3.3.6. DNA purification from agarose gels

To extract DNA from an agarose gel, the respective band was cut out from the gel using a scalpel. The DNA was then purified from the gel fragment using the Qiaquick gel extraction kit according to the manufacturer's instructions (Qiagen, Hilden, Germany). Extracted DNA was kept for short term storage at 4 °C and for long term storage at -20 °C.

2.3.3.7. Restriction digest of DNA

Restriction digest of plasmid DNA or PCR fragments was performed using 2-5 µg DNA, 1.5 µl restriction enzyme (NEB, Ipswich, MA, USA), and 5 µl of 10 x restriction buffer in a 50 µl reaction volume. In case of a double digest, the compatibility of both restriction enzymes was first checked using the double digest finder tool at the NEB website (<http://www.neb.com/nebecomm/DoubleDigestCalculator.asp>). The reaction was incubated

for 2 h at 37 °C. Finally, the restriction digest was examined and purified by gel electrophoresis and subsequent DNA gel extraction.

2.3.3.8. Ligation

Ligation was performed using T4 Ligase (NEB, Ipswich, MA, USA) and approximately 1 μg of insert, 0.4 μg of vector, and 2 μl 10 x reaction buffer in a total volume of 20 μl . The reaction was incubated for 10 min at room temperature. For transformation into DH5 α competent cells, 10 μl of the ligation reaction was used. The rest was stored at 4 °C.

2.3.3.9. Site-directed mutagenesis

Transcription factor binding sites (TFBS) in the TMEM132D promoter sequence determined by *in silico* analysis (see section 2.5.3) were mutated by site-directed mutagenesis. For this, primers introducing the mutation were designed using the QuikChange Primer Design Program (Agilent Technologies, Böblingen, Germany) assuring that no alternative putative transcription factor binding sites arise from mutagenesis. PCR with pGL3T604, pGL3T829, or pGL3T300 template amplified in dam⁺ E. coli bacteria, i.e. expressing the DNA adenine methyltransferase gene, was performed using the long range polymerase Herculase II DNA polymerase (Agilent technologies). Here, 100 ng of template was added to the reaction mix that comprised 10 μl reaction buffer, 125 ng of each forward and reverse primer, 500 μM of each dNTP, 1 μl Herculase II DNA polymerase, and H₂O in a total volume of 50 μl . The thermal cycling consisted of a 5 min initial denaturation step at 98 °C followed by 18 cycles of a 30 s denaturation step, a 1 min annealing step at 60 °C, and an elongation step at 68 °C for 1 min/kb. Subsequently, the template was digested by adding 20 U/ml restriction enzyme *dpnI*, which specifically recognizes dam-methylated DNA sequences, to the reaction mix and incubating it at 37 °C for 1.5 h resulting in a degradation of the template DNA but not the PCR product. Finally, the mutated plasmid DNA was transformed into DH5 α bacteria, amplified, and checked for successful mutagenesis by sequencing.

Table 2.9.: **In-vitro-mutagenesis primers.** Primer listed induce either a deletion (del) or a point mutation (mut); for = forward primer, rev = reverse primer

Name	Sequence 5' → 3'
GCMFdel_for	cgg cct ggg atg ctg cgg gcc agg
GCMFdel_rev	cct ggc ccg cag cat ccc agg ccg
MyTdel_for	cgc acc cgc caa tgg gtg ccg
MyTdel_rev	cgg cac cca ttg gcg ggt gcg
HESFdel_for	gca aaa ctt tgg gtg ccg gac ccg agc ccc
HESFdel_rev	ggg gct cgg gtc cgg cac cca aag ttt gg
MTFdel_for	ctc cga gcc gcc tct gcg tcc cg
MTFdel_rev	cgg gac gca gag gcg gct cgg ag
NRF1.2del_for	cgc cgc ctg cgc cac cgc tag cc
NRF1.2del_rev	ggc tag cgg tgg cgc agg cgg cg
ZFXYdel_for	gtc gtc gcc tcc ctg gcc atg gac tg
ZFXYdel_rev	cag tcc atg gcc agg gag gcg acg ac
NRF1mut_for	cgc caa act ttg ggt gcc gga ttt tgc gcg cgc ccg
NRF1mut_rev	cgg gcg cgc gca aaa tcc ggc acc caa agt ttg gcg
HESFmut_for	ccg gag cgc gct tgc gcc cga gcc
HESFmut_rev	ggc tcg ggc gca agc gcgc tcc gg
ZF5Fmut_for	ccg gag cgc gct ctc tcc cga gcc ccg
ZF5Fmut_rev	cgg ggc tcg gga gag agc gcg ctc cgg
EGRFmut_for	gtc ctt gcg gag cgg agc caa aaa acc tgc tgg cag gag gca gc
EGRFmut_rev	gct gcc tcc tgc cag cag gtt ttt tgg ctc cgc tcc gca agg ac
NFKBmut_for	ccc ccg ggc gca gga aaa agc ccc gcg tct cc
NFKBmut_rev	gga gac gcg ggg ctt ttt cct gcg ccc ggg gg
SP1mut_for	ccc cag ccg ggc ccg gaa aaa agc ggg ccg agg cgg cg
SP1mut_rev	cgc cgc ctc ggc ccg ctt ttt tcc ggg ccc ggc tgg gg
HAMLmut_for	gtc gaa gga ggg agg taa agt ttg cct gcg cgc gt
HAMLmut_rev	acg cgc gca ggc aaa ctt tac ctc cct cct tcg ac

2.3.4. RT-PCR for semi-quantitative detection of gene expression

RNA was isolated from eukaryotic cells as described in section 2.3.3.1 and reverse transcribed to cDNA as described in section 2.3.3.3. PCR was performed using the Taq DNA polymerase (Invitrogen, Grand Island, NY, USA). Up to 5 μ l of cDNA was added to the reaction mix that comprised 1 x reaction buffer, 0.2 mM of each dNTP, 10 pmol of each forward and reverse primer, 1.5 mM MgCl₂, 2 units Taq DNA polymerase, and H₂O. The thermal cycling included an initial denaturation interval of 5 min at 95 °C and 30-40 cycles of 30 s denaturation at 95 °C, 30 s primer annealing at 58-62 °C, and 30 s elongation at 72 °C. A final elongation of 3 min at 72 °C concluded the thermal cycling. For each primer pair the annealing temperature, the

2. Materials and Methods

cycle number and the amount of cDNA template input were optimized to assure that the PCR remained in the linear amplification phase. Finally, the sample was mixed with 5 x sample loading dye and analyzed by agarose gel electrophoresis. Bands on the documented gel image were quantified using the ImageJ software (Rasband, W.S., ImageJ, U.S. National Institutes of Health Bethesda, Maryland, USA, <http://rsb.info.nih.gov/ij/>, 1997-2009).

Table 2.10.: **RT-PCR primers.** Primers for detection of gene expression levels amplifying short, 100-500 bp long, fragments; for = forward primer, rev = reverse primer

Name	Sequence 5' → 3'
GAPDH_for	gag tca acg gat ttg gtc gt
GAPDH_rev	ttg att ttg gag gga tct cg
β -actin_for	cta caa tga gct gcg tgt ggc
β -actin_rev	cag gtc cag acg cag gat ggc
TMEM132D_for	cat aca gcc tca gcc aat ga
TMEM132D_rev	cat gga tgc tcc acc tga gt
HES1_for	gca gat gac ggc tgc gct ga
HES1_rev	ggc tgc ccg ggg tag gtc at
ZNF219_for	gtt gct gga gtt gga aga gc
ZNF219_rev	cta tgc agg atg tgc agg tg
ZFP161_for	tgg tga gtg gtt gac caa ga
ZFP161_rev	ggg caa tca aga ttg agg aa
ZFX_for	cat ccc ctg tgt gct tag gt
ZFX_rev	att tgg gct gga gtt cac ac
MTF1_for	atc tga agg ctg cag caa at
MTF1_rev	cca tta ctg ggg cag aag aa
NRF1_for	ctt aca agg tgg ggg aca ga
NRF1_rev	ggt gac tgc gct gtc tga ta
MYT1_for	atg aca agg acg agg aca cc
MYT1_rev	tca cgc ttc tca gct ctt ga
SP1_for	gcc acc atg agc gac caa gat ca
SP1_rev	ctc ggg ccc tgg gag ttg ttg
HAML_for	ccg caa gtc gcc acc tac ca
HAML_rev	ctc cag ggt gct gtg tct tcc tcc
MZF1_for	gtc cag agg tac gct cca ag
MZF1_rev	tct gga gtt gga ggc tca gt
NFKB1_for	ctg gaa gca cga atg aca ga
NFKB1_rev	tga ggt cca tct cct tgg tc

2.4. Cell culture

The MO3.13 cell line was a kind gift from Neil Cashman, University of Toronto, Canada; the HOG cell line was a kind gift from Glyn Dawson, University of Chicago, IL, USA. The cell lines used in this thesis were cultivated in Roswell Park Memorial Institute (RPMI) medium (Invitrogen) supplemented with 10 % fetal calf serum (FCS) (Invitrogen, Grand Island, NY, USA) and 1 % antibiotic-antimycotic (Invitrogen) in case of MO3.13 cells or in Dulbecco's modified Eagle's medium (DMEM) medium (Invitrogen) supplemented with 10 % FCS, 1 % antibiotic-antimycotic, and 1 % sodium-pyruvate (Invitrogen) in case of HOG, HEK293, A172, or SK-N-MC cells. All cells were cultured at 37 °C and 5 % CO₂ in an incubator (CO₂ Incubator Heracell 240i, Thermo Scientific, Waltham, MA, USA or CO₂ Incubator, Heraeus, Mannheim, Germany). All work with cell lines was performed in a LaminAir HB2448 flow hood (Heraeus, Mannheim, Germany) to reduce the risk of contamination. All solutions were prewarmed to 37 °C in a waterbath (Waterbath Typ 1003, GFL, Burgwedel, Germany). Cell growth was examined visually using an Olympus CK30 microscope (Olympus, Hamburg, Germany)

2.4.1. Cell line subcultivation

For passaging of cells the growth medium was removed, cells were washed once with prewarmed PBS (Invitrogen), and incubated shortly with trypsin-EDTA (Invitrogen). When cells detached they were suspended in prewarmed growth medium and seeded out into a new culture plate in an appropriate dilution.

2.4.1.1. Freezing and thawing of cells

For cryopreservation cells were detached from the dish with trypsin-EDTA, collected in growth medium, and centrifuged. The cell pellet was resuspended in 1 ml freezing medium (FCS supplemented with 10 % DMSO) and transferred into a cryo-tube. The cells were frozen as fast as possible at -80 °C. For long term storage the cells were later transferred to a nitrogen-tank.

2. Materials and Methods

For thawing a new batch of cells, a 15 ml falcon tube was filled with growth medium and cryopreserved cells were thawed as fast as possible in a 37 °C water bath. Thawed cells were transferred immediately into the 15 ml falcon tube and centrifuged. The cell pellet was resuspended in growth medium and transferred to a 10 cm dish filled with 9 ml growth medium.

2.4.1.2. Mycoplasma test

To test cultured cells for contamination with mycoplasmae, a commercially available Mycoplasma Test Kit was applied according to the manufacturer's instructions (Biological Industries, Kibbutz Beit-Haemek, Israel). Here, mycoplasma contamination was analyzed by a PCR-based method using cell culture supernatant.

2.4.1.3. Cell counting

To seed out a defined number of cells, the concentration of a cell suspension has to be estimated. After trypsinization and resuspension of the cells in growth medium an aliquot of the cell suspension was diluted in growth medium and supplemented with trypan blue dye (Sigma-Aldrich, St. Louis, MO, USA) to stain dead cells. The cell concentration of this suspension was then determined using a Neubauer counting chamber (Paul Marienfeld GmbH & Co. KG, Lauda Königshofen, Germany).

2.4.2. TMEM132D overexpression

For overexpression of TMEM132D, MO3.13 cells were seeded on cover slips placed in a 12 well plate at a concentration of 40000 cells per well to reach a confluency of 70 % the next day. Then 0.7 µg of a murine TMEM132D-pEGFP N1 construct (gift from J. Deussing, MPI of Psychiatry, Munich) or empty pEGFP N1 vector as control diluted in 100 µl 150 mM NaCl solution was transfected by lipofection using 2.2 µl of the linear polyethylenimine (PEI) solution ExGen500 (Fermentas, St-Leon-Rot, Germany). After thorough vortexing, the reaction mix was incubated for 20 min at room temperature and 100 µl was then transferred to each well. After 48 h incubation at 37 °C and 5 % CO₂, the cells were fixed in 4 % PFA,

counterstained with the nuclear stain DAPI, and the cover slips were mounted on glass slides for analysis at an Olympus IX81 confocal microscope (Olympus, Hamburg, Germany).

2.4.3. Reporter gene assay

Phosphate buffer pH 7.8

0.5 M KH_2PO_4
0.5 M K_2HPO_4
adjust to pH 7.8

Passive lysis buffer

100 mM Phosphate buffer pH 7.8
0.2 % Triton X-100

Firefly substrate solution

2.5 mM MgCl_2
2 mM ATP
100 μM D-Luciferin
in H_2O

Phosphate buffer pH 5.1

0.5 M KH_2PO_4
0.5 M K_2HPO_4
adjust to pH 7.8

Gaussia substrate solution

1.1 M NaCl
2.2 mM Na_2EDTA
0.22 M Phosphate buffer pH 5.1
0.44 mg/ml BSA
3 $\mu\text{g/ml}$ Coelenterazin

TMEM132D promoter activity was studied using reporter gene assays. To perform a reporter gene assay the promoter region of interest was cloned upstream of a firefly luciferase (from *Photinus pyralis*) encoded in the pGL3 basic plasmid (section 2.3.3 and Figure 3.11). When this promoter-containing pGL3 plasmid is transfected into a eukaryotic cell, the reporter gene, i.e. firefly luciferase, is expressed proportionally to the promoter activity. To minimize variations due to slight differences in transfection efficiencies or cell numbers, a reference plasmid containing a constitutively active promoter, in this case a CMV promoter-driven gaussia luciferase plasmid (Gaussia-KDEL, gift from T. Rein, Max Planck Institute of Psychiatry), was co-transfected for normalization of the firefly luciferase signals. The gaussia luciferase (from *Gaussia princeps*) expressed by the Gaussia-KDEL plasmid was modified by a C-terminal KDEL amino acid sequence, which serves as a retention signal for the endoplasmatic reticulum. This inhibits the secretion of gaussia and enables the measurement of both gaussia and firefly luciferase in the cell lysate. Importantly, firefly and gaussia luciferase catalyze the oxidation of different substrates, namely D-Luciferin and Coelenterazin, resulting in the emission of light. This bioluminescence can be detected in the luminometer and, provided that the enzyme is saturated with substrate, reflects the reporter gene expression

2. Materials and Methods

which is proportional to the promoter activity.

For the reporter gene assays performed in this study, 8000 MO3.13 cells per well were seeded in a 96-well plate. The next day, when cells reached a confluency of approximately 70 %, both the reporter gene and reference plasmids were transfected by lipofection: 50 ng/well of the TMEM132D promoter driven firefly luciferase plasmid and 10 ng/well of the CMV promoter driven gaussia luciferase plasmid were diluted in 150 mM NaCl solution and supplemented with 0.6 μ l of the linear polyethylenimine (PEI) solution ExGen500 (Fermentas, St. Leon-Rot, Germany). The reaction mix was then thoroughly vortexed and incubated for 20 min at room temperature allowing formation of liposomes. The mix was then added to the cells leaving some wells untransfected as a background control. Finally, the 96-well plate was centrifuged for 5 min at 250 x g at room temperature to improve transfection efficiency before the cells were then incubated for 48 h at 37 °C and 5 % CO₂.

Finally, luciferase activity was measured at a Tristar luminometer (Berthold, Bad Wildbad, Germany). For this, the cells were lysed in passive lysis buffer for 30 min at room temperature shaking at 700 rpm. Subsequently, 20 μ l of the lysate was transferred into wells of a white Nunc96 plate (Nunc GmbH & Co. KG, Langenselbold, Germany). The luminometer first injected 100 μ l of firefly substrate solution and after shaking for 1 s, measured the bioluminescence over the period of 10 s. Then, 100 μ l gaussia substrate solution was injected into the same well, thereby quenching the firefly signal by decreasing the pH. The plate was shaken for 1 s and after a 2 s delay, the bioluminescence was measured over a period 5 s.

For data analysis, the background signal intensity generated by lysates of untransfected cells was subtracted from each data point. Then, for normalization the firefly/gaussia ratio was calculated. The data are presented normalized to the expression value of the constitutive active firefly luciferase plasmid (pGL3SV40) that was transfected in each experiment. In all performed assays each experimental conditioned was represented in triplicates.

2.4.4. MO3.13 differentiation assay

MO3.13 cells were grown to approximately 70 % confluency. Then, to induce differentiation normal growth medium was exchanged to FCS-free RPMI medium containing 100 nM phorbol 12-myristate 13-acetate (PMA) according to previously described protocols (Buntinx et al., 2003). Differentiation was monitored by assessing the morphological change using an inverted microscope (Olympus CK30 microscope, Olympus, Hamburg, Germany). After three days of differentiation RNA was isolated as described in section 2.3.3.1. RT-PCR for TMEM132D mRNA and the candidate transcription factor mRNAs was performed in differentiated versus non-differentiated MO3.13 cells as described in section 2.3.4. For visualization of the morphological changes, differentiated and non differentiated MO3.13 cells were stained with the TexasRed-labeled cell surface marker wheat germ agglutinin (WGA) (Invitrogen). For this purpose, MO3.13 cells were grown on glass cover slips. After differentiation, cells were fixed in 4 % PFA, washed with PBS, stained with TexasRed-WGA and counterstained with the nuclear stain DAPI. Finally, cover slips were mounted on slides and analyzed using an Olympus IX81 confocal microscope (Olympus, Hamburg, Germany).

2.4.5. siRNA mediated knock-down of TMEM132D

To answer the question if TMEM132D is necessary for oligodendrocyte differentiation, a knock-down using TMEM132D-specific siRNA was performed (Dharmacon, Lafayette, CO, USA), and transfected MO3.13 cells were subsequently subjected to PMA-induced differentiation (see section 2.4.4). For this purpose, 120000 MO3.13 cells were plated into each well of a 6 well plate. The next day, when cells had reached approximately 70 % confluency, TMEM132D-specific or control siRNA was transfected via lipofection using the DharmaFECT reagent (Dharmacon, Lafayette, CO, USA) according to the manufacturer's specifications. 6 h later, the medium was exchanged to either control (normal growth medium) or 100 nM PMA containing medium and cells were cultivated for at least three more days. Then, cell morphology was analyzed using an Olympus CK30 microscope (Olympus, Hamburg, Germany) and cells were harvested for RT-PCR analysis (see section 2.3.4).

2.5. Bioinformatical methods

A comprehensive *in silico* analysis was performed to study TMEM132D. Sequence information was retrieved from the databases at the National Center for Biotechnology Information (NCBI) (<http://www.ncbi.nlm.nih.gov>), the UCSC Genome Browser (<http://genome.ucsc.edu/>), the Ensemble Genome Browser (<http://www.ensembl.org/>), and the UniProtKB database (<http://www.uniprot.org>). Sequence alignments were performed with the NCBI Basic local alignment tool (BLAST), e.g. for analyzing sequence results during cloning. Primers (see Tables 2.7, 2.8, 2.9, 2.10) were designed using the NCBI Primer-BLAST program.

Table 2.11.: **Employed bioinformatical tools.** Listed are all bioinformatical tools used in this study, their developers, as well as a description of the intended use.

Tool	Developed by	Application
Sequence databases		
NCBI gene, nucleotide, and protein databases	National Center for Biotechnology Information (NCBI)	Sequence retrieval
UniProtKB	European Bioinformatics Institute (EBI), Swiss Institute of Bioinformatics (SIB), Protein Information Resource (PIR)	Protein sequence retrieval
UCSC Genome Browser	Genome Bioinformatics Group of UC Santa Cruz	Sequence retrieval
Ensembl Genome Browser	European Molecular Biology Laboratory - European Bioinformatics Institute (EMBL-EBI) and Sanger Institute	Sequence retrieval
NCBI GEO DataSets	National Center for Biotechnology Information (NCBI)	Retrieval of gene expression data
Sequence alignments and phylogenetic analysis		
BLAST	National Center for Biotechnology Information (NCBI)	Comparison of protein sequences (blastp, psi-blast), nucleotide sequences (blastn), or for primer design (Primer-BLAST)
T-Coffee	Center for Genomic Regulation (CRG), Barcelona (Notredame et al., 2000)	Multiple sequence alignment of TMEM132D paralogs
BOXSHADE 3.21	K. Hofmann and M. Baron, Swiss Institute of Bioinformatics	Illustration of multiple sequence alignment

WebLogo	University of California, Berkeley (Crooks et al., 2004)	Illustration of consensus sequence of multiple sequence alignment
Phylogeny.fr platform (MUSCLE + PhyML + TreeDyn)	A. Dereeper, V. Guignon (Dereeper et al., 2008)	Phylogeny analysis: MUSCLE multiple sequence alignment + PhyML phylogenetic analysis + TreeDyn Tree rendering
HHPred	Max-Planck Institute for Developmental Biology (Soding et al., 2005)	Detection of homologous protein domains
COILS/PCOILS	Max-Planck Institute for Developmental Biology (Lupas et al., 1991)	Detection of coiled-coil domains
<i>In silico</i> TMEM132D promoter analysis		
Gene2Promoter	Genomatix Software GmbH (Munich, Germany)	Extraction of the TMEM132D promoter sequence
MatInspector	Genomatix Software GmbH (Munich, Germany) (Cartharius et al., 2005)	Identification of transcription factor binding sites
DiAlignTF/GEMS Launcher	Genomatix Software GmbH (Munich, Germany) (Cartharius et al., 2005)	TFBS in aligned regions of orthologous promoters
TFSEARCH	Yutaka Akiyama, http://www.rwcp.or.jp/papia/	Identification of transcription factor binding sites
EMBOSS CpGPlot	European Molecular Biology Laboratory - European Bioinformatics Institute (EMBL-EBI) (Rice et al., 2000)	Detection of CpG Islands
ECR Browser	NCBI Dcode.org Comparative Genomics Developments (Loots and Ovcharenko, 2007)	Evolutionary conservation of multiple genomes; conservation of human and murine TMEM132D promoter

2.5.1. Analysis of phylogenetic conservation of TMEM132D proteins

Human TMEM132D paralogs were identified by blastp search of the TMEM132D protein sequence against the UniProtKB/Swiss-Prot database (<http://blast.ncbi.nlm.nih.gov>). A multiple sequence alignment of TMEM132D was performed to identify conserved regions employing the T-Coffee method (www.tcoffee.org). The multiple sequence alignment was illustrated using BOXSHADE3.21 (http://www.ch.embnet.org/software/BOX_form.html)

and a graphical representation was produced applying the WebLogo tool (<http://weblogo.berkeley.edu/>). Orthologs of the TMEM132D protein were retrieved from the ENSEMBL database (<http://www.ensembl.org>). The sequences of homologous proteins were submitted to phylogeny analysis at <http://www.phylogeny.fr> (Dereeper et al., 2008).

2.5.2. Identification of homologous protein domains of TMEM132D

As so far the protein function of TMEM132D is unknown, an *in silico* analysis of functional protein domains was performed using the HHPred tool (<http://toolkit.tuebingen.mpg.de/hhpred>). Based on a hidden markov model (HMM)-hidden markov model (HMM) comparison the HHPred tool detects homologous protein domains (Söding, 2005). Only protein domain hits with a probability higher than 60 were taken into account. Subsequently, the COILS/PCOILS program (<http://toolkit.tuebingen.mpg.de/pcoils>) was applied to confirm a potential coiled-coil domain identified by HHPred.

2.5.3. TMEM132D *in silico* promoter analysis

The prediction of the TMEM132D promoter region was performed using the Genomatix Gene2promoter tool (<http://www.genomatix.de/products/Gene2Promoter>) by entering the human TMEM132D mRNA sequence (NCBI Reference Sequence: NM_133448.2) into the input mask. Subsequently, the retrieved TMEM132D promoter sequence was analyzed for the presence of transcription factor binding site motifs using either the Genomatix MatInspector tool (<http://www.genomatix.de/products/MatInspector>) or the TFSEARCH program (<http://www.cbrc.jp/research/db/TFSEARCH.html>). To restrict further analyses to the most important transcription factor binding sites (TFBS), phylogenetic conservation of transcription factor binding sites was analyzed using the Genomatix DiAlignTF tool of the GEMS Launcher Package (<http://www.genomatix.de/products/GEMSLauncher>). This tool identifies TFBS motifs in a multiple alignment of the human and murine TMEM132D promoter sequence. Additionally, conservation of the more distally located human and murine

promoter regions (position chr12:128953500-128959000 of the human genome) was analyzed using the ECR Browser (<http://ecrbrowser.dcode.org/>). Finally, analysis of CpG islands was performed by entering the human TMEM132D promoter sequence into the EMBOSS CpG Plot input mask (<http://www.ebi.ac.uk/Tools/emboss/cpgplot>).

2.5.4. NCBI GEO DataSet analyses

The NCBI GEO DataSets (<http://www.ncbi.nlm.nih.gov/gds/>) store gene expression data from microarray experiments. In a first analysis, TMEM132D expression data from a published microarray study were retrieved from NCBI GEO DataSets (accession number GDS2044) (Vallender and Lahn, 2006). For the array experiments, primary dermal fibroblasts have been treated with the DNA methyltransferase inhibitor 5-aza-2'-deoxycytidine (Aza-dC) for 96 hours followed by gene expression analysis on an Affymetrix Mouse Genome 430 2.0 Array. Here, TMEM132D expression values were retrieved from the NCBI GEO DataSets website and were analyzed for statistical significance by applying a student's *t*-test.

In a second analysis, data on immunoglobulin gene expression in human blood samples of PTSD patients and controls were retrieved from NCBI GEO DataSets (accession number GDS1020). In the respective study blood from trauma survivors admitted to the emergency room has been collected few hours and 4 months after exposure to a traumatic event. Subjects have been assigned to control and PTSD groups based on the expression of PTSD symptoms (Segman et al., 2005). Here, expression values for Ig κ light chain (IGK), Ig λ light chain (IGL), IgG1 heavy chain (IGHG1), IgA2 heavy chain (IGHA2), and IgM heavy chain (IGHM) transcripts were extracted and analyzed for statistical significance by applying a two-way ANOVA and Bonferroni post-tests.

2.6. Statistics

Statistical analyses were performed using the software Excel 2003TM (Microsoft Deutschland GmbH, Unterschleißheim, Germany) and GraphPad Prism 5TM (GraphPad Software Inc., La Jolla, CA, USA). Statistical significance was calculated using the two-tailed student's *t*-test

or ANOVA and Bonferroni post-hoc tests when appropriate. The p-values were classified into four groups: t $p < 0.1$, * $p < 0.05$, ** $p < 0.01$, *** $p < 0.001$.

2.6.1. Pearson correlation

Correlation studies were performed according to published procedures (Wu et al., 2007; Zink et al., 2010) employing GraphPad Prism 5TM: For each individual mouse its mean relative synapsin, synaptophysin, or homer 1b/c protein expression value on day 60 after shock (calculated from three technical replicates) was correlated with the values representing the intensities of either its contextual fear, generalized fear, or acoustic startle response on days 28-30 after shock by calculating the Pearson correlation coefficient.

3. Results I: Transcriptional regulation of the human TMEM132D gene

This thesis aimed at analyzing the hitherto completely unknown transcriptional regulation of transmembrane protein 132 D (TMEM132D), a recently identified candidate gene for anxiety disorders. Changes in TMEM132D expression have been associated to anxiety phenotypes (Erhardt et al., 2011) as well as oligodendrocyte differentiation (Nomoto et al., 2003) as described in section 1.6. In order to identify mechanisms leading to these expression changes, this thesis concentrated on elucidating the hitherto completely unexplored transcriptional regulation of TMEM132D and in particular the structure and regulatory mechanisms of the TMEM132D promoter.

3.1. Analysis of TMEM132D gene structure and prediction of possible protein functions

Prior to analyzing the TMEM132D promoter region in detail, a brief *in silico* analysis of the TMEM132D gene and protein was performed. As listed in the gene database of the National Center for Biotechnology Information (NCBI) (<http://www.ncbi.nlm.nih.gov>), TMEM132D (Gene ID: 121256) is a nine exon containing gene located on chromosome 12q24.32-q24.33 and spans a region of about 830 kb. Transcription results in a 5777 bp long mRNA (NCBI accession number NM_133448.2) with a 328 bp spanning 5' untranslated region, an open reading frame of 3300 bp, and a 3' untranslated region of 2149 bp. Translation produces a 1099 amino acid long protein (NCBI accession number NP_597705.2). TMEM132D has been predicted to be a single-pass type I transmembrane protein, i.e. a protein anchored in the lipid membrane with the N-terminus oriented towards the extracellular space, with a 30 amino acid signal peptide, a long extracellular domain (885 amino acids), a short transmembrane region

3. Results I: Transcriptional regulation of the human *TMEM132D* gene

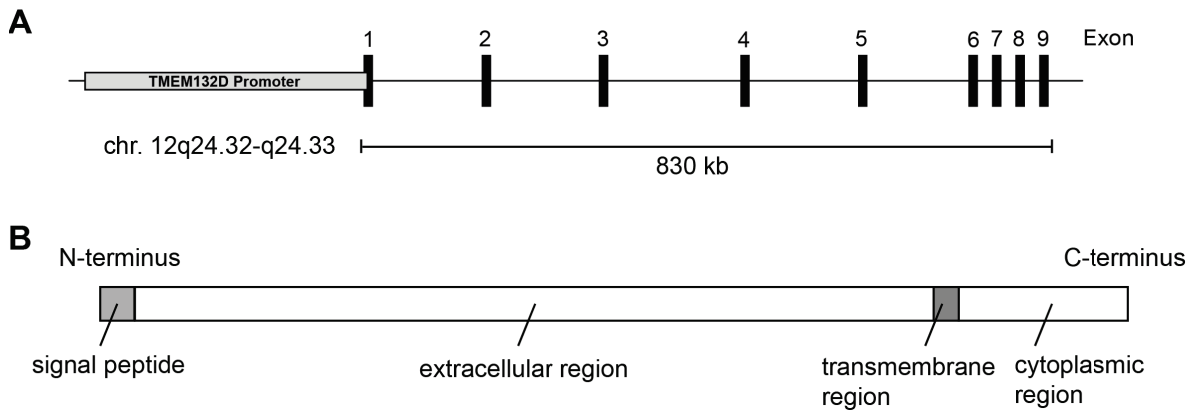


Figure 3.1.: **Schematic illustration of the human *TMEM132D* gene and protein structure based on information retrieved from the NCBI and UniProtKB databases.** (A) The *TMEM132D* gene locus spanning 830 kilobases (kb) on chromosome 12q24.32-q24.33 is depicted. (B) *TMEM132D* is a potential type I transmembrane protein with a short cytoplasmic residue and a long extracellular region.

(amino acids 916-936), and a short cytoplasmic domain (163 amino acids) (www.uniprot.org; accession number Q14C87-1), as illustrated in Figure 3.1. Translation of an alternative splice variant of the *TMEM132D* transcript described in the uniprot database (www.uniprot.org; accession number Q14C87-2) is predicted to result in a protein that lacks the first 462 amino acids and thus, exhibits a shorter extracellular domain.

Here, the transmembranous localization of *TMEM132D* was experimentally confirmed by overexpression of an EGFP-tagged murine *TMEM132D* (construct was a generous gift from J. Deussing, MPI of Psychiatry, Munich, Germany) in MO3.13 oligodendroglial cells: while control cells overexpressing EGFP only show an evenly distributed green fluorescence across the cell, in *TMEM132D* overexpressing cells the green fluorescence was predominantly restricted to the cell membrane (Figure 3.2), thereby visualizing the numerous small cellular processes that are characteristic of these cells (cf. Figure 3.21).

As besides displaying a cell surface marker during oligodendrocyte differentiation (Nomoto et al., 2003), the protein function of *TMEM132D* is hitherto unknown, an *in silico* analysis of homologous sequences of *TMEM132D* was performed: a search for human *TMEM132D* paralogs using the NCBI protein-protein BLAST (blastp) or the NCBI position specific iterative (PSI)-BLAST (both accessed via the webpage <http://blast.ncbi.nlm.nih.gov>) on the

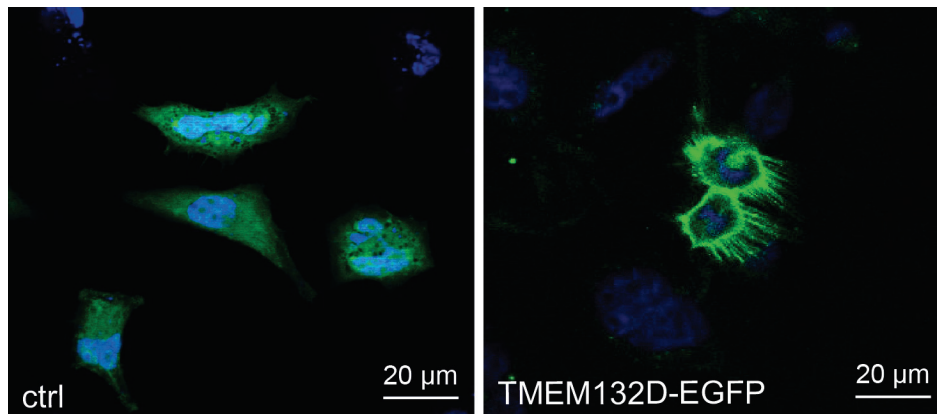


Figure 3.2.: **Overexpression of EGFP-tagged TMEM132D reveals its transmembranous localization.** Murine TMEM132D-EGFP was overexpressed in MO3.13 cells, control cells overexpressed EGFP only. After 48 h of overexpression, cells were prepared for analysis by confocal microscopy.

swiss-prot protein database revealed the five known members of the TMEM132 protein family, namely TMEM132A, TMEM132B, TMEM132C, TMEM132D, and TMEM132E. UniProtKB database search (<http://www.uniprot.org>) furthermore revealed that all of the TMEM132 proteins (TMEM132A - accession Q24JP5, TMEM132B - accession Q14DG7, TMEM132C - accession Q8N3T6, TMEM132D - accession Q14C87, and TMEM132E - accession Q6IEE7) are predicted to be single-pass type I transmembrane proteins with a large extracellular domain and a short intracellular domain and have an approximate size of 1000 amino acids. Subsequent phylogenetic analysis demonstrated TMEM132D to exhibit the highest conservation with TMEM132C and TMEM132B, and the lowest similarities with TMEM132A (Figure 3.3). According to the blastp results, sequence identity of TMEM132D was 61 % with TMEM132C, 51 % with TMEM132B, 36 % with TMEM132E, and 30 % with TMEM132A. Conserved regions in the TMEM132D paralogs were analyzed by performing a multiple sequence alignment. Interestingly, TMEM132D paralogs showed a high conservation of the putative transmembrane region (Figure 3.4, see Appendix A.1 for detailed sequence information). Moreover, the regions flanking the predicted transmembrane region were not very well conserved in the TMEM132D paralogs, while in the extracellular region multiple segments exhibited high sequence similarity (Figure 3.4, see Appendix A.1 for detailed sequence information). However, so far not much is known about the protein function of these

3. Results I: Transcriptional regulation of the human TMEM132D gene

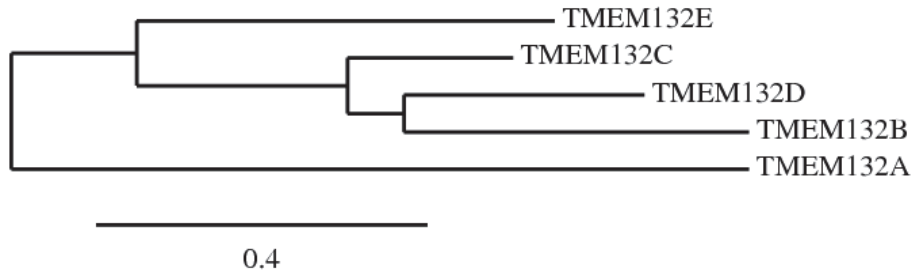


Figure 3.3.: **Phylogenetic tree of human TMEM132D paralogs.** Sequence information of TMEM132D paralogs were extracted from the blastp database search and submitted to phylogeny analysis at http://www.phylogeny.fr/version2_cgi/phylogeny.cgi. The length of the branches is scaled to the degree of change in amino acid sequence.

TMEM132D homologous proteins. Only the function of TMEM132A has been previously studied revealing it to play a role in neurite-like process formation as well as cell survival (Oh-hashii et al., 2010).

Next, to study the inter-species conservation of TMEM132D, phylogenetic conservation of TMEM132D orthologs was analyzed. For this purpose, all TMEM132D orthologous protein sequences were extracted from the ENSEMBL database (only complete sequences,

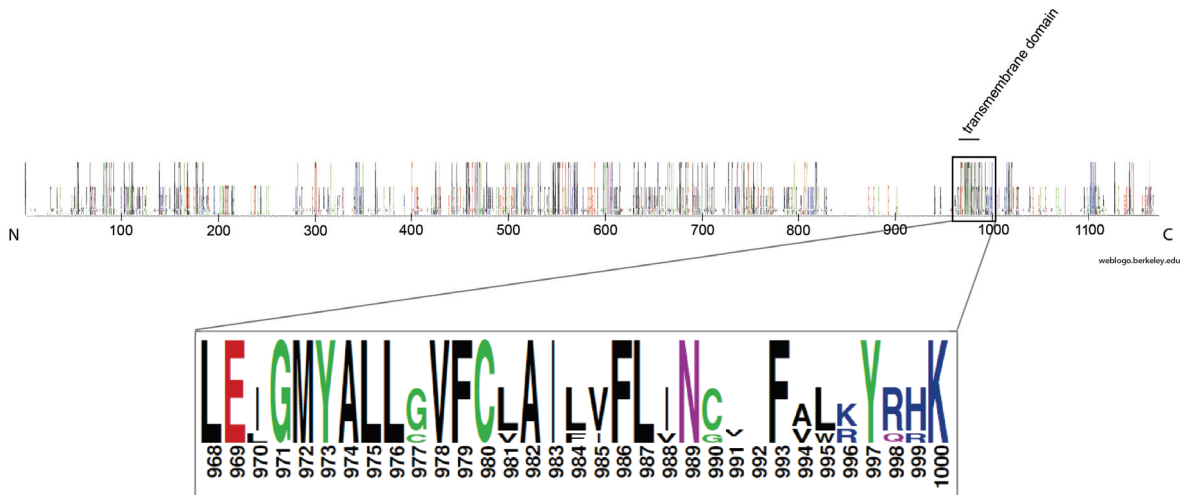


Figure 3.4.: **Illustration of conserved regions in a multiple sequence alignment of TMEM132D paralogs.** Multiple sequence alignment was performed employing the multiple sequence alignment server T-Coffee (www.tcoffee.org/). The consensus sequence was illustrated as a sequence logo using the weblogo tool at <http://weblogo.berkeley.edu/>. The N- and C-terminus as well as the sequence positions are indicated. The highly conserved potential transmembrane region is highlighted and depicted in the magnification.

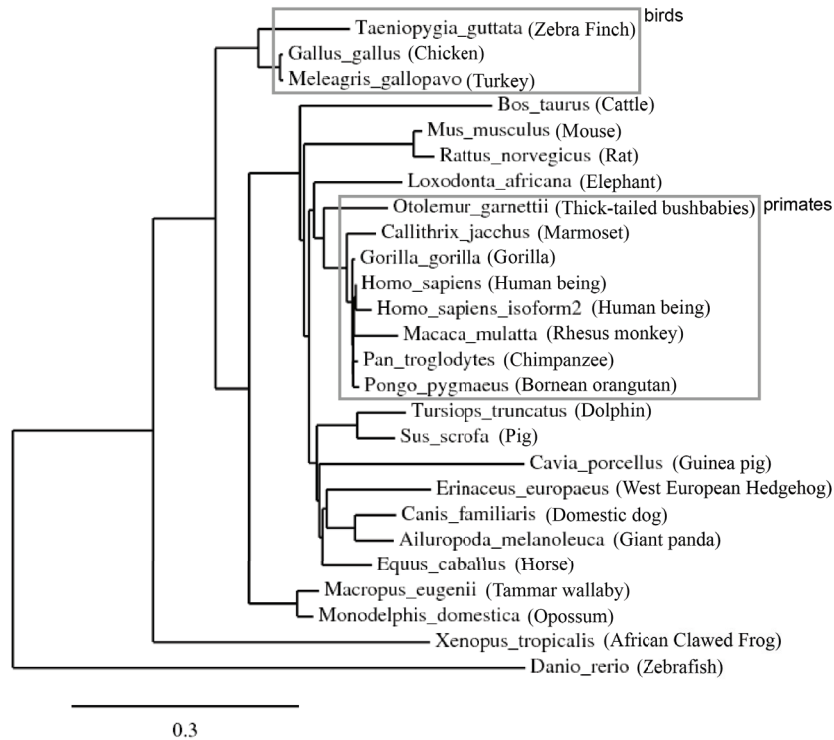


Figure 3.5.: **Phylogenetic conservation of the TMEM132D orthologs.** TMEM132D protein orthologs were retrieved from the ENSEMBL database and submitted to phylogeny analysis at http://www.phylogeny.fr/version2_cgi/phylogeny.cgi. The length of the branches is scaled to the degree of change in amino acid sequence of TMEM132D orthologs.

i.e. no sequence fragments, were taken into account) and a phylogenetic tree was generated employing the phylogeny.fr tool (http://www.phylogeny.fr/version2_cgi/phylogeny.cgi). So far, TMEM132D homologs have been found in several vertebrates including mammals and birds as well as amphibians (*Xenopus tropicalis*) and fish (*Danio rerio*). However, no homologs have been found in invertebrates yet (Figure 3.5).

As conventional BLAST analysis did not reveal any significant homologous proteins with known function, a search for conserved protein domains was performed next. For this purpose, the HHpred tool at <http://toolkit.tuebingen.mpg.de/hhpred> was employed, which is based on a different algorithm than blastp and PSI-BLAST, i.e. the Hidden Markov Model (HMM) (Söding, 2005). In contrast to blastp, which performs a sequence-sequence comparison, and PSI-BLAST, which compares protein profiles to protein sequences, the HHpred tool compares HMM profiles to HMM profiles. In addition to amino acid sequence information,

3. Results I: Transcriptional regulation of the human TMEM132D gene

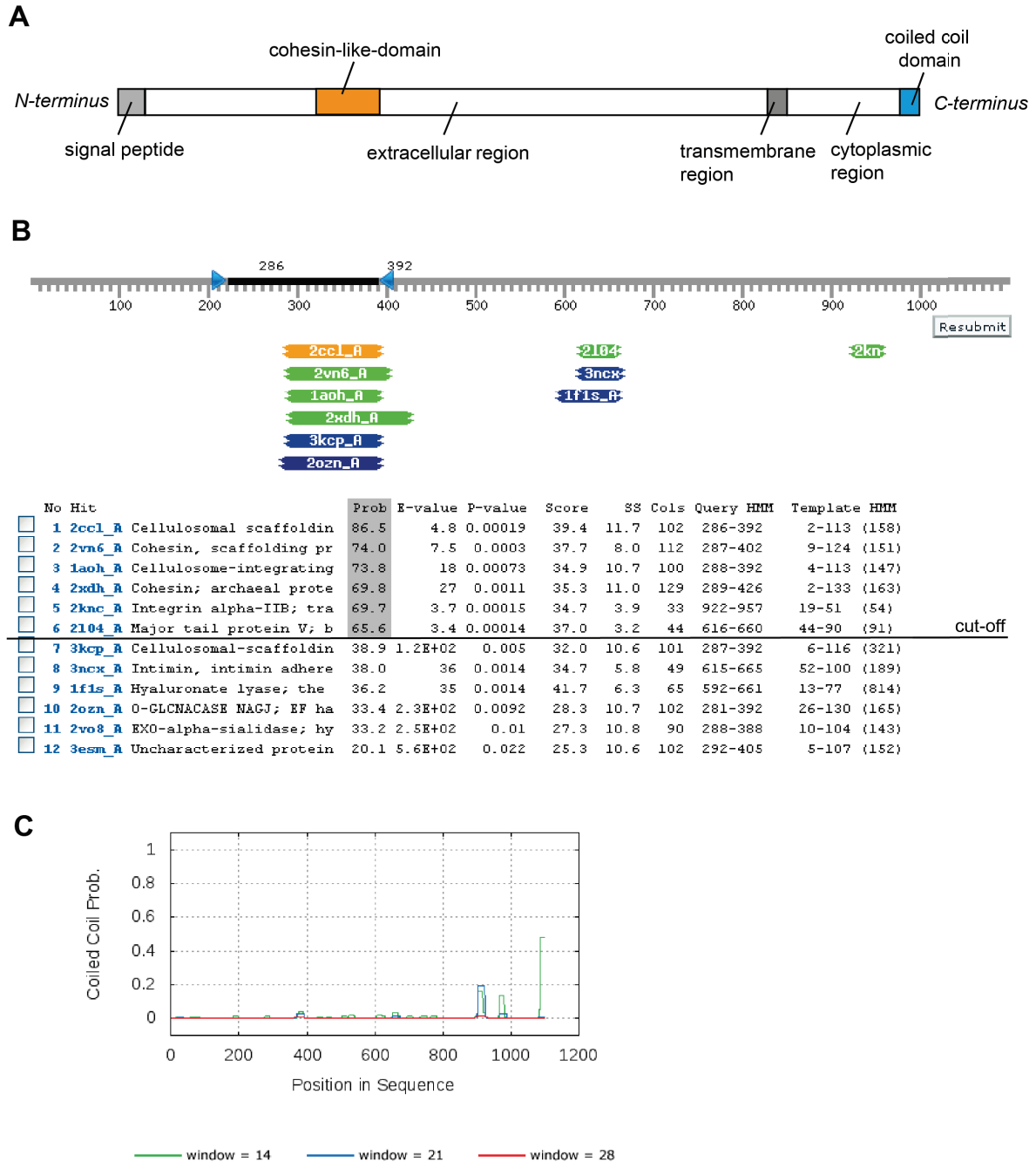


Figure 3.6.: **Prediction of conserved protein domains employing the HHpred tool.** (A) Schematic illustration of the localization of the cohesin-like domain and the coiled coil domain predicted by HHpred. (B) Results of the HMM-HMM comparison retrieved by submitting the TMEM132D protein sequence (NP_597705.2) to the HHpred tool at <http://toolkit.tuebingen.mpg.de/>. The cut-off is indicated and probability values are highlighted in gray. (C) Results of the COILS/PCOILS analysis of the TMEM132D protein sequence (NP_597705.2) at <http://toolkit.tuebingen.mpg.de/>.

3.1. Analysis of TMEM132D gene structure and prediction of possible protein functions

this method also includes position-specific probability values for insertions and deletions of amino acids along the alignment, which was reported to improve the alignment sensitivity (Söding, 2005). Subjection of the TMEM132D protein sequence (NCBI accession number NP_597705.2) to HHpred analysis resulted in 12 conserved protein domain hits. Only 6 hits exhibited a probability higher than 60, which was defined as a cut-off criterion: 4 of these hits pointed at a cohesin-like domain at amino acid position 286-392 in the extracellular domain of TMEM132D (Figure 3.6 A, B). Due to the extracellular localization and strong and highly specific interactions of bacterial cohesins with dockerins (Bayer et al., 2004), a cohesin-like domain might be important for cell adhesion processes. Interestingly, the fifth hit, the transmembrane domain of the integrin α -IIB protein, another single-pass type I transmembrane protein, is homologous to the potential transmembrane domain of TMEM132D at amino acid position 916-936 (Figure 3.6 A, B) and thus further confirms the identity of this region. The HHpred tool further indicated the presence of a coiled coil domain at the C-terminus of the TMEM132D protein, which was subsequently confirmed by applying the COILS/PCOILS tool (<http://toolkit.tuebingen.mpg.de/pcoils>). Coiled coil domains can mediate oligomerization and are predominantly found in proteins involved in intracellular transport (Burkhard et al., 2001) (Figure 3.6 C).

Taken together, *in silico* analyses revealed TMEM132D to constitute a nine exon containing gene located on chromosome 12q24.32-q24.33 and encoding a 1099 amino acid long predicted transmembrane protein. The transmembranous localization was experimentally confirmed by microscopic analysis of cells overexpressing a EGFP-tagged TMEM132D. Addressing TMEM132D protein function, a blastp-search of homologous proteins revealed TMEM132A, TMEM132B, TMEM132C, and TMEM132E to be paralogs of TMEM132D, as was to be expected from their classification into the same protein family. However, as these proteins are as poorly characterized as TMEM132D itself, they could not contribute to the elucidation of TMEM132D protein function. Finally, prediction of conserved protein domains using an alternative method revealed a cohesin-like domain in the extracellular region of TMEM132D, which might point at a potential role of TMEM132D in cell adhesion processes.

3.2. *In silico* analysis of the TMEM132D promoter

After *in silico* analysis of the TMEM132D protein and gene structure, the TMEM132D promoter was analyzed to decipher the regulatory mechanisms of TMEM132D expression. Experimental analysis of the TMEM132D promoter was preceded by an extensive *in silico* analysis that is illustrated in Figure 3.7. For this purpose, first the TMEM132D promoter was predicted employing the Gene2Promoter tool (www.genomatix.de), which has been successfully employed in previous promoter studies (Lindermayr et al., 2008; Palmieri et al., 2008). By mapping the TMEM132D mRNA sequence (NCBI Reference Sequence NM_133448) to the human genome, the Genomatix Gene2Promoter tool (www.genomatix.de) detected four possible promoters for TMEM132D, which were all located on the minus strand (Figure 3.7 A). For further analyses one of the predicted possible promoters was selected, i.e. that one that was considered to be the most important since it regulates the expression of the primary transcript of the TMEM132D gene, that is the nine exon containing transcript (Figure 3.1/Figure 3.7). This promoter spans the region of 829 bp upstream to 101 bp downstream of the start codon (Figure 3.8). Second, the TMEM132D promoter identified *in silico*, i.e. promoter I, was screened for the presence of transcription factor binding sites (TFBS) using the MatInspector tool (www.genomatix.de), that is widely used in promoter studies, e.g. in the characterization of promoter polymorphisms in the serotonin transporter gene (Ehli et al., 2012). Employing this tool yielded approximately 170 hits (Figure 3.7 B). To select the most important TFBS, human and murine promoter sequences were aligned and a TFBS search was conducted in the aligned sequence. Alignment and subsequent TFBS identification were performed using the DiAlignTF tool (www.genomatix.de) and resulted in 9 conserved TFBS (Figure 3.7 C) that were then analyzed *in vitro*. Finally, to identify additional, non-conserved TFBS, the TMEM132D promoter region was screened using the alternative tool TFSEARCH that contributed successfully to previous promoter characterizations (Wu et al., 2012; Banerjee and Nandagopal, 2007) and here, identified 30 hits in the TMEM132D promoter (Figure 3.7 D). TFBS identified by both TFSEARCH and MatInspector were selected for further *in vitro* analysis.

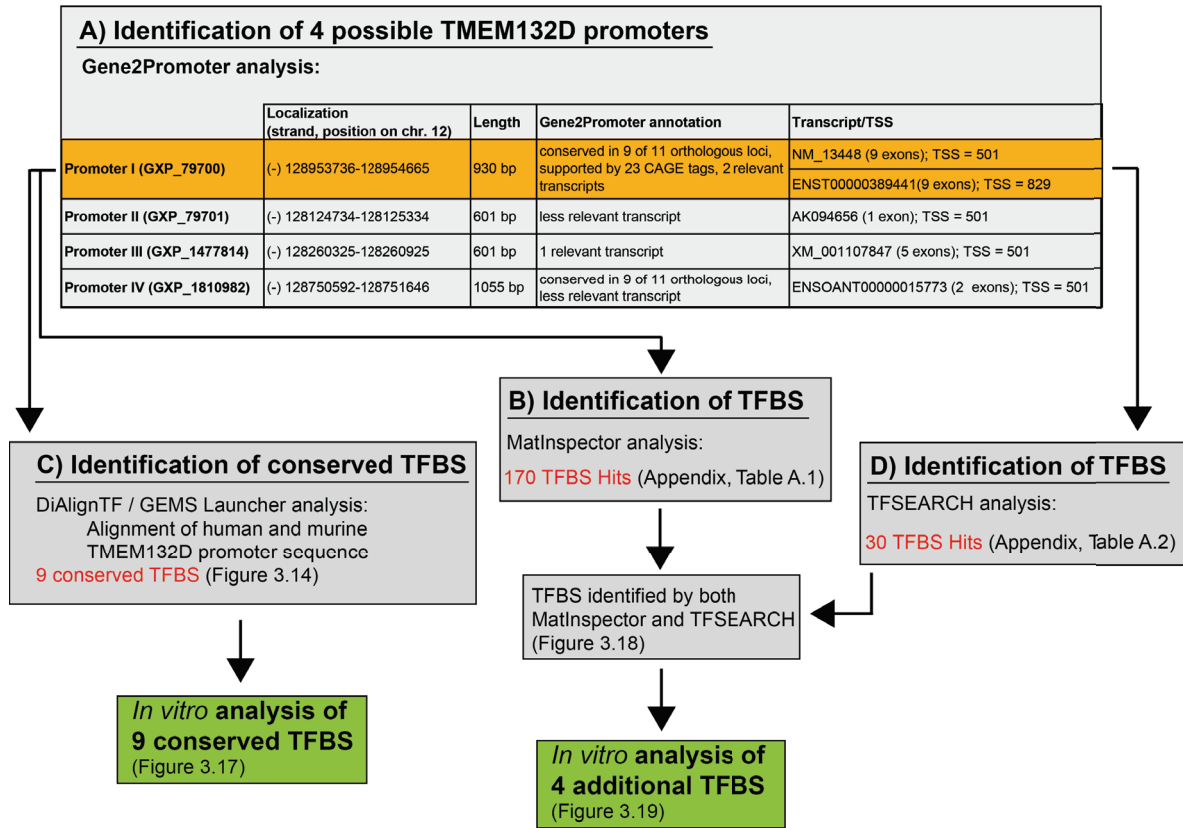


Figure 3.7.: **Workflow of *in silico* TMEM132D promoter analysis.** A) Employing the Gene2Promoter tool (www.genomatix.de) 4 possible TMEM132D promoters were identified. Promoter I (highlighted in orange) was selected to be the most important and was subjected to further analyses. B) Transcription factor binding site (TFBS) motifs were identified using the MatInspector tool (www.genomatix.de) resulting in 170 TFBS hits, listed in Appendix, Table A.1. C) TFBS search in a sequence alignment of the human and murine TMEM132D promoter identified 9 conserved TFBS (Figure 3.14), that were subjected to *in vitro* analysis (Figure 3.17). D) For identification of additional TFBS, the TFSEARCH tool (<http://www.cbrc.jp/research/db/TFSEARCH.html>) was employed, resulting in 30 TFBS hits (listed in Appendix, Table A.2). TFBS identified by both MatInspector and TFSEARCH were subjected to *in vitro* analysis (Figure 3.18 and 3.19).

The promoter, that is the DNA sequence involved in regulation and initiation of transcription of a gene, comprises both binding sites for general transcription factors and RNA polymerase II for the formation of the initiation complex as well as binding sites for other regulatory proteins, i.e. transcription factors that control the rate of assembly of the initiation complex (Riethoven, 2010). Among the 170 TFBS hits of the MatInspector analysis, several core elements for

3. Results I: Transcriptional regulation of the human *TMEM132D* gene

```

1  TTGCGGAGCG GAGCCXCPECCCGTF2BGCCTF2BTGCTGGC AGGAGGCAGC TGC GTTGCTC GGCCGCGTCC
61  CCGAGCCGGC GGGCCCTCCT CCGCGCACAT CTGGCCCGCC TCCCCGGGC GCAGGGGGGA
121  GCCCCGCGTC TCCGGAGCCT GCAGTGCGCT CGGCGCGCGT AGAGCCCCGC GAGCCCCAGC
181  CGGGCCCGGG GCCGGGCGGG CCGAGGCGGC GGCCGGGGAG CAGCCGCACC CGCCAAACTT
241  TGGGTGCCGG AGCGCGCGCG CGCCGAGCC CCGAGGCGCA GCGGCCGGCC TGGGATGGGG
301  GCTGCGGGCC AGGGAGCCCC GGGCCGCCA GCGAGCCCGG CCACCCGCC GGGGGGCTCC
361  GAGCCGCCTC TGCCCGCGTC CCGGCTCCG CAGCCCCGCC ACCCCGGCGC CGCCTGCGCC
421  AGCGCCCGCT AGCCAGCCCG GGAGCAGCTG GAGCCCGCGG MTENAGCCCTGCGC CTGGAGGCGC
481  CCCTCCTTGG GCCACCGGGG MTENGCCACTCTTC MTENGCTCGGGTAA ACAGGAAAGG AAATACCCCC
541  TGTGGATTAA AATTTAAAAA AAATTCTGTT GGGGTCAAG GAGGGAGGTG GGGTTTGCTT
601  GCGCGCGTGT TGGACTCCGG AGAGCAACTC AGGAGCCCGC GCGGTCTGTC CCTCCGGCC
661  TGGCCATGGA CTGGCGGGAA GAGMTENGGAGCAG MTENGGCGCCCGG MTENCTGCTCGGGC MTENCCCTAGCCGG
721  XCPEGCGCTCCCTC XCPEGCCACCGGC CCGCTGCGGG CCTCTAGGGG InrACTGAGACGG TCTCTTGTTT
781  GCCTGGACGG CGCCGGGGAG CGGAGGATCT GCGCTCCGGG TCTCCAGGAT GTGCCCGTCT
841  GAGATGGGGA CGCTGTGGCA CCACTGGTCG CCGGTACTCA TCAGCCTGGC CGCCCTGTTT
901  TCCAAAGGTG AGGACGCCGC GGCCGCCAGG

```

Figure 3.8.: **Core elements required for transcription initiation in the *TMEM132D* promoter.** The core sequence of core promoter elements in the *TMEM132D* promoter is highlighted by red frames. The start codon is printed in bold. Abbreviations: XCPE = Activator-, mediator- and TBP-dependent core promoter element for RNA polymerase II transcription from TATA-less promoters; TF2B = RNA polymerase II transcription IIB; MTEN = core promoter motif ten elements; Inr = core promoter initiator element

initiation of RNA Polymerase II-driven transcription were identified (Figure 3.8). Similar to other human promoters, in the human *TMEM132D* promoter sequence no TATA-box was identified. Instead, a core promoter initiator element (Inr), typically located at position -2 to +4 relative to the transcription start site (TSS) (Jin et al., 2006), was found approximately 75 bp upstream of the *TMEM132D* start codon. In general, the first step in the assembly of the initiation complex is the binding of the general transcription factor TFIID to the DNA. In presence of a TATA box, TFIID binds via its TATA binding protein (TBP) subunit, while in

TATA-less promoters the TBP-associated factor (TAF) subunits of TFIID bind to the initiator element (Inr) (Smale, 1997). This is followed by assembly of the other general transcription factors, namely TFIIB, TFII E, TFII F, and TFII H as well as the RNA polymerase II to the initiation complex. Finally, transcription is induced by TFII H mediated unwinding of the DNA and phosphorylation of RNA polymerase II (Baumann et al., 2010). Besides binding of general transcription factors, core promoter elements also integrate the activating and repressive influences of transcription factors bound at distal sites (Smale and Kadonaga, 2003). Several core promoter motif ten elements (MTEN) were identified in the TMEM132D promoter sequence. In general, MTENs are located at position +18 to +27 relative to the TSS and have been reported to promote initiation of transcription in the presence of an Inr (Lim et al., 2004). In the TMEM132D promoter sequence, however, all identified MTENs were located upstream of the identified Inr. In addition to Inr and MTEN, the *in silico* analysis performed here identified two activator-, mediator- and TBP-dependent core promoter elements for RNA polymerase II transcription from TATA-less promoters (XCPE). XCPEs are typically located at position -8 to +2 relative to the TSS (Tokusumi et al., 2007): here, in the TMEM132D promoter one XCPE site was found to be located approximately 32 bp upstream of the potential TSS whose presumable existence was concluded from the presence of the Inr. The second XCPE was located far more upstream, approximately 740 bp upstream of the start codon. This second XCPE site was found to overlap with a RNA polymerase II transcription IIB (TF2B) binding site, that is typically located -37 to -32 bp upstream of the TSS and is an important element involved in the RNA polymerase II recruitment (Jin et al., 2006). Taken together, from the core promoter elements identified by MatInspector analysis it is not possible to reach an ultimate conclusion on the transcription start site of TMEM132D: the localization of the identified Inr suggests a TSS at position -75 of the start codon. In contrast, the transcription start site that can be deduced from the 5' sequence of the TMEM132D transcript NM_133448.2 listed in the NCBI nucleotide data base is at position -329 of the start codon, however, MatInspector analysis detected no core promoter elements that supported the presence of this TSS.

In general, besides the core promoter elements important for recruitment of RNA polymerase

3. Results I: Transcriptional regulation of the human *TMEM132D* gene

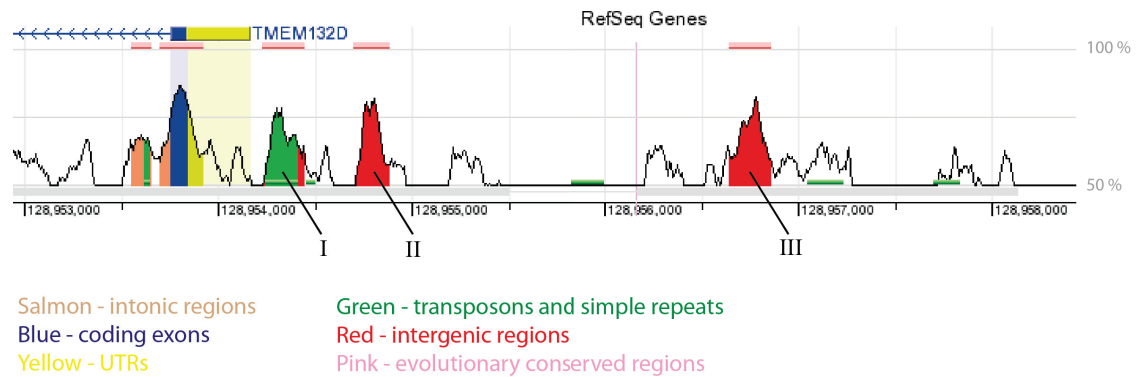


Figure 3.9.: **Conservation of the 5 kb region upstream of the *TMEM132D* start codon.** Conservation of the human and murine *TMEM132D* promoter region was analyzed using the ECR Browser (<http://ecrbrowser.dcode.org/>). Three clusters (I-III) of evolutionary conserved regions were detected.

II and initiation of transcription which are located in close proximity to the transcription start site, also both proximal and distal enhancer and repressor elements can substantially influence promoter activity. Striving to identify distal regulatory elements, a conservation analysis of the region spanning 5 kb upstream of the start codon was performed employing the ECR Browser (<http://ecrbrowser.dcode.org/>) (Figure 3.9). Comparing human and murine *TMEM132D* promoter sequences, three conserved regions emerged (Figure 3.9). The first one (630 to 401 bp upstream of the start codon) lies within the promoter identified by Gene2Promoter (Figure 3.7), the second is located in close proximity to the latter (1036 to 903 bp upstream of the start codon) and the third cluster lies more distal (3012 to 2830 bp upstream of the start codon) (Figure 3.9). Evolutionary conserved regions often contain essential functional elements regulating promoter activity (Loots and Ovcharenko, 2007). The third cluster of conservation might thus harbour functional distal regulatory elements like enhancers or silencers, while cluster I and II probably contain more proximal regulatory elements (Figure 3.9).

Besides the presence of core promoter elements and evolutionary conserved regions, CpG islands, i.e. genomic regions with a high frequency of CG dinucleotides, are well-known indicators of promoter regions (Yamashita et al., 2005). A CpG island reaching from 1118 bp upstream to 285 bp downstream of the start codon was identified using the EMBOSS CpG Island Plot (<http://www.ebi.ac.uk/Tools/emboss/cpgplot/>) (Figure 3.10 A)

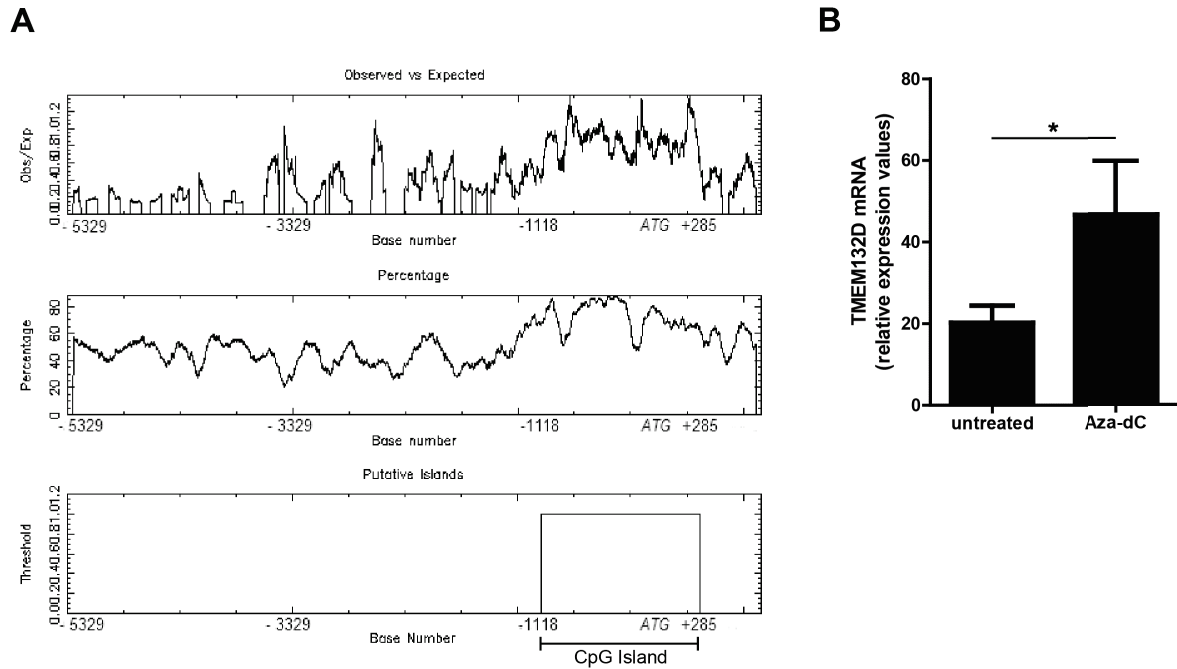


Figure 3.10.: **Identification of a CpG island in the TMEM132D promoter.** (A) EMBOSS CpG Island Plot of the TMEM132D promoter region (<http://www.ebi.ac.uk/Tools/emboss/cpgplot/>). The CpG island identified reached from -1118 to +285 relative to the start codon of TMEM132D. (B) Results of the statistical analysis of TMEM132D expression data extracted from a microarray dataset (from NCBI GEO DataSets (GDS2044); <http://www.ncbi.nlm.nih.gov/geo/>) showing an upregulation of TMEM132D mRNA after Aza-dC treatment (leading to DNA demethylation) of primary mouse fibroblasts. Data represent means \pm SD, $n = 3$. Statistical significance was calculated using a student's *t*-test and is indicated by * $p < 0.05$.

which further supports the identity of the here identified TMEM132D promoter region. Additionally, a potential role of CpG methylation in transcriptional regulation of TMEM132D was concluded from publicly available microarray data retrieved from NCBI GEO DataSets (Accession number: GDS2044) (<http://www.ncbi.nlm.nih.gov/geo/>): samples of primary mouse fibroblasts treated with the DNA methyltransferase inhibitor 5-aza-2'-deoxycytidine (Aza-dC) were submitted to the microarray. For the analysis performed in the thesis at hand, TMEM132D expression data were extracted from the database and statistically analyzed revealing an increased TMEM132D gene expression in Aza-dC treated, i.e. DNA-demethylated, fibroblasts (Figure 3.10 B; $t = 3.314$, $df = 4$, $p = 0.030$), indicating that epigenetic mechanisms play an important role in the regulation of TMEM132D expression.

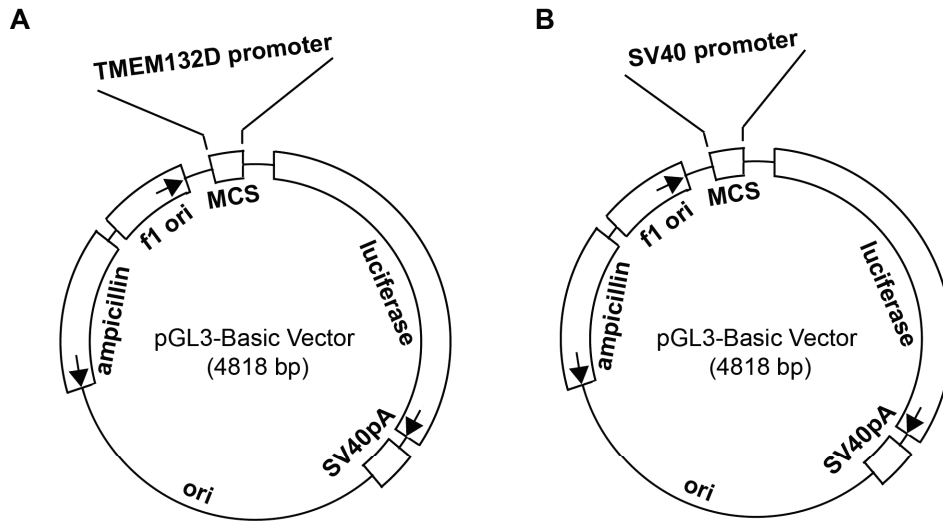


Figure 3.11.: **Cloning strategy of the TMEM132D promoter luciferase constructs.** TMEM132D promoter segments or, for cloning of a corresponding positive control vector, the simian virus 40 (SV40) promoter were inserted into the multiple cloning site (MCS) of the pGL3-Basic Vector that comprises a firefly luciferase element downstream of the MCS, followed by a SV40 polyadenylation site (SV40pA). The vector backbone additionally contains an ampicillin resistance element for selective amplification in *E. coli*; the origin of replication (ori) in *E. coli* and origin of replication derived from filamentous phage (f1 ori) are labeled.

3.3. Analysis of TMEM132D promoter activity in the oligodendrocytic MO3.13 cell line

In order to experimentally verify the promoter region identified *in silico*, a reporter gene analysis was performed with progressive 5' deletion mutants of the region spanning 5 kb upstream of the start codon, and thus including all three evolutionary conserved regions identified in this thesis (Figure 3.9). For this purpose, segments of the TMEM132D promoter region were isolated from human genomic DNA by PCR and cloned into the pGL3-basic reporter vector that encodes a firefly luciferase downstream of the multiple cloning site (MCS) and contains no further promoter or enhancer elements (Figure 3.11 A). As a positive control, the constitutively active simian virus 40 (SV40) promoter was inserted into the MCS of the pGL3-basic reporter vector (Figure 3.11 B), while the pGL3-basic vector without any inserts was used to determine the background firefly luciferase signal.

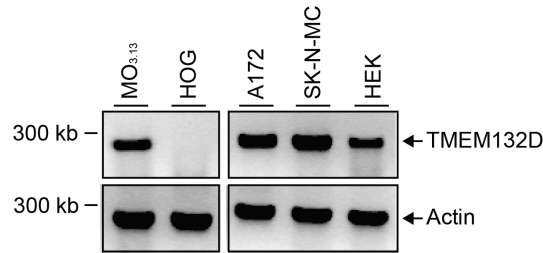


Figure 3.12.: **TMEM132D mRNA expression in neuronal and non-neuronal cell lines.** mRNA extracted from either the oligodendroglial cell lines MO3.13 or HOG, the astroglial cell line A172, the neuroblastoma cell line SK-N-MC, or the embryonic kidney cell line HEK293 was analyzed for expression of *TMEM132D* and, for control, β -actin mRNA by RT-PCR. n = 1; 2 technical replicates.

Due to the reported association of *TMEM132D* with oligodendrocyte differentiation (Nomoto et al., 2003), the reporter gene assays were performed in the human oligodendrocyte MO3.13 cell line (Buntinx et al., 2003), even though RT-PCR analyses performed here revealed also other neural (SK-N-MC, A172) and non-neural (HEK293) cell lines to express *TMEM132D* (Figure 3.12). *TMEM132D* expression has so far not been studied in cell lines but it has been previously reported to be expressed not only in brain tissue, but also in lung, pancreas, and testis (Nomoto et al., 2003).

To perform the reporter gene assay, both the firefly luciferase plasmid containing either the *TMEM132D* or the SV40 promoter (positive control) and the gaussia luciferase plasmid, which served as a control for normalization, were co-transfected into MO3.13 cells. The activity of the luciferases expressed by the transfected MO3.13 cells was assessed by measuring the bioluminescence emitted during enzymatic conversion of the respective luciferase substrates. For data evaluation the firefly luciferase activity was normalized to the gaussia luciferase activity resulting in a data value that corresponds to the activity of the promoter element tested. The different segments upstream of the *TMEM132D* start codon analyzed here exhibited promoter activity, i.e. were able to induce the expression of the luciferase gene in the reporter gene assay (Figure 3.13). Moreover, the first 604 bp upstream of the *TMEM132D* start codon were identified as the most potent promoter activating region (Figure 3.13). However, compared to the positive control, the SV40 promoter driven luciferase construct, *TMEM132D* promoter activity was rather low, reaching a maximum of approximately 7 % of the SV40

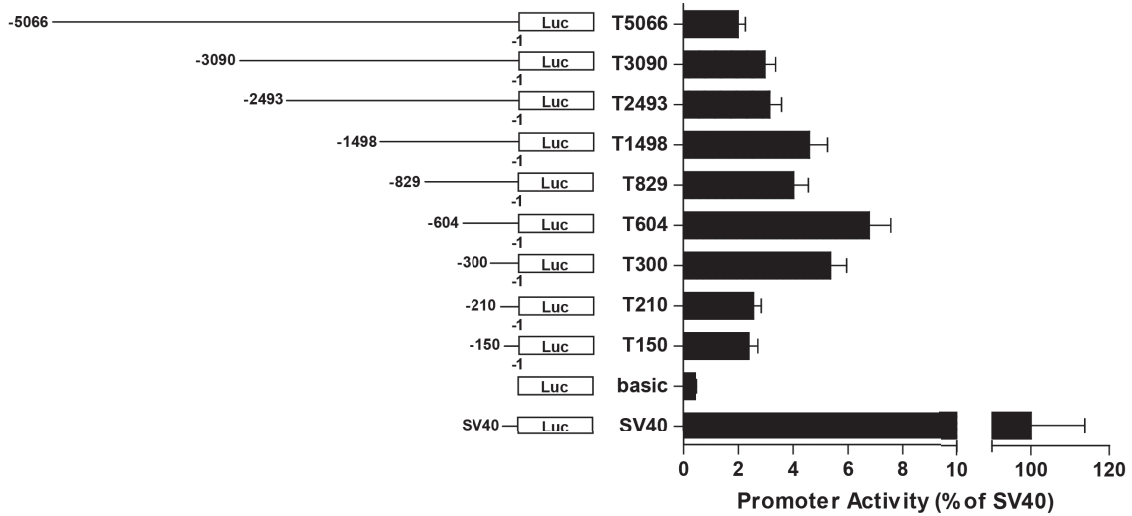


Figure 3.13.: **Reporter gene assay of 5' deletion mutants of the *TMEM132D* promoter sequence in MO3.13 cells.** Left site: scheme of 5' deletion constructs, indicated are the start sites of the construct relative to the start codon (position -1). The 'basic' construct contains no promoter sequences, i.e. is identical to the empty pGL3-basic vector representing the background signal. Right site: promoter activity of 5' deletion constructs is presented as percentage of the SV40 promoter activity set at 100 %. Values plotted are means \pm SEM of 3 independent experiments performed in triplicates.

promoter activity (Figure 3.13). Interestingly, the construct containing the 300 bp region upstream of the start codon exhibited no major decrease in luciferase activity when compared to the luciferase activity of the 604 bp construct, although the transcription start site (TSS) reported in the NCBI database is located at position 329 upstream of the start codon and thus is lacking in the 300 bp construct (Figure 3.14). Without expressing the core promoter elements for recruiting RNA polymerase II and for subsequent initiation of transcription, one would expect the promoter activity of the 300 bp construct to be considerably reduced. The fact that this was not the case points at the importance of the alternative TSS which was identified by Gene2Promoter analysis and is identical with the start codon (Figure 3.7) as well as the potential TSS that is located approximately 75 bp upstream of the start codon and was suggested by the presence of the initiator element identified by MatInspector analysis (Figure 3.8). In addition, the functionality of these alternative TSS are further supported by the 150 bp *TMEM132D* promoter construct which still exhibits considerably higher promoter activity than the empty pGL3-basic luciferase construct (Figure 3.13).

3.3. Analysis of TMEM132D promoter activity in the oligodendrocytic MO3.13 cell line

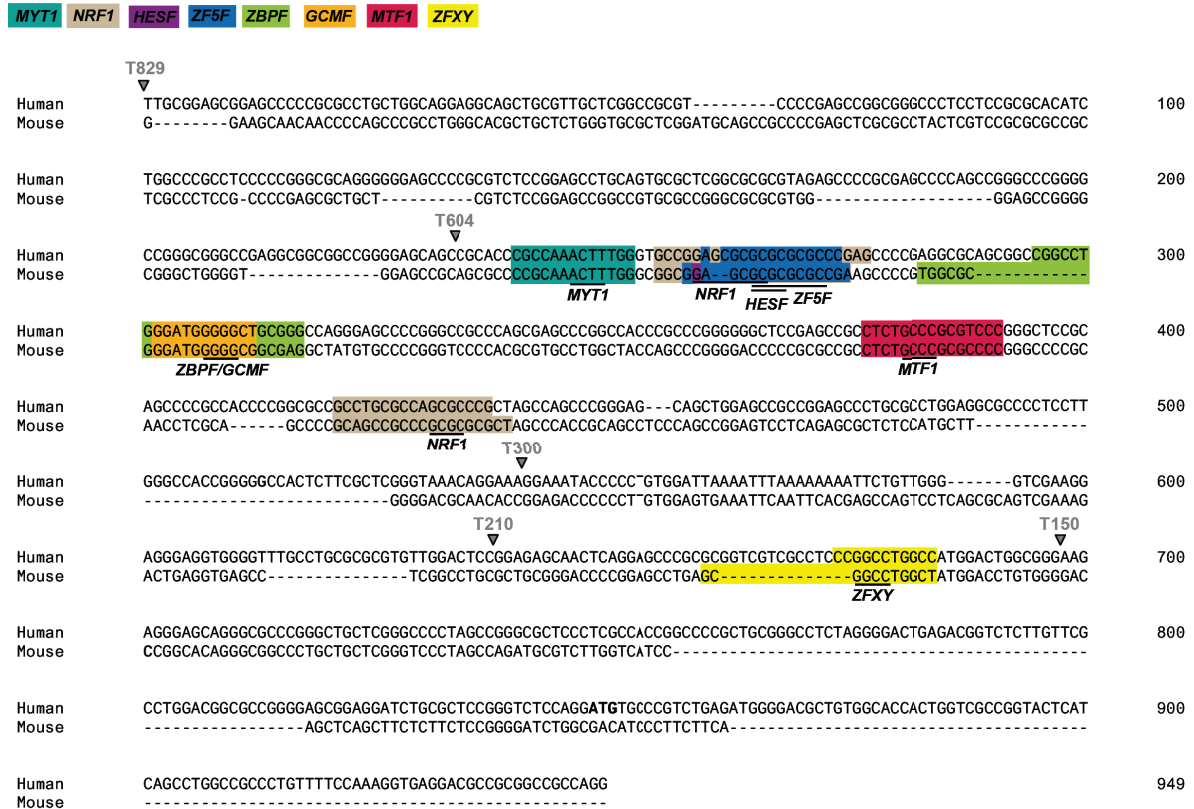


Figure 3.14.: **Conserved transcription factor binding sites in the TMEM132D core promoter.** Alignment of the murine and human nucleotide sequence of the TMEM132D promoter sequence identified by Gene2Promoter. Indicated are the start sites of the 5' deletion constructs (arrowheads) as well as conserved transcription factor binding sites (colored, core sequence is underlined) subjected to deletion analysis as depicted in Figure 3.17. The start codon of the human sequence is printed in bold.

Next, the impact of different regulatory elements on promoter activity was addressed. For this purpose, the impact of transcription factor binding sites conserved in the human and murine promoter sequence (highlighted in Figure 3.14 and described in Table 3.1; see also Figure 3.7) on TMEM132D promoter activity was analyzed in reporter gene assays. To analyze the functionality of the conserved TFBSs identified *in silico*, reporter gene assays using TMEM132D promoter constructs with mutated, i.e. dysfunctionalized, TFBS were performed. Mutated TMEM132D promoter constructs were generated by site-directed mutagenesis (Figure 3.15): primers introducing the dysfunctionalizing mutation were designed. Using these primers and the long-range DNA polymerase Herculanase the complete TMEM132D

3. Results I: Transcriptional regulation of the human *TMEM132D* gene

Table 3.1.: **Conserved transcription factor binding sites in the *TMEM132D* promoter.** Listed are transcription factor binding sites conserved in the human and murine sequence of the *TMEM132D* promoter shown in Figure 3.14 as well as the description of their biological functions according to the respective gene ontology (GO)-terms.

Transcription factor family	Transcription factors	Description
HESF (Vertebrate homologues of enhancer of split complex)	BHLHB2, BHLHB3, HELT, HES1, HES2, HES3, HES4, HES5, HES6, HES7, HEY1, HEY2, ITGB3BP	notch signaling, negative regulation of neuron differentiation
NRF1 (Nuclear respiratory factor 1)	NRF1	response to cold and stress
ZF5F (ZF5 POZ domain zinc finger)	ZFP161	negative regulation of transcription
MYT1 (Myelin transcription factor)	MYT1, MYT1L, ST18	regulates oligodendrocyte differentiation; downregulation in mature oligodendrocytes
ZBPF (Zinc binding protein factors)	ZNF148, ZNF202, ZNF219, ZNF281	negative regulation of transcription; cellular defense, lipid metabolism
GCMF (Chorion-specific transcription factors with a GCM DNA binding domain)	GCM1, GCM2	astrocyte fate, anatomical structure morphogenesis, absence of GCM: neuron development; presence of GCM: development of neurons and glia (astrocytes)
MTF1 (Metal induced transcription factor)	MTF1, MTF2	response to metal ion, positive regulation of transcription
ZFX (Zfx and Zfy - transcription factors implicated in mammalian sex determination)	ZFX	endocrine system, embryonic structures

promoter plasmid was amplified generating a TFBS mutation containing plasmid. Finally, the template plasmid was enzymatically degraded as schematically illustrated in Figure 3.15.

Except for the ZFX site, all TFBS were located in the region 300 bp to 604 bp upstream of the start codon. According to the results of the reporter gene assay performed with the 5' deletion mutants, in which promoter activity of the 300 bp construct was slightly lower compared to the 604 bp construct, it was expected that the conserved TFBS exert at least in part activating

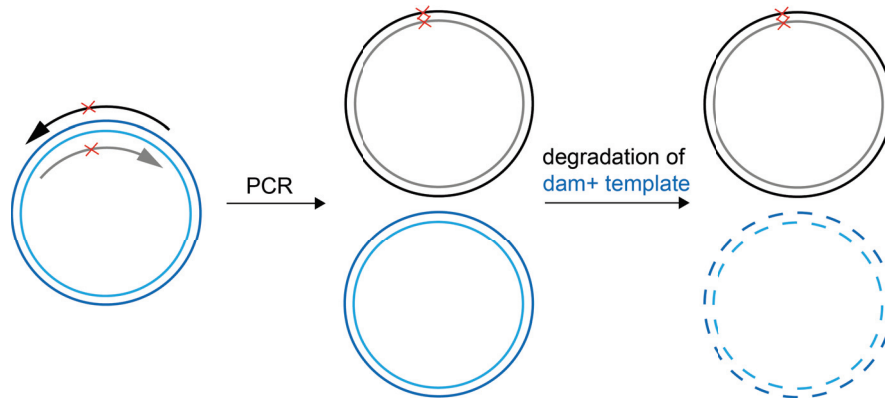


Figure 3.15.: **Site-directed mutagenesis of selected transcription factor binding sites.** PCR-based amplification of the template plasmid using primers introducing the respective mutation was followed by subsequent enzymatic degradation with the restriction endonuclease *dpnI*, which recognizes DNA adenine methylase (*dam*) methylation of DNA introduced during replication in *E. coli*.

effects on promoter activity, i.e. that mutation of these binding sites would decrease the activity of the 604 bp promoter construct. Surprisingly, the promoter activity was found to be increased when the conserved transcription factor binding sites for MYT1, HESF, GCMF, ZBPF, and MTF1 were mutated in the 604 bp TMEM132D promoter construct (Figure 3.17 A; MYT1del: $t = 3.048$, $df = 34$, $p = 0.004$; HESFdel: $t = 2.990$, $df = 34$, $p = 0.005$; HESFmut: $t = 1.807$, $df = 25$, $p = 0.083$; GCMF/ZBPF: $t = 3.059$, $df = 34$, $p = 0.004$; MTF1: $t = 2.094$, $df = 34$, $p = 0.044$), indicating an inhibitory effect of these binding sites on TMEM132D promoter activity. Mutation of binding sites for ZF5F and ZFX Y, however, had no effect on promoter activity (Figure 3.17 A; ZF5Fmut: $t = 0.367$, $df = 25$, $p = 0.717$; ZFX Ydel: $t = 0.991$, $df = 34$, $p = 0.329$). Two conserved NRF1 sites were mutated, the more distal one increased promoter activity (Figure 3.17 A; NRF1mut: $t = 2.065$, $df = 25$, $p = 0.049$), while the more proximal did not influence it (Figure 3.17 A; NRF1del: $t = 0.691$, $df = 34$, $p = 0.494$).

To further confirm these results, selected transcription factors (TF) binding to the conserved binding sites (TF \rightarrow TFBS: MYT1L \rightarrow MYT1, HES1 \rightarrow HESF, NRF1 \rightarrow NRF1, ZFP161 \rightarrow ZF5F, ZNF219 \rightarrow ZFBP, GCM1 \rightarrow GCMF, MTF1 \rightarrow MTF1, ZFX \rightarrow ZFX Y) were cloned into a pcDNA3.1(-) expression vector and were overexpressed together with the wildtype 604 bp TMEM132D promoter construct in MO3.13 cells to study the influence of these

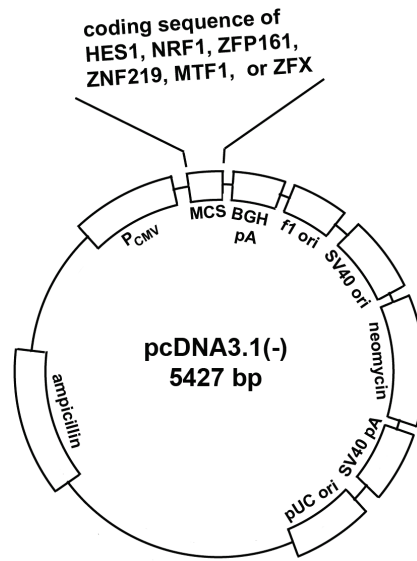


Figure 3.16.: **Cloning strategy of transcription factor expression plasmids.** The coding sequence (open reading frame) of the human HES1, NRF1, ZFP161, ZNF219, MTF1, or ZFX gene was inserted into the multiple cloning site (MCS) of the pcDNA3.1(-) vector. A constitutively active CMV promoter element (P_{CMV}) is located upstream of the MCS, and a bovine growth hormone polyadenylation (BGHpA) is located downstream of the MCS. The vector backbone additionally contains an ampicillin resistance gene for selective amplification in *E. coli*, as well as a neomycin resistance gene for selective amplification in eukaryotic cells. Additional abbreviations used: f1 ori - origin of replication derived from filamentous phage; SV40 ori - simian virus 40 promoter and origin of replication; SV40pA - simian virus 40 polyadenylation site; pUC ori - origin of replication of pUC vector

transcription factors on *TMEM132D* promoter activity in a reporter gene assay (Figure 3.17 B). For cloning, the coding sequence of human HES1, NRF1, ZFP161, ZNF219, MTF1, and ZFX was amplified from reverse transcribed human mRNA and inserted into the multiple cloning site of the pcDNA3.1(-) vector (Figure 3.16). Expression plasmids for MYT1L and GCM1 were purchased from PlasmID (see section 2.3.3). The subsequently performed reporter gene assay confirmed the inhibitory effect of MYT1L/MYT1, HES1/HESF, ZNF219/ZFBP, GCM1/GCMF, and MTF1/MTF1 that was suggested previously by the TFBS mutation analysis (Figure 3.17 B; MYT1L: $t = 5.863$, $df = 13$, $p < 0.001$; HES1: $t = 4.008$, $df = 25$, $p < 0.001$; ZNF219: $t = 3.301$, $df = 25$, $p = 0.003$; GCM1: $t = 6.518$, $df = 13$, $p < 0.001$; MTF1: $t = 4.735$, $df = 16$, $p < 0.001$). Additionally, the inactivity of the ZF5F site, as shown

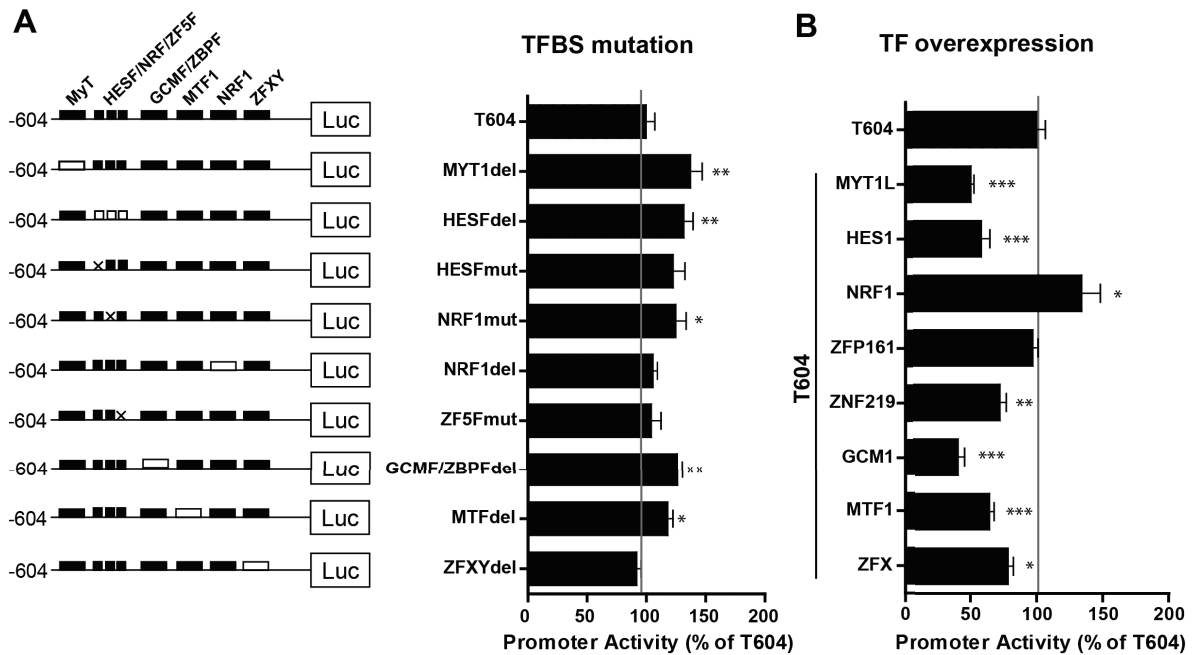


Figure 3.17.: **Reporter gene assays in MO3.13 cells analyzing the effect of conserved transcription factor binding sites.** (A) Left site: scheme of transcription factor binding site mutation, empty boxes indicate deletion mutations, x indicates point mutations. Right site: results of the reporter gene assay showing the promoter activity of the mutated *TMEM132D* promoter constructs. (B) Overexpression of transcription factors binding to the respective binding sites and measurement of the activity of the wildtype T604 promoter construct in the reporter gene assay. Promoter activity (after normalization to SV40 promoter activity) is represented as percentage of the wildtype T604 promoter construct set at 100 %. Values plotted are means \pm SEM of 3 independent experiments in triplicates. Statistical significance was calculated using student's *t*-test to compare each group to the control group, i.e. the wildtype T604 *TMEM132D* promoter, and is indicated by *** $p < 0.001$, ** $p < 0.01$, * $p < 0.05$.

by overexpression of ZFP161, was confirmed (Figure 3.17 B; ZFP161: $t = 0.395$, $df = 25$, $p = 0.696$). In contrast to the results of the TFBS mutation analyses (Figure 3.17 A), NRF1 overexpression resulted in increased promoter activity (Figure 3.17 B; NRF1: $t = 2.276$, $df = 15$, $p = 0.038$) and ZFX overexpression led to a weak decrease of promoter activity (Figure 3.17 B; ZFX: $t = 2.778$, $df = 16$, $p = 0.013$), although the previously performed mutation of the ZFX site had no effect on promoter activity.

The binding sites analyzed above were all located between 604 bp and 300 bp and thus cannot elicit the prominent differences in promoter activity between the T829 and T604 constructs as

3. Results I: Transcriptional regulation of the human *TMEM132D* gene

```

1 TTGCGGAGCG GAGCC604CCCCG GCCTGCTGGC AGGAGGCAGC TGCCTTGCTC GGCCGCGTCC
      EGRF
61 CCGAGCCGGC GGGCCCTCCT CCGCGCACAT CTGGCCCGCC TCCCCGGGC GCAGGGGGGA
      NFKB
      MZF1
121 GCCCCGCGTC TCCGGAGCCT GCAGTGCCT CGGCGCGCT AGAGCCCCGC GAGCCCCAGC
      SP1
181 CGGGCCCGGG GCGGGGCGG CCGAGGGCGG GGCCGGGAG CAGCGCACC CGCCAAACTT
      SP1
241 TGGGTGCCGG AGCGCGCGCG CGCCGAGCC CCGAGGCGCA GCGGCCGGCC TGGGATGGGG
301 GCTGCGGGCC AGGGAGCCCC GGGCCGCCCA GCGAGCCCG CCACCCGCC GGGGGGCTCC
361 GAGCCGCCTC TGCCCGCGTC CCGGGCTCCG CAGCCCCGCC ACCCCGGCGC CGCCTGCGCC
421 AGCGCCCGCT AGCCAGCCCG GGAGCAGCTG GAGCCGCCG AGCCCTGCGC CTGGAGGCGC
481 CCCTCCTTGG GCCACCGGG GCCACTCTT GCTCGGGTAA ACAGGAAAG300 AAATACCCC
541 TGTGGATTAA AATTTAAAA AAATTCTGTT GGGTCTGAAG GAGGGAGGTG GGGTTTGCCT210
      HAML
601 GCGCGCGTGT TGGACTCCG AGAGCAACTC AGGAGCCCG GCGGTCGTGC CCTCCCGGCC
      150
661 TGGCCATGGA CTGGCGGGA GAGGGAGCAG GGCGCCGGG CTGCTCGGGC CCCTAGCCGG
721 GCGCTCCCTC GCCACCGGCC CCGTGCGGG CCTCTAGGG ACTGAGACGG TCTTTGTTC
781 GCCTGGACGG CGCCGGGAG CGGAGGATCT GCGTCCGGG TCTCCAGGAT GTGCCCGTCT
841 GAGATGGGGA CGCTGTGGCA CCACTGGTCG CCGTACTCA TCAGCCTGGC CGCCCTGTTT
901 TCAAAGGTG AGGACGCCGC GGCCGCCAGG

```

Figure 3.18.: **Additional transcription factor binding sites in the *TMEM132D* promoter sequence.** The core sequence of additional transcription factor binding sites in the *TMEM132D* promoter identified with Matinspector and TFSEARCH (see also Figure 3.7) is highlighted by red frames. The start sites of the 5' deletion mutants are indicated. The start codon is printed in bold.

well as between the T300 and T210 constructs. To address these promoter subregions potential TFBS identified by Matinspector were compared with TFBS found by the alternative tool TFSEARCH (<http://www.cbrc.jp/research/db/TFSEARCH.html>), as illustrated in Figure 3.7. The TFBS identified in both Matinspector and TFSEARCH analysis (summarized in Table 3.2 and Figure 3.18) were then mutated by site-directed mutagenesis as described above (Figure 3.15), and reporter gene assays were performed.

As expected from the reporter gene assays with the progressive 5' deletion analysis (Figure 3.13), mutation of the NFKB/MZF1 site as well as the SP1 site in the T829 promoter construct

Table 3.2.: **Additional transcription factor binding sites in the *TMEM132D* promoter sequence identified with MatInspector and TFSEARCH.** Presented are names and abbreviations of the identified transcription factor families as well as the description of their biological functions according to the respective gene ontology (GO)-terms.

Transcription factor family	Transcription factors	Description
MZF1 (Myeloid zinc finger 1)	MZF1	hematopoiesis
EGRF (Early growth response family)	EGR1, EGR2, EGR3, EGR4, WT1	differentiation, mitogenesis
NFKB (Nuclear factor of kappa light polypeptide gene enhancer in B-cells)	NFKB1, NFKB2	negative regulation of cytokine production, toll-like receptor signaling pathway
SP1 (Specificity protein 1)	SP1	trophectodermal cell differentiation, ossification, liver development
HAML (Human acute myelogenous leukemia factors)	AML1, AML2, AML3	induction of apoptosis, axon guidance, cell proliferation

resulted in an increased promoter activity (Figure 3.19 A; NFKBmut: $t = 3.273$, $df = 16$, $p = 0.005$; SP1mut: $t = 4.801$, $df = 16$, $p < 0.001$). In contrast, mutating the EGRF site led to a weak but significant decrease in promoter activity (Figure 3.19 A; EGRF: $t = 2.700$, $df = 16$, $p = 0.016$). Nevertheless, these analyses suggest that overall the TFBS sites in the region between T829 and T604 analyzed here have an inhibitory effect on promoter activity, which could explain the increased promoter activity of the T604 construct compared to the T829 construct (Figure 3.13). However, this does not exclude that also other binding sites that have not been analyzed here modulate *TMEM132D* promoter activity. Next, transcription factors binding to these TFBS were overexpressed: all transcription factor expression plasmids used in this assay were purchased from PlasmID (see section 2.3.3). Overexpression of MZF1, NFKB1, and SP1 together with the wildtype T829 promoter construct confirmed the inhibitory effect of these transcription factors on *TMEM132D* promoter activity (Figure 3.19 B; MZF1: $t = 14.78$, $df = 22$, $p < 0.001$; NFKB1: $t = 10.26$, $df = 22$, $p < 0.001$; SP1: $t = 11.22$, $df = 22$, $p < 0.001$). The activating effect of the EGFR site, however, could not be validated by overexpressing WT1 (Figure 3.19 B; WT1: $t = 2.681$, $df = 22$, $p = 0.014$). To analyze the strong decrease in promoter activity of the T210 construct compared to the T300 construct

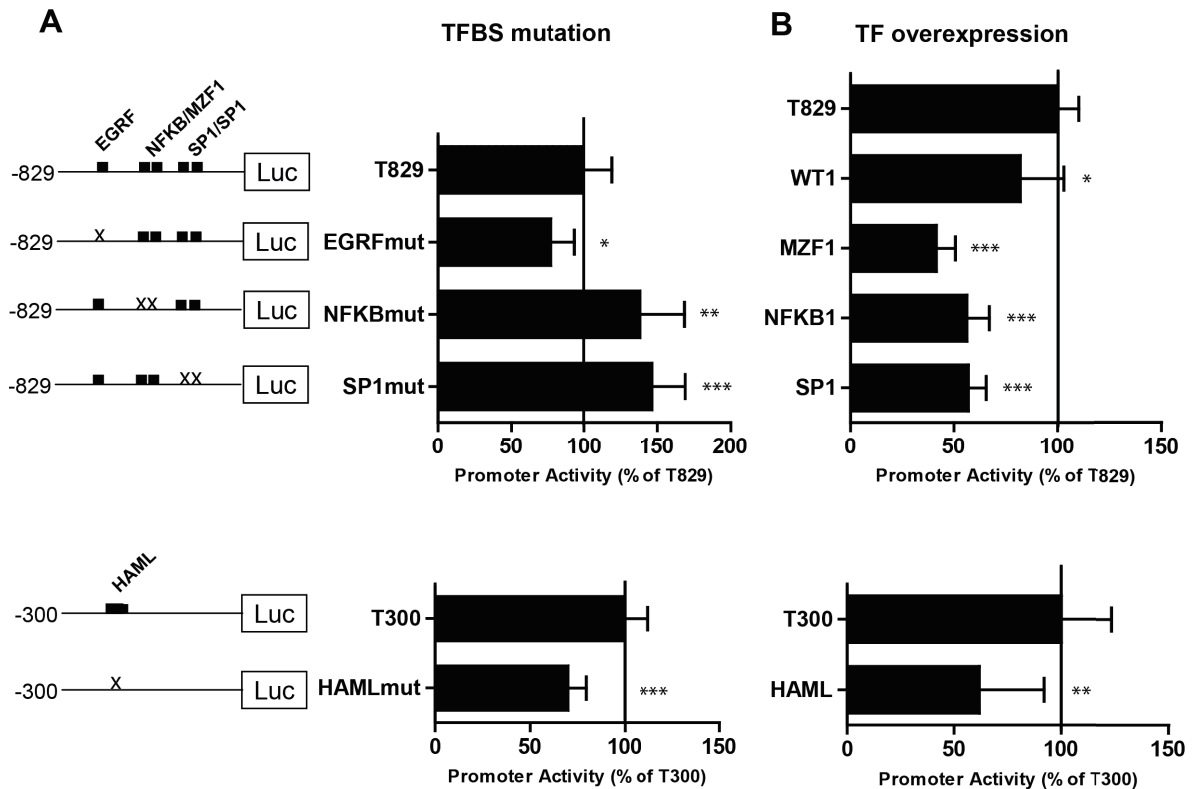


Figure 3.19.: **Reporter gene assays in MO3.13 cells analyzing the effect of additional transcription factor binding sites.** (A) Left site: scheme of transcription factor binding site mutation. Right site: results of the reporter gene assay showing the promoter activity of the mutated TMEM132D promoter constructs. (B) Overexpression of transcription factors binding to the respective binding sites and measurement of the activity of the wildtype T829 or T300 promoter construct in the reporter gene assay. Promoter activity (after normalization to SV40 promoter activity) is represented as percentage of the wildtype T829 or T300 promoter construct set at 100 %. Values plotted are means \pm SEM of 3 independent experiments in triplicates. Statistical significance was calculated using student's *t*-test to compare each group to the control group, i.e. the wildtype TMEM132D promoter activity, and is indicated by *** $p < 0.001$, ** $p < 0.01$, * $p < 0.05$.

that has been observed in the 5' deletion analysis (Figure 3.13), the HAML binding site was mutated in the T300 construct resulting in reduced promoter activity (Figure 3.19 A; HAMLmut: $t = 5.761$, $df = 16$, $p < 0.001$). This indicates that this activating TFBS might be responsible for the drop of promoter activity of the T210 promoter construct. Overexpression of HAML, however, did not confirm this effect (Figure 3.19 B; HAML: $t = 2.987$, $df = 16$, $p = 0.009$).

Taken together, reporter gene analysis of the 5' sequence upstream of the start codon and mutation of TFBS as well as overexpression of the respective transcription factors revealed several candidate TFBS important for regulation of TMEM132D gene expression, namely MYT1, HES1, ZNF219, MTF1, MZF1, NFkB1, and SP1, while the other transcription factors analyzed here either did not influence TMEM132D promoter activity (ZFX, ZFP161) or exhibited variable, contradictory results in the TFBS mutation analysis and the TF overexpression analysis (NRF1, EGRF, HAML).

3.4. Transcriptional regulation of TMEM132D during oligodendrocyte differentiation

Next, the 13 transcription factors analyzed above, namely MYT1, HES1, ZNF219, GCM1, MTF1, MZF1, NFkB1, SP1, ZFX, ZFP161, NRF1, WT1, and HAML were studied for their role in regulating TMEM132D expression in the context of oligodendrocyte differentiation in a cell culture assay. It has been shown that TMEM132D is expressed in mature oligodendrocytes, while immature oligodendrocytes lack TMEM132D expression (Nomoto et al., 2003). To confirm this finding the human oligodendrocyte cell line MO3.13 was treated with serum-free medium containing 100 nM phorbol 12-myristate 13-acetate (PMA) for 3 days, which has been previously shown to effectively induce differentiation in this cell line (Buntinx et al., 2003). Differentiation was reflected by a substantially changed morphology mainly characterized by the outgrowth of processes and an overall flattening of the cells (Figure 3.20).

As expected from the findings of Nomoto et al. (2003), TMEM132D gene expression was upregulated in response to PMA treatment (Figure 3.21; $t = 4.676$, $df = 8$, $p = 0.001$). Next, the expression of transcription factors identified here to regulate TMEM132D promoter activity was compared between non-differentiated and PMA-differentiated cells. Indeed, several of the transcription factors identified as inhibitors of TMEM132D promoter activity, namely MYT1, HES1, ZNF219, and SP1, were found to be downregulated in differentiated MO3.13 cells, which was paralleled by the upregulation of TMEM132D expression in the

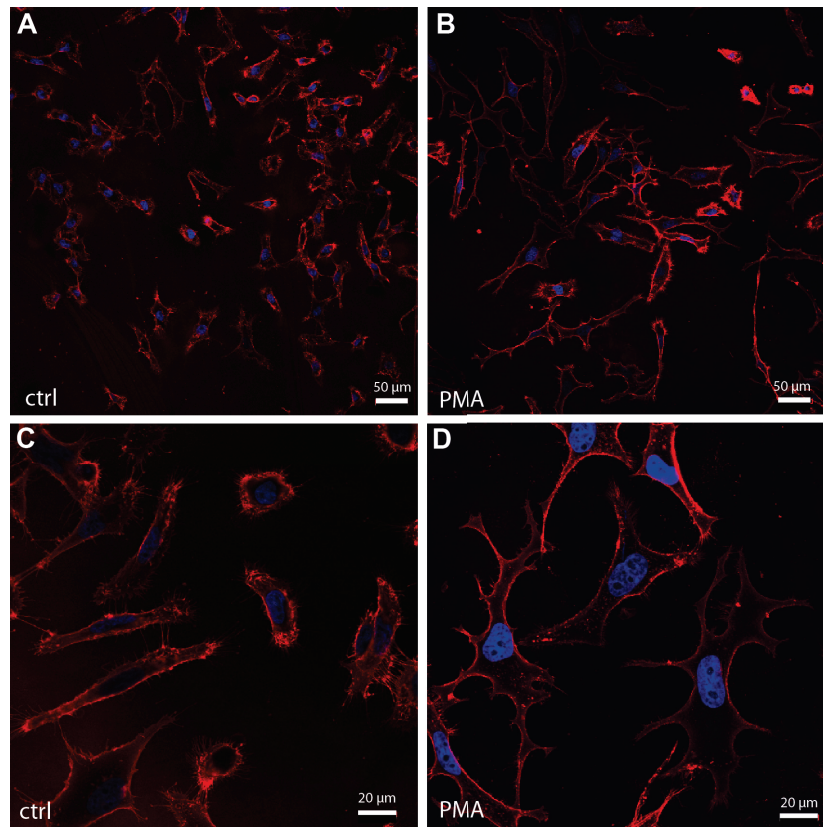


Figure 3.20.: **PMA-induced differentiation of MO3.13 oligodendrocytic cells.** MO3.13 cells were treated with 100 nM PMA to induce differentiation. After 3 days of treatment, cells were fixed and stained with the fluorescently labeled cell surface marker wheat-germ-agglutinin (WGA). Nuclei were counterstained with DAPI (blue). Presented are images of representative cell batches; $n = 5$ per treatment group from two independent experiments. The scalebar is $50 \mu\text{m}$ in (A, B) and $20 \mu\text{m}$ in (C, D).

differentiated cells (Figure 3.21; MYT1: $t = 3.423$, $df = 8$, $p = 0.009$; HES1: $t = 10.690$, $df = 8$, $p < 0.001$; ZNF219: $t = 4.604$, $df = 8$, $p = 0.002$; SP1: $t = 2.691$, $df = 8$, $p = 0.028$). GCM1 and WT1 could not be detected in MO3.13 cells and all the other detected transcription factors were not significantly altered and thus do not seem to be involved in the oligodendrocyte differentiation process (Figure 3.21; MTF1: $t = 0.081$, $df = 8$, $p = 0.938$; NRF1: $t = 1.295$, $df = 8$, $p = 0.231$; ZFP161: $t = 0.244$, $df = 8$, $p = 0.813$; ZFX: $t = 1.556$, $df = 8$, $p = 0.158$; NFKB1: $t = 1.363$, $df = 8$, $p = 0.210$; HAML: $t = 0.682$, $df = 8$, $p = 0.515$; MZF1: $t = 0.779$, $df = 8$, $p = 0.458$). However, they might still have an impact on *TMEM132D* regulation in other biological contexts.

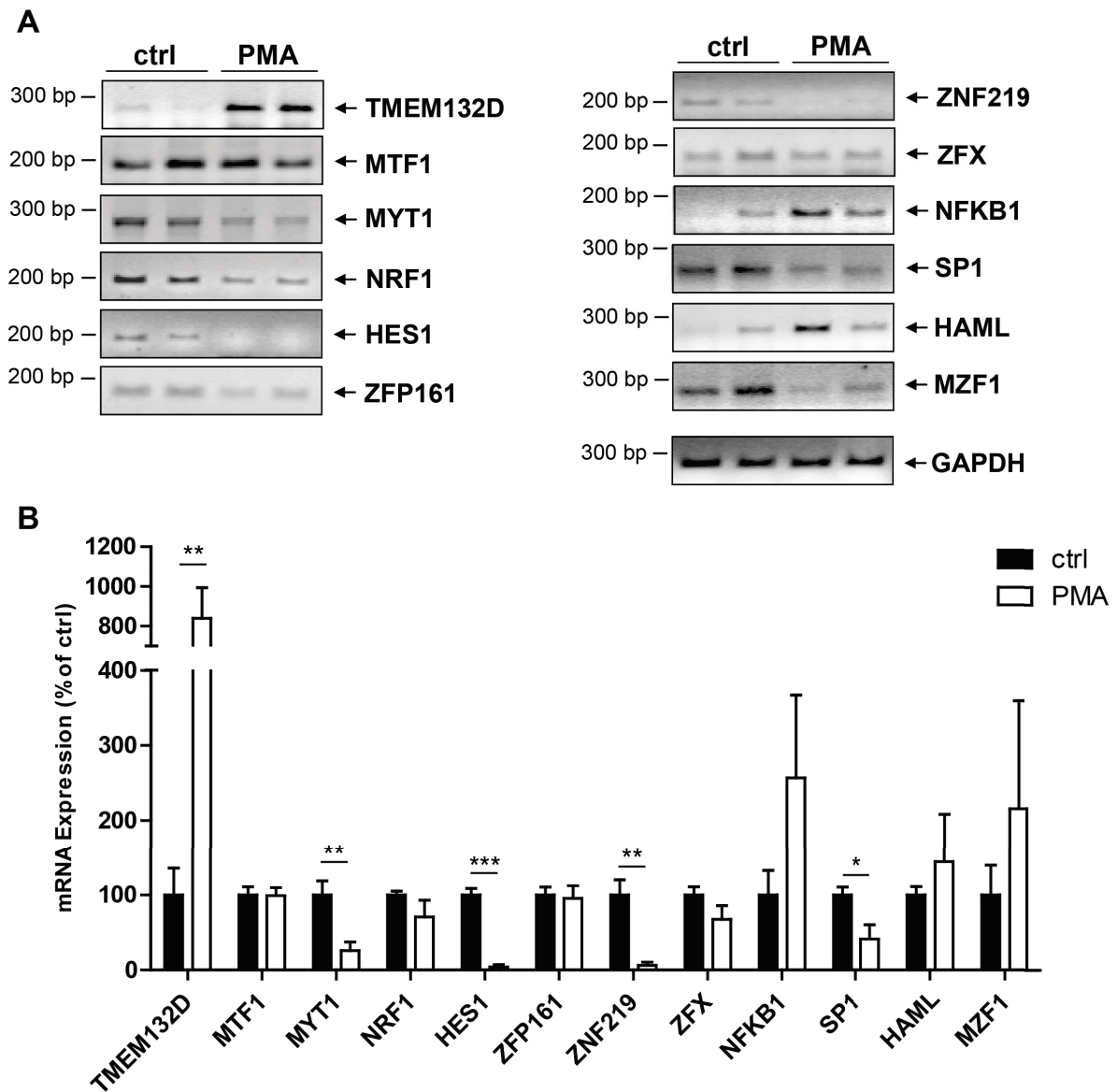


Figure 3.21.: mRNA expression levels of *TMEM132D* and candidate transcription factors in differentiated and non-differentiated oligodendrocytic MO3.13 cells. (A) RT-PCR analysis of *TMEM132D* and the transcription factors MTF1, MYT1, NRF1, HES1, ZFP161, ZNF219, ZFX, NFKB1, SP1, HAML, MZF1 in non-differentiated and PMA-differentiated MO3.13 cells. (B) Quantification of (A). Expression values were normalized to constitutive GAPDH expression and are presented as percentage of those of control cells (% of control). Plotted data are means \pm SD, $n = 5$ from two independent experiments. Statistical significance was calculated using student's *t*-test and is indicated by *** $p < 0.001$, ** $p < 0.01$, * $p < 0.05$.

3. Results I: Transcriptional regulation of the human *TMEM132D* gene

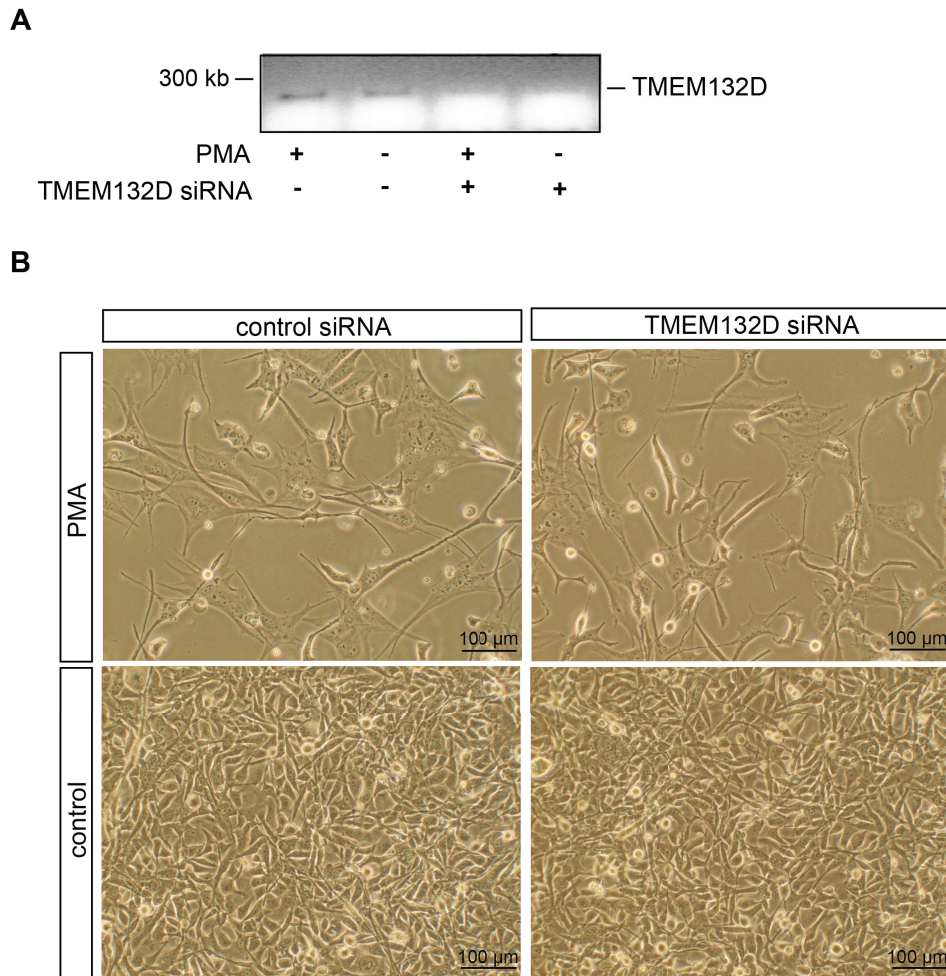


Figure 3.22.: **Impact of *TMEM132D* knockdown on oligodendrocyte differentiation.** (A) RT-PCR analysis of *TMEM132D* expression in MO3.13 cells treated either with control or PMA-containing medium and transfected with either control siRNA or *TMEM132D* specific siRNA, $n = 3$ per treatment group. (B) Representative images of analyzed samples ($n = 3$). Microscopic analysis of cell morphology revealed no influence of *TMEM132D* knockdown on MO3.13 differentiation.

To further analyze the impact of *TMEM132D* on oligodendrocyte differentiation, MO3.13 cells were transfected with either *TMEM132D* siRNA to diminish *TMEM132D* expression or with control siRNA, which leaves *TMEM132D* expression undisturbed, and these transfected cell batches were compared regarding their differentiation properties. Although the siRNA-mediated knockdown clearly reduced, but not completely abolished, *TMEM132D* transcript levels in MO3.13 cells by approximately 70 % (Figure 3.22 A), these cells exhibited no obvious morphological differences after PMA treatment, i.e. their differentiation resulted

in a cellular morphology microscopically indistinguishable from that of differentiated cells transfected with control siRNA (Figure 3.22 B). This indicates that either tiny levels of TMEM132D expression are sufficient to mediate oligodendrocyte differentiation, or, although TMEM132D expression is upregulated during this differentiation process, it might not be absolutely necessary for it - at least in the oligodendrocyte model tested here.

3.5. Summary of Results I

To sum up, experimental analysis of the transcription factor binding sites in the TMEM132D promoter region predicted *in silico* revealed eight inhibitory transcriptional regulators of TMEM132D gene expression, i.e. HES1, MYT1, ZNF219, GCM1, MTF1, NFKB1, MZF1, and SP1. Employing a cell culture model of oligodendrocyte differentiation the previously published increase in TMEM132D gene expression in differentiated oligodendrocytes (Nomoto et al., 2003) was confirmed. Furthermore, gene expression levels of a subset of the identified inhibitory transcriptional regulators of TMEM132D gene expression, i.e. HES1, MYT1, ZNF219, and SP1, were found to be decreased in the population of differentiated oligodendrocytes suggesting these transcription factors to be essential for the differentiation associated upregulation of TMEM132D mRNA levels. The role of TMEM132D in oligodendrocyte differentiation, however, remains unclear: searching for conserved protein domains *in silico* revealed a conserved cohesin-like domain in the extracellular region of the TMEM132D protein suggesting a potential role of TMEM132D in cell adhesion processes. Nevertheless, oligodendrocyte differentiation could not be prevented by TMEM132D knock-down, indicating that either the residual TMEM132D levels suffice to mediate differentiation or that TMEM132D upregulation is not the sole determining factor in the oligodendrocyte differentiation process.

4. Results II: Identification of PTSD candidate proteins in a mouse model of PTSD

To identify novel PTSD protein biomarkers, expression levels of a set of selected candidate proteins was compared in different brain regions and in the blood of traumatized and mock treated control mice (PTSD mouse model was introduced in section 1.5.1).

4.1. Behavioral analyses (PTSD mouse model)

Trauma-related symptoms, i.e. the conditioned fear response and the generalized fear response as well as hyperarousal, were assessed in male C57BL/6NCrl mice 28-30 days after subjecting them to an electrical footshock or to control treatment (no shock) (Figure 4.1 A), respectively. As expected and published previously (Siegmund and Wotjak, 2007; Golub et al., 2011), shocked mice exhibited a PTSD-like syndrome. Here, the behavioral characteristics of this PTSD-like syndrome are exemplified by showing representative data of mouse batch PTSD I (see Table 2.2 for an overview of all mouse batches employed in this thesis). In particular, hyperarousal was assessed by measuring the amplitude of the acoustic startle response to noise bursts of different intensities, namely 50, 75, 90, 105, and 115 dB. The amplitude of the acoustic startle response was significantly increased in shocked mice compared to non shocked mice (Figure 4.1 B; $F_{1,28shock} = 6.39$, $p = 0.017$) and showed an interaction with noise burst intensity (Figure 4.1 B; $F_{4,116INTxshock} = 2.91$, $p = 0.024$), thus confirming previously published results (Golub et al., 2011). The generalized fear response was tested by measuring the freezing response in two experimental contexts differing in several features from the shock context. As expected, shocked mice exhibited a significantly increased freezing response in both environments, i.e. first, in a neutral context differing completely from the shock context

4. Results II: Identification of PTSD candidate proteins in a mouse model of PTSD

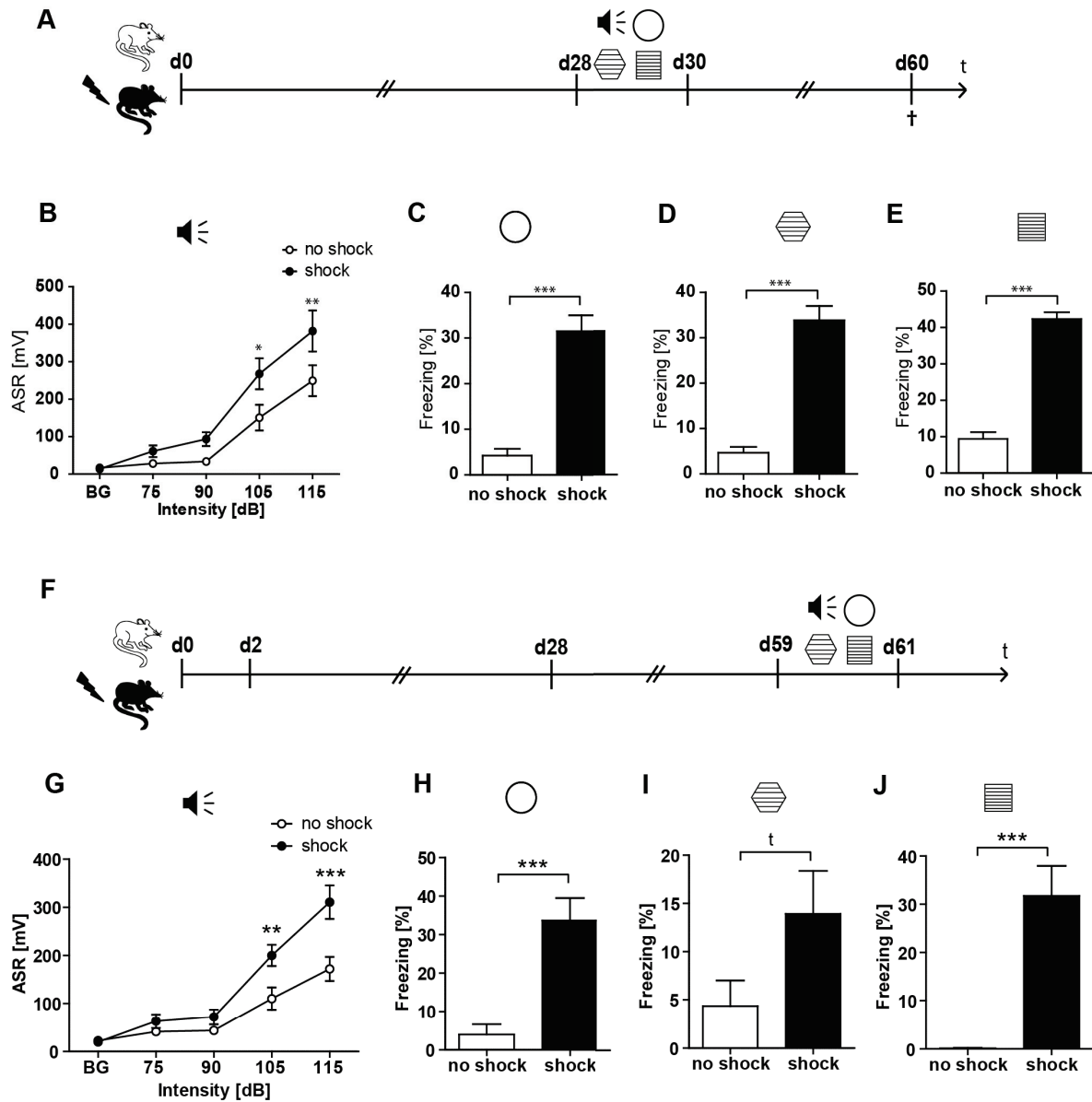


Figure 4.1.: **Behavioral analyses in the PTSD mouse model.** Course of experiment: C57BL/6NCrl mice were subjected to a single electric footshock and behavioral testing was performed on days 28-30 (A-E) or on days 59-61 (F-J): To assess hyperarousal the acoustic startle response (ASR) was measured at 50 dB (background, BG), 75, 90, 105, and 115 dB (B,G). Fear generalization was assessed by measuring the freezing response both in a neutral context (C,H) and in a grid context similar to the shock chamber (D,I). The conditioned fear response was tested by measuring the freezing response in the shock context (E,J). Freezing duration was normalized to the 3 min observation intervals (% freezing). Presented data are means \pm SEM, $n = 16$ (Batches PTSD I and V, see Table 2.2). Statistical analysis was performed using student's t -test and, in case of the acoustic startle response (ASR), using two-way repeated measures ANOVA and is indicated by t $p < 0.1$, * $p < 0.05$, ** $p < 0.01$, *** $p < 0.001$. Figure adopted from (Herrmann et al., 2012)

(Figure 4.1 C; $t = 7.442$, $df = 29$, $p < 0.001$) and second, in an experimental context displaying the metal grid as a dominant reminder of the shock context (Figure 4.1 D; $t = 8.582$, $df = 28$, $p < 0.001$), indicating an increased generalized fear response. Finally, the conditioned fear response, assessed by analyzing the freezing response in the shock context, was increased in shocked mice (Figure 4.1 E; $t = 12.36$ $df = 29$, $p < 0.001$), confirming previously published data (Siegmund and Wotjak, 2007). Taken together, 28 days after exposure to the electric footshock, shocked mice exhibited a PTSD-like syndrome, i.e. an increased acoustic startle response as well as increased conditioned and generalized fear responses. For subsequent molecular analyses, these mice were sacrificed 30 days after termination of the behavioral testing, i.e. on day 60 after footshock. In a different batch of mice, batch PTSD V, the PTSD-like behavior, i.e. increased acoustic startle response as well as increased generalized and conditioned fear responses, was demonstrated to persist for at least 60 days after footshock (Figure 4.1 G, acoustic startle response d59-61: $F_{1,28shock} = 21.490$, $p < 0.001$; $F_{4,140INTxshock} = 4.710$, $p = 0.001$; Figure 4.1 H, neutral context d59-61: $t = 4.423$, $df = 28$, $p < 0.001$; Figure 4.1 I, grid context d59-61: $t = 1.787$, $df = 28$, $p = 0.085$; Figure 4.1 J, shock context d59-61: $t = 4.868$, $df = 23$, $p < 0.001$).

4.2. Screening for PTSD candidate molecules

Potential candidate proteins were selected and compared between shocked and non shocked mice at different time-points after shock and in different brain regions. First, expression levels of neurostructural marker proteins and proteins of the glutamatergic system, which was found associated both with animal models of stress (Knox et al., 2010) and animal models of anxiety (Riaza Bermudo-Soriano et al., 2012) as well as with human PTSD (Heresco-Levy et al., 2009), were analyzed. Finally, in the last part of this section a serendipitous finding of a potential novel immune system associated candidate protein for PTSD is described.

4.2.1. Neurostructural proteins

The analyzed neurostructural proteins included synapsin and synaptophysin, two presynaptic vesicle proteins that have been previously found to be regulated in various animal models of stress (Adlard et al., 2011; Afadlal et al., 2010; Aisa et al., 2009; Alfonso et al., 2006; Elizalde et al., 2010; Sterlemann et al., 2010), as well as the postsynaptic protein homer 1b/c, the dendritic marker MAP-2, and the pan-neuronal cytoskeleton protein neurofilament H that have so far been hardly studied in the context of stress. Protein expression levels were examined in the hippocampus and prefrontal cortex, two brain regions known to be implicated in the neurocircuitry of PTSD (see section 1.2.4), as well as in the cerebellum (CER), which is supposed not to be involved in the PTSD pathogenesis.

4.2.1.1. Synapsin and synaptophysin protein expression is differentially regulated in mice exposed to repetitive acute stress

In pilot experiments, male 129SvJ/C57BL/6 mice were subjected to repetitive acute stressors, i.e. different restraint as well as combined restraint and forced swim stressors as illustrated in Figures 4.2 and 4.3, and the expression levels of the presynaptic vesicle proteins synapsin Ia-b/IIa and synaptophysin were analyzed in the hippocampus, prefrontal cortex, and in the cerebellum of stressed and mock treated mice.

The synapsin protein family, comprising synapsin Ia-b, IIa-b, and IIIa-c in the adult mammalian brain (Cesca et al., 2010), is known to be involved in the organization of presynaptic vesicle pools. In particular, synapsins attach the vesicles to each other and to the actin cytoskeleton. Upon phosphorylation of synapsin the vesicles detach and may fuse with the membrane of the active zone to release their neurotransmitter content into the synaptic cleft (Fdez and Hilfiker, 2006). The role of synaptophysin, however, is less clear. So far, it is believed to play a role in synaptic vesicle endocytosis (Gordon et al., 2011).

In a first experiment, to analyze short term effects of acute stress, male 129SvJ/C57BL/6 mice were exposed to a 15-min restraint stressor or control treatment and sacrificed 24 h later (Figure 4.2 A). Western blot analyses of synapsin Ia-b/IIa and synaptophysin expression in the hippocampus (HC), prefrontal cortex (PFC), and cerebellum (CER) revealed no significant

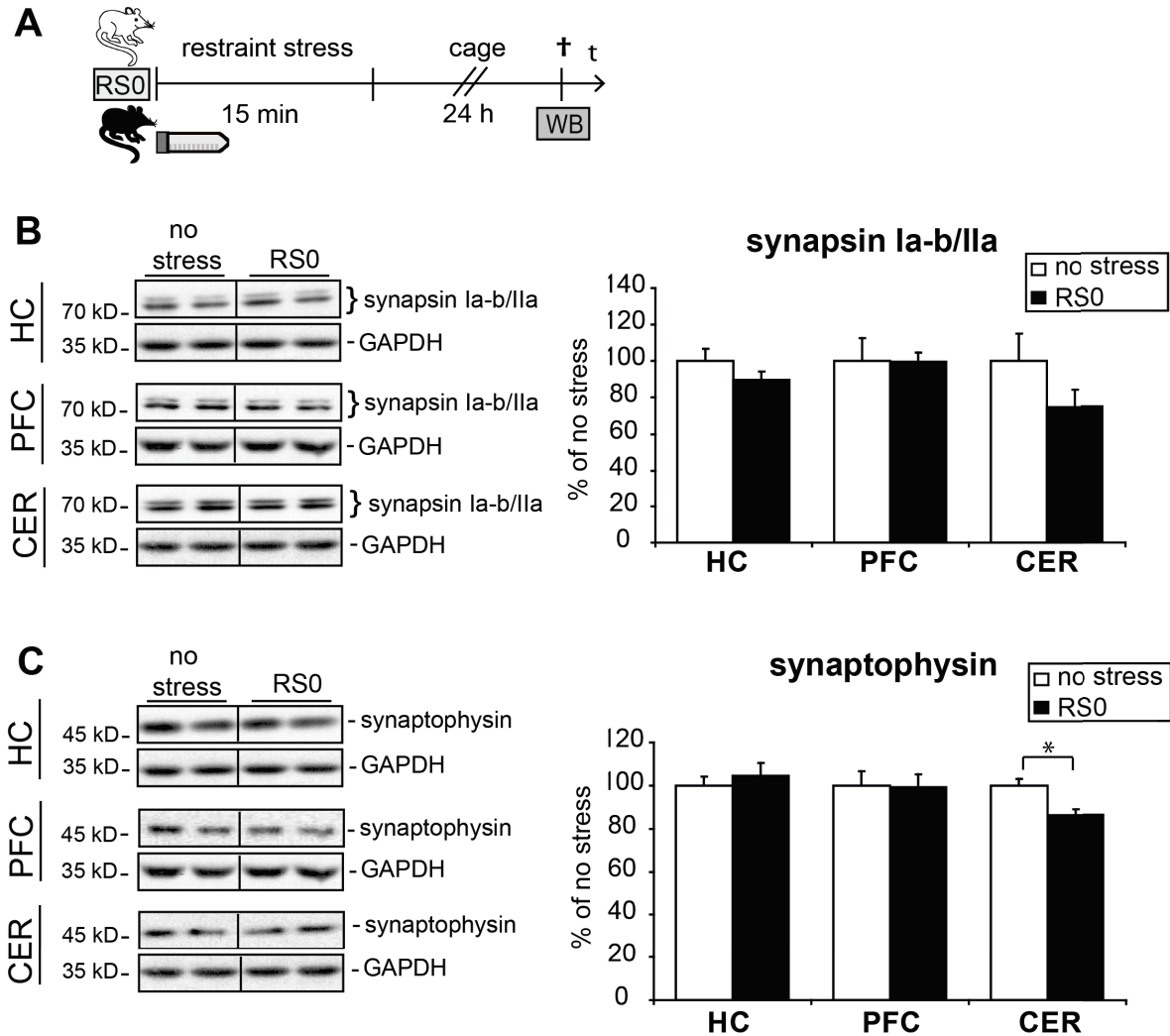


Figure 4.2.: **Synapsin and synaptophysin expression 24 h after exposure to acute restraint stress.** 129SvJ/C57BL/6 mice were subjected to a 15-min restraint stressor and sacrificed 24h later (A). Hippocampus (HC), prefrontal cortex (PFC), and cerebellum (CER) were isolated from sacrificed mice for subsequent western blot analysis (WB) of synapsin Ia-b/IIa (B) or synaptophysin (C) expression levels: depicted are representative western blots. Graphs show relative expression levels of synapsin Ia-b/IIa or synaptophysin after normalization to glyceraldehyd-3-phosphat-dehydrogenase (GAPDH) presented in percent of those of non stressed mice (set at 100 %). Plotted data represent means \pm SEM, $n = 9$ (batch Acute Restraint Stress, RS0, see Table 2.2), 2-3 technical replicates. Statistical analysis was performed using student's t -test, indicated are only significant changes: * $p < 0.05$.

4. Results II: Identification of PTSD candidate proteins in a mouse model of PTSD

expression level changes of any protein tested (Figure 4.2 B, C; HC – synapsin Ia-b/IIa: $t = 1.242$, $df = 16$, $p = 0.233$; PFC – synapsin Ia-b/IIa: $t = 0.035$, $df = 16$, $p = 0.972$; CER – synapsin Ia-b/IIa: $t = 1.402$, $df = 16$, $p = 0.180$; HC – synaptophysin: $t = 0.633$, $df = 16$, $p = 0.535$; PFC – synaptophysin: $t = 0.098$, $df = 16$, $p = 0.922$), except for a slight significant decrease of synaptophysin in the cerebellum of stressed mice (Figure 4.2 C; $t = 2.850$, $df = 12$, $p = 0.015$).

In a second experiment, medium-term effects of combined restraint and forced swim stressors were addressed. The batch of mice employed here for the analysis of synaptic protein expression has previously been investigated for hippocampal expression of glucocorticoid receptor and FKBP51, which was published recently (Touma et al., 2011). Here, male 129SvJ/C57BL/6 mice were exposed to a 15-min restraint stressor and to a 6-min forced swim stressor (FSS) followed by an additional exposure to a 6-min FSS 24 h later (Figure 4.3 A, RSI paradigm). A different group of mice was exposed to a 60-min restraint stressor combined with a 6-min forced swim stressor 24 h later (Figure 4.3 A, RSII paradigm), which was considered to be more stressful as indicated by higher plasma corticosterone levels (Touma et al., 2011). In both paradigms, mice were sacrificed 8 days after stress exposure and hippocampus, prefrontal cortex, and cerebellum were dissected (Figure 4.3 A). Western blot analysis revealed a significantly decreased protein expression of synapsin Ia-b/IIa in both the hippocampus and the prefrontal cortex of mice subjected to the RSI or RSII paradigm compared to mock treated control mice (Figure 4.3 B; HC: $F_{2,17} = 8.626$, $p = 0.003$; PFC: $F_{2,17} = 8.813$, $p = 0.002$). In the cerebellum, synapsin expression was not altered (Figure 4.3 B; CER: $F_{2,17} = 1.925$, $p = 0.180$). In contrast, synaptophysin protein expression in the hippocampus and the prefrontal cortex was not affected by the RSI stress paradigm, and interestingly, synaptophysin protein levels increased 8 days after subjecting the mice to the RSII stress paradigm (Figure 4.3 C; HC: $F_{2,17} = 12.62$, $p < 0.001$; PFC: $F_{2,17} = 8.813$, $p = 0.002$). As expected, synaptophysin expression was not altered in the cerebellum of mice subjected to the RSI or the RSII paradigm compared to mock treated control mice (Figure 4.3 C; CER: $F_{2,17} = 0.507$, $p = 0.611$).

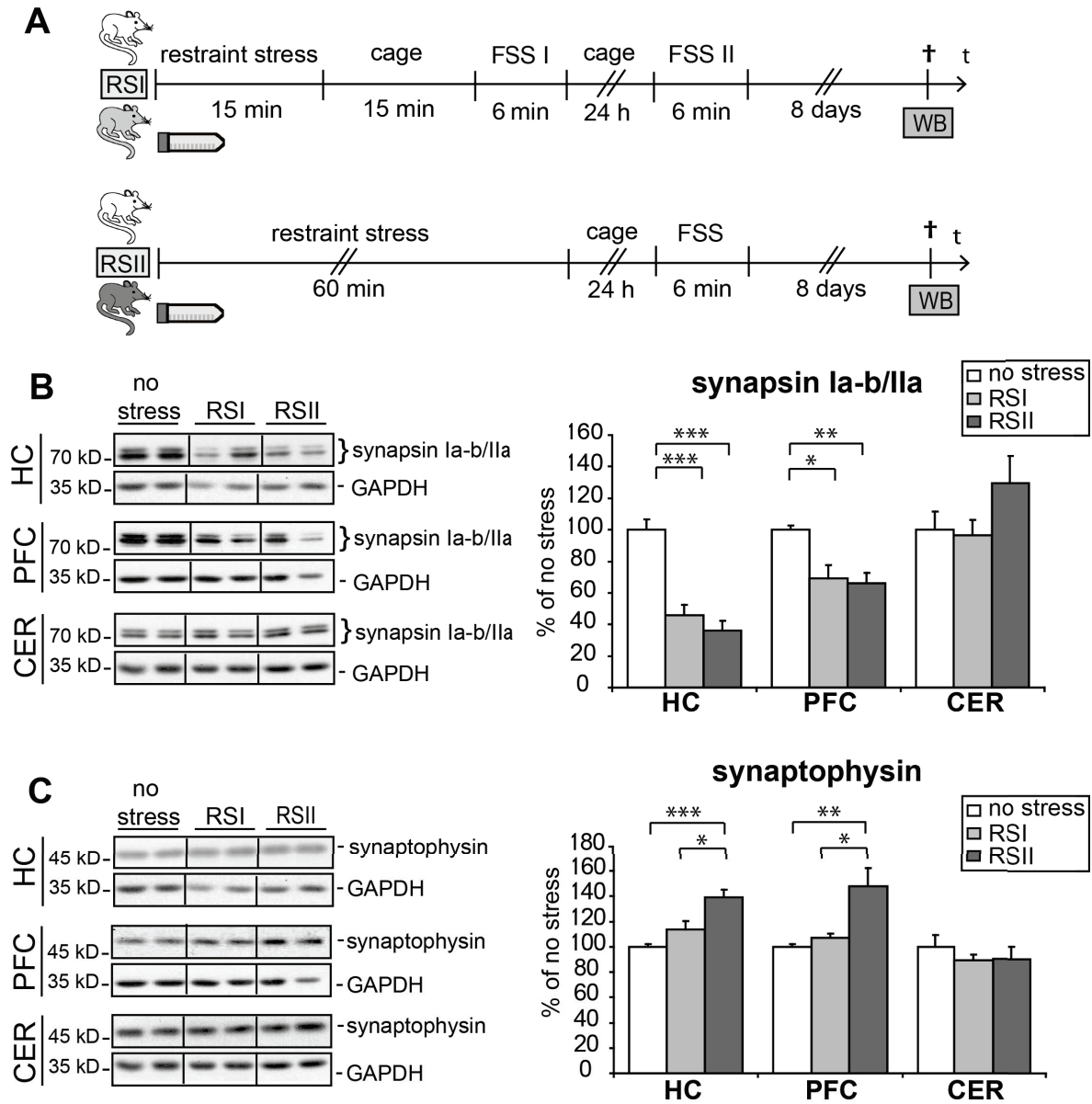


Figure 4.3.: Synapsin and synaptophysin expression 8 days after exposure to combined restraint and forced swim stress paradigms. To study medium-term effects, 129SvJ/C57BL/6 mice were stressed with either a 15-min restraint stressor followed by two intervals of forced swim stress (FSS) (RSI paradigm) or by a 60-min restraint stressor followed by one interval of FSS (RSII paradigm) and sacrificed 8 days later (A). Hippocampus (HC), prefrontal cortex (PFC), and cerebellum (CER) were isolated from sacrificed mice for subsequent western blot analysis (WB) of synapsin Ia-b/IIa (B) or synaptophysin (C) expression levels. Shown are representative western blots and graphs as described in Figure 4.2. Plotted data represent means \pm SEM, $n = 6$ (batch Repetitive Acute Stress, RSI/RSII, see Table 2.2), 2-3 technical replicates. Statistical analysis was performed using one-way ANOVA and Bonferroni post-hoc tests. Significant changes of Bonferroni post-hoc tests are indicated by * $p < 0.05$, ** $p < 0.01$, *** $p < 0.001$.

4.2.1.2. Traumatic footshock stress reduces hippocampal synaptic protein expression

Synapsin and synaptophysin expression analyses presented above point at an involvement of the synapse or synaptic plasticity in the brain's adaptation processes to repetitive acute stress. Reduction of synaptic proteins might also contribute to the hippocampal shrinkage that was recently found in footshocked mice of the PTSD mouse model employed here (Golub et al., 2011). Motivated by this assumption and by the findings of the pilot experiments, expression levels of synaptic proteins were analyzed in the PTSD mouse model. Traumatized and control mice were sacrificed either 2, 28, or 60 days after footshock or control treatment. Then, hippocampus, prefrontal cortex, and cerebellum were dissected for subsequent western blot analysis (Figure 4.4 A), which revealed that cerebral synapsin Ia-b/IIa levels were reduced in traumatized mice. Interestingly, this was true only for the hippocampus, but not for the prefrontal cortex and, as expected, also not for the cerebellum (Figure 4.4 B-D; d2: PFC $t = 0.603$, $df = 10$, $p = 0.560$, CER $t = 0.398$, $df = 10$, $p = 0.698$; d28: PFC $t = 1.279$, $df = 10$, $p = 0.229$, CER $t = 0.044$, $df = 10$, $p = 0.965$; d60: PFC $t = 1.408$, $df = 22$, $p = 0.173$, CER $t = 0.540$, $df = 10$, $p = 0.601$). Downregulation of hippocampal synapsin levels in shocked mice were detectable already 2 days after footshock (Figure 4.4 B; $t = 2.631$, $df = 10$, $p = 0.025$). The hippocampal synapsin reduction in traumatized mice maintained in the long-term, namely until day 60 after shock, although on day 28 after footshock only a trend towards a reduction was measured (Figure 4.4 C, D; d28: $t = 1.963$, $df = 10$, $p = 0.078$; d60: $t = 4.332$, $df = 22$, $p < 0.001$).

To analyze if traumatic stress induces a specific downregulation of synapsin or if it rather results in an overall alteration of the synaptic structure, additional synaptic marker proteins were tested. Since synapsin Ia-b/IIa expression was altered only in the hippocampal region, and motivated by the finding that the hippocampal volume is reduced both in traumatized patients and in footshocked mice of the PTSD mouse model used in this study (Golub et al., 2011), further analyses concentrated on the hippocampus.

Next, synaptophysin was analyzed in hippocampal lysates prepared from mice sacrificed on days 2, 28, or 60 after footshock. Synaptophysin is located together with synapsin on vesicles of the presynapse (Wiedenmann and Franke, 1985). Results from the pilot experiments indicated

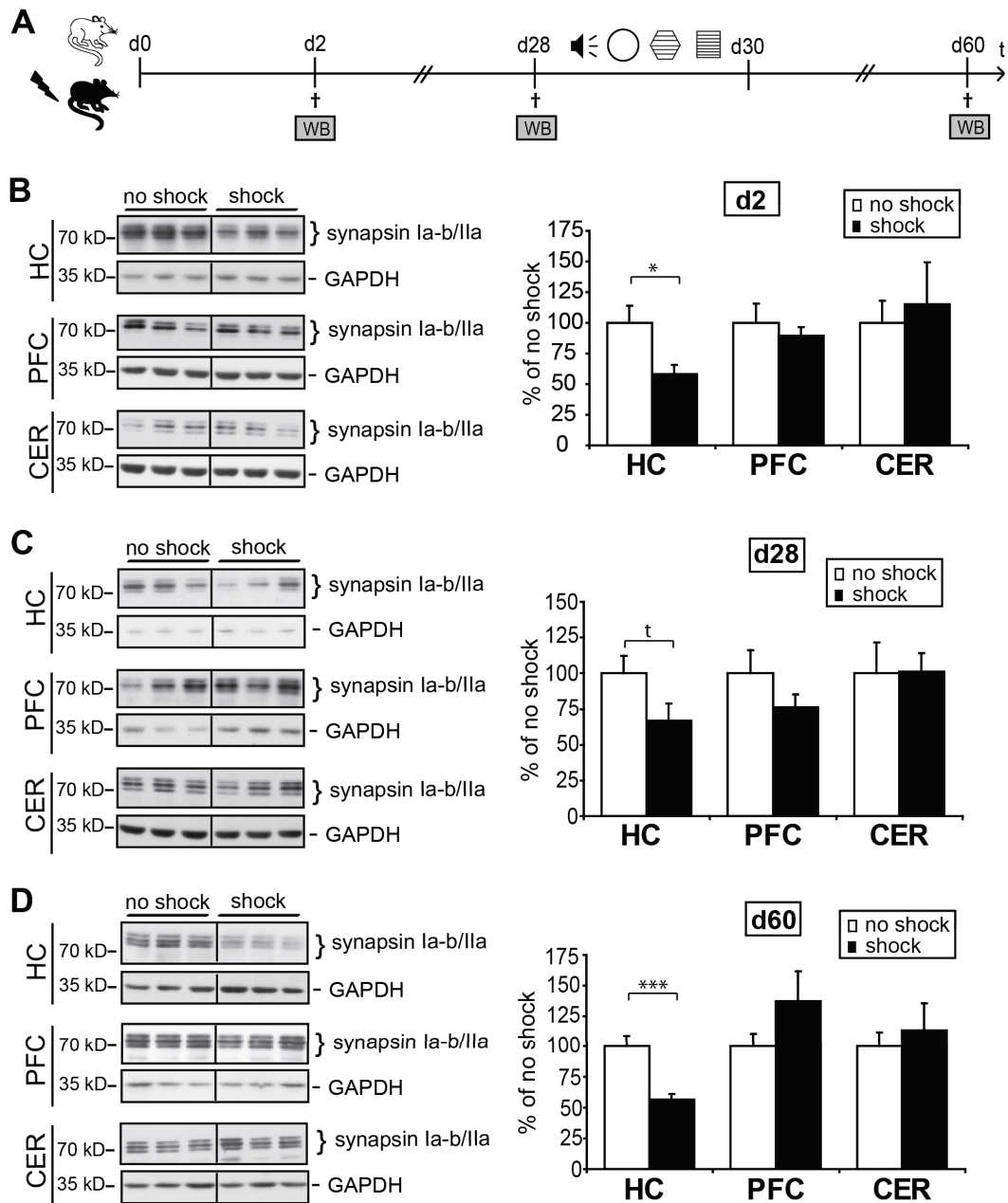


Figure 4.4.: Synapsin expression in the PTSD mouse model. (A) C57BL/6NCrl mice were subjected to a single electric footshock and sacrificed either 2, 28, or 60 days later. At each time-point, hippocampus (HC), prefrontal cortex (PFC), and cerebellum (CER) were isolated for subsequent western blot analysis (WB). (B–D) Shown are representative western blots of synapsin Ia-b/IIa or, for control, glycerinaldehyd-3-phosphat-dehydrogenase (GAPDH) of shocked and non shocked mice. Graphs show expression levels of synapsin Ia-b/IIa after normalization to GAPDH presented in percent of those of non shocked mice (set at 100%). Plotted data represent means \pm SEM, $n = 6$ for d2 and d28 (batch PTSD I), $n = 12$ for d60 (batch PTSD I + II, see Table 2.2), 2-3 technical replicates. Statistical significance was calculated using student's *t*-test and is indicated by *t* $p < 0.1$, * $p < 0.05$, *** $p < 0.001$. Figure adapted from (Herrmann et al., 2012)

4. Results II: Identification of PTSD candidate proteins in a mouse model of PTSD

an increased expression of synaptophysin in stressed animals (Figure 4.3). In contrast to those findings, the single electric footshock induced a reduction of hippocampal synaptophysin levels in the long-term: while on day 2 a trend in reduction was detectable (Figure 4.5 B; $t = 1.869$, $df = 10$, $p = 0.091$), and on day 28 again no significant protein level changes were present (Figure 4.5 B; $t = 1.209$, $df = 10$, $p = 0.254$), synaptophysin levels were significantly decreased on day 60 after footshock (Figure 4.5 B; $t = 2.351$, $df = 10$, $p = 0.040$). These results indicate that rather than a specific reduction of synapsin protein levels, overall changes in the synaptic vesicle number or even in the number of synapses might be induced by the traumatic footshock. To further explore this, a postsynaptic marker protein, namely homer 1b/c, was analyzed next. Homer 1b/c is located in the postsynaptic density and is involved in the clustering and trafficking of metabotropic glutamate receptors (mGluR) (Kammermeier, 2006). Western blot analyses revealed that in hippocampal lysates of traumatized and control mice homer 1b/c expression was significantly decreased on day 60 after footshock (Figure 4.5 C; $t = 3.552$, $df = 22$, $p = 0.001$), while at earlier time-points no significant alterations in homer 1b/c expression were detected (Figure 4.5 C; d2: $t = 1.573$, $df = 10$, $p = 0.147$; d28: $t = 0.259$, $df = 8$, $p = 0.801$). Thus, in the long-term not only pre- but also post-synaptic proteins are reduced suggesting a loss of synaptic structures in mice showing a PTSD-like phenotype. The fact that all proteins that were found to be reduced on day 60 after footshock were not significantly changed on day 28 after footshock suggests that the behavioral testing on days 28-30 might constitute at least a minor stressor leading to an amplification of the stress-induced molecular alterations.

Next, to obtain more information on the involvement of the different hippocampal subregions in stress-mediated synapsin reduction, immunohistochemical stainings for synapsin I/II were performed in brain slices of traumatized and control mice sacrificed on day 60 after shock (Figure 4.6). The cornus ammonis area 3 (CA3) and the hilus region of the dentate gyrus (DG) exhibited the most intense staining, while the CA1 region showed a weaker intensity. These findings correspond well with findings of other rodent studies analyzing hippocampal synapsin protein expression using immunohistochemistry (Melloni et al., 1993; Vaynman et al., 2004; Nowicka et al., 2003). The pronounced expression in the CA3 and hilus region of the

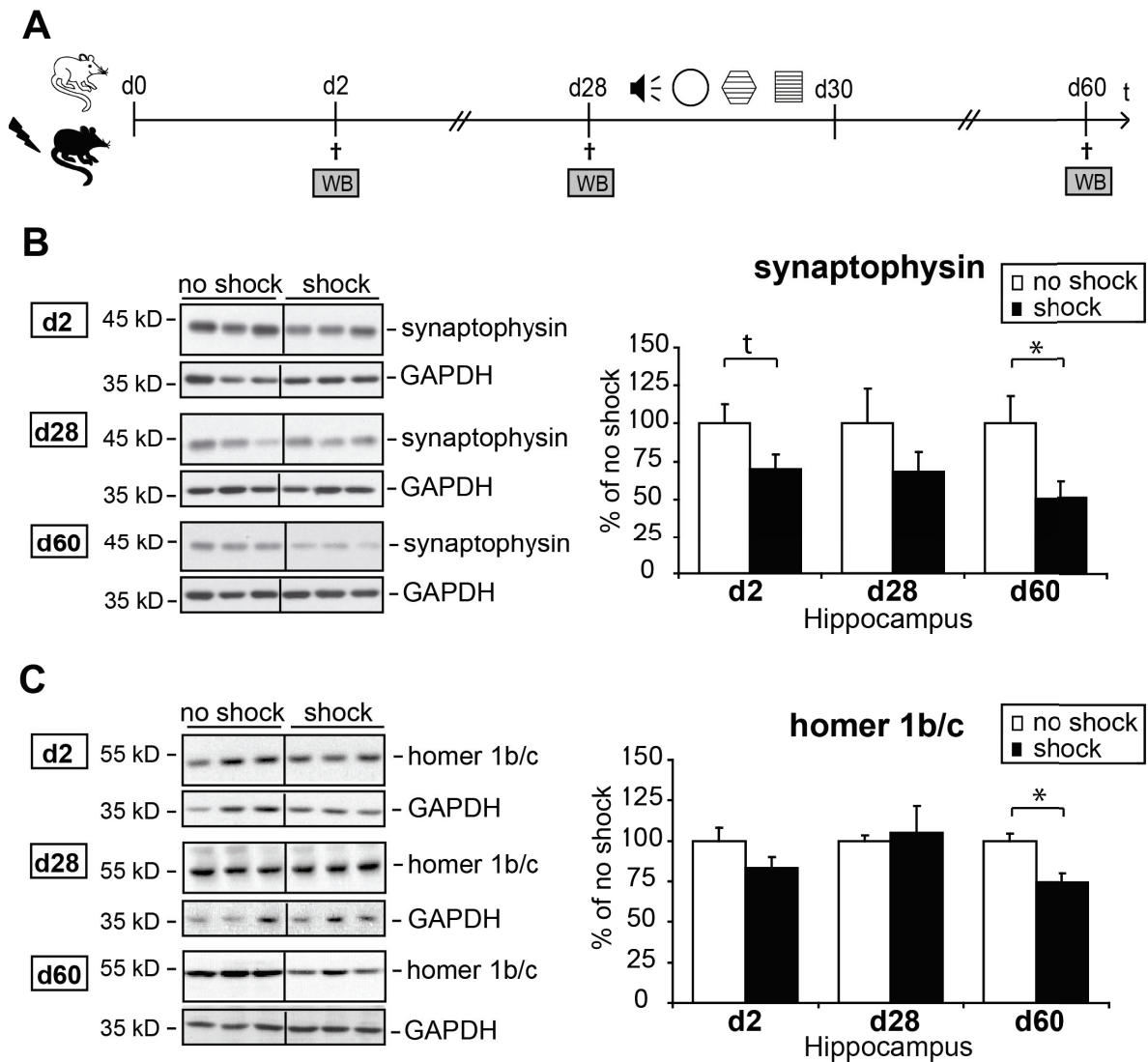


Figure 4.5.: **Hippocampal synaptophysin and homer 1b/c expression in the PTSD mouse model.** Synaptophysin and homer 1b/c expression was analyzed in hippocampal lysates of C57BL/6NCr1 mice subjected to a single electric footshock and sacrificed either 2, 28, or 60 days later (A). Shown are representative western blots of synaptophysin (B) and homer 1b/c (C) or, for control, glycerinaldehyd-3-phosphat-dehydrogenase (GAPDH) analyzed in shocked and non shocked mice. Graphs show relative expression levels after normalization to GAPDH presented in percent of those of non shocked mice set at 100 %. Plotted data represent means \pm SEM, $n = 6$ for d2 and d28 (batch PTSD I, see Table 2.2), $n = 12$ for d60 (batch PTSD I + II)(except for synaptophysin where only one batch $n=6$, batch PTSD I was employed), 2-3 technical replicates. Statistical significance was calculated using student's t -test and is indicated by t $p < 0.1$, * $p < 0.05$. Figure adapted from (Herrmann et al., 2012)

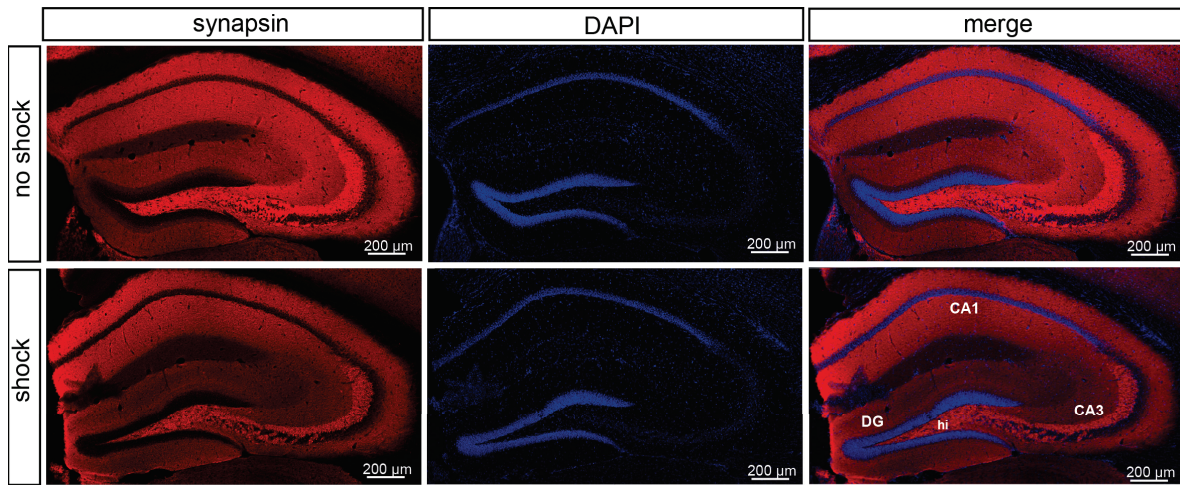


Figure 4.6.: **Immunohistochemical assessment of synapsin expression in the PTSD mouse model.** Shown are representative images ($n = 6$, batch PTSD II, see Table 2.2) of coronal hippocampal sections from shocked and non shocked mice sacrificed 60 days after shock and stained with anti-synapsin I/II antibody followed by a fluorescently labeled secondary antibody (left panel). Slices were counterstained with DAPI (middle panel). The overlay of DAPI and anti-synapsin stained sections is presented in the right panel (merge). Abbreviations used: Cornu ammonis areas 1 and 3 (CA1, CA3), dentate gyrus (DG), hilus region (hi). Figure adopted from (Herrmann et al., 2012)

DG furthermore suggests that these regions possibly contribute more than other hippocampal areas to the trauma stress-induced reduction of hippocampal synapsin expression and possibly also to the trauma stress-induced hippocampal volume reduction.

4.2.1.3. Hippocampal expression of neurofilament H, but not MAP-2, is reduced in mice subjected to a single electric footshock

To investigate if a loss of neurons contributes to the trauma stress-induced hippocampal volume loss, the pan-neuronal marker protein neurofilament H and the dendritic marker protein microtubule-associated protein 2 (MAP-2) were analyzed. Both proteins constitute major elements of the neuronal cytoskeleton and are therefore crucial for the neuronal cell morphology. Interestingly, a slight reduction in neurofilament H expression was evident on day 2 after footshock (Figure 4.7 B; $t = 2.422$, $df = 10$, $p = 0.035$), while no changes on day 28 (Figure 4.7 B; $t = 0.537$, $df = 10$, $p = 0.603$), and a statistical trend towards a reduction on day 60 after footshock (Figure 4.7 B; $t = 1.873$, $df = 21$, $p = 0.075$) were detectable.

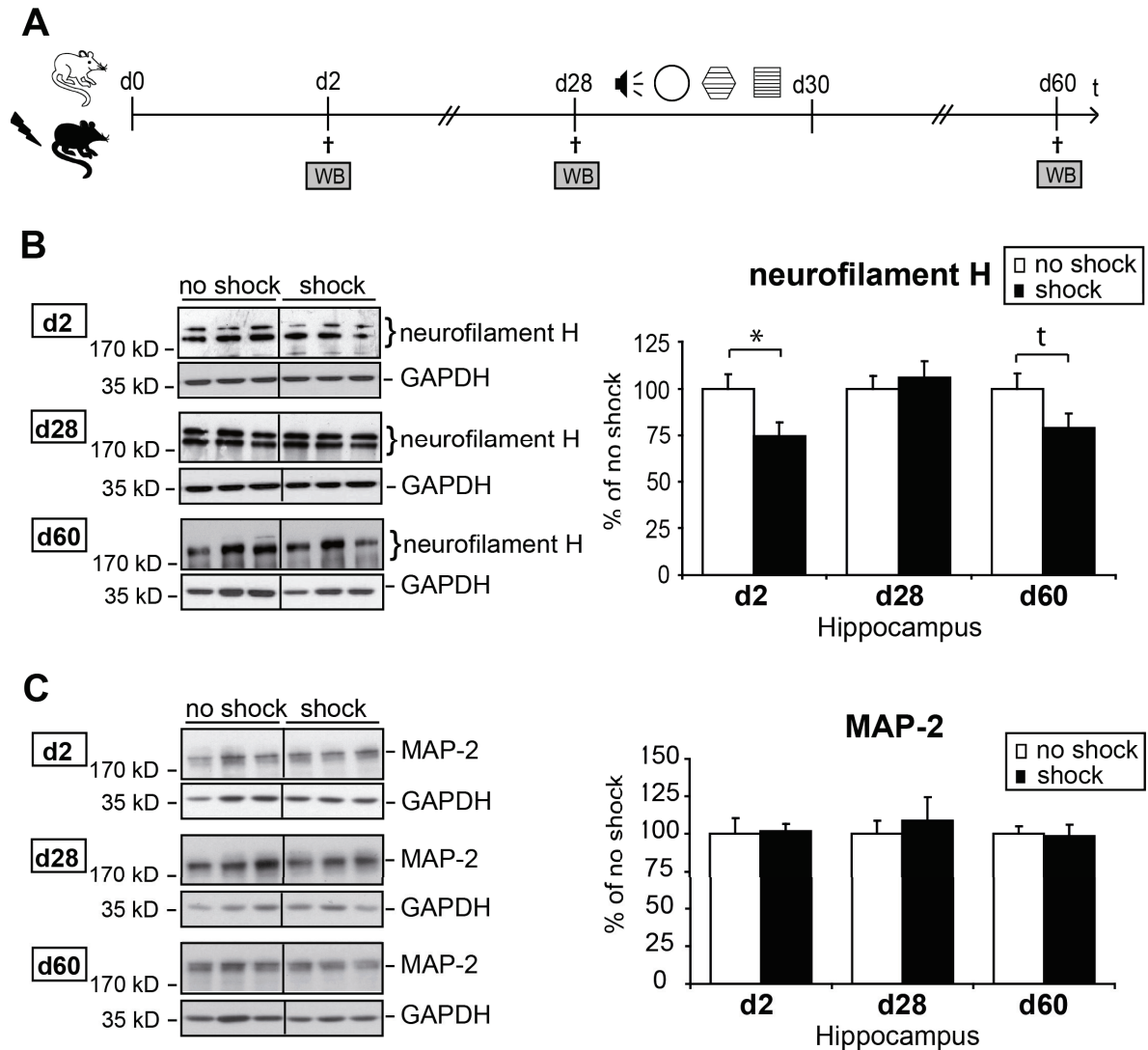


Figure 4.7.: **Hippocampal neurofilament H and MAP-2 expression in the PTSD mouse model.** Neurofilament H and MAP-2 expression was analyzed in hippocampal lysates of C57BL/6NCrl mice subjected to a single electric footshock and sacrificed either 2, 28, or 60 days later (A). Shown are representative western blots of neurofilament H (B) and MAP-2 (C) or, for control, glyceralaldehyd-3-phosphat-dehydrogenase (GAPDH) analyzed in shocked and non shocked mice. Graphs show relative expression levels after normalization to GAPDH presented in percent of those of non shocked mice set at 100 %. Plotted data represent means \pm SEM, $n = 6$ for d2 and d28 (batch PTSD I, see Table 2.2), $n = 12$ for d60 (batch PTSD I + II), 2-3 technical replicates. Statistical significance was calculated using student's t -test and is indicated by t $p < 0.1$ * $p < 0.05$. Figure adapted from (Herrmann et al., 2012)

In contrast, MAP-2 exhibited no significant expression level differences between shocked and control mice at any time-point tested (Figure 4.7 C; d2: $t = 0.155$, $df = 10$, $p = 0.879$; d28: $t = 0.495$, $df = 10$, $p = 0.631$; d60: $t = 0.152$, $df = 22$, $p = 0.881$).

The fact that expression of MAP-2 remains unchanged points at a steady number of neuronal cells and furthermore implicates that dendritic morphology is not excessively altered. Neurofilament proteins are enzymatically degraded in synaptic structures (Fasani et al., 2004). Therefore, the reduction in neurofilament H protein levels probably does not reflect a synaptic loss but rather points at a possible retraction of axonal elements.

Interestingly, the expression of none of the protein analyzed here was altered in traumatized and control mice sacrificed on day 28 after footshock, i.e. in mice that received the electric footshock on day 0 and were sacrificed on day 28 after footshock without further behavioral testing. In contrast, traumatized mice sacrificed on day 60 after footshock and subjected to behavioral testing on days 28 to 30 after footshock exhibited a significantly reduced synaptic protein and neurofilament H expression suggesting an amplification of the molecular alterations by re-exposure to the shock context. However, as between day 28 and day 60 no additional stressors were presented, the synaptic protein expression changes persisting until day 60 after footshock can be regarded as stress-induced and re-exposure triggered long-term molecular alteration, which in case of homer 1b/c occurred with delayed onset.

4.2.1.4. Hippocampal synaptic protein expression correlates with the conditioned and generalized fear response but not with the acoustic startle response

To get an idea of the impact of the hippocampal synaptic protein loss on the development of distinct PTSD symptoms, a correlation analysis was performed according to previously published procedures (Wu et al., 2007; Zink et al., 2010). In particular, by calculating the Pearson correlation coefficients, the intensity of the freezing behavior in either the shock context or the grid context (conditioned and generalized fear response, respectively), or the intensity of the startle response (representing the hyperarousal phenotype) of traumatized and control mice assessed on days 28-30 after footshock was correlated with the protein expression values of synapsin Ia-b/IIa, synaptophysin, or homer 1b/c assessed on day 60 after footshock.

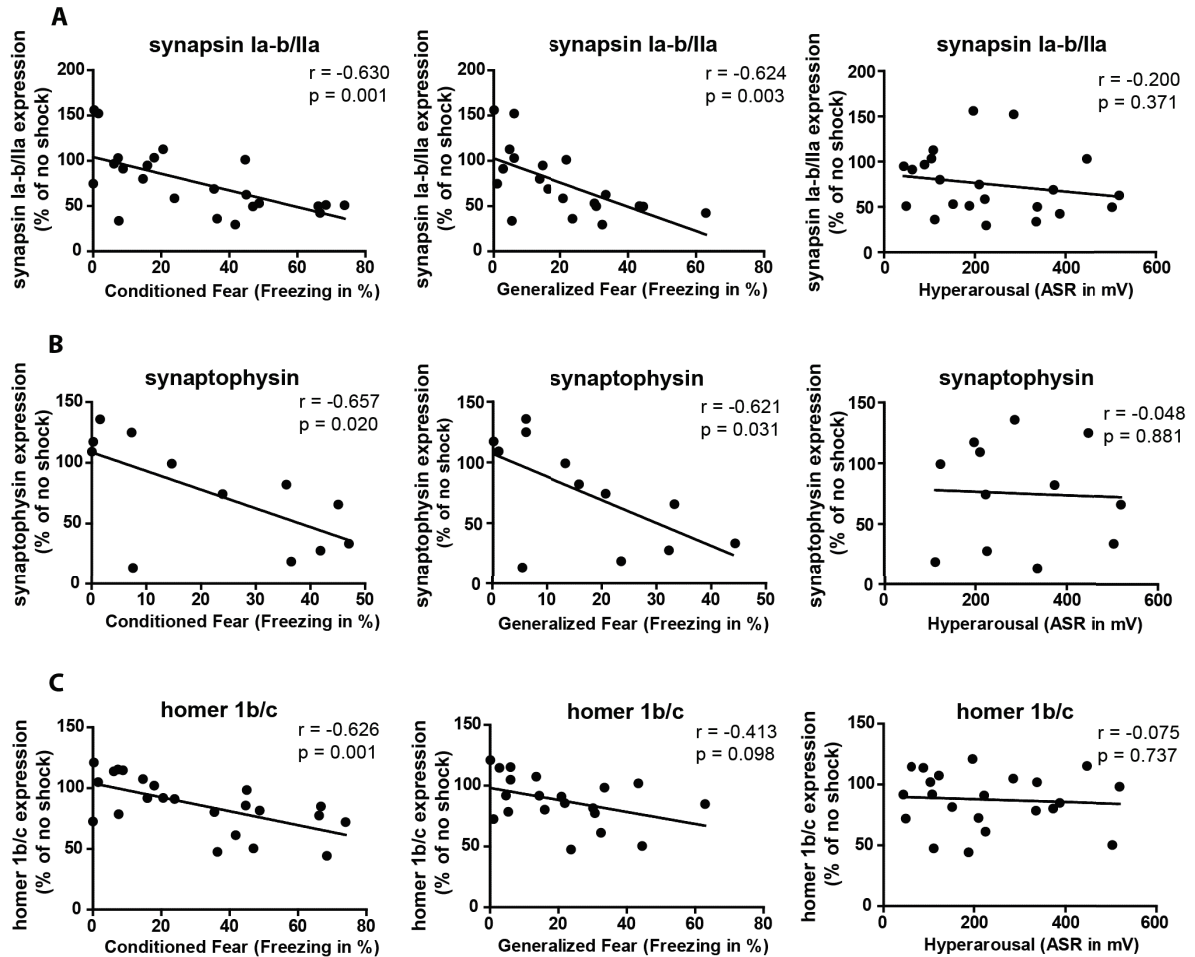


Figure 4.8.: **Correlation of PTSD-like symptoms with hippocampal synaptic protein expression.** Intensities of PTSD-like behaviors on days 28-30 after shock, i.e. the conditioned fear response, the generalized fear response, and the acoustic startle response (ASR), were plotted against the relative day-60 expression levels (% of no shock) of synapsin Ia-b/IIa (A), synaptophysin (B), and homer 1b/c (C) of both shocked and non shocked mice. Freezing duration was normalized to the 3 min observation intervals (% freezing). Pearson correlation coefficients (r) were calculated, followed by a student's t -test (p); $n = 12$ per group for synapsin Ia-b/IIa and homer 1b/c (batch PTSD I + II, see Table 2.2), $n = 6$ per group for synaptophysin (batch PTSD I). Figure adapted from (Herrmann et al., 2012)

Plotted protein expression values of each mouse were normalized to the mean expression value of the group of non shocked mice (Figure 4.8; depicted as % of no shock). The analysis revealed a statistically significant negative correlation of the intensity of the conditioned fear response with the expression of all synaptic proteins analyzed (Figure 4.8; synapsin Ia-b/IIa: $r = -0.630$, $p = 0.001$; synaptophysin: $r = -0.657$; $p = 0.020$; homer 1b/c: $r = -0.626$; $p = 0.001$). Furthermore, the analysis detected also a significant negative correlation of the intensity of the generalized fear response with the protein expression levels of both synapsin and synaptophysin (Figure 4.8; synapsin Ia-b/IIa: $r = -0.624$, $p = 0.003$; synaptophysin: $r = -0.621$, $p = 0.031$). The correlation of homer 1b/c expression with the intensity of generalized fear response was weaker, but still revealed a trend (Figure 4.8; $r = -0.413$; $p = 0.098$). In contrast, the expression of neither protein correlated with the hyperarousal phenotype (Figure 4.8; synapsin Ia-b/IIa: $r = -0.200$, $p = 0.371$; synaptophysin: $r = -0.048$, $p = 0.881$; homer 1b/c: $r = -0.075$, $p = 0.737$). Thus, the reduction of hippocampal synaptic proteins might differentially impact on the distinct symptoms of the PTSD-like syndrome in mice.

4.2.1.5. Chronic fluoxetine treatment increases synaptic vesicle protein expression in mice subjected to a single electric footshock

Chronic fluoxetine treatment has been previously shown to effectively ameliorate PTSD-like symptoms in shocked mice of the PTSD mouse model employed here (Siegmund and Wotjak, 2007). As fluoxetine treatment has additionally been reported to increase synaptophysin expression in a mouse model of learned helplessness (Reinés et al., 2008), it was investigated next whether chronic fluoxetine treatment is able to repair the footshock-elicited loss of hippocampal synaptic proteins. For this purpose, shocked mice were subjected to either 20 mg/kg per day fluoxetine treatment via the drinking water or control treatment (normal tap water) for 4 weeks starting the day after application of the footshock (Figure 4.9 A). The efficacy of fluoxetine treatment was tested by measuring the freezing response in response to a neutral tone in the neutral context on day 28 after footshock. As expected, fluoxetine treatment reduced the generalized fear response on day 28 after footshock (Figure 4.9 B: $t = 7.516$, $df = 28$, $p < 0.001$). Then, the fluoxetine dose was halved for three more

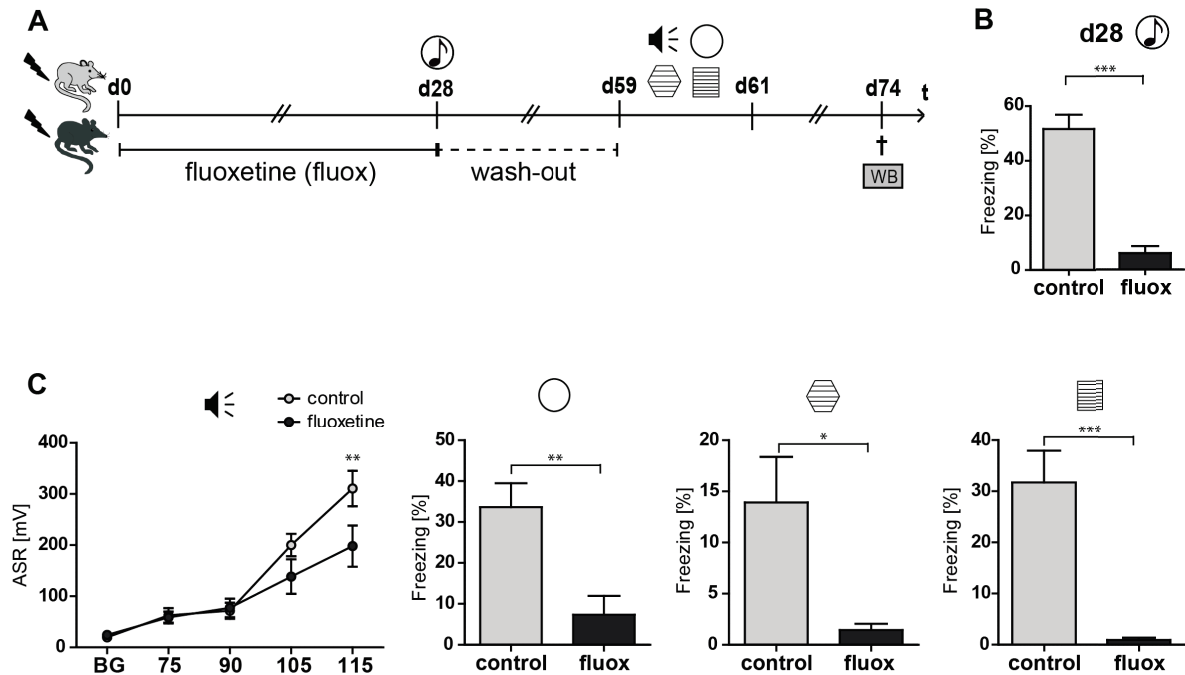


Figure 4.9.: **Fluoxetine treatment of shocked mice ameliorates PTSD-like behavior.**

(A) Course of experiment: C57BL/6NCrl mice were subjected to a single electric footshock on day 0 and subsequently received 20 mg/kg/d fluoxetine or control treatment. On day 28, the generalized fear response was assessed (B) during presentation of a neutral tone in the neutral context. After a 4-week washout period, mice were tested on days 59-61 for their acoustic startle response, the generalized, and conditioned fear response (C). Presented data are means \pm SEM, $n = 16$ (ctrl), $n = 14$ (fluox) (batch Fluoxetine in PTSD, see Table 2.2). Statistical significance was calculated by two-way ANOVA (startle response) or student's t -test (freezing response) and is indicated by * $p < 0.05$, ** $p < 0.01$, *** $p < 0.001$. Figure adapted from (Herrmann et al., 2012)

days before discontinuing the fluoxetine treatment. PTSD-like behavior was tested 4 weeks later on days 59 to 61 after footshock. As expected, fluoxetine treatment reduced the acoustic startle response (Figure 4.9 C; two-way ANOVA: $F_{1,112\text{fluoxetine}} = 2.072$, $p = 0.161$; $F_{4,112\text{INT}} = 56.54$, $p < 0.001$; $F_{4,112\text{INT} \times \text{fluoxetine}} = 4.325$, $p = 0.003$; Bonferroni post-hoc test, 115 dB: $t = 3.474$, $p < 0.01$) and both generalized (Figure 4.9 C; neutral cylinder: $t = 3.475$, $df = 28$, $p = 0.002$, grid hexagon: $t = 2.607$, $df = 28$, $p = 0.015$) and conditioned fear responses (Figure 4.9 C; shock chamber $t = 4.736$, $df = 23$, $p < 0.001$).

Analysis of hippocampal protein expression of the control or fluoxetine treated shocked mice on day 74 after footshock revealed a significant upregulation of synapsin Ia-b/IIa

4. Results II: Identification of PTSD candidate proteins in a mouse model of PTSD

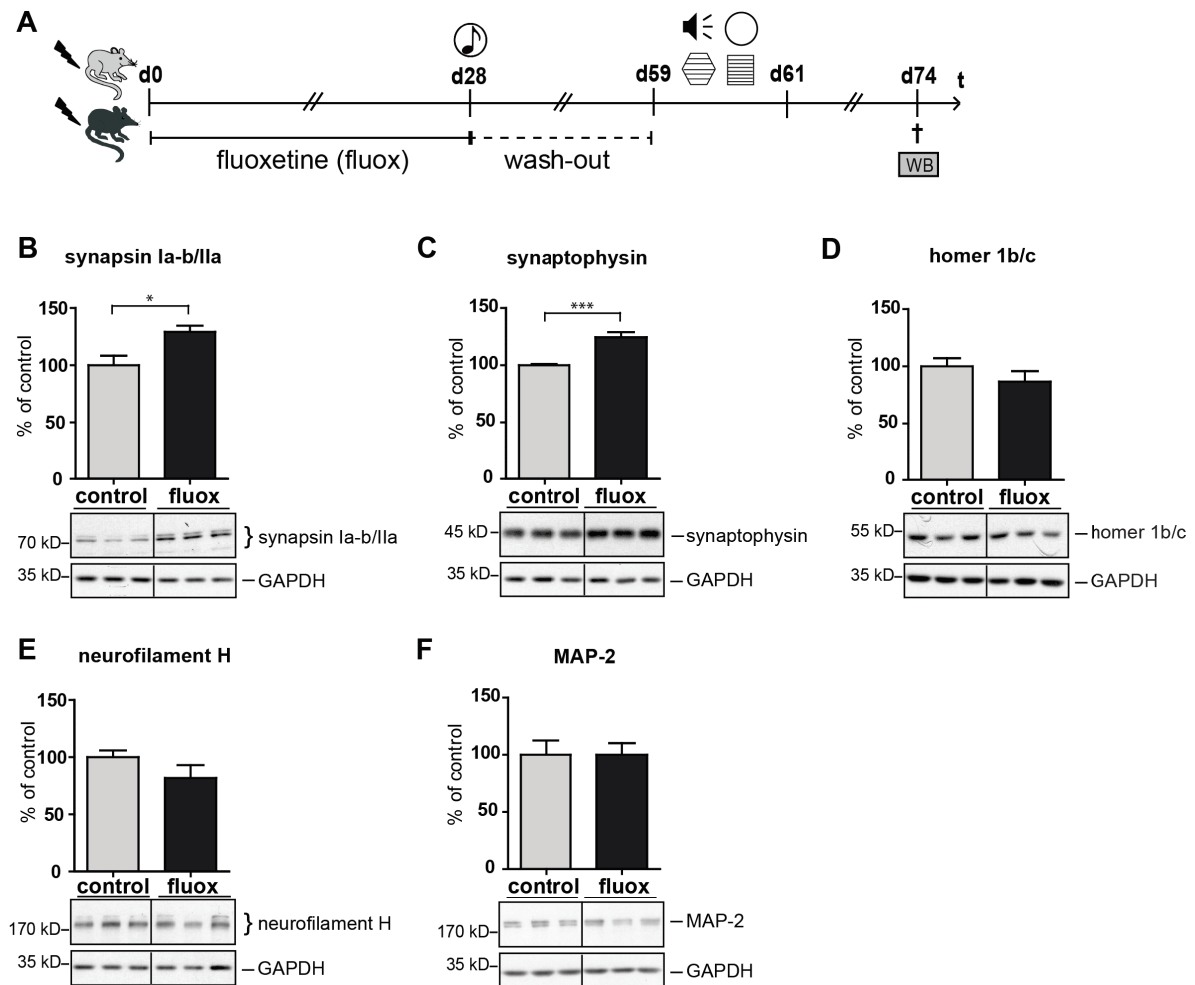


Figure 4.10.: Fluoxetine treatment of shocked mice increases hippocampal presynaptic protein expression. (A) Course of experiment, see legend of Figure 4.9 for detailed explanation of behavioral analyses. Representative immunoblots of all candidate proteins and, for control, glycerinaldehyd-3-phosphat-dehydrogenase (GAPDH) analyzed in hippocampal lysates of footshocked control (ctrl) or fluoxetine (fluox) treated mice, respectively. Graphs show relative expression levels of synapsin Ia-b/IIa (B), synaptophysin (C), homer 1b/c (D), neurofilament H (E), and MAP-2 (F) after normalization to GAPDH 74 days after shock in the hippocampus of footshocked control and footshocked fluoxetine treated mice, respectively. Candidate protein expression levels of fluoxetine treated mice are presented in percent of those of control mice set at 100 % (% of control). Plotted data represent means \pm SEM, $n = 6$ (batch Fluoxetine in PTSD, see Table 2.2), 2-3 technical replicates. Statistical significance was calculated using student's *t*-test and is indicated by * $p < 0.05$, *** $p < 0.001$. Figure adapted from (Herrmann et al., 2012)

and synaptophysin, while the expression of homer 1b/c, neurofilament H, and MAP-2 was not altered significantly (Figure 4.10; synapsin Ia-b/IIa: $t = 2.929$, $df = 10$, $p = 0.015$; synaptophysin: $t = 5.239$, $df = 10$, $p < 0.001$; homer 1b/c: $t = 1.150$, $df = 10$, $p = 0.277$; neurofilament H: $t = 1.433$, $df = 10$, $p = 0.182$; MAP-2: $t = 0.007$, $df = 10$, $p = 0.995$). Thus, the upregulation of presynaptic proteins by fluoxetine treatment paralleled the remission of PTSD symptoms suggesting that hippocampal synaptic protein loss is causally linked to the pathogenesis of PTSD-like symptoms in mice.

Taken together, in this section a trauma stress-induced pronounced reduction of hippocampal synaptic proteins and a decrease in the expression of the cytoskeleton protein neurofilament H was demonstrated, while further analyses revealed that the expression of the dendritic marker protein MAP-2 was not altered (summarized in Table 4.1). This points at a trauma stress-induced hippocampal synaptic protein loss accompanied by axonal degradation, while the overall number of neuronal cells probably remains constant. Furthermore, decreased synaptic protein levels correlated with distinct symptoms of the PTSD-like syndrome in mice, namely with the conditioned and generalized fear response, but not with hyperarousal. Finally, treatment of shocked mice with fluoxetine counteracted both the PTSD-like behavior and the footshock-induced reduction of presynaptic proteins.

Table 4.1.: **Summary of hippocampal expression changes of neurostructural proteins.** Summarized are significant expression changes observed in shocked (s) versus non shocked (ns) mice of batches PTSD I and II as well as expression changes observed in footshocked fluoxetine (fluox) versus control (ctrl) treated mice of batch ‘Fluoxetine in PTSD’. t = statistical trend

Candidate protein	PTSD I & II			Fluoxetine in PTSD
	d2	d28	d60	d74
synapsin Ia-b/IIa	s < ns	s < ns ^t	s < ns	fluox > ctrl
synaptophysin	s < ns ^t	s = ns	s < ns	fluox > ctrl
homer 1b/c	s = ns	s = ns	s < ns	fluox = ctrl
neurofilament H	s < ns	s = ns	s < ns ^t	fluox = ctrl
MAP-2	s = ns	s = ns	s = ns	fluox = ctrl

4.2.2. Glutamate transporters

After the analysis of neurostructural proteins, protein expression levels of glutamate transporters were analyzed in the PTSD mouse model. Alterations in the glutamatergic systems are known to play a role in stress-associated and anxiety disorders (Nair and Singh Ajit, 2008; Sanacora et al., 2012; Rianza Bermudo-Soriano et al., 2012). As glutamate is the major excitatory neurotransmitter in the brain, the prolonged presence of increased extracellular glutamate levels can result in toxic effects. Thus, tight regulation of extracellular glutamate levels is essential. This regulation is mediated mainly by the excitatory amino acid transporters (EAAT) which remove extracellular glutamate by a Na⁺- and K⁺-coupled mechanism. Most of this glutamate transport is accomplished by the astrocytic glutamate transporters, that is GLT1 (EAAT2 in humans) in the forebrain and GLAST (EAAT1) in the cerebellum (Danbolt, 2001). This study concentrated on the analysis of GLT1. In addition to the vesicular glutamate transporters that are responsible for the uptake of glutamate into the synaptic vesicles, also neurons express some glutamate transporters in the cell membrane. The so far best characterized neuronal glutamate transporter, EAAC1 (EAAT3), was analyzed here (Danbolt, 2001).

4.2.2.1. Hippocampal glutamate transporter expression is reduced in mice subjected to a single electric footshock

Since significant alterations of synapsin expression levels were detected only in the hippocampus of footshocked mice, and moreover, since this thesis aimed at deciphering the molecular basis of stress-induced hippocampal shrinkage, most analyses in the thesis at hand concentrated on the hippocampus, in this chapter on hippocampal glutamate transporter expression. Protein expression of GLT1 was analyzed in hippocampal lysates of footshocked and control mice sacrificed either 2 days, 28 days, or 60 days after traumatic footshock (batch PTSD I). GLT1 expression was impressively reduced on day 2 after footshock (Figure 4.11 B; $t = 4.699$, $df = 10$, $p < 0.001$). However, on day 28 and day 60 after footshock the expression was not significantly altered (Figure 4.11 B; d28: $t = 1.666$, $df = 10$, $p = 0.126$; d60: $t = 1.560$, $df = 10$, $p = 0.149$).

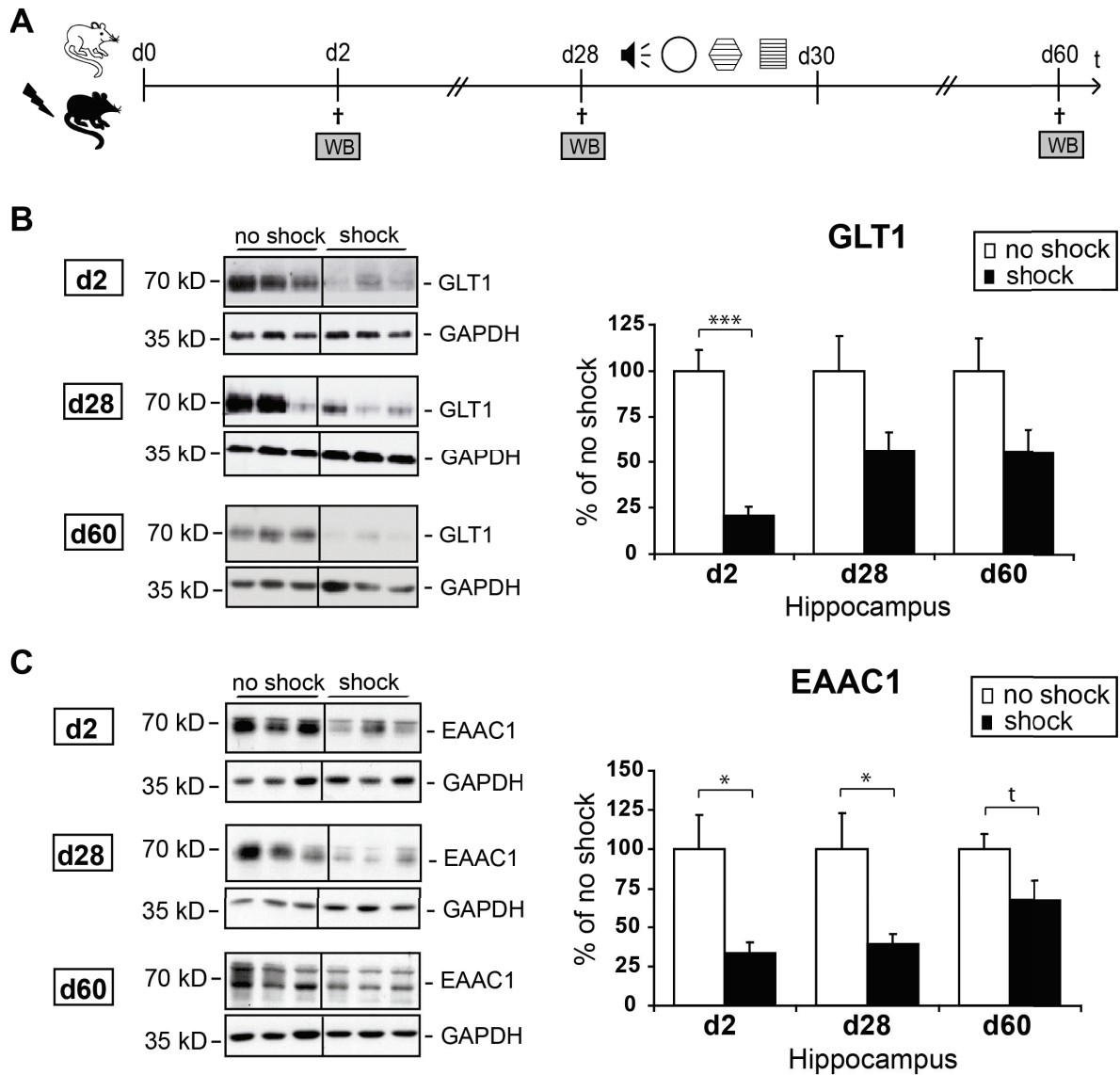


Figure 4.11.: **Hippocampal glutamate transporter expression in traumatized and control mice.** GLT1 and EAAC1 expression was analyzed in hippocampal lysates of C57BL/6NCr1 mice subjected to a single electric footshock and sacrificed either 2, 28, or 60 days later (A). (B-C) Shown are representative western blots of GLT1, EAAC1, or, for control, glycerinaldehyd-3-phosphat-dehydrogenase (GAPDH) analyzed in shocked and non shocked mice. Graphs show relative expression levels of GLT1 or EAAC1 after normalization to GAPDH presented in percent of those of non shocked mice set at 100 %. Plotted data represent means \pm SEM, $n = 6$ (batch PTSD I, see Table 2.2), 2-3 technical replicates. Statistical significance was calculated using student's t -test and is indicated by t $p < 0.1$; * $p < 0.05$; *** $p < 0.001$.

Although the main effect on glutamate clearance is accomplished by the astroglial glutamate transporters, neuronal glutamate transporter expression was also analyzed. So far, three neuronal glutamate transporters have been identified, namely EAAC1 (EAAT3), EAAT4 and EAAT5. In the adult mammalian brain EAAT4 is predominantly expressed by Purkinje cells of the cerebellum. In contrast, not much is known on the cellular localization and function of EAAT5. The third neuronal glutamate transporter EAAC1, however, is mainly expressed in the hippocampus, cerebellum, and basal ganglia (Danbolt, 2001). As this study focused on alterations in hippocampal protein expression, the analysis of neuronal glutamate transporters was restricted to EAAC1. Analysis of EAAC1 expression levels in footshocked and control mice revealed a trauma stress-induced reduction in EAAC1 protein expression in traumatized mice on day 2 and day 28 after footshock (Figure 4.11 C; d2: $t = 2.398$, $df = 10$, $p = 0.037$; d28: $t = 2.268$, $df = 10$, $p = 0.046$), but only showed a trend towards a reduction on day 60 after footshock (Figure 4.11 C; $t = 2.207$, $df = 10$, $p = 0.051$).

4.2.2.2. GFAP protein expression remains unchanged in footshocked mice

As reduced protein levels in GLT1 may also be explained by reduced astrocytic cell numbers, expression levels of the glial fibrillary acidic protein (GFAP), an astrocyte specific cytoskeleton protein, were assessed. However, no changes in hippocampal GFAP expression were detectable at any time-point analyzed (Figure 4.12 B; d2: $t = 1.116$, $df = 10$, $p = 0.290$; d28: $t = 0.666$, $df = 10$, $p = 0.520$; d60: $t = 0.338$, $df = 22$, $p = 0.738$) suggesting a stable number of astrocytes and thus a possibly specific trauma stress-induced effect on glutamate transporter expression. Furthermore, the results of the MAP-2 expression analysis presented in section 4.2.1.3 (Figure 4.7), namely that MAP-2 expression remained unchanged after traumatic stress, suggest that the decreased levels of EAAC1 do not result from reduced neuronal cell numbers.

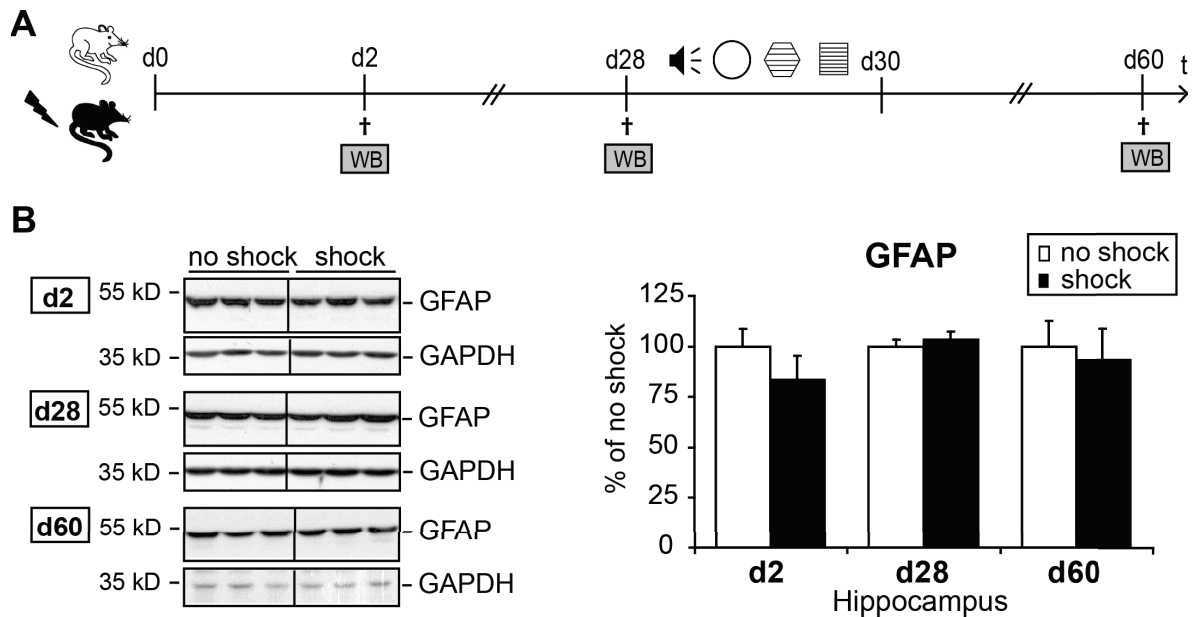


Figure 4.12.: **Hippocampal GFAP expression in traumatized and control mice.**

GFAP expression was analyzed in hippocampal lysates of C57BL/6NCrl mice subjected to a single electric footshock and sacrificed either 2, 28, or 60 days later (A). (B) Shown are representative western blots of GFAP or, for control, glycerinaldehyd-3-phosphat-dehydrogenase (GAPDH) analyzed in shocked and non shocked mice. Graphs show relative expression levels of GFAP after normalization to GAPDH presented in percent of those of non shocked mice set at 100 %. Plotted data represent means \pm SEM, $n = 6$ for d2 and d28 (batch PTSD I, see Table 2.2), $n = 12$ for d60 (batches PTSD I, II), 2-3 technical replicates. Statistical significance was calculated using student's *t*-test.

4.2.2.3. Fluoxetine treatment increases GLT1 but not EAAC1 and GFAP protein expression

Finally, it was investigated whether fluoxetine treatment, which has been demonstrated here to improve PTSD-like symptoms and to increase synaptic protein expression in footshocked mice (see section 4.2.1.5), also affects glutamate transporter expression. Analyzing the same hippocampal lysates as in section 4.2.1.5, fluoxetine treatment was found to significantly increase GLT1 expression in footshocked mice (Figure 4.13 B; $t = 2.657$, $df = 10$, $p = 0.024$), while it did not affect the expression of neither EAAC1 nor GFAP (Figure 4.13 C, D; EAAC1: $t = 0.312$, $df = 10$, $p = 0.754$; GFAP: $t = 0.139$, $df = 10$, $p = 0.892$).

4. Results II: Identification of PTSD candidate proteins in a mouse model of PTSD

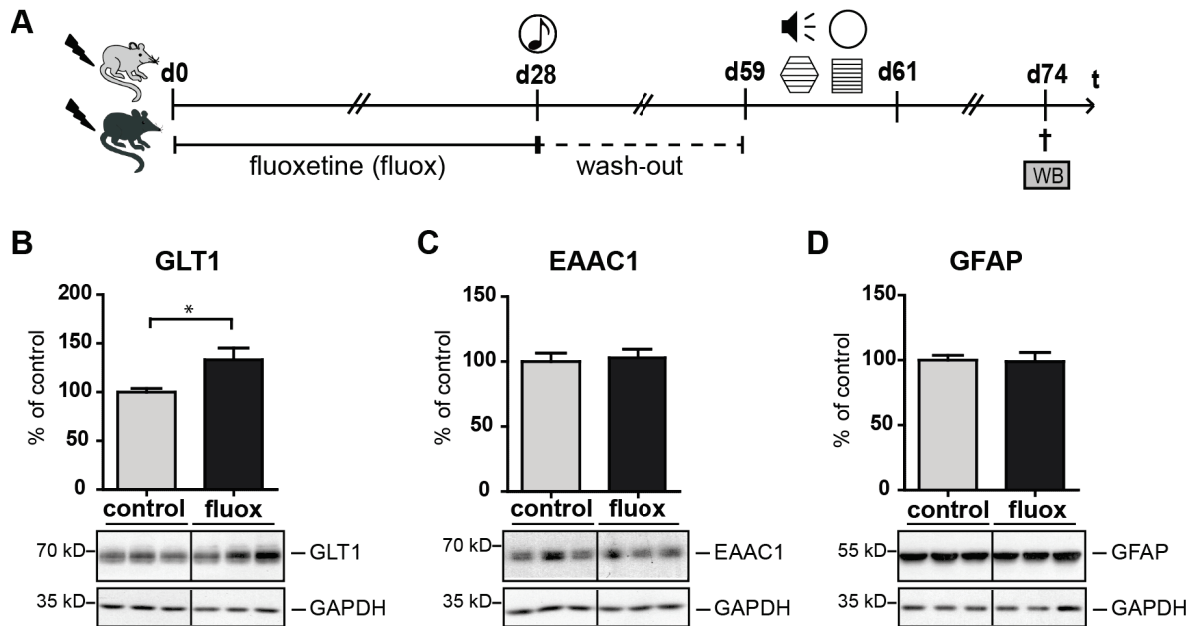


Figure 4.13.: Expression of glutamate transporter proteins in footshocked fluoxetine treated and control mice. (A) Course of experiment, see Figure 4.9 for details. (B-D) Representative western blots of GLT1, EAAC1, GFAP, and, for control, glyceraldehyd-3-phosphat-dehydrogenase (GAPDH) analyzed in hippocampal lysates of shocked control or fluoxetine (fluox) treated mice sacrificed on day 74 after shock. Graphs show relative expression levels after normalization to GAPDH. Expression levels are presented in percent of those of control mice set at 100 % (% of control). Plotted data represent means \pm SEM, $n = 6$ (batch Fluoxetine in PTSD, see Table 2.2), 2-3 technical replicates. Statistical significance was calculated using student's *t*-test and is indicated by * $p < 0.05$.

Taken together, the results of the glutamate transporter expression analysis presented here and summarized in Table 4.2 point towards a trauma stress-induced modulation of the glutamatergic system.

Table 4.2.: **Summary of hippocampal expression changes of glutamate transporter proteins.** Summary of significant expression changes observed in shocked (s) versus non shocked (ns) mice of batch PTSD I and expression changes observed in shocked fluoxetine (fluox) versus control (ctrl) mice of batch 'Fluoxetine in PTSD'. t = statistical trend

Candidate protein	PTSD I			Fluoxetine in PTSD
	d2	d28	d60	d74
GLT1	s < ns	s = ns	s = ns	fluox > ctrl
EAAC1	s < ns	s < ns	s < ns ^t	fluox = ctrl
GFAP	s = ns	s = ns	s = ns	fluox = ctrl

4.2.3. Immune system proteins

As a third group of candidates, proteins associated with the immune system were analyzed for differential expression patterns in mice subjected to the electric footshock or control treatment. Although several lines of evidence suggest a potential role of the immune system in stress-related disorders (Costa-Pinto and Palermo-Neto, 2010), the effect of the first candidate, immunoglobulin G, was found by serendipity.

4.2.3.1. An immunoglobulin G immunoreactive band is detected in the C57BL/6 mouse brain

Using an immunoglobulin G (IgG) Fab-specific anti-mouse antibody in western blot experiments analyzing murine C57BL/6 total brain tissue samples, a prominent 25 kDa band of unknown origin was repeatedly detected (Figure 4.14 B). This band possibly represents endogenously expressed immunoglobulin (Ig) light chains, which are known to have a molecular weight of approximately 25 kD (Schroeder and Cavacini, 2010); this hypothesis is supported by few studies that have detected immunoglobulins in murine brain tissue (Weiner and Chun, 1997; Yoshimi et al., 2002; Upender et al., 1997; Hazama et al., 2005; Huang et al., 2008). To confirm this assumption, the western blot analysis was repeated using murine C57BL/6 spleen lysate, which is known to contain plenty endogenous antibodies. As expected, a similar banding pattern, i.e. containing the 25 kD band, was found in spleen lysate (Figure 4.14 B). In addition to the 25 kDa band, a weak 70 kDa band was detected in both the spleen and the brain lysates, possibly representing a dimer of an Ig light chain (25 kDa) and an Ig heavy chain (50 kDa). To further validate this finding of immunoglobulin expression in the brain, the same brain and spleen lysates were analyzed using antibodies specifically detecting different epitopes of the immunoglobulin G molecule. An antibody molecule typically consists of either two Ig κ or Ig λ light chains which are linked to two Ig heavy chains determining the isotype of the antibody (Schroeder and Cavacini, 2010), as illustrated in Figure 4.14 A.

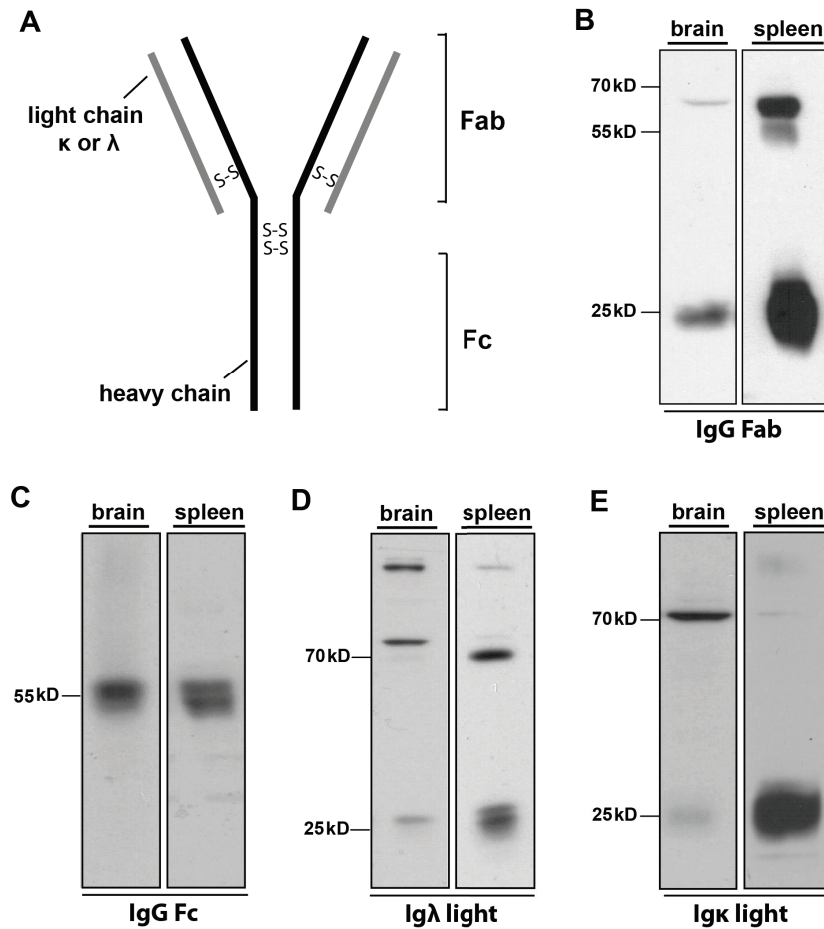


Figure 4.14.: **Immunoglobulin expression in total brain and spleen tissue lysate of wildtype C57BL/6 mice.** (A) Schematic drawing of an immunoglobulin molecule. Indicated are the Fab and the Fc regions as well as the heavy chain (black) and the light chain (grey) that are either of the κ or λ type. The subchains are connected by disulfid bonds (S-S). Western blots using total brain and spleen lysates of C57BL/6 mice are depicted for IgG Fab (B), IgG Fc (C), Ig λ light chain (D), or Ig κ light chain (E) specific antibodies.

As expected from the analysis of murine C57BL/6 brain and spleen lysates employing the IgG Fab-specific antibody (Figure 4.14 B), immunoblot analysis using antibodies specifically detecting the Ig κ light chain, the Ig λ light chain, or the Fc γ heavy chain revealed a comparable banding pattern of the respective subchains in total brain and spleen lysates of C57BL/6 mice (Figure 4.14 C-E).

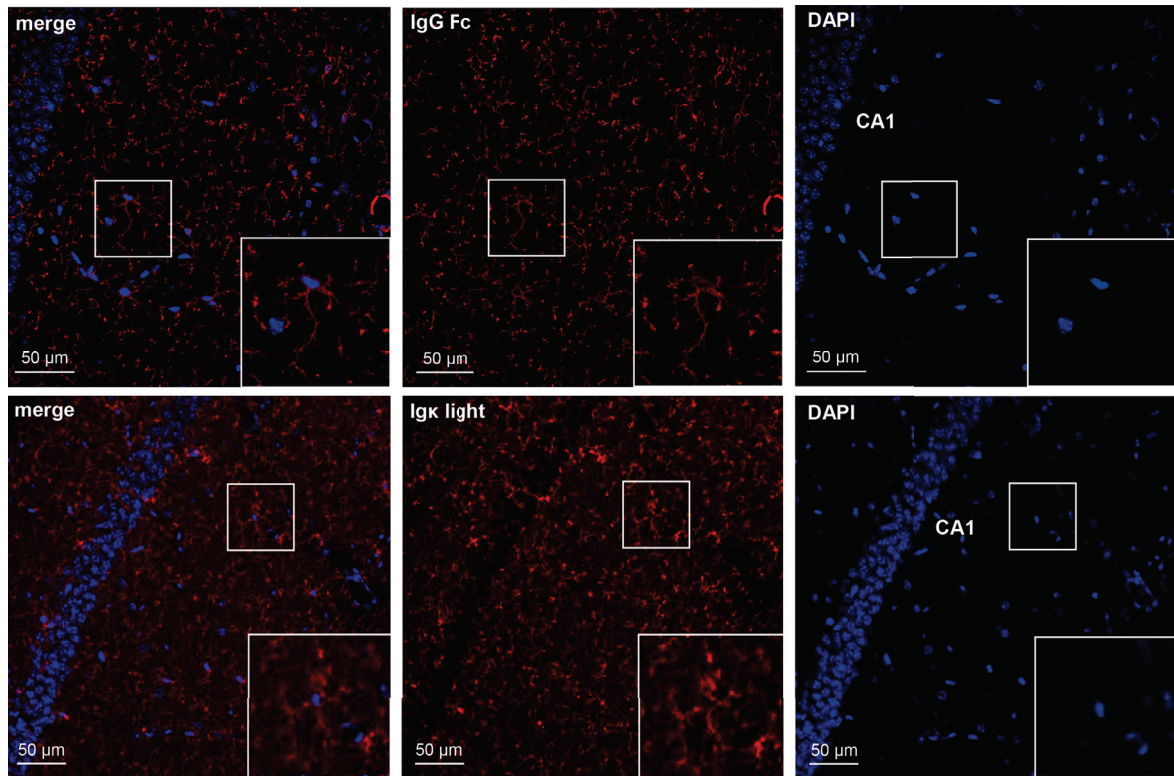


Figure 4.15.: **Immunohistochemical assessment of immunoglobulin expression in the brain.** Shown are representative images of the CA1 region in hippocampal slices of wildtype C57BL/6 mice ($n = 2$) that were stained with either IgG Fc or the Ig κ light chain specific antibodies followed by a fluorescently labeled secondary antibody (middle panel). Slices were counterstained with the nuclear stain DAPI (right panel). The overlay of the DAPI and anti-IgG Fc or anti-Ig κ light chain stained sections is presented in the left panel (merge). Inserts show a 2-fold magnification of the framed area.

To further evaluate the cerebral immunoglobulin expression patterns, immunohistochemical stainings were performed with antibodies detecting the Fc γ heavy chain or the κ light chain. Remarkably, in both cases the antibodies stained specific cellular structures exhibiting numerous branched processes and a small cell body (Figure 4.15).

To identify the cell type in which cerebral IgG expression occurs, immunohistochemical costainings were performed in brain slices of wildtype C57BL/6 mice using an IgG Fab specific antibody and a GFAP specific antibody staining specifically astrocytes, which, however, revealed no colocalization of GFAP with IgG (Figure 4.16). Next, CD31, an endothelial cell marker, was analyzed for colocalization with IgG. The CD31 specific antibody stained

4. Results II: Identification of PTSD candidate proteins in a mouse model of PTSD

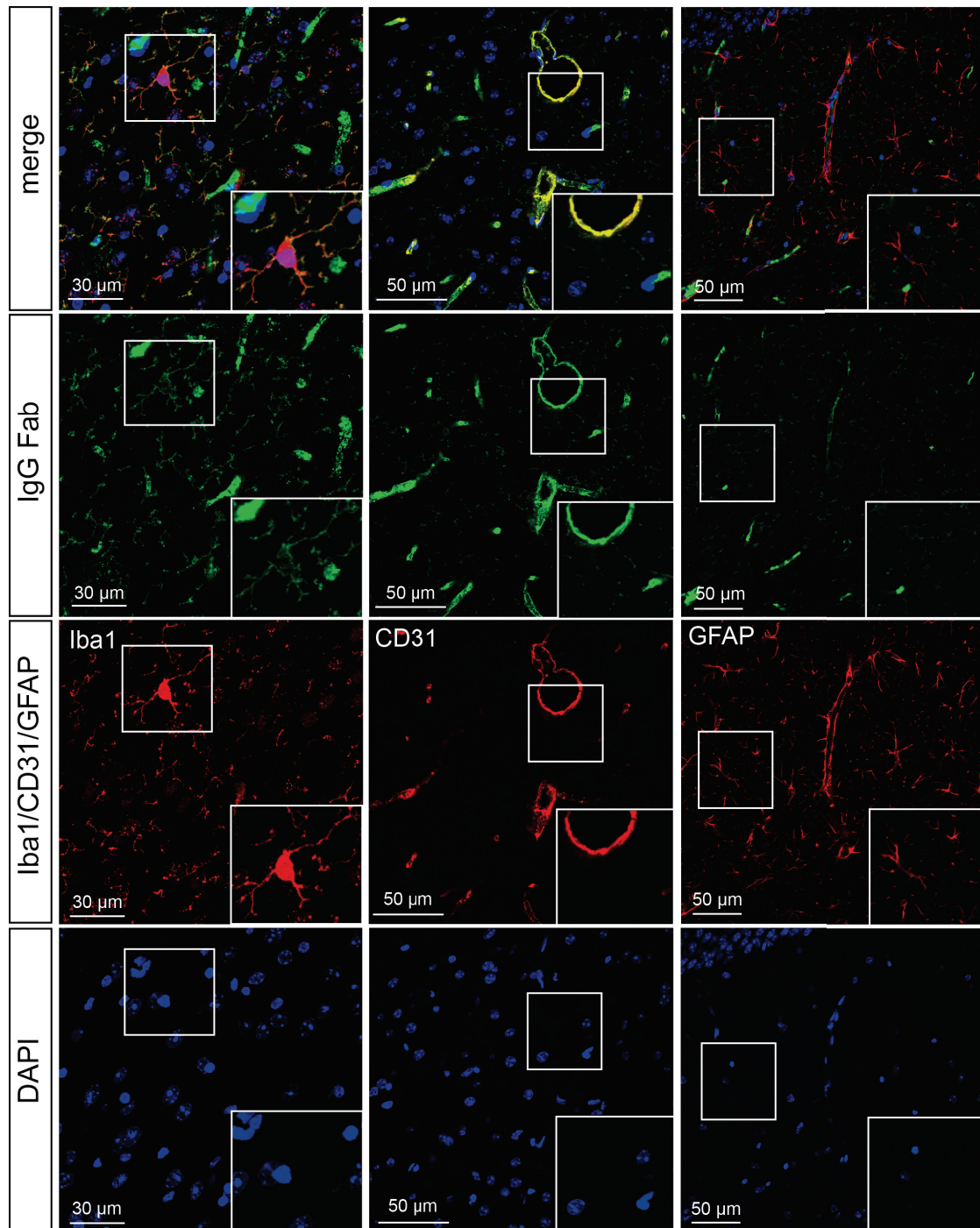


Figure 4.16.: **Identification of IgG associated cell types.** Co-immunostainings were performed on brain slices of unstressed wildtype C57BL/6 mice ($n = 2$) aged 18 weeks. The IgG Fab staining (green) was combined with a staining of either Iba1, CD31, or GFAP (red). All slices were counterstained with the nuclear stain DAPI (blue). An overlay of the IgG Fab and the respective Iba1, CD31, or GFAP staining with DAPI is presented in the panels labeled 'merge', showing a colocalization of IgG Fab with Iba1 and CD31. Inserts show a 1.5-fold magnification of the framed area.

blood vessels in the brain slices. The blood vessels were also stained with the IgG Fab specific antibody resulting in a colocalization of CD31 and IgG in the blood vessels (Figure 4.16). The small cellular structures of unknown origin that were stained by the IgG Fab specific antibody, however, were not stained with the CD31 specific antibody. This suggests, that in addition to endothelial cells another cell type in the brain expresses IgG. Finally, costainings using the IgG Fab specific antibody together with an antibody detecting the microglial marker protein Iba1, which is expressed in both resting and activated microglia, were performed. Here, a clear colocalization of the Iba1 and IgG Fab staining was observed (Figure 4.16). Taken together, the immunohistochemical analyses performed here identified IgG to be associated with microglia and endothelial cells; both of these cell types are known to express the IgG binding $Fc\gamma$ receptors (Quan et al., 2009; Montoyo et al., 2009).

4.2.3.2. IgG expression is increased in mice subjected to a single electric footshock

Next, immunoglobulin G expression was assessed in hippocampus, prefrontal cortex, and cerebellum of traumatized and control mice of the PTSD mouse model. Interestingly, employing the IgG Fab-specific antibody, on day 2 after application of the traumatic footshock no changes in hippocampal IgG levels were detectable (Figure 4.17 A; HC d2: $t = 0.116$, $df = 23$, $p = 0.909$), while at later time-points there was a significant increase of IgG in the hippocampus both on day 28 (Figure 4.17 A; HC d28: $t = 2.144$, $df = 24$, $p = 0.042$) and on day 60 (Figure 4.17 A; HC d60: $t = 2.536$, $df = 47$, $p = 0.015$). In the prefrontal cortex, employing the same IgG Fab-specific antibody, IgG expression did not change significantly on days 2 and 28 (Figure 4.17 B; PFC d2: $t = 0.185$, $df = 24$, $p = 0.855$; PFC d28: $t = 0.112$, $df = 24$, $p = 0.912$), but increased significantly on day 60 (Figure 4.17 B; PFC d60: $t = 2.231$, $df = 47$, $p = 0.031$). In contrast, using the IgG Fab-specific antibody no significant changes in IgG levels were detectable in the cerebellum at any time-point analyzed (Figure 4.17 C; CER d2: $t = 0.851$, $df = 24$, $p = 0.403$; CER d28: $t = 1.317$, $df = 20$, $p = 0.203$; CER d60: $t = 1.510$, $df = 47$, $p = 0.138$).

Further investigations concentrated on the hippocampal region, where a significant increase was detectable both on day 28 and 60 after footshock. To validate and further characterize

4. Results II: Identification of PTSD candidate proteins in a mouse model of PTSD

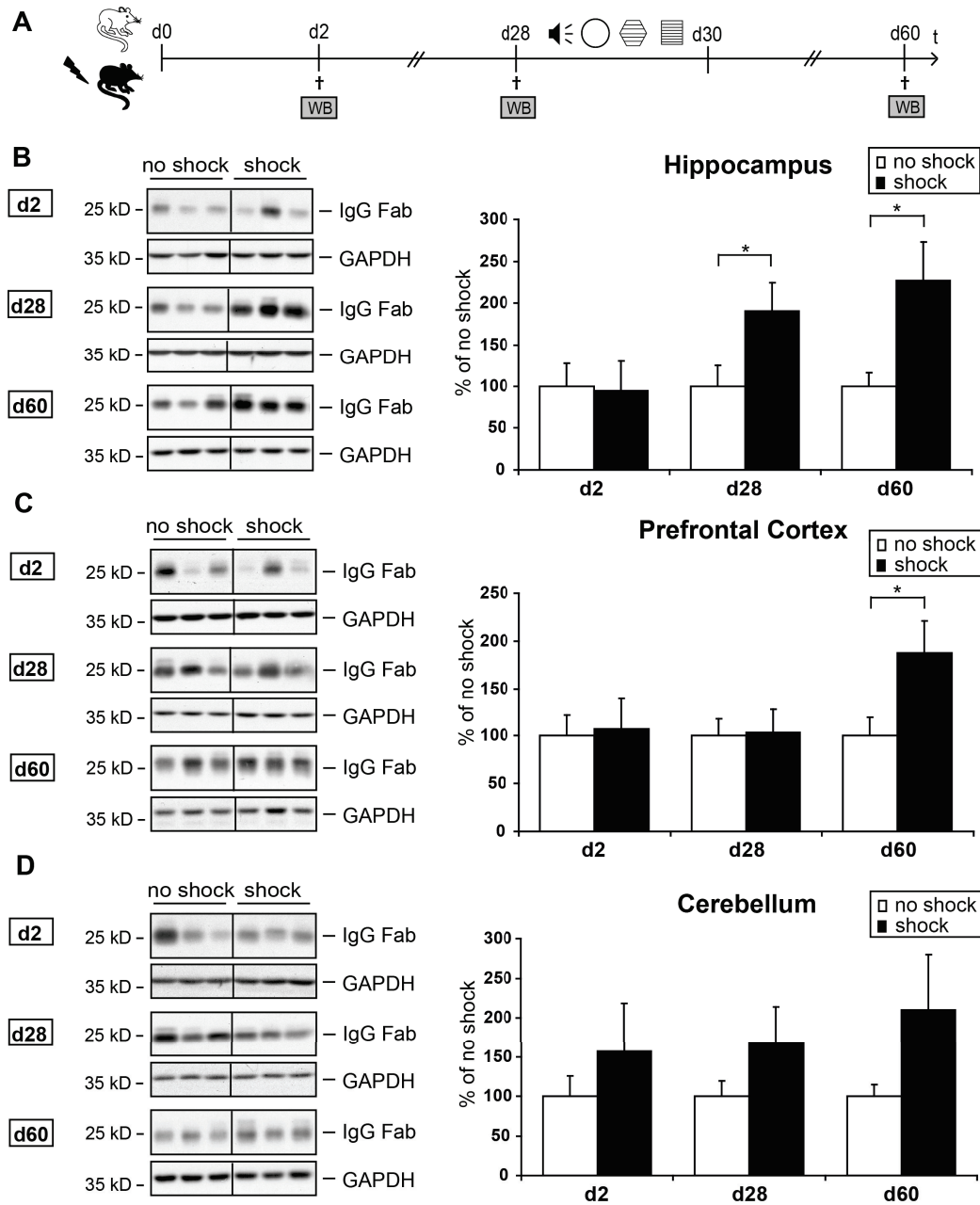


Figure 4.17.: **IgG Fab expression in traumatized and control mice.** C57BL/6NCrI mice were subjected to a single electric footshock and sacrificed either 2, 28, or 60 days later. At each time-point hippocampus (HC), prefrontal cortex (PFC), and cerebellum (CER) were isolated for subsequent western blot analysis (WB). Shown are representative western blots of IgG Fab or, for control, glyceraldehyd-3-phosphat-dehydrogenase (GAPDH) of shocked and non shocked mice in HC (A), PFC (B), and CER (C). Graphs show expression levels of IgG Fab after normalization to GAPDH presented in percent of those of non shocked mice (set at 100 %). Plotted data represent means \pm SEM from all batches analyzed, $n = 13$ (d2, d28; batch PTSD I + IV), $n = 25$ (d60, batch PTSD I-IV, see Table 2.2), 2-3 technical replicates. Statistical significance was calculated using student's *t*-test and is indicated by t $p < 0.1$, * $p < 0.05$.

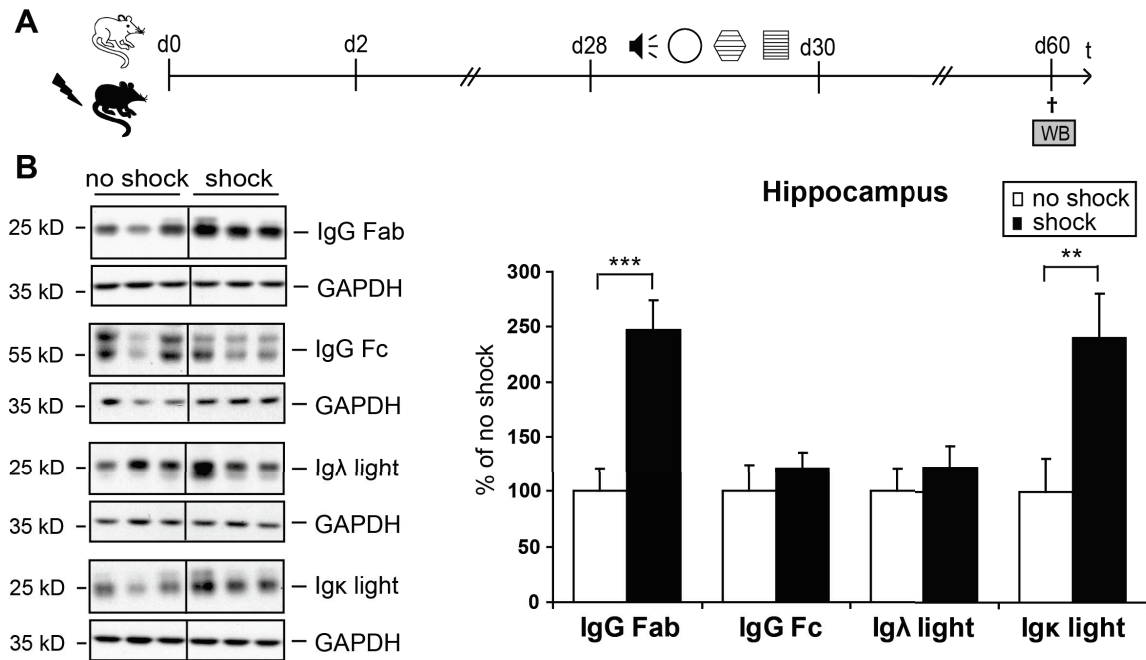


Figure 4.18.: **Hippocampal immunoglobulin expression in traumatized and control mice.** Immunoglobulin expression was analyzed in hippocampal lysates of C57BL/6NCrl mice subjected to a single electric footshock and sacrificed 60 days later by employing antibodies specifically detecting the IgG Fab fragment, the IgG Fc fragment, the Igλ light chain, or the Igκ light chain. Shown are representative western blots of IgG Fab, IgG Fc, Igλ, and Igκ light chain or, for control, glyceraldehyd-3-phosphat-dehydrogenase (GAPDH) analyzed in shocked and non shocked mice. Graphs show relative IgG expression levels after normalization to GAPDH presented in percent of those of non shocked mice set at 100 %. Plotted data represent means \pm SEM, $n = 6$ (batch PTSD III, see Table 2.2), 2-3 technical replicates. Statistical significance was calculated using student's t -test and is indicated by ** $p < 0.01$, *** $p < 0.001$.

the increase in IgG in hippocampal lysates of mice subjected to the electric footshock, antibodies detecting different epitopes of the immunoglobulin molecule were employed in the western blot analysis: hippocampal lysates of mice sacrificed on day 60 after footshock were analyzed employing antibodies specifically detecting the Fcγ heavy chain, the Igκ light chain, or the Igλ light chain. Interestingly, the trauma stress-induced long-term increase in IgG expression levels determined by employing the IgG Fab specific antibody (Figure 4.18; $t = 5.914$, $df = 9$, $p < 0.001$) could be confirmed by using the Igκ light chain specific antibody (Figure 4.18; $t = 4.164$, $df = 9$, $p = 0.002$) but not by using the Igλ light chain specific antibody (Figure 4.18; $t = 0.942$, $df = 9$, $p = 0.371$) or the Fcγ heavy chain specific antibody

4. Results II: Identification of PTSD candidate proteins in a mouse model of PTSD

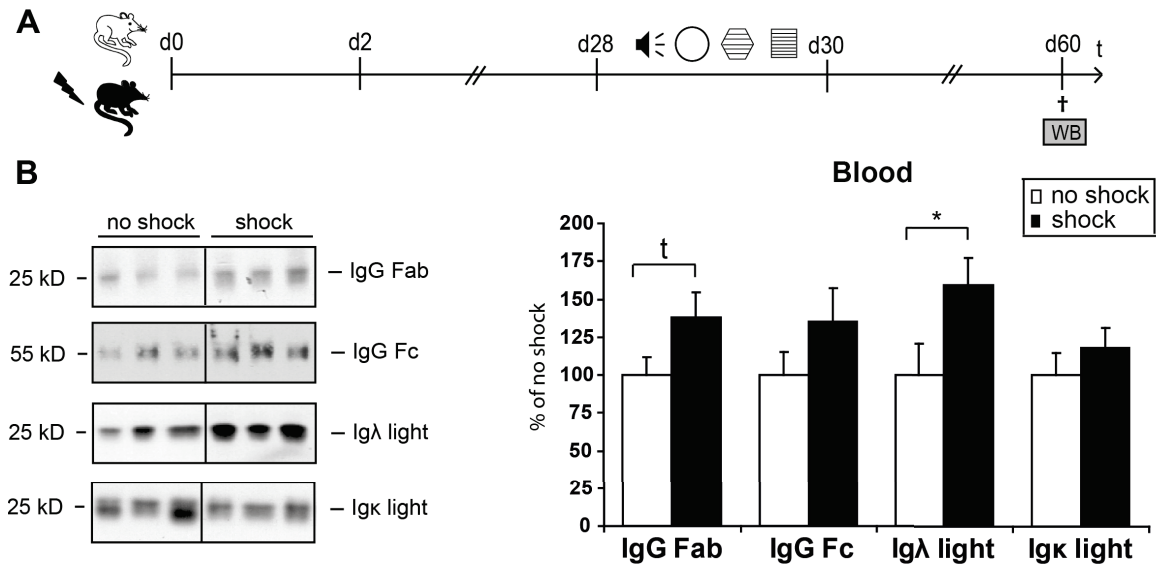


Figure 4.19.: **Immunoglobulin expression in blood samples of traumatized and control mice.** Immunoglobulin expression was analyzed in blood samples of C57BL/6NCrI mice subjected to a single electric footshock and sacrificed 60 days later by employing antibodies specifically detecting the IgG Fab fragment, the IgG Fc fragment, the Igλ light chain, or the Igκ light chain. Shown are representative western blots of IgG Fab, IgG Fc, Igλ, and Igκ light chain analyzed in shocked and non shocked mice. Graphs show relative IgG expression levels presented in percent of those of non shocked mice set at 100 %. Plotted data represent means ± SEM, n = 6 (batch PTSD III, see Table 2.2), 2-3 technical replicates. Statistical significance was calculated using student's *t*-test and is indicated by t p < 0.1, * p < 0.05.

(Figure 4.18; $t = 1.052$, $df = 9$, $p = 0.320$). These experiments show for the first time a stress-induced regulation of immunoglobulin proteins, and in particular of the κ light chain containing immunoglobins.

Although sporadic reports exist demonstrating that IgG is produced by neurons (Huang et al., 2008), most studies investigating the presence of immunoglobulin G molecules in the brain suggest that neurons or microglia take up IgG delivered into the brain via the blood (Yoshimi et al., 2002; Upender et al., 1997; Hazama et al., 2005), which carries antibodies produced by plasma cells. Therefore, IgG expression levels were analyzed in blood of traumatized and mock treated control mice (Figure 4.19). Interestingly, employing the IgG Fab specific antibody, the increase in IgG in the blood of traumatized mice was detectable only at the level of a statistical trend (Figure 4.19; $t = 2.250$, $df = 9$, $p = 0.051$). Moreover, in contrast to

the results obtained by analyzing IgG expression level differences in hippocampal lysates, no protein expression level differences were found in the blood using the Ig κ light chain specific antibody (Figure 4.19; $t = 0.877$, $df = 9$, $p = 0.403$), while employing the Ig λ light chain specific antibody yielded an increase in immunoglobulin expression in blood of mice subjected to the footshock (Figure 4.19; $t = 2.297$, $df = 9$, $p = 0.047$). As expected from analysis of hippocampal lysates, no IgG expression level differences were measured in the blood using the Fc γ heavy chain specific antibody (Figure 4.19; $t = 1.514$, $df = 9$, $p = 0.164$). Thus, although the immunoglobulins detected in the brain might originate from the blood, trauma stress differentially regulates the expression of Ig κ and Ig λ carrying antibodies in brain and blood.

4.2.3.3. IgG expression is reduced in HAB compared to LAB mice

To investigate if the regulation of IgG protein expression is a specific characteristic of traumatic stress or a general feature of stress and anxiety-related phenotypes, IgG expression was also assessed in 19 week old mice showing high anxiety-related behavior (HAB) or low anxiety-related behavior (LAB), representing a model of extremes in trait anxiety (introduced in 1.5.2) (Krömer et al., 2005). Assessment of IgG expression in the HAB/LAB mouse model revealed strong differences between HAB and LAB mice: employing the IgG Fab specific antibody HAB mice were found to express considerably lower hippocampal and cerebellar IgG protein levels than the LAB mice (Figure 4.20 A; HC: $t = 8.007$, $df = 9$, $p < 0.001$; CER: $t = 6.010$, $df = 9$, $p < 0.001$). The prefronto-cortical samples of this mouse batch were used in other experiments and were therefore not analyzed for IgG expression. In contrast to the PTSD mouse model (Figure 4.17), the changes in IgG expression seem to affect the whole brain, as decreased IgG expression levels were found in HAB mice in all brain regions tested. Employing the Fc γ heavy chain specific antibody (Figure 4.20 B; HC: $t = 2.870$, $df = 9$, $p = 0.019$; CER: $t = 4.595$, $df = 9$, $p = 0.001$) and the Ig κ light chain specific antibody (Figure 4.20 D; HC: $t = 4.347$, $df = 9$, $p = 0.002$; CER: $t = 4.077$, $df = 9$, $p = 0.003$) revealed decreased expression levels both in the hippocampus and in the cerebellum of HAB compared to those of LAB mice. In contrast, increased expression levels were detected in hippocampal

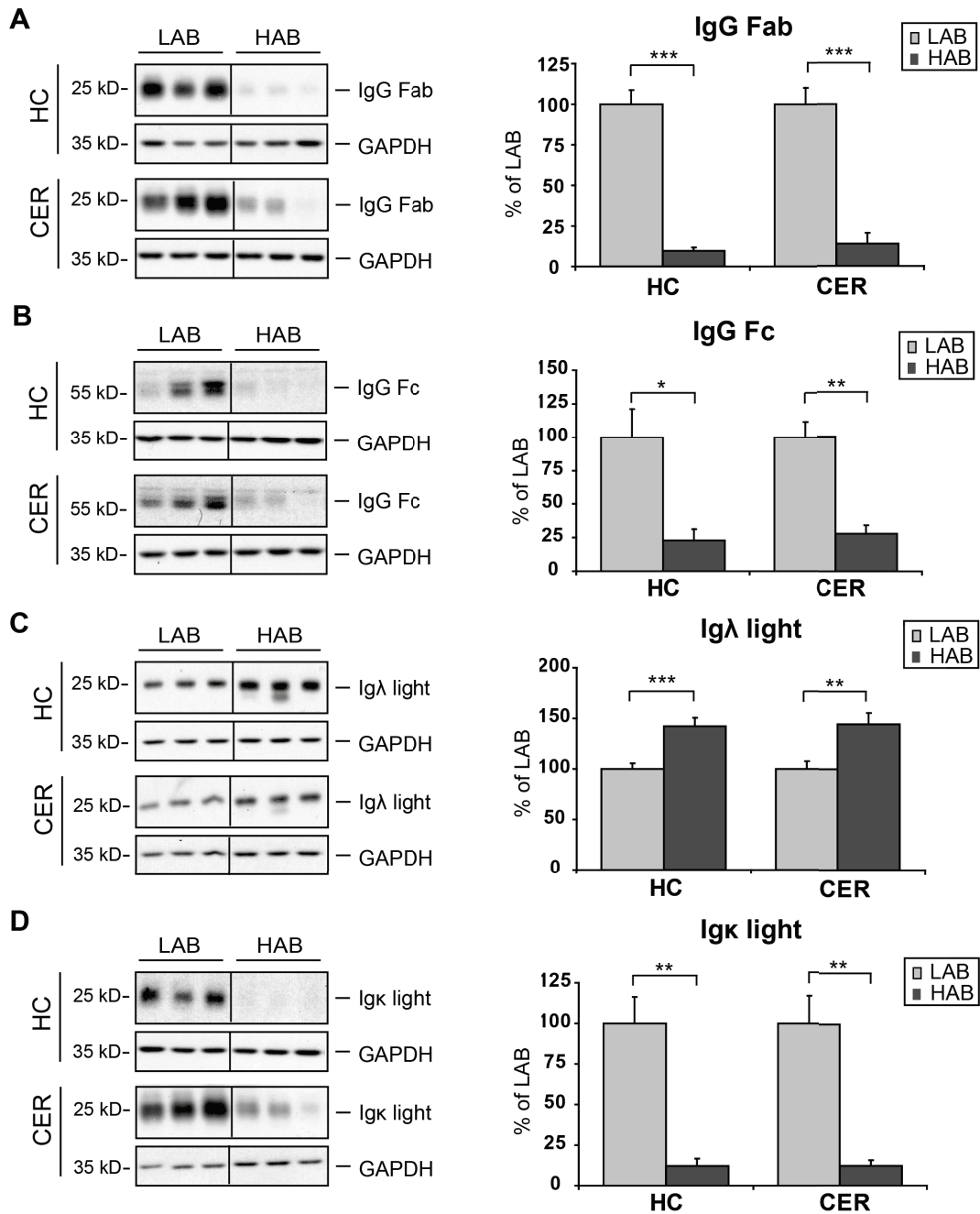


Figure 4.20.: **Immunoglobulin expression in HAB and LAB mice.** IgG expression was analyzed employing the IgG Fab, IgG Fc, Igλ, and Igκ light chain specific antibody in hippocampal and cerebellar lysates of HAB and LAB mice aged 19 weeks. Shown are representative western blots using the IgG Fab (A), IgG Fc (B), Igλ (C), and Igκ (D) light chain specific antibody or, for control, a glyceraldehyd-3-phosphat-dehydrogenase (GAPDH) specific antibody. Graphs show relative expression levels after normalization to GAPDH presented in percent of those of LAB mice set at 100 %. Plotted data represent means ± SEM, n = 7 (LAB), n = 4 (HAB) (batch HAB/LAB, see Table 2.2), 2-3 technical replicates. Statistical significance was calculated using student's *t*-test and is indicated by * $p < 0.05$, ** $p < 0.01$, *** $p < 0.001$.

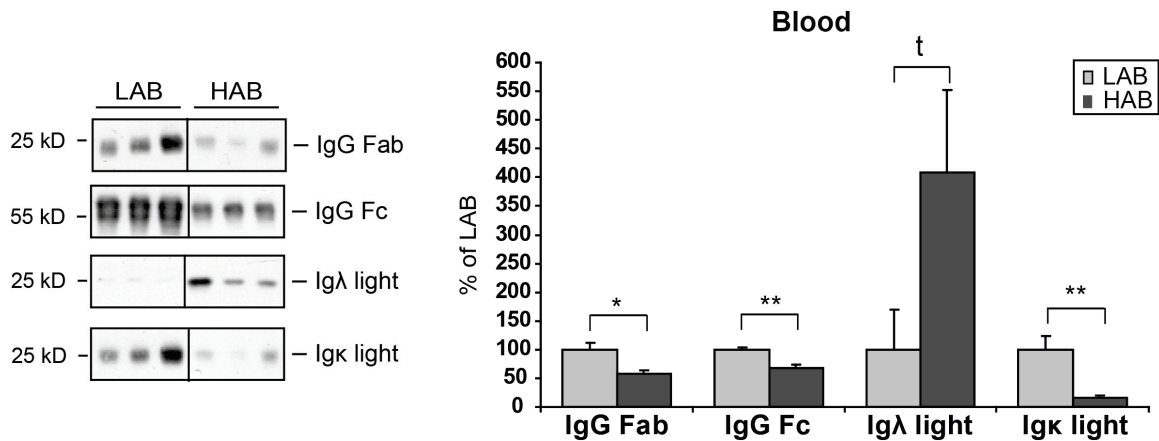


Figure 4.21.: **Immunoglobulin expression in the blood of HAB and LAB mice.** IgG expression was analyzed employing the IgG Fab, IgG Fc, Igλ, and Igκ light chain specific antibody in the blood of HAB and LAB mice. Shown are representative western blots using the IgG Fab, IgG Fc, Igλ, and Igκ light chain specific antibody. Graphs show relative expression levels presented in percent of those of LAB mice set at 100 %. Plotted data represent means \pm SEM, $n = 7$ (LAB), $n = 4$ (HAB) (batch HAB/LAB, see Table 2.2), 2-3 technical replicates. Statistical significance was calculated using student's *t*-test and is indicated by * $p < 0.05$, ** $p < 0.01$, *** $p < 0.001$.

and cerebellar lysates of HAB mice using the Igλ light chain specific antibody (Figure 4.20 C; HC: $t = 5.399$, $df = 9$, $p < 0.001$; CER: $t = 4.331$, $df = 9$, $p = 0.002$). Finally, the analysis of HAB and LAB blood samples yielded results comparable to those gained by analysis of the brain, i.e. decreased immunoglobulin expression levels using the IgG Fab, the IgG Fcγ heavy chain, and the Ig κ light chain specific antibody as well as increased immunoglobulin expression levels in HAB mice compared to LAB mice employing the Ig λ light chain specific antibody (Figure 4.21; IgG Fab: $t = 2.974$, $df = 12$, $p = 0.012$; IgG Fc: $t = 3.824$, $df = 12$, $p = 0.002$; Igλ light chain: $t = 1.948$, $df = 12$, $p = 0.075$; Igκ light chain: $t = 3.386$, $df = 12$, $p = 0.005$).

Interestingly, IgG expression analysis employing antibodies specifically detecting different epitopes of the immunoglobulin protein revealed differences in the trauma stress-induced regulation of Igκ and Igλ carrying antibodies in the hippocampus and the blood of mice subjected to the electric footshock, while in the HAB/LAB mouse model IgG expression level differences in the blood largely reflect the IgG expression level differences in the brain.

4. Results II: Identification of PTSD candidate proteins in a mouse model of PTSD

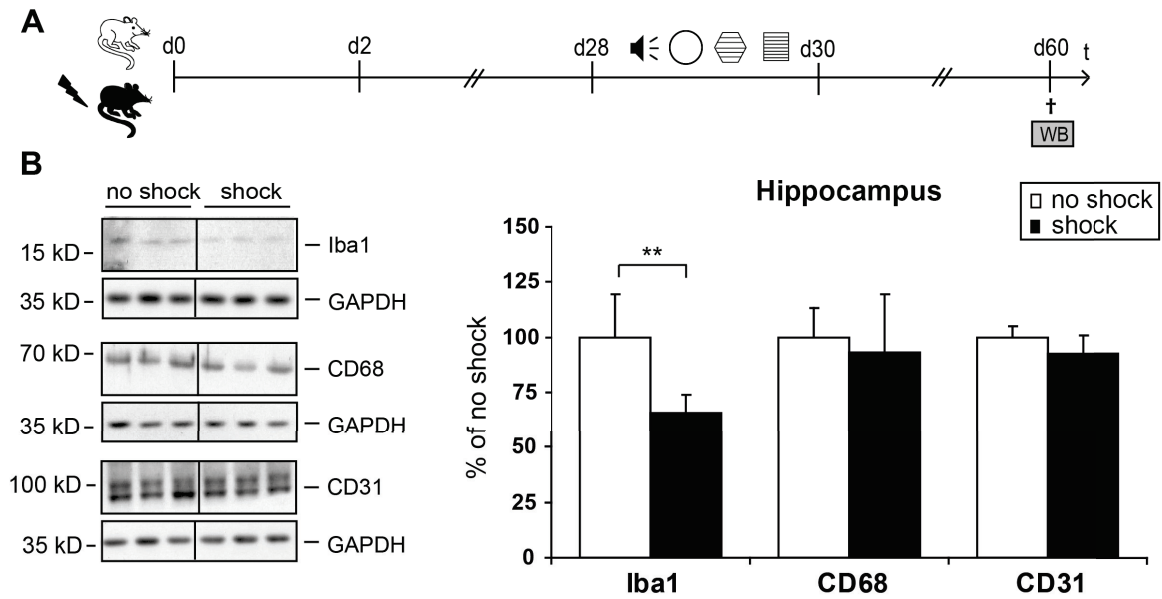


Figure 4.22.: **Expression of microglial and endothelial cell markers in the PTSD mouse model.** Expression of Iba1, CD68, and CD31 was analyzed in hippocampal lysates of C57BL/6NCrl mice subjected to a single electric footshock and sacrificed 60 days later. Shown are representative western blots of Iba1, CD68, and CD31 or, for control, glyceraldehyd-3-phosphat-dehydrogenase (GAPDH) analyzed in shocked and non shocked mice. Graphs show relative expression levels of Iba1, CD68, and CD31 after normalization to GAPDH presented in percent of those of non shocked set at 100 %. Plotted data represent means \pm SEM, $n = 6$ (batch PTSD III, see Table 2.2), 2-3 technical replicates. Statistical significance was calculated using student's *t*-test and is indicated by ** $p < 0.01$.

4.2.3.4. Analysis of microglial and endothelial marker protein expression levels in the PTSD and the HAB/LAB mouse model

Immunohistochemical costainings revealed an association of IgG with microglial and endothelial cells (Figure 4.16). Next, to assess the influence of state anxiety (PTSD mouse model) and trait anxiety (HAB/LAB mouse model) on the expression of microglial and endothelial marker proteins, expression levels of the microglial marker protein Iba1, of CD68, which specifically detects activated microglia, and of the endothelial cell marker CD31 were measured. These analyses revealed no significant alterations of CD31 protein levels neither in the hippocampus of footshocked and mock treated control mice sacrificed 60 days after footshock or mock treatment nor in the hippocampus or the cerebellum of HAB and LAB mice

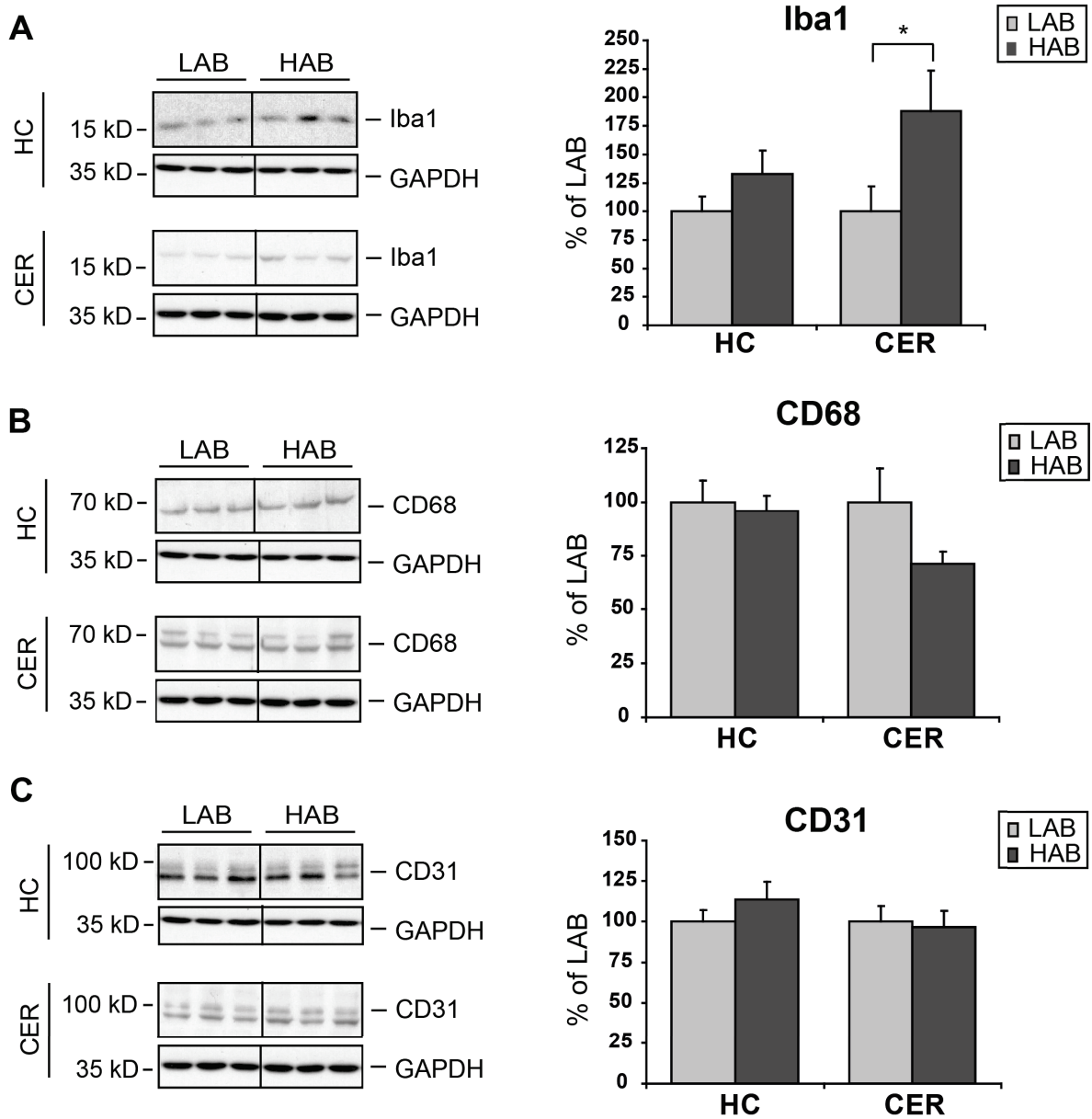


Figure 4.23.: **Expression of microglial and endothelial cell markers in HAB and LAB mice.** Expression of Iba1, CD68, and CD31 was analyzed in hippocampal and cerebellar lysates of HAB and LAB mice. Shown are representative western blots of Iba1 (A), CD68 (B), and CD31 (C) or, for control, glyceraldehyd-3-phosphat-dehydrogenase (GAPDH). Graphs show relative expression levels of Iba1, CD68, and CD31 after normalization to GAPDH presented in percent of those of LAB mice set at 100 %. Plotted data represent means \pm SEM, $n = 4$ (HAB), $n = 7$ (LAB) (batch HAB/LAB, see Table 2.2), 2-3 technical replicates. Statistical significance was calculated using student's t -test and is indicated by * $p < 0.05$, ** $p < 0.01$.

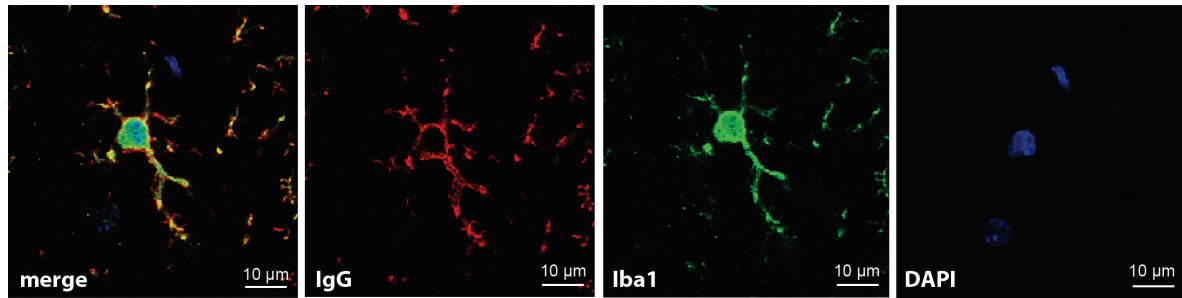


Figure 4.24.: **IgG is associated to the cell surface of microglia.** Shown are representative images of brain slices of unstressed C57BL/6 wildtype ($n = 2$) mice that were stained with an IgG Fc (red) and an Iba1 (green) specific antibody followed by appropriate fluorescently labeled secondary antibodies. Slices were counterstained with the nuclear stain DAPI (blue). The overlay of anti-IgG Fc and anti-Iba1 staining with DAPI is presented in the left panel (merge).

(Figure 4.22, Figure 4.23 C; HC PTSD: $t = 0.789$, $df = 9$, $p = 0.450$; HC HAB/LAB: $t = 1.420$, $df = 9$, $p = 0.189$; CER HAB/LAB: $t = 0.270$, $df = 9$, $p = 0.793$). In contrast, protein expression levels of Iba1 were reduced in the hippocampus of traumatized mice sacrificed 60 days after footshock (Figure 4.22; $t = 2.990$, $df = 9$, $p = 0.015$) and increased in the cerebellum but not in the hippocampus of HAB versus LAB mice (Figure 4.23 A; HC: $t = 1.423$, $df = 9$, $p = 0.188$; CER: $t = 2.317$, $df = 9$, $p = 0.045$). Interestingly, the decrease of Iba1 expression levels in traumatized mice was paralleled by increased IgG expression levels (Figure 4.17), while increased Iba1 expression levels in HAB mice in the cerebellum were accompanied with a decreased expression of IgG (Figure 4.20). Finally, assessment of CD68 expression levels revealed no significant changes of this marker protein for activated microglia in either mouse model (Figure 4.22, Figure 4.23; PTSD HC: $t = 0.320$, $df = 9$, $p = 0.755$; HAB/LAB HC: $t = 0.369$, $df = 9$, $p = 0.720$; HAB/LAB CER: $t = 1.812$, $df = 9$, $p = 0.103$).

Detailed microscopical analysis of immunohistochemical costainings of IgG and the microglial marker Iba1 suggest that IgG is associated to the cell surface of microglia rather than to the cytosol which was not stained by the IgG specific antibody (Figure 4.24). The cell surface localization of IgG might be mediated via Fc receptors, e.g. $Fc\gamma RI$, that is able to bind the Fc fragment of IgG antibodies (Sondermann and Oosthuizen, 2002). In microglial cells, $Fc\gamma$ receptor signaling induces processes like phagocytosis and cytokine production by activating the MAPK signaling pathway, Ca^{+} mobilization and actin reorganization (Takai,

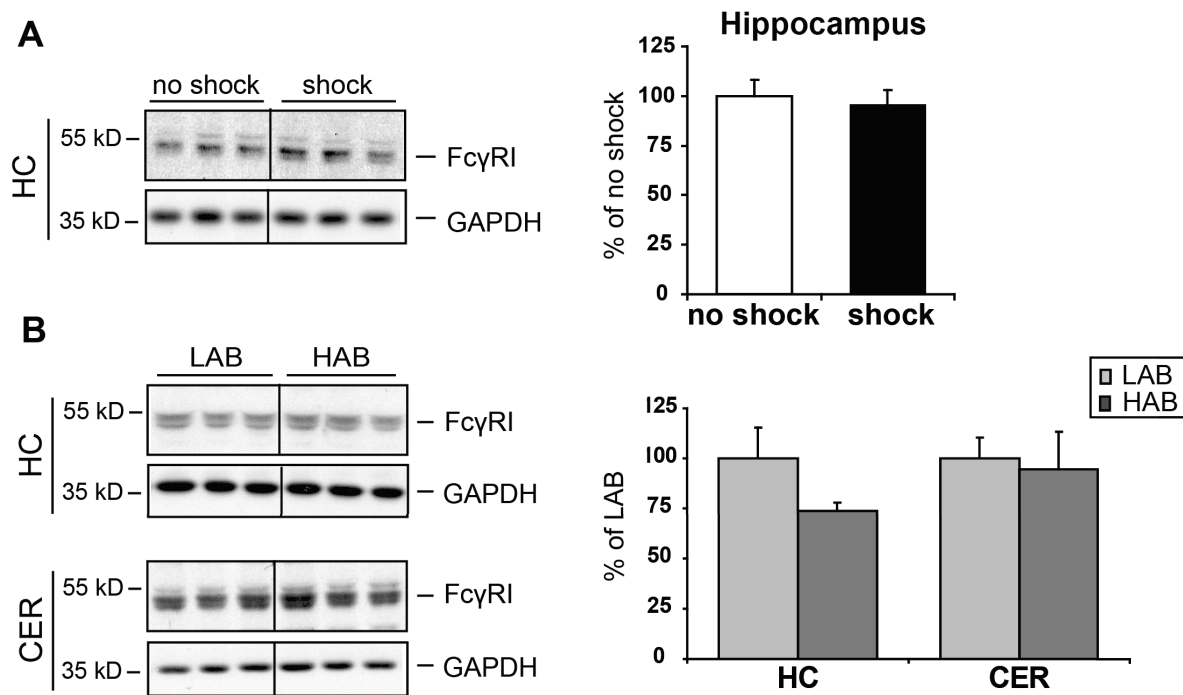


Figure 4.25.: **Fc γ RI expression analysis in the PTSD and the HAB/LAB mouse model.** Fc γ RI expression was analyzed in hippocampal lysates of shocked and non shocked mice sacrificed 60 days after footshock (A) and in hippocampal (HC) and cerebellar (CER) lysates of HAB and LAB mice (B). Shown are representative western blots of Fc γ RI or, for control, glyceraldehyd-3-phosphat-dehydrogenase (GAPDH). Graphs show relative expression levels of Fc γ RI after normalization to GAPDH presented in percent of those of LAB mice set at 100 % (% of LAB) or of non shocked mice set at 100 % (% of no shock). Plotted data represent means \pm SEM, $n = 6$ (batch PTSD III, see Table 2.2), $n = 4$ (HAB), $n = 7$ (LAB) (batch HAB/LAB, see Table 2.2), 2-3 technical replicates. Statistical significance was calculated using student's t -test and revealed no significant changes.

2002). Stress-induced microglial Fc γ R expression changes have so far not been studied. The analysis of Fc γ RI levels by western blotting performed here revealed no expression changes in the PTSD mouse model and also not in the HAB/LAB mouse model (Figure 4.25; HC PTSD: $t = 0.474$, $df = 9$, $p = 0.646$; HAB/LAB HC: $t = 1.227$, $df = 9$, $p = 0.250$; HAB/LAB CER: $t = 0.989$, $df = 9$, $p = 0.348$). Nevertheless, this result does not exclude a possible increase in activation of the Fc γ receptor associated signaling pathway. To clarify this, it will be required to analyze downstream molecules of the Fc γ receptor, for example the src-family kinases that play a role in the phosphorylation of the Fc γ receptor (Takai, 2002).

Table 4.3.: **Summary of expression level changes of immune system proteins.**

Summary of significant expression changes observed in shocked (s) versus non shocked (ns) mice of batch PTSD III and in HAB versus LAB mice of the HAB/LAB batch. Iba1, CD68, CD31, and Fc γ RI were not detected in blood samples (n.d.). t = statistical trend

Candidate protein	PTSD III		HAB/LAB		
	HC d60	blood	HC	CER	blood
IgG Fab	s > ns	s > ns ^t	HAB < LAB	HAB < LAB	HAB < LAB
IgG Fc	s = ns	s = ns	HAB < LAB	HAB < LAB	HAB < LAB
Ig λ light	s = ns	s > ns	HAB > LAB	HAB > LAB	HAB > LAB ^t
Ig κ light	s > ns	s = ns	HAB < LAB	HAB < LAB	HAB < LAB
Iba1	s < ns	n.d.	HAB = LAB	HAB > LAB	n.d.
CD68	s = ns	n.d.	HAB = LAB	HAB = LAB	n.d.
CD31	s = ns	n.d.	HAB = LAB	HAB = LAB	n.d.
Fc γ RI	s = ns	n.d.	HAB = LAB	HAB = LAB	n.d.

Taken together, as summarized in Table 4.3, IgG levels were increased in the hippocampus and in the blood of traumatized mice 60 days after application of the electric footshock. In addition, IgG expression levels were also altered in a different mouse model, the HAB/LAB trait anxiety mouse model: high anxiety mice (HAB) expressed considerably lower amounts of IgG in the hippocampus, the cerebellum, and the blood. Furthermore, IgG was identified to be associated with microglial cells, which was paralleled by a decreased hippocampal expression of the microglial marker protein Iba1 in mice subjected to the electric footshock and an increased cerebellar expression of Iba1 in HAB mice. The protein expression levels of the microglial IgG receptor Fc γ RI, however, remained unchanged in all samples analyzed.

4.2.3.5. *In silico* analysis of immunoglobulin expression in PTSD patients

To translate the findings of the animal research presented above and summarized in Table 4.3 to the patient, immunoglobulin mRNA expression was analyzed in publicly available microarray data from trauma exposed controls and trauma survivors admitted to the emergency room displaying PTSD symptoms at admittance and 4 month later (Segman et al., 2005). Assessing overall peripheral blood mononuclear cell (PBMC) gene expression profiles in PTSD, Segman et al. (2005) have described a distinct alteration in expression of genes involved in immune activation (Segman et al., 2005). In this thesis, the expression of different immunoglobulin

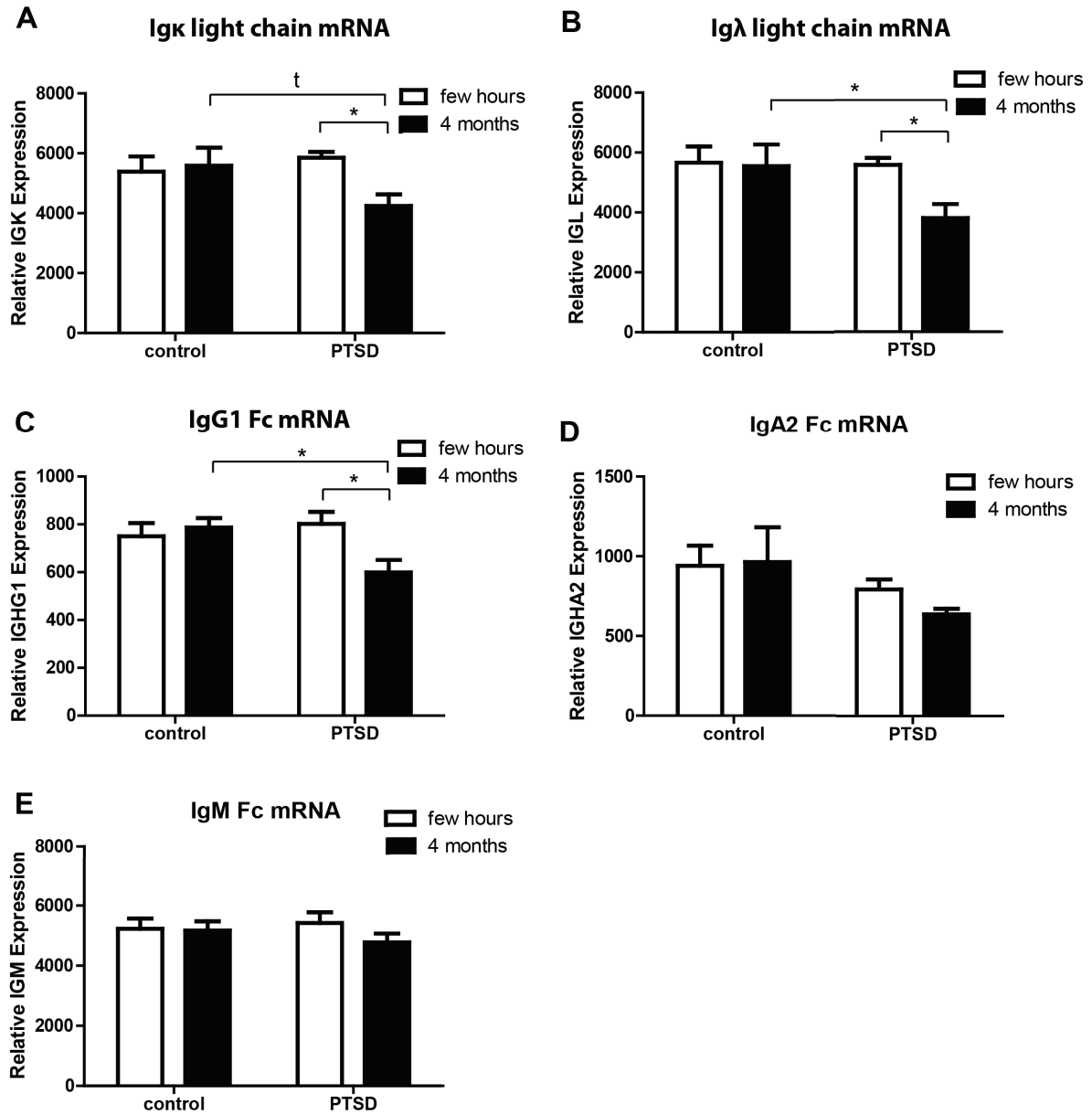


Figure 4.26.: *In silico* analysis of IgG mRNA expression in human peripheral mononuclear blood cells (PBMC) of PTSD patients in comparison to trauma-exposed controls. Microarray gene expression data generated by Segman et al. (2005) was retrieved from the publicly available NCBI GEO DataSets (accession number GDS1020). Expression data for Igκ light chain, Igλ light chain, IgG1 heavy chain, IgA2 heavy chain, and IgM heavy chain transcripts from trauma survivors with (PTSD) or without (control) PTSD symptoms either few hours or 4 month after the traumatic event were statistically analyzed. Plotted data represent mean \pm SEM, $n = 9$. Statistical significance was calculated using two-way ANOVA and Bonferroni post-tests and is indicated by t $p < 0.1$; * $p < 0.05$.

4. Results II: Identification of PTSD candidate proteins in a mouse model of PTSD

Table 4.4.: **Summary of immunoglobulin expression changes in animal models and PTSD patients.** Summary of significant expression changes observed in the blood of PTSD patients and controls 4 month after the traumatic event, in blood of shocked (s) versus non shocked (ns) mice of batch PTSD III, and in blood of HAB versus LAB mice of the HAB/LAB batch. IgG Fab was not detected in blood samples of PTSD patients (n.d.), IGHA2 and IGHM were not detected in murine blood samples (n.d.).

Candidate protein	Blood		
	PTSD patients [mRNA]	mouse batch PTSD III d60 blood [protein]	mouse batch HAB/LAB blood [protein]
IgG Fab	n.d.	s > ns	HAB < LAB
IgG Fc	PTSD < control	s = ns	HAB < LAB
Ig λ light	PTSD < control	s > ns	HAB > LAB
Ig κ light	PTSD < control	s = ns	HAB < LAB
IGHA2	PTSD = control	n.d.	n.d.
IGHM	PTSD = control	n.d.	n.d.

transcripts were now analyzed in further detail employing an *in silico* approach. For this, microarray gene expression data in PBMCs of trauma survivors and trauma exposed controls were retrieved from the NCBI GEO DataSets (accession number GDS1020). Expression levels of Ig κ light chain, Ig λ light chain, IgG1 heavy chain, IgA2 heavy chain, and IgM heavy chain transcripts were statistically analyzed (Figure 4.26). Ig κ light chain and Ig λ light chain mRNA expression was significantly reduced in PTSD patients 4 month but not few hours after the traumatic event (Figure 4.26 A, B; two-way ANOVA plus Bonferroni post-test; PTSD_(fewhours,4month): Ig κ light chain: $t = 2.555$, $p < 0.05$; Ig λ light chain: $t = 2.385$, $p < 0.05$; 4 month_(control,PTSD): Ig κ light chain: $t = 2.205$, $p < 0.1$; Ig λ light chain: $t = 2.417$, $p < 0.05$). Among the analyzed heavy chain transcripts only IgG1 showed a significant reduction in PTSD patients 4 month after the traumatic event, while the expression of IgA2 and IgM was not significantly altered (Figure 4.26 C-E; two-way ANOVA plus Bonferroni post-test; PTSD_(fewhours,4month): IgG1 Fc: $t = 2.960$, $p < 0.05$; IgA2 Fc: $t = 0.823$, $p > 0.05$; IgM Fc: $t = 1.443$, $p > 0.05$; 4 month_(control,PTSD): IgG1 Fc: $t = 2.820$, $p < 0.05$).

Taken together, as summarized in Table 4.4, IgG expression was decreased in PTSD patients and HAB mice, while it was increased in traumatized mice of the PTSD mouse model. Although it might have been expected to detect increased expression of IgG in PTSD patients

similar to the here presented observation in traumatized mice, this nevertheless suggests that immune system associated proteins and specifically immunoglobins are an important stress-modulated parameter not only in the animal model but also in human patients. Besides probable species specific effects, an important difference between the human and the animal data is that the microarray study analyzed mRNA expression while in the animal models IgG protein expression was assessed.

4.3. Summary of Results II

To sum up, several novel candidate proteins of PTSD have been identified in the second part of this thesis. First, analysis of neurostructural proteins revealed a pronounced long-term reduction of the synaptic proteins synapsin, synaptophysin, and homer 1b/c and the neuronal cytoskeleton protein neurofilament H in the hippocampus of mice subjected to a traumatic footshock, which, in contrast, did not affect the expression of the dendritic protein MAP-2 and the astroglial marker protein GFAP (summarized in Table 4.1). Second, the electric footshock elicited a marked decrease of both neuronal (EAAC1) and glial (GLT1) glutamate transporter expression (summarized in Table 4.2), which was most pronounced on day 2 after footshock. Chronic fluoxetine treatment alleviated both the PTSD-like symptoms and the reductions in synapsin, synaptophysin, and GLT1 protein expression. Finally, footshocked mice showed a delayed onset hippocampal increase in IgG expression which was accompanied by a decreased expression of Iba1, a marker protein of microglial cells, that has been demonstrated here to express IgG. Alterations in IgG expression, although in the opposite direction, were also observed in a mouse model of extremes in trait anxiety and in publicly available gene expression microarray data of PTSD patients and trauma-exposed controls (summarized in Table 4.3). Nevertheless, the alteration of IgG expression in different mouse models of anxiety disorders and in different species suggest IgG to play an important role in the pathobiology of anxiety disorders like PTSD. Altogether, these results indicate that in mice traumatic stress induces substantial and mostly long-lasting alterations in their hippocampal cytoarchitecture, their cerebral glutamate homeostasis, and their immune system.

5. Discussion

To date, the precise molecular mechanisms underlying anxiety diseases like PTSD and panic disorder are not completely understood. The first part of this thesis strived to elucidate the transcriptional regulation of the previously identified anxiety disorder candidate gene TMEM132D (Erhardt et al., 2011). In a cell culture model of oligodendrocyte differentiation the transcription factors MYT1, HES1, ZNF219, and SP1 were identified as regulators of TMEM132D gene expression.

Aiming to identify novel candidate proteins for PTSD that might contribute to the elucidation of PTSD pathogenesis and might serve as diagnostic biomarkers as well as potential drug targets, in the second part of this thesis, cerebral expression levels of a set of selected marker proteins were compared between traumatized and control mice. In summary, this screen revealed that traumatic stress induces alterations of the cerebral protein levels of synaptic proteins, namely synapsin Ia-b/IIa, synaptophysin, and homer 1b/c, of the glutamate transporter proteins GLT1 and EAAC1, as well as of the immune factor IgG and of the microglial marker protein Iba1.

5.1. Identification of transcription factors targeting

TMEM132D, a candidate molecule for anxiety disorders

TMEM132D was recently identified as a potential candidate gene for panic disorder (Erhardt et al., 2011). TMEM132D function, however, remains elusive and the regulation of its expression has so far never been studied. In the thesis at hand, for the first time, mechanisms regulating TMEM132D expression were studied by performing a promoter characterization of the human TMEM132D gene. Using *in silico* analysis methods and follow-up reporter gene assays, members of 13 transcription factor families were analyzed for their potential to regulate TMEM132D expression: 8 of these transcription factor binding sites revealed

inhibitory effects on TMEM132D promoter activity in the reporter gene assays (HESF, MYT1, ZBPF, GCMF, MTF1, NFKB, MZF1, SP1), while the others exhibited variable (NRF1, ZFXF, EGRF, HAML) or no effect (ZF5F) (Figures 3.17 and 3.19, summarized in Table 5.1 A, B). The fact that here only inhibitory regulators of TMEM132D expression were identified might explain the low endogenous gene expression levels of TMEM132D that have been reported in different human tissues (Nagase et al., 2001). According to Nagase et al. (2001) the highest TMEM132D expression levels are found in the brain, another study reported also considerable TMEM132D mRNA expression in human lung, pancreas, and testis (Nomoto et al., 2003). In accordance, the mRNA TMEM132D expression analyses performed in this thesis support a more widespread expression of TMEM132D since it was found to be expressed in oligodendroglial, astroglial and neuroblastoma cell lines as well as in an embryonic kidney cell line (Figure 3.12). Hence, TMEM132D expression is not restricted to the brain. The present study concentrated on elucidating TMEM132D regulation in oligodendroglial cells: TMEM132D upregulation during oligodendrocyte differentiation (Nomoto et al., 2003) was confirmed here in PMA-differentiated MO3.13 oligodendrocytic cells. Upregulation of TMEM132D in differentiated MO3.13 cells was accompanied by a downregulation of some of the inhibitory TMEM132D targeting transcription factors identified in this thesis, namely HES1, MYT1, ZNF219, and SP1 (Figure 3.21, summarized in Table 5.1 C). These four transcription factors showed concordant results in all analyses performed (highlighted in Table 5.1). The distinct mechanisms leading to the determination of the oligodendroglial cell fate are still not fully understood. Epigenetic as well as miRNA mediated, i.e. posttranscriptional, mechanisms have been described to control oligodendrocyte differentiation (Liu and Casaccia, 2010; Yu et al., 2010; Dugas and Notterpek, 2011). In accordance with the findings presented here, three of the identified regulators of TMEM132D gene expression, namely SP1, HESF, and MYT1, have been previously shown to be involved in oligodendrocyte differentiation: SP1 is a common transcription factor that binds to GC-rich motifs and plays a major role in various biological processes including cell proliferation and growth (Wierstra, 2008). Interestingly, SP1 has been linked to oligodendrocyte differentiation by modulating the expression of the myelin gene MBP (Guo et al., 2010).

Table 5.1.: Summary of TMEM132D regulating transcription factors Shown are the results of the three analyses performed in the thesis at hand. A) Reporter gene assay of TFBS mutant TMEM132D promoter constructs. Arrows represent the promoter activity of the mutant TMEM132D promoter construct in relation to the respective wildtype TMEM132D promoter construct. B) Reporter gene assay of TMEM132D promoter constructs with overexpressed transcription factors (TF). Arrows represent the change in promoter activity in the presence of overexpressed TFs compared to promoter activity in the presence of endogenous TF expression. C) Changes in TF expression in differentiated versus non-differentiated MO3.13 cells. D) Summary of the effects of the transcription factor families on TMEM132D promoter activity. Candidates showing concordant functions in all analyses are highlighted in yellow. n.d. = not detected

	HESF	NRF1	ZFPF	MYT1	ZBPF	GCMF	MTF1	ZFXY	EGRF	NFKB	MZF1	SP1	HAML
Analyses													
A TFBS mutant TMEM132D promoter activity compared to wildtype (Figure 3.17 A and 3.19 A)	↑	↑ / ↔	↔	↑	↑	↑	↑	↔	↑	↑	↑	↑	↑
B Effect of TF overexpression on wildtype TMEM132D promoter activity (Figure 3.17 B and 3.19 B)	↑	↑	↔	↑	↑	↑	↑	↑	↑	↑	↑	↑	↑
C TF expression in differentiated versus non-differentiated MO3.13 cells (Figure 3.21)	↑	↔	↔	↑	↑	n.d.	↔	↔	n.d.	↔	↔	↑	↔
D Effect of TFBS on TMEM132D promoter activity	inhibitory	variable	no effect	inhibitory	inhibitory	inhibitory	inhibitory	variable	variable	inhibitory	inhibitory	inhibitory	variable

MYT1 (Myelin transcription factor 1) is important for the induction of myelin gene expression, in particular MYT1 has been shown to increase the expression of the myelin component proteolipid protein (PLP) (Kim and Hudson, 1992). Myelination of axons is probably the most important function of mature oligodendrocytes. Furthermore, MYT1 has been shown to be downregulated in differentiated oligodendrocytes (Armstrong et al., 1995). The downregulation of MYT1 levels (paralleling TMEM132D upregulation) in differentiated MO3.13 cells presented in Figure 3.21 confirmed the findings of Armstrong et al. (1995) on MYT1 downregulation during oligodendrocyte maturation. Furthermore, the phylogenetic analysis of the TMEM132D promoter using the GEMS Launcher tool revealed the MYT1 binding site to exhibit conservation in the human, murine, and equine TMEM132D promoter sequence, while none of the other transcription factor binding sites was conserved in all three species thereby further stressing the importance of MYT1 for TMEM132D regulation.

The HES transcription factors, especially HES1 and HES5, have been reported to inhibit oligodendrocyte differentiation (Wu et al., 2003). Interestingly, HES1 was shown to be upregulated by the Notch signaling pathway thereby inhibiting oligodendrocyte differentiation (Li et al., 2011; Ohtsuka et al., 1999). Thus, downregulation of HES1 during MO3.13 oligodendrocyte differentiation (Figure 3.21) and inhibition of TMEM132D transcription by HES1 (Figure 3.17), as observed in this study, confirm the findings of Wu et al. (2003).

Identification of a GCM1 (glial cells missing homolog) binding site further supports a potential implication of TMEM132D in oligodendrocyte differentiation. It has been shown that the absence of GCM1 determines the neuronal cell fate, while the presence of GCM1 enables the development of both neurons and glia (Altshuller et al., 1996; Iwasaki et al., 2003). However, it was not possible to detect GCM1 expression in the MO3.13 cell line, but overexpression of GCM1 resulted in a reduction of TMEM132D promoter activity (Figure 3.17). Taken together, the fact that four regulatory sites known to play a role in oligodendrocyte differentiation were identified strongly argues for a pivotal role of TMEM132D in this process.

Although ZNF219 has so far not been associated to oligodendrocyte differentiation, it has been discussed to be involved in the differentiation of another cell type, i.e. chondrocytes (Takigawa et al., 2010). In addition, ZNF219 has been reported to generally function as a

transcriptional repressor (Sakai et al., 2003), which was also confirmed in the thesis at hand by identifying ZNF219 as an inhibitory regulator of *TMEM132D* gene expression.

Nevertheless, the other identified inhibitory transcription factors, MTF1, NFKB1, and MZF1, i.e. those factors that revealed concordant results in the reporter gene analyses but did not show expression level changes in differentiated versus non-differentiated MO3.13 oligodendrocytes, might be important for *TMEM132D* transcriptional regulation in other, not yet identified, biological contexts. Furthermore, the regulatory elements analyzed in this study were all located in the region up to 829 bp upstream of the start codon, while potentially conserved transcription factor binding sites in the more distally located clusters of conservation (Figure 3.9) remain to be analyzed in future experiments.

The identification of a cohesin-like domain in the extracellular region of *TMEM132D* further stresses the importance of *TMEM132D* in oligodendrocyte differentiation. This conserved protein domain resembles bacterial cohesins, which are cell adhesion proteins expressed in the cellulosome, a multienzyme complex degrading plant cell wall polysaccharides. In these cellulosomes, cohesins exert a high affinity interaction with dockerins forming a scaffoldin complex which is attached to the cell surface of the bacterium (Bayer et al., 2004). The cohesin-like domain identified in the extracellular region of *TMEM132D* most likely mediates cohesin-like function, i.e. extracellular high affinity interactions in cell adhesion processes, and thus alludes to a potential role of *TMEM132D* in cell adhesion. The latter is of great importance inter alia in oligodendroglial differentiation especially in myelination during which cell adhesion proteins mediate interactions between the axon and the oligodendrocytic processes (Laursen and French-Constant, 2007). However, knockdown of *TMEM132D* was not able to prevent differentiation in the MO3.13 model (Figure 3.22). This suggests that the low residual expression of *TMEM132D* might be sufficient to stimulate oligodendrocyte differentiation, or that *TMEM132D*, although upregulated during differentiation, might not be absolutely necessary for the morphological alterations observed during differentiation of the cell line studied. Independent from that, *TMEM132D* might still play an important role for the mature oligodendrocytic cell function, e.g. in neuron-glia interactions during the process of axon myelination.

5. Discussion

The fact that TMEM132D is involved in oligodendrocyte differentiation, as reported previously (Nomoto et al., 2003), was confirmed in this study, and it was further elucidated by the identification of transcriptional regulators of TMEM132D gene expression with known functions in oligodendrocyte differentiation processes (MYT1, HES1, SP1). Together with the fact that TMEM132D has been identified as novel candidate gene for panic disorder, this motivates the speculation that oligodendrocyte differentiation might play a role in the pathobiology of anxiety disorders. Although the exact role of oligodendrocytes in the pathobiology of anxiety disorders remains to be identified, recent reports note a role of myelin proteins in the context of anxiety phenotypes (Kodama et al., 2008; Klempan et al., 2009; Pasquini et al., 2011; Ono et al., 2008), as described in further detail in section 1.6. Additionally, oligodendrocyte dysfunction has also been related to other psychiatric diseases like schizophrenia (Martins-de-Souza, 2010; Takahashi et al., 2011).

In conclusion, this is the first study which explored the regulatory mechanisms of TMEM132D expression. Here, the transcription factors MYT1, HES1, ZNF219, and SP1 were found to inhibit TMEM132D expression. In addition, the downregulation of these four TFs was found to parallel TMEM132D upregulation in a cell culture model of oligodendrocyte differentiation. With exception of ZNF219, these regulators have already been implicated in oligodendrocyte differentiation as discussed above.

This study provides the first insights into TMEM132D regulation - further studies are clearly needed to extend them: Addressing the upstream signalling pathways of these transcription factors might open up opportunities to pharmacologically modulate TMEM132D expression levels both during oligodendrocyte differentiation and eventually also in anxiety disorders. To further elucidate the role of TMEM132D regulation in anxiety disorders, in future experiments it would be interesting to analyze expression levels of the candidate transcription factors identified here in cingulate cortex samples of HAB and LAB mice which have been previously reported to differentially express TMEM132D in this brain region. Additionally, it might also be interesting to investigate TMEM132D function in other cell types like neuronal cells.

5.2. Identification of novel PTSD candidate proteins

5.2.1. Traumatic stress induces a long-lasting hippocampal synaptic protein loss

The thesis at hand revealed a long-lasting decrease in the hippocampal expression of the synaptic proteins synapsin Ia-b/IIa, synaptophysin, and homer 1b/c to accompany a PTSD-like syndrome in mice (Figure 4.4 and 4.5), while in this mouse model of traumatic stress the expression levels of the dendritic marker protein MAP-2 (Figure 4.7) and the glial marker protein GFAP (Figure 4.12) were not significantly altered. Moreover, traumatic stress combined with re-exposure stress was found to induce a long-lasting decrease in hippocampal expression of the neuronal marker neurofilament H in the long-term (Figure 4.7). Stressing the validity and significance of these results, treatment with the antidepressant fluoxetine was found to alleviate the behavioral symptoms and to counteract the observed synaptic protein loss (Figure 4.9 and 4.10). Statistical analyses revealed the expression of these synaptic proteins to specifically correlate with the intensity of the conditioned and generalized fear response but not with the intensity of the hyperarousal phenotype (Figure 4.8). Pointing to an overall significance of synaptic proteins in the cerebral stress response, hippocampal synapsin Ia-b/IIa protein was found to be reduced also in another mouse model, namely in mice having been subjected to acute repetitive stress. This decrease of synapsin protein levels was, in contrast to footshocked mice (Figure 4.4), accompanied by an increase in synaptophysin protein levels both in the hippocampus and interestingly also in the prefrontal cortex (Figure 4.3).

Hippocampal synapsin and synaptophysin expression changes on mRNA and protein levels have been widely studied in various animal models of stress: both in rats and mice, stress-induced reduction of hippocampal synapsin and synaptophysin has been repeatedly reported in various paradigms of chronic and acute stress including prenatal stress, early life stress, chronic social stress, chronic footshock, and chronic restraint stress (Briones et al., 2012; Cunha et al., 2006; Dągryte et al., 2011; Khurana and Devaud, 2007; Llorente et al., 2011; Lui et al., 2011; Silva et al., 1996; Thome et al., 2001; Xu et al., 2004; Adlard et al., 2011;

Afadlal et al., 2010; Aisa et al., 2009; Alfonso et al., 2006; Elizalde et al., 2010; Sterlemann et al., 2010). In contrast to these studies, one single study in rats and another study in mice also reported a stress-induced upregulation of hippocampal synapsin (Revest et al., 2010) and synaptophysin (Gao et al., 2006). The expression of both synapsin and synaptophysin were repeatedly reported to be regulated by different drugs, i.e. by the steroid pregnenolone (Shirayama et al., 2005) as well as by atypical antipsychotics (Guest et al., 2010) and, more importantly, by the antidepressant fluoxetine (O’Leary et al., 2009; Reines et al., 2008), which, like other SSRI-antidepressants, is frequently used in PTSD treatment. Against this literature background, the findings presented in the thesis at hand demonstrate for the first time a long-lasting reduction of hippocampal synapsin and synaptophysin protein levels in a mouse model of PTSD, and furthermore, confirm fluoxetine to be able to counteract this synaptic protein loss.

In contrast to synapsin and synaptophysin, not much is known about the regulation of homer 1b/c in the cerebral stress response of rodents. So far, expression of the isoforms homer 1a and homer 2a/b has been reported to be modulated by stress exposure (Ary et al., 2007; Qi et al., 2010). One single study showed decreased interaction of homer 1b/c with the metabotropic glutamate receptor in mice subjected to immobilization stress thereby alluding the stress responsivity of the homer 1b/c protein (Tronson et al., 2010). Since the protein expression of this postsynaptic protein has never been shown to be regulated by stress, the thesis at hand provides the first evidence for a stress-induced downregulation of homer 1b/c expression.

Furthermore, this thesis comprises the first study addressing the long-term molecular sequelae of acute traumatic stress, which is of special importance in PTSD pathogenesis, as symptoms usually appear with a delayed-onset of at least 4 weeks, and furthermore, are reinforced by re-exposure to traumatic cues.

In accordance with previous studies showing a differential regulation of different synaptic proteins (Thome et al., 2001; Müller et al., 2011), here, acute repetitive stress was demonstrated to differentially regulate synapsin and synaptophysin in the hippocampus and, in contrast to traumatic footshock stress, also in the prefrontal cortex (Figure 4.3). The opposite regulation of synaptophysin in the two different mouse models of stress employed here

emphasizes the complex regulation of synaptic proteins which is crucial for synaptic plasticity. The expression levels of other plasticity-related proteins, i.e. the cell adhesion molecules of the immunoglobulin superfamily (NCAM), have been shown to depend on the intensity of the electric footshock stressor and the post-stress time-interval (Merino et al., 2000).

The post-stress time-interval also plays an important role for the molecular alterations in the PTSD mouse model employed here: while on day 2 after footshock the expression of synaptic proteins was significantly reduced, on day 28 after footshock, i.e. in mice not subjected to the stressful behavioral testing, the expression of none of the synaptic proteins tested was significantly altered. Remarkably, on day 60 after footshock, i.e. in mice subjected to behavioral testing on days 28-30 after footshock, the expression levels of all synaptic proteins were significantly reduced (Figure 4.5 and 4.4). This leads to the conclusion that the stressful behavioral testing on days 28-30 after footshock, which includes re-exposure to the shock chamber, amplifies the trauma stress-elicited synaptic protein loss, probably by acting as a retraumatizing stressor. As from day 28 on this synaptic protein loss sustainably persisted to at least day 60 after footshock without any application of additional stressors, this justifies classifying the then observed changes in protein levels as ‘long-term alterations’.

The fact that chronic fluoxetine treatment counteracted these long-term molecular alterations in the hippocampus and, furthermore, alleviated the PTSD-like symptoms strongly suggests the hypothesis that hippocampal synaptic protein loss contributes to the pathogenesis of the murine PTSD-like syndrome. Although in addition to the hippocampus, also prefrontal cortex and amygdala play a major role in the fear circuitry and have been repeatedly proposed to play a role in the pathogenesis of PTSD (Shin et al., 2006; Rauch et al., 2006; Gamo and Arnsten, 2011; Hughes and Shin, 2011), the prefrontal cortex has not been studied extensively and molecular changes in the amygdala have not been investigated at all since the thesis at hand concentrated on deciphering the molecular correlates of the PTSD-associated hippocampal volume loss (as introduced in section 1.2.4.1).

The fact that acute repetitive stress, which was considered to be more stressful than the single electric footshock, led to a reduction of synapsin expression not only in the hippocampus but also in the prefrontal cortex (Figure 4.3), and together with the findings of a recent report

demonstrating that in rats the hippocampus was found to be the most vulnerable region during the extremely stressful condition of experimental sepsis (Semmler et al., 2005), this suggests the hypothesis that the hippocampus might exhibit a higher stress-responsivity than the prefrontal cortex.

Hippocampal shrinkage has been frequently associated with stress-related disorders like major depression and post-traumatic stress disorder (McEwen, 1997; Apfel et al., 2011; Gurvits et al., 1996; Cole et al., 2011). The molecular correlates of this stress-associated hippocampal volume loss, however, remain unknown. As published recently, the development of PTSD-like symptoms in footshocked mice of the PTSD mouse model used here is also accompanied by a hippocampal shrinkage (Golub et al., 2011). This leads to the hypothesis that the footshock induced synaptic protein loss observed here might causally contribute to footshock induced hippocampal shrinkage. This hypothesis and the results presented in the thesis at hand are in accordance with previous reports suggesting that synapse loss contributes to stress induced hippocampal volume loss (Tata and Anderson, 2010). Besides synapse loss, a reduction in neuronal and glial cell numbers as well as dendritic atrophy have been discussed previously as other possible correlates of hippocampal shrinkage (Czeh and Lucassen, 2007). In rats subjected to chronic unpredictable stress or to chronic glucocorticoid administration, the total number of DG-CA3 synapses of the mossy fiber pathway was reported to be reduced in comparison to untreated control rats (Sousa et al., 2000). Interestingly, recovery from stress or glucocorticoid exposure resulted in increased synapse numbers (Sousa et al., 2000), arguing for a potential reversibility of both the synapse loss and the hippocampal volume loss. Importantly, the hippocampal shrinkage and the behavioral symptoms observed in the PTSD mouse model employed here have been previously shown to be prevented by environmental enrichment (Golub et al., 2011). In addition, a reversibility of hippocampal shrinkage has also been reported after exercise training in humans (Erickson et al., 2011) as well as after antidepressant treatment of stressed tree shrews (Czeh et al., 2001; van der Hart et al., 2002). Together with the reversibility of hippocampal shrinkage and PTSD-like symptoms in the animal model, a clinical study reporting PTSD duration to negatively correlate with hippocampal volume (Felmingham et al., 2009) suggests that hippocampal

volume loss not exclusively represents a vulnerability factor, as it has been suggested by twin studies (Gilbertson et al., 2002; Pitman et al., 2006), but rather underlies the behavioral alterations.

A reduction in astrocyte numbers has been previously suggested to contribute to stress-induced hippocampal volume loss (Czeh et al., 2006). The fact that in traumatized mice hippocampal GFAP expression levels remained unchanged (Figure 4.12) argues against a major contribution of a loss of astrocytes to the hippocampal shrinkage in the PTSD mouse model analyzed here. Furthermore, neuronal cell loss due to increased apoptosis or decreased neurogenesis has been discussed repeatedly to underlie hippocampal shrinkage (Czeh and Lucassen, 2007; DeCarolis and Eisch, 2010). However, most studies failed to detect a reduction in neuronal cell numbers (Lucassen et al., 2001), which is in agreement with the results presented in Figure 4.7 showing that the dendritic marker protein MAP-2 was not significantly altered at any time-point of the analysis. In addition, the fact that both the volume reduction and the associated behavioral effects are reversible upon treatment strongly argues against neuronal cell death. In contrast to apoptosis, decreased neurogenesis has been shown to be reversible and has previously been associated with an increase of the hippocampus volume (Czeh et al., 2001; van der Hart et al., 2002). However, as hippocampal neurogenesis is a rare event that only occurs in the dentate gyrus, some authors regard decreased neurogenesis to be not sufficient to explain the marked hippocampal volume loss associated with stress (Czeh and Lucassen, 2007). Finally, hippocampal dendritic atrophy has been repeatedly reported in animal studies of chronic stress (Bock et al., 2011; Eiland and McEwen, 2012). However, the fact that footshocked and mock treated mice did not exhibit significant differences in their hippocampal levels of the dendritic marker protein MAP-2 (Figure 4.7), strongly suggests that dendritic atrophy most likely does not grossly contribute to the hippocampal shrinkage in the PTSD mouse model employed here. The fact that these results differ from literature findings might result from the mouse strains or the stress paradigms employed here, and moreover, it is feasible that although both chronic and acute stress paradigms result in hippocampal volume loss, their underlying ultrastructural correlates might be different.

Interestingly, PTSD patients have been reported to exhibit the most pronounced hippocampal

volume loss in the CA3/DG region (Wang et al., 2010b). This agrees well with the findings of the immunohistochemical analysis presented in Figure 4.6 which shows that synapsin is mainly expressed in the CA3/DG region.

Hippocampal shrinkage as well as a general hypoactivity of the hippocampus have been associated with cognitive impairments in PTSD patients (Dickie et al., 2011; Hayes et al., 2011). The fact that synapsin knockout mice show a pronounced impairment in their cognitive performance (Corradi et al., 2008; Silva et al., 1996) leads to the speculation that the here observed trauma stress induced loss of synapsin protein might causally contribute to PTSD-associated cognitive impairment in mice. The correlation analysis presented in Figure 4.8 showing a significant correlation of synaptic protein expression levels with the conditioned and generalized fear response but not with the intensity of the hyperarousal behavior furthermore suggests that synaptic proteins differentially contribute to fear and hyperarousal phenotypes and thus derive from different pathogenetic mechanisms.

As hippocampal shrinkage is associated with both the murine (Golub et al., 2011) and the human (Gurvits et al., 1996) PTSD syndrome and as fluoxetine not only alleviates the PTSD-like symptoms in mice but also leads to PTSD symptom reduction in humans (Berger et al., 2009), it can be speculated that fluoxetine treatment might also counteract synaptic protein loss in PTSD patients. Hence, synapsin, synaptophysin, and homer 1b/c might possibly represent novel candidate molecules for the neuropathology of PTSD. Synaptic protein alterations have already been detected in *post-mortem* brain specimens of patients with other psychiatric disorders like schizophrenia and bipolar depression (Beasley et al., 2005; Eastwood et al., 1995; Eastwood et al., 2000; Porton and Wetsel, 2007; Vawter et al., 2002), but not in patients who had suffered from major depression (Beasley et al., 2005; Müller et al., 2001). To date, there are no studies having analyzed synaptic protein expression in *post-mortem* brain specimens of PTSD patients.

Interestingly, synapsin expression has been reported to influence the expression of other synaptic marker proteins: experimental depletion of synapsin in neuronal cultures as well as in the mouse model was found to be accompanied by a downregulation of other synaptic vesicle proteins like synaptophysin and synaptotagmin (Ferreira et al., 1994; Rosahl et al.,

1995). These reports suggest that restoring synapsin expression levels can also have beneficial effects on other synaptic proteins or even the structure of the whole synapse and stresses the fact that synapsin protein expression is highly dynamic and presents an attractive target to modulate the stress induced effects on the synapse.

In order to pharmacologically target synaptic protein expression, the mechanisms underlying synaptic protein loss have to be elucidated. The fact that glucocorticoids have been repeatedly reported to induce synapsin expression in animals (Nestler et al., 1981; Garcia-Caceres et al., 2010; Wu et al., 2007) and the fact that human PTSD has been associated with decreased glucocorticoid levels (Yehuda, 2009) as exemplified in further detail in section 1.2.1, lead to the speculation that decreased corticosterone levels might underlie the here observed trauma stress induced hippocampal synaptic protein loss. In contrast to glucocorticoids, the effects of epinephrine or norepinephrine, which are known to be increased in human PTSD (Dikanović et al., 2011), on synapsin expression have so far not been studied, but it has been repeatedly shown that norepinephrine increases synapsin phosphorylation and thereby modulates synaptic activity (Mobley and Greengard, 1985; Parfitt et al., 1991).

In conclusion, in this thesis the synaptic proteins synapsin, synaptophysin, and homer 1b/c were identified as novel candidate proteins for the murine PTSD-like syndrome and especially for the accompanying hippocampal shrinkage (Golub et al., 2011). To further confirm the hypothesis of synaptic degeneration, in future experiments synapse structure and numbers should be analyzed by electron microscopy of hippocampal slices of traumatized and control mice. Furthermore, in order to translate these findings to the clinical setting, i.e. to the diagnosis and treatment of PTSD patients, and to evaluate the synaptic candidate proteins as future PTSD biomarkers, analysis of synaptic protein expression in human *post-mortem* specimens as well as blood plasma and CSF samples of PTSD patients will be necessary. As most *post-mortem* brain samples, however, derive from medicated patients it might be problematic to confirm the findings from the animal models because, as discussed above, many drugs used in pharmacotherapy of PTSD have been reported to modulate synaptic protein expression (O'Leary et al., 2009; Iwata et al., 2006).

5.2.2. Traumatic stress induces a reduction of glutamate transporter expression

In addition to the trauma stress-induced hippocampal synaptic protein loss, also the expression levels of the glutamate transporter proteins GLT1 and EAAC1 were found to be decreased in the hippocampus of footshocked mice with the most pronounced effects appearing early, i.e. on day 2, after footshock (Figure 4.11), while the expression levels of the astrocytic marker protein GFAP remained unchanged at any time point tested (Figure 4.12). Interestingly, chronic fluoxetine treatment of footshocked mice enhanced the expression of GLT1 but not the expression of EAAC1 or GFAP (Figure 4.13).

So far, there was no report on the association of GLT1 with the murine PTSD-equivalent syndrome, but only one study reporting a reduction of GLT1 protein expression in response to sub-chronic immobilization stress in mice (Zoppi et al., 2011). In rats, however, several research groups have analyzed the effect of mainly chronic and early life stress on glutamate transporter expression resulting in inconsistent findings: while some reported a reduction of GLT1 (García-Bueno et al., 2007; Madrigal et al., 2003; Zink et al., 2010), others observed increased GLT1 expression after stress exposure (Martisova et al., 2012; Wood et al., 2004; Raudensky and Yamamoto, 2007; Reagan et al., 2004). Similarly, animal studies on stress-induced expression changes of the glutamate transporter EAAC1 provided inconsistent results (García-Bueno et al., 2007; Madrigal et al., 2003; Zink et al., 2010). This thesis demonstrates for the first time GLT1 and EAAC1 expression to be associated with the stress response in a mouse model of PTSD. Furthermore, in agreement with previous reports showing the tricyclic antidepressant amitriptyline, the mood stabilizer valproic acid (VPA), as well as the β -lactam antibiotic ceftriaxone and, most importantly, the SSRI antidepressant fluoxetine to induce glutamate transporter expression (Tai et al., 2006; Perisic et al., 2009; Valentine and Sanacora, 2009; Zink et al., 2011), in this thesis chronic fluoxetine treatment of footshocked mice was found to increase hippocampal GLT1 protein levels (Figure 4.13) and, moreover, to alleviate PTSD-like symptoms (Figure 4.9).

Typically, glutamate homeostasis in the synaptic cleft is tightly controlled by astrocytes which wrap the pre- and postsynapse thereby forming a tripartite synapse (Perea et al., 2009)

(Figure 5.1 A). The fact that the expression levels of both the dendritic marker protein MAP-2 as well as the astrocytic marker protein GFAP were not changed in footshocked mice (Figure 4.7 and 4.12), leads to the hypothesis that a decrease in neuronal or astrocytic cell numbers does not grossly contribute to trauma-induced reduction of glutamate transporter expression. The decrease of glutamate transporter expression levels in mice subjected to a single electric footshock motivates the speculation that glutamate clearance from the synaptic cleft might be reduced in traumatized mice which, in turn, might lead to increased extracellular concentrations of glutamate. Unbalanced levels of glutamate can result in excitotoxicity (Forder and Tymianski, 2009; Dong et al., 2009) which, in turn, might probably also contribute to the synaptic protein loss discussed in section 5.2.1.

These speculations are corroborated by the fact that increased glutamate release from presynaptic terminals has been discussed as a crucial step in the trauma stress-induced hippocampal volume loss (Musazzi et al., 2011). Moreover, excessive glutamate levels are well known to be tightly involved in the stress-induced structural remodeling of synapses by initiating excitotoxic processes via NMDA receptor mediated calcium influx (McEwen, 2010). This leads to the speculation that the degradation of synapses suggested by the here reported footshock induced long-term downregulation of synaptic proteins might represent an adaptation mechanism inhibiting further trauma stress-induced harmful excitatory input. To test this hypothesis of trauma stress-induced increase in glutamate levels in the synaptic cleft, microdialysis measurements of extracellular glutamate levels in the hippocampus should be performed in future experiments.

The findings that the antidepressant fluoxetine is able to counteract both the trauma stress-induced decrease of GLT1 protein levels (Figure 4.13) and the behavioral symptoms in mice (Figure 4.9) reveal GLT1 as an interesting candidate molecule for clinical PTSD trials and *post-mortem* studies. The fact that anti-glutamatergic drugs like lamotrigine have been reported to effectively alleviate symptoms in PTSD patients (Hertzberg et al., 1999) leads to the speculation that the glutamate homeostasis is disturbed not only in mice but also in humans with PTSD symptoms.

In summary, the trauma stress-induced loss of hippocampal glutamate transporters observed

here suggest that a disturbed glutamate homeostasis probably contributes to the development of hippocampal shrinkage in the PTSD mouse model used here. As the effects on glutamate transporter expression were most pronounced on day 2 after footshock (Figure 4.11), the observed glutamatergic alterations probably represent early events in the pathogenesis of the mouse PTSD-like syndrome and might contribute to the induction of other long-term molecular changes, e.g. the here described synaptic protein loss, which was demonstrated to be counteracted by fluoxetine treatment (Figure 4.13).

5.2.3. The expression of immune system associated molecules is altered both in mice exhibiting a PTSD-like syndrome and in PTSD patients

In contrast to the three synaptic proteins, GLT1, and EAAC1 which were all found to be decreased in traumatized mice (see sections 4.2.1 and 4.2.2), the protein expression levels of the antibody molecule immunoglobulin G (IgG) were found to be increased in the hippocampus, the prefrontal cortex, and in the blood of footshocked mice (Figures 4.17 and 4.19); this increase occurred with a delayed-onset. On the contrary, in an *in silico* analysis employing data from Segman et al. (2005) IgG gene expression levels were found to be decreased in peripheral blood mononuclear cells (PBMC) of PTSD patients in comparison to trauma-exposed controls (Figure 4.26) suggesting that IgG plays a role both in human PTSD and its murine equivalent but is obviously regulated differentially in different species. In addition, these contrary findings in mice and human patients might also result from the fact that in mice IgG expression was determined on the protein level and in the clinical study on the mRNA level. However, in agreement with the data comparing mRNA expression levels in PTSD patients and controls, reduced IgG protein levels were found to occur in another mouse model for anxiety disorders, i.e. the high anxiety-related behavior (HAB) mice (Krömer et al., 2005) which in comparison to low anxiety-related behavior (LAB) mice expressed considerably lower amounts of IgG in the blood and in all brain regions analyzed, i.e. in the hippocampus and the cerebellum (Figures 4.20 and 4.21). The observation that the Ig λ and κ light chain carrying antibodies were differentially expressed in the hippocampus and blood samples of shocked mice (Figures 4.18 and 4.19) suggests that preferably Ig κ carrying antibody molecules extravasate from the blood

by a still to be determined mechanism. This region-specificity was not detectable in HAB and LAB mice which, in contrast to the PTSD mouse model, do not represent temporary changes but rather reflect permanent alterations of an extreme anxiety phenotype. Interestingly, HAB mice compared to LAB mice expressed increased Ig λ light chain levels, while they exhibited reduced expression levels of Ig κ light chain, IgG Fc, and IgG Fab (Figure 4.20). However, as only 5 % of murine antibodies carry the Ig λ light chain, the increase of the Ig λ light chain levels observed here might probably have a small impact on total immunoglobulin levels, and therefore this finding does not contradict the reduction of total IgG levels found here in HAB mice.

Furthermore, by immunohistochemical analyses in brains of untreated C57BL/6 mice IgG was identified to be associated with microglial and endothelial cells (Figure 4.16). Western blot analysis revealed a decreased hippocampal expression of the microglial marker protein Iba1 in footshocked mice (Figure 4.22), while in HAB mice compared to LAB mice an increased cerebellar expression of Iba1 was found (Figure 4.23). The opposite regulation of immunoglobulin IgG and the microglial marker Iba1 in traumatized mice and in HAB mice might result from the different mouse strains, but most likely, it derives from the fact that footshocked mice suffer from state anxiety while HAB mice suffer from trait anxiety since they were selectively bred for an high anxiety phenotype for more than 40 generations (Krömer et al., 2005). In contrast to Iba1, protein expression levels of the endothelial cell marker CD31, of CD68, a marker protein for activated microglia, and of the microglial IgG receptor Fc γ RI were not significantly altered in both the PTSD mouse model and the HAB/LAB mouse model (Figures 4.22, 4.23 and 4.25).

Increasing amount of evidence supports the immune system to be a major player in stress adaptation (García-Bueno et al., 2008; Bauer et al., 2010) as well as in the pathogenesis of stress-related disorders like PTSD (Pace and Heim, 2011). So far, in clinical studies, altered expression of the cytokines IL-1 β , IL-6, TNF- α , IL-2, and IL-8 in blood as well as the CSF of PTSD patients have been reported (Spivak et al., 1997; von Känel et al., 2007; Maes et al., 1999; Baker et al., 2001; Song et al., 2007). Furthermore, alterations of immune cell functions like impaired natural killer cell activity (Gotovac et al., 2010), enhanced T cell

function (Boscarino and Chang, 1999; Sommershof et al., 2009), and altered epigenetic profiles of immune system associated genes (Uddin et al., 2010) have been reported in PTSD patients. So far, only few studies employing animal models have addressed the molecular mechanisms underlying the immune system's contribution to the psychological stress response. Employing a predator stress mouse model of PTSD, it has been shown that regulatory T cells suppress the individual's ability to adapt to psychosocial stress (Cohen et al., 2006). In addition, another study showed recently that mice exposed to early life stress exhibit decreased expression levels of lipopolysaccharide binding protein (LBP), an innate immune system protein, which is required for synaptic pruning during hippocampal development (Wei et al., 2012).

Sporadic studies have reported increased salivary IgA levels in humans in response to environmental stress (Kugler et al., 1996; Mishra et al., 2011), but so far no systematic study neither in human patients nor in animal models has analyzed immunoglobulin expression in response to psychological stress and in the context of stress-related disorders. Against this background, this thesis shows for the first time a trauma stress-induced upregulation of immunoglobulin G expression in both the brain and the blood of traumatized mice.

The presence of IgG in the healthy CNS of rodents has already been shown in both neuronal (Yoshimi et al., 2002; Upender et al., 1997) and microglial cells (Hazama et al., 2005); these reports are in agreement with the findings presented in Figure 4.16 showing IgG to be associated with microglial cells.

While stress-induced alterations of protein expression levels of the endothelial cell marker CD31 and the microglial immunoglobulin G receptor Fc γ RI have not been analyzed before, several reports demonstrated microglial alterations to occur in the aftermath of stress exposure. Most publications report a stress-induced increase of microglial activation and of total microglial cell numbers (Diz-Chaves et al., 2012; Espinosa-Oliva et al., 2011; Tynan et al., 2010). Microglial activation and functions like cytokine secretion have been suggested to be at least in part mediated by glucocorticoids (Frank et al., 2012) and epinephrine (Wohleb et al., 2011). In contrast to these reports, decreased levels of the microglia marker protein Iba1 and unchanged expression of the activated microglia marker CD68 (Figure 4.22) in the aftermath of traumatic footshock suggest a reduction of total microglia cell numbers and an

increase in the proportion of activated microglia. Here, western blot analysis revealed IgG to be upregulated in footshocked and downregulated in HAB mice, while Iba1 expression was reduced in footshocked animals and increased in HAB animals. This finding, i.e. that increased IgG levels were accompanied by decreased Iba1 levels, was unexpected as IgG by binding to its Fc receptors can induce the activation, and therewith proliferation, of microglia (Lunnon et al., 2011).

However, the origin of IgG found in the brain remains elusive. By RT-PCR analysis and in situ hybridization others already have excluded that microglia synthesize IgG, and moreover, it has been proposed that IgG from the blood is taken up via microglial Fc receptors (Hazama et al., 2005). The blood-brain barrier (BBB) normally prevents the transfer of many blood proteins into the CNS, but it has been shown that IgG can pass the BBB during epinephrine-induced transient hypertension (Kuang et al., 2004). Some studies also showed a stress-induced increase in BBB permeability (Skultéyová et al., 1998; Esposito et al., 2001; Esposito et al., 2002), which, however, was not confirmed by others (Park et al., 2008; Amourette et al., 2009). Provided that the increased epinephrine levels observed in PTSD patients (Dikanović et al., 2011) are also found in mice subjected to the electric footshock, the epinephrine-induced BBB leakage might explain the origin of IgG in the brain. Furthermore, a differential sensitivity of the analyzed brain regions to stress or epinephrine induced BBB permeability, which has been reported before (Skultéyová et al., 1998), might explain the region-specific increase of IgG levels in the PTSD mouse model.

Strikingly, no evidence for a direct glucocorticoid-dependent regulation of IgG exists, although glucocorticoids are well-known for their anti-inflammatory properties and are commonly used in the therapy of chronic inflammatory diseases (Barnes, 2011). Nevertheless, the hypocortisolism associated with PTSD patients (Yehuda, 2009) motivates the speculation of a reduced repression of inflammation which, in turn, could possibly contribute to the increased levels of IgG in traumatized mice. Furthermore, it has been shown that the stress hormone epinephrine, which is tightly involved in the complex regulation of the immune response (Elenkov et al., 2000) and is found to be chronically elevated in PTSD patients (Dikanović et al., 2011), increases IgG production in B cells via β_2 -adrenergic receptors (Podojil and

Sanders, 2003). From this it can be speculated that anti- β -adrenergic drugs like propranolol, which have already been used successfully in the treatment of PTSD patients (see section 1.4), could counteract IgG upregulation and might possibly also alleviate PTSD-like symptoms in mice. However, in a recent study one single administration of propranolol did not ameliorate PTSD-like behavior in a predator scent based PTSD mouse model (Cohen et al., 2011). Nevertheless, future analysis of the behavioral consequences of anti- β -adrenergic treatment in footshocked mice might contribute to the elucidation of the mechanism of the here observed trauma-stress induced IgG upregulation.

Rather than inducing inflammation in the brain physiological levels of IgG might mediate neuroprotective effects, as suggested recently (Hulse et al., 2008). Physiological levels of IgG have been shown to prevent glutamate induced excitotoxicity in rat hippocampal slices by activating microglia and subsequent TNF α release (Hulse et al., 2008), which, in turn, has been reported to enhance synaptic efficacy (Beattie et al., 2002). Thus, a moderate increase of IgG levels in the hippocampus of footshocked mice could possibly reflect a compensatory mechanism to counteract glutamate excitotoxicity and synaptic loss.

Surprisingly, here, a decreased IgG expression was found in an *in silico* analysis of PBMC gene expression data of PTSD patients (Figure 4.26). However, as protein and mRNA expression levels do not necessarily correlate, IgG protein expression in human PTSD blood samples should be addressed in future experiments to investigate the potential increase in IgG expression levels, that might be expected both from the analysis of the PTSD mouse model presented here and from the repeatedly reported elevated inflammatory parameters in PTSD patients (Spivak et al., 1997; von Känel et al., 2007; Maes et al., 1999; Baker et al., 2001; Gotovac et al., 2010; Boscarino and Chang, 1999; Sommershof et al., 2009). Importantly, here, both in PTSD patients and in traumatized mice, alterations of IgG were only detectable in the long-term, but not shortly after the trauma leading to the speculation that these changes contribute to the delayed-onset occurrence of PTSD-like symptoms, i.e. the fear generalization behavior in mice that is also characteristic of the human PTSD syndrome.

In summary, this thesis revealed distinct alterations in immune system proteins by analysis of two different mouse models of pathological anxiety as well as by an *in silico* analysis of PBMC

gene expression of PTSD patients. Whether these changes present a cause or a consequence of the events leading to the development of anxiety disorders like PTSD remains unresolved and will be addressed in future studies.

5.2.4. Model conception of the speculated trauma stress-induced synapse loss

Figure 5.1 summarizes all factors analyzed in this thesis that possibly contribute to the speculated trauma stress-induced hippocampal synapse loss in the PTSD mouse model. It is well-known that astrocytic processes tightly contact the synapse to build the so called tripartite synapse (Perea et al., 2009) and, by expressing glutamate transporter proteins, mediate the clearance of glutamate from the synaptic cleft (Danbolt, 2001). In addition to astrocytes, also microglia have been recently reported to modulate synaptic structures: besides the secretion of immune molecules like cytokines (Fourgeaud and Boulanger, 2010), microglia also physically interact with the synapse by forming a quadripartite synapse (Tremblay and Majewska, 2011) (Figure 5.1 A). Activated by homeostatic imbalances microglia have been reported to induce synaptic stripping (Perry and O'Connor, 2010), which leads to a separation of pre- and postsynapse to protect the neurons from further harmful synaptic input (Blinzinger and Kreutzberg, 1968; Trapp et al., 2007; Tremblay et al., 2010). This leads to the speculation that the loss of glutamate transporter proteins in response to the traumatic footshock reported in the thesis at hand (Figure 4.11) probably prevents effective glutamate clearance and subsequently results in elevated extracellular glutamate levels. Furthermore, it can be speculated that this imbalance in glutamate homeostasis might activate synaptic stripping to protect the neurons from glutamate induced excitotoxicity (Figure 5.1 B). Ultimately, both synaptic stripping and excitotoxic effects could result in the here observed loss of synaptic proteins.

5.2.5. Conclusions

In conclusion, educated guess-driven screening for novel candidate molecules for PTSD in a mouse model of PTSD revealed alterations in the expression of hippocampal synaptic proteins. This synaptic protein loss is speculated to reflect a trauma-stress induced synaptic loss, which

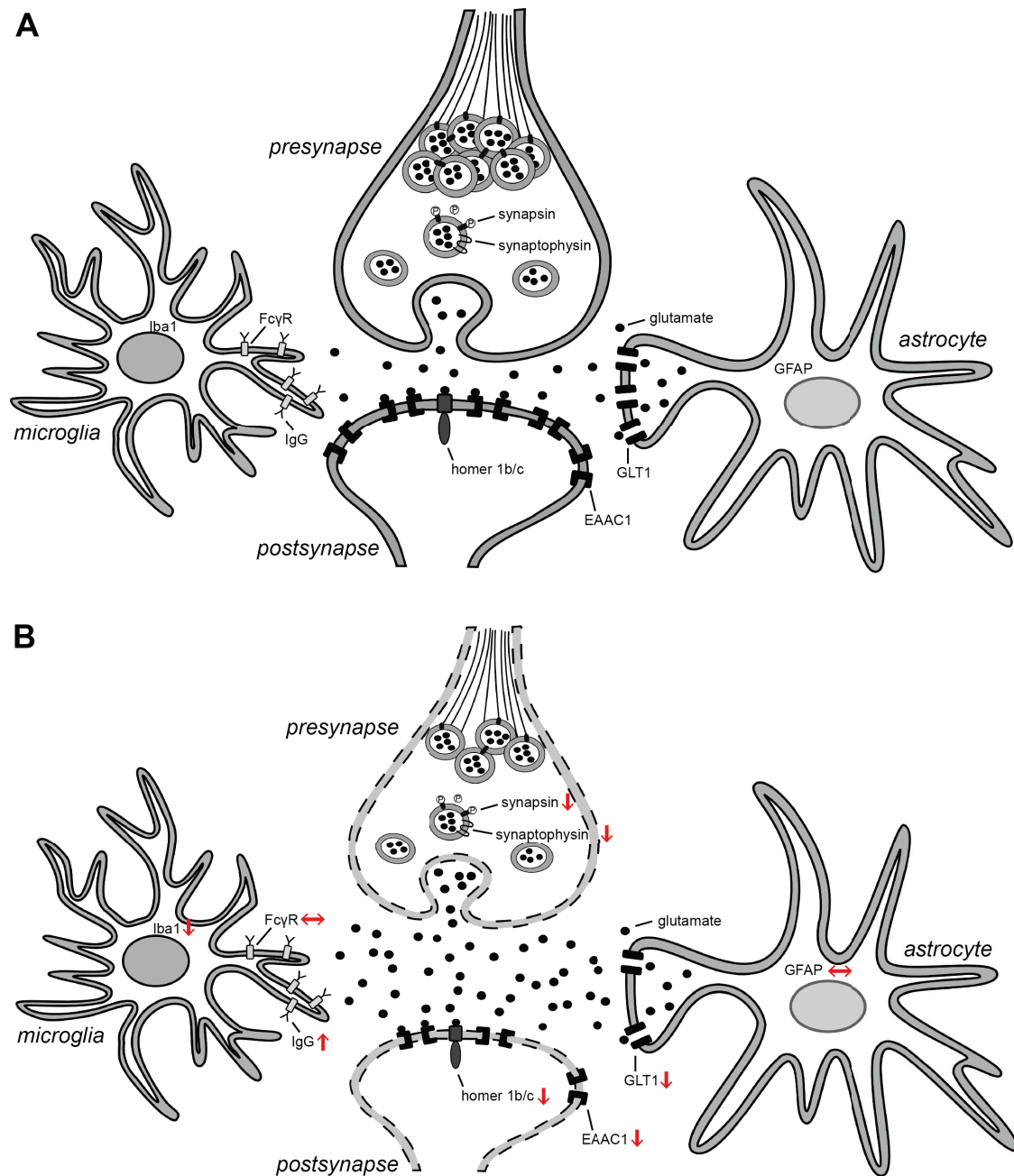


Figure 5.1.: **Model conception of the speculated trauma stress-induced synapse loss.** (A) Scheme of the quadripartite synapse as proposed by Tremblay and Majewska (2011), consisting of pre- and postsynapse, astrocytic and microglial processes. (B) Red arrows indicate trauma stress-induced alterations of candidate proteins identified here: synapsin, synaptophysin, homer 1b/c, GLT1, EAAC1, GFAP, IgG, Iba1, Fc γ R. The here observed synaptic protein loss motivates the speculation of a trauma stress-induced synaptic loss, which might possibly be induced by insufficient glutamate clearance due to a trauma stress-induced loss of glutamate transporter proteins and subsequent excitotoxic processes. IgG has been reported to mediate neuroprotective effects, however, the role of the immune system in synaptic plasticity has not been fully elucidated yet.

might contribute to hippocampal shrinkage observed in both the PTSD mouse model employed here and in human patients. The here observed pronounced decrease of glutamate transporter expression is speculated to result in increased extracellular glutamate levels. This in turn leads to the speculation that glutamate induced excitotoxicity might contribute to the here observed trauma stress-induced synaptic protein loss and possibly also to hippocampal shrinkage. These neurodegenerative processes might speculatively be counteracted by possible neuroprotective effects mediated by the here observed increase of hippocampal immunoglobulin G protein levels in traumatized animals. Whether the trauma stress-induced IgG increase is actually protective or rather promotes the hippocampal synaptic loss, or whether it has a completely different function, has to be addressed by future experiments.

A. Appendix

A. Appendix

```

TMEM132A 1 MCARMAGRRTTMAPRGPYGPLVCLVALALDVRVDCGQ-----APLDPVYVPAALELLDAPEHFRVQVGH--YPP 69ANRNSLSL
TMEM132B 1 MFGAASRMDL-----AVCTGGVTSRGLVDS-LOKISSPAYLPTNLHISNAEESFFLKEANO--DLT 61RNSLSQA
TMEM132C 1 MRSEGAAPGPAP--L CGA--LSLLCALLKVVEGHVTDN--LORFSSLPYLPVSYHLRAETSFFLKEANO--DLL 72RNSLSQA
TMEM132D 1 MCPSEMGLL-WHH--WSP--VLSLALFVSKVTEGRGLES--LORFSLPTVLPVTHLNNADYSFFLKEANO--DJM 70RNSLSQS
TMEM132E 1 MAPGMSRGGG-----ALLCLSLALLAHAS-GRSHPASPSPPGPOASPVLPVSVRLSHRLAFFLREARPPSPAV 68ANRSLQ-

TMEM132A 77 HSETEFLLLQPWPAQPLLRASVYPPFATQVVVPPRVTETP-----HORPVPVDRVAVSVEAAVTPAEYPARV 142FHLKCDQWPPG--
TMEM132B 69 RVEPEFLIYR--ARTPLLNASVYGFPSVEKLTPOEELLSLSTAFGNVDKPFNMLKSHDSSLYSNRPKVOVLL 139FYVTGMGWDSDL
TMEM132C 80 RVESEFTYK--TRQPPVLNASVYGFPSVEKVVPLDMLTSLNFGPTNKFSFDKMLKALHDKVYLSRPKVOVLL 150FHLMGRDWDHGA
TMEM132D 78 RVESEFLIYK--SRRLPVLNASVYGFPSLEQVVRQDMLLSNPRGFTNKFSLNMLKKAHLRDKVYLSRPKVOVLL 148FHLMGRDWDHRSV
TMEM132E 75 RSEPEVVFQ--TKELPVLNVSLYGFPSLQVARELLOPSTLDIRLTVNKKVRAFTVRSHPVAPSPVVOVLL 145FYVAGRDWDDGVA

TMEM132A 154 SGLPCARLHATHPMGTAHQALRFQPSLQACVVELELPSHW-SQA-----STIRALAY 207LEPAALGPGGCGSGEEND
TMEM132B 153 TLDLPCVKMFAPIEAREVAASCRLLQCAPGLCAVELELPEWFSGLDLEPEEIPALLGCTMELFF 219TLYPADK-AGCCPLEEEGK
TMEM132C 164 GEKLPCLRVFAFREIREVRGSCRLKGLGLCAVELELSSWFSAPTVGAGRKKSVDQPEGTPVELLY 230TVHPGNE-RGDCAGGDF-R
TMEM132D 162 GEKLPCLRVFAFREIREVRGSCRLKGLGLCAVELELSSWFSAPTVVAGRRKKSVDQPEGTPVELLY 228TVHPGGE-RGDCVREDAR
TMEM132E 159 TERLPCVRLHAFRAREH----- 176-----

TMEM132A 227 -----PGEQALPVGGVELEHPADPPQYQVPLDEAVTLRVVDMVVRPQOLFSS 272ATLLLRHNF-----TASLLLRHK
TMEM132B 238 WENNIHSGLESPPQAFPARERIGSVVYVPTQDCLKVLSLDENVVSVPLNLVREGDTA 298FLVSLTSS-----VADQTLRIK
TMEM132C 248 KGNALRPKDDGLEETTSHQRIQIYVYVYHAQPSAQLSELRGLDGNVWLPSPRPVKQEVVIT 308AYVITSSS-----VDLELRAK
TMEM132D 246 RSNGLRTRGHSIDDESGLPQRIQISFLYQTHRKPSSRELRDLSVAHYIYKTVKGDVLT 306FPVSI SRNS-----TEDRFLRAK
TMEM132E 177 -----PLLRIQSLHPPRRRLQERLRDLSNLMRLDRIRKPGEMVLS 220ILLYAPNSSSPSSPVEHFTLRK

TMEM132A 292 VVKGLHVTAAAPQAQTLWTAKLDRFKGSRHITLITCHRAGLTF-PDSSSPELSS 345FVWVDFVVEVNSGGGVAVRPVWQLEVYPG
TMEM132B 318 AAGGWKITAVRYS-DMVAQELDNGSTQTSALTCGWRHPDT-OSRV-NGSFY 370ELQVDEGDNSS--DAGAQOITVOVEYPI
TMEM132C 328 VVKGVNLSAOTREPROGVKQEVGSGKRVITAVACORLGPSP-RNRS-SSLFN 380VVCNNEIASFS--SLSGQITVOVEYPR
TMEM132D 326 VVKGVNIGVASSPSVDVKERTDYTGKVAAPVLCQKKAAS-ENSA-DGASY 378VMQIDVEVLEPG--DLPATQITVOVEYPR
TMEM132E 246 AKKGVTLTGKSRSGOHVHSELLTGAKHSIAVDVAWAQSTPLPPRE-GQGPL 298ELQLDLMEVNF--SOSVKRRIWHHTVIRG

TMEM132A 377 QAPEAEKDKMWELEVSERDIRALIPAKAEELVNTAPIITGVPHVYVR 425LVTVDGGALVEVTEHYVGEESANTQVLQVSEACDAV
TMEM132B 400 EDSM--SELVYSEIFVSOITFVGI VPLAMDTIELNTALITGKPVSVVVK 446VWVQEDGSSVVDVSESVECKSADIEDVIKVSNNCDSTF
TMEM132C 410 KG-T--TDIAYSEIFVSOQDLVGI VPLAMDTIELNTAVITGKTVAMPVK 455VSVLENSAVNDI SESVECKSDEEDVIKVSERCDFV
TMEM132D 408 EI-T--SDLVGSKIVYVSPKDLIGVYPLAMEIETLNTALITGKTVAVPVK 453VSVVEDDGTITLLESVECKSDEEDVIKVSERCDFV
TMEM132E 328 HGAIPDLERAVITLTVTRDVOALTEPLAMDTIELNTALITGRTVAVPVK 376VATEVNLVLDISALVECKSDEEDVIKVSERCDFV

TMEM132A 463 VAGKESRQARGVRVDFWWRRLRASRLVYVWAPLPLRIELTDT 505TLEQVRGWRVYGPAGPAEPAASDEAL--R--RARGGCHLQ
TMEM132B 484 VNGKEMKSVDTINNFITHQHTSQVYVWAPRPLQIEVSDT 526ELSOIKGWRVYVMAANRRPTIHSDDDELE--K--KRGGGSQ
TMEM132C 493 VNGKELGKMDAVNFTVYGLSAPLCTVYVWAPRPLQIEVSDT 535ELSOIKGWRVYVITNRRPTIHSDEDELE--R--RGRGGALQ
TMEM132D 491 VNGKEMKGVNVNFTVYHLSAPLCTVYVWAPRPLQIEVSDT 533ELNOIKGWRVYVSSRRRPAQDSDEDELE--R--RGRGGTLO
TMEM132E 414 VSGKESRGSNNARVITFRYDVLNAPLEMTVWVWPKLPLHLESDA 456MLSSQVKGWRVYVLPDRRSVRESDEDELEERROSASRGCTLO

TMEM132A 544 YORAGVRFVAPFAHPLDGGRRITHLGFDWLLDVSH 580VAPHARVLDNRVASLEGRRVVVGRPGVYVISEVRSPLSDS--GEQALA
TMEM132B 565 YOHATVRVLTQFVAFSPDLGQPTMYLGPDWDFDTH 600LVTEFMKVEETIAQLQDGRITAGREGPITVGVVSPSDS--LAEKTVI
TMEM132C 574 YOHATVRVLTQFVAGPWCOPYVLSLSPINWDFDTH 610LVTEFMKVEETIAQLQDGRITAGREGVYVITVGVVSPSDS--LAEKTVI
TMEM132D 572 YOHATVRVLTQFVAAAGPGGCHLHLGSDWDFDTH 608LVTEFMKVEETIAQLQDGRITAGREGVYVITVGVVSPSDT--LAEKTVI
TMEM132E 500 YOHATLRVLTQFHTTSSSEGTDCVVTMLGPDWCEVETD 536VSDFMVWGDPRVAHVVDSTLAGLEPGTTPPKVVSPLTEAVLGEITLL

TMEM132A 630 VTDKVSVLEIRVQVVMGILSITLSRGTAPHP 660EVTAICWASALPANKQEVALSILWSSFSHTWAPAEVDRRDLGLSVSAEEPGL
TMEM132B 650 VLDKRVITAEIGVQVAGMSLSLQPHRADKR 680AVTAAALDQLSQEQEAVSSWVLESQVSTPEDIVDKDYVTVSSVAVV
TMEM132C 660 VLDKRVITAEIQVAGLSVALYVNAENSK 690AVTAVTAEVLELQKQEAFTWQFSDGVSVPLDIDVDKDYVHAATISQDAVW
TMEM132D 658 VLDKRVITAEIGVQVAGMSLSLQSPGSS 688AVTAAVAGLELQRPKQEAASVWQFSDGVSVPLDIDVDKDYVMAATISQDAVW
TMEM132E 586 VTEKVSITQLQAVVAVSLALSLRSPGSSH 616TILATTAAVQQLSFLKQEAALLSILWSSYSDGITAPLSTVSPHYGLVSSVLEHVA

TMEM132A 716 LPAEEQGAQLGVVSGAGAEGPLPH 740VALHPPIPRRGRHRVPLASGTAWLGLPPASTPAPALPSSPAVSPATIEATMGGKQVAGS
TMEM132B 736 SVQANLESKMPVVAEAGEGQPLIK 760LEVMISEPCKTKRKSVALVKGKGNVVKVLEPSSDEHGGGNDIEGIRRE-----YKDH
TMEM132C 746 SVQPPSPRMPVVAEAGEGQPLIR 770VDMVTAAACOKSKRKSVALVGVGNVVKVQNDADSSPGGDY--EEDL-----IKNN
TMEM132D 744 SHODPKFKMPLTAAETEGQGLLVK 768VEMVISESOKSKRKSVALAVGTANI KVKFGQNDANPNTSDSRHTGAGVH-----MENN
TMEM132E 672 TVTQDR--APPLVVAFAEGSEFLR 694AETTAESCKTKRKSVALTPVGLRVHFGRDEFDPTY-D-Y-P-----

TMEM132A 802 VGGNTGVRGKFAEELAR 820-----TPVQGEIST--NKSTIPQSPMEGKNLLKS-----GGVDAFHSPTQKSP--A
TMEM132B 814 LNSNIREGNGERAVQEF 832HRG--SIPVEREELGALRRATITARSLLD--NKVVKNSRADGGRLAGEGQLQNIPIDFINFAHVDLP
TMEM132C 821 ASDRRQKQGHERTGODGH 839LYG--SSPVEREELGALRRATITARSLLD--NKVVKNSRADGGRLAGEGQLQNIPIDFINFAHVDLP
TMEM132D 822 VSDRRPKKPSQEWGSEGO 840YGG--SSSNGLMEG--RGTITDRSILQ--KKKQGESELLD-----NSHLQTI--SDLSFSAQVLDLP
TMEM132E 736 -----GPSQPGGGGDEAR 750GAGPPGSALPAPAP--GPTASPVV-----PPTEDFLP

TMEM132A 827 REEEEEEEEMVP 839AQHWTELELGMVALLGVFCVATIFILVNGVVFVLRVYQRKEPHDSATDPTSPQPHNWWLGTDOEELSRQLDR
TMEM132B 880 DPN--NPSDITV 889TSRGLTDELEGMVALLGVFCVLAIVFLVNCVAFAMKVRHKRFVAVSPOG-NIPHSHDWWLGNVEVLELNPVDI
TMEM132C 903 KAGSGLLENDLVQ 915TPRGLSDLEIGMVALLGVFCVLAIVFLVNCVTFALKYRHKQVPLFQGA-SMTSHSDWWLGNVAELLENSMGDA
TMEM132D 896 RNSGEMDGNLMO 908ASKGLSDLEIGMVALLGVFCVLAIVFLVNCVTFALKYRHKQVPLFQGE-GMSHDWWLGNVNRTELELLENHINF
TMEM132E 783 -----LPTGFLQ 789VPRGLTDELEGMVALLGVFCVLAIVFLVNCVTFALKYRHKRIPPEGQT-SMDSHSHWVLENGGQPLR-VQGEL

TMEM132A 913 QSPGPPK 919GEGSCPCESGGG-EAPTL-APGPPGTT-S-----SSSTLARKEAGGRKRKVEVITFAPAPVAQS
TMEM132B 962 T--LPS 965EECTIMDRGLQF-EERNF-LL--NGSOKTFHSCOLLRPSD-Y--VYEKEIKNEPWNSSGPKRKRKVFISYITLIPEDG
TMEM132C 988 P--PPQ 991DEHTTIDRGPAGCESNHLLL--NGGSHKVSQIHRSAQ-SGGRQGREQKODPLHSPTSRRKRKVFITFTTILPPDD
TMEM132D 981 A--SSQ 984DEQITAI DRGMDI-EESKY-LL--STNSOKSINGOLFPLG-PIIIGDKDKRSEPTSPTSRRKRKVFITFTTILPSSDDE
TMEM132E 861 S--PPA 864GN--PLEETVAF-CHGDH-HS--SGSCTVSQVQVHGRGSSGGSARDQAE DPASPTSRKRKVFITFTTILPSEEL

TMEM132A 978 P 978EEPVGAQVQSLVAGEEDI RWVCEDMG---LKDPEELRNYMERIRGSS 1024
TMEM132B 1038 -- 1037----GPTNSTLFDSDDNK KWCQDMG----LQSDQDFRNVESIQDM 1078
TMEM132C 1068 -- 1067----CPTVNSI VSNDEDI KWCQDVA----VGAPKELRNYLEKLDKA 1108
TMEM132D 1059 -- 1058----YPTRNSI VMSSEDDI KWCQDLD----PGDCKELHNYMERI HENV 1099
TMEM132E 937 A 937YD--SVPAGE-EEDEEEEDLGGWCPDVAGPTRPTAPDPLHNYMRRIRKAI 984

```

Figure A.1.: Multiple sequence alignment of TMEM132D paralogs employing T-coffee (www.tcoffee.org/). Visualization of multiple sequence alignment was performed using BOXSHADE 3.21 (http://www.ch.embnet.org/software/BOX_form.html).

Table A.1.: Transcription factor binding sites in the TMEM132D promoter identified by MatInspector (www.genomatix.de).

Family	Detailed Family Information	Matrix	position from-to	strand	Matrix sim.	Sequence (capitals: sequence)	core
V\$EGRF	EGR/nerve growth factor induced protein C & related factors	V\$WT1.01	8-24	(-)	0.959	aggcgCGGggtccgc	
V\$NRF1	Nuclear respiratory factor 1	V\$NRF1.01	10-26	(+)	0.782	ggaGCCccgcctcgc	
V\$ZBPf	Zinc binding protein factors	V\$ZF9.01	10-32	(+)	0.896	ggagcccCGCgctctggcag	
O\$XCPE	Activator-, mediator- and TBP-dependent core promoter element for RNA polymerase II transcription from TATA-less promoters	O\$XCPE1.01	12-22	(-)	0.823	gcGGGgggct	
V\$STAF	Selenocysteine tRNA activating factor	V\$ZNF76_143.01	12-34	(-)	0.783	tcctGCCAgcaggcggggct	
O\$TF2B	RNA polymerase II transcription factor II B	O\$BRE.01	17-23	(+)	1.000	cgcCGCC	
V\$CTCF	CTCF and BORIS gene family, transcriptional regulators with 11 highly conserved zinc finger domains	V\$CTCF.02	18-44	(+)	0.699	cgcgcctgctggcaggaGCAgctgcg	
V\$MYOD	Myoblast determining factors	V\$MYOD.01	18-34	(-)	0.891	tcctGCCAgcaggcgcg	
V\$ETSf	Human and murine ETS1 factors	V\$ETS2.01	24-44	(+)	0.841	tgctggcAGGAggcagctgcg	
V\$BTBF	BTB/POZ (broad complex, TramTrack, Bric-a-brac/pox viruses and zinc fingers) transcription factor	V\$KAISO.01	26-36	(-)	0.988	cctcCTGCCag	
V\$HAND	Twist subfamily of class B bHLH transcription factors	V\$HEN1.02	29-49	(-)	0.823	agcaacgcaGCTGcctctctgc	
V\$HAND	Twist subfamily of class B bHLH transcription factors	V\$HEN1.02	30-50	(+)	0.866	caggaggcaGCTGcgttgctc	
V\$MYOD	Myoblast determining factors	V\$MYOD.01	31-47	(+)	0.897	aggaGGCAGctgcttg	
V\$XBBF	X-box binding factors	V\$RFX1.01	41-59	(-)	0.920	gacggccgaGCAAcgca	
V\$DEAF	Homolog to deformed epidermal autoregulatory factor-1 from D. melanogaster	V\$NUDR.01	46-64	(+)	0.759	fgcTCGGccggtccccga	
V\$CTCF	CTCF and BORIS gene family, transcriptional regulators with 11 highly conserved zinc finger domains	V\$CTCF.01	50-76	(-)	0.824	gggcccgggctcGGGacggggcgc	

V\$CTCF	CTCF and BORIS gene family, transcriptional regulators with 11 highly conserved zinc finger domains	V\$CTCF.04	51-77	(+)	0.876	ggcgcgtccccgagcCGGCggggcct
V\$ZF5F	ZF5 POZ domain zinc finger	V\$ZF5.01	80-90	(-)	0.963	atgtGGCGgga
V\$RP58	RP58 (ZFP238) zinc finger protein	V\$RP58.01	84-96	(+)	0.937	cgcaCATctggcc
V\$NEUR	NeuroD, Beta2, HLH domain	V\$NGN_NEUROD.01	85-97	(-)	0.982	gggcCAGAtgfgc
V\$SPLF	GC-Box factors SPI/GC	V\$SP2.01	91-105	(-)	0.800	ggggggcgGGC'ag
V\$EGRF	EGR/nerve growth factor induced protein C & related factors	V\$CKROX.01	92-108	(-)	0.920	ccggGGGAgggcgggcca
V\$ZBPF	Zinc binding protein factors	V\$ZBP89.01	92-114	(+)	0.948	tggcccgctCCCcgggcg'cag
V\$CTCF	CTCF and BORIS gene family, transcriptional regulators with 11 highly conserved zinc finger domains	V\$CTCF.01	93-119	(-)	0.851	ccccctg'cgcccGGG'Gagcgggcc
V\$MAZF	Myc associated zinc fingers	V\$MAZ.01	94-106	(-)	0.919	ggggGAGGcgggc
V\$NOLF	Neuron-specific-olfactory factor	V\$OLF1.02	95-117	(+)	0.899	ccgccTCCCcgggcg'cagggg
V\$OAZF	Olfactory associated zinc finger protein	V\$ROAZ.01	98-114	(-)	0.743	ctGGC'ccgggggaggc
V\$CTCF	CTCF and BORIS gene family, transcriptional regulators with 11 highly conserved zinc finger domains	V\$CTCF.01	101-127	(+)	0.898	tccccggggcg'cagGGG'gagccccgc
V\$ZBPF	Zinc binding protein factors	V\$ZNF219.01	103-125	(-)	0.916	ggggctcCCCCctgcgccggggg
V\$PAX5	PAX-5 B-cell-specific activator protein	V\$PAX5.01	104-132	(+)	0.808	ccgggCGC'Agggggagcccccg'ctctc
V\$KLFS	Kruppel like transcription factors	V\$KLF.01	105-123	(+)	0.913	ccggcgcaGGG'ggagcc
V\$ZBPF	Zinc binding protein factors	V\$ZBP89.01	107-129	(-)	0.941	acgcgggctCCC'cctgcgcc
V\$CHRE	Carbohydrate response elements, consist of two E box motifs separated by 5 bp	V\$CHREBP_MLX.01	112-128	(+)	0.881	CAG'ggggagccccgcg
V\$MZF1	Myeloid zinc finger 1 factors	V\$MZF1.01	114-124	(+)	0.995	ggGGG'Gagccc
V\$NFKB	Nuclear factor kappa B/c-rel	V\$NFKAPPAB50.01	114-126	(+)	0.943	gggGGG'Agccccg
V\$NFKB	Nuclear factor kappa B/c-rel	V\$NFKAPPAB50.01	115-127	(-)	0.876	g'cgGGG'ctcccc
O\$MTEN	Core promoter motif ten elements	O\$DMTE.01	137-157	(-)	0.857	cgcgcgAGC'gactgcaggg
V\$MTF1	Metal induced transcription factor	V\$MTF-1.01	142-156	(+)	0.900	cagtGGC'tegggc
V\$PAX3	PAX-3 binding sites	V\$PAX3.01	149-167	(+)	0.767	cTGG'cgcgctagagccc
V\$DEAF	Homolog to deformed epidermal autoregulatory factor-1 from D. melanogaster	V\$NUDR.01	155-173	(-)	0.748	ctcGGG'ggcictacgc
V\$AHRR	AHR-arnet heterodimers and AHR-related factors	V\$AHRARNT.02	156-180	(-)	0.770	gctgggctcGGG'ggctacgcg
V\$AP2F	Activator protein 2	V\$AP2.01	181-195	(+)	0.906	cggGCC'ggggcgg
V\$STAF	Selenocysteine tRNA activating factor	V\$ZNF76_143.01	182-204	(-)	0.798	toggCCC'cgccccggggccc

V\$SPIF	GC-Box factors SPI/GC	V\$SP1.01	185-199	(+)	0.898	cccgggGcggg
V\$SPIF	GC-Box factors SPI/GC	V\$SP1.01	190-204	(+)	0.916	ggccGGCgggcca
V\$NRSF	Neuron-restrictive silencer factor	V\$NRSE.01	197-227	(-)	0.714	ggggtgtcccGGCggcgctcgccccg
V\$CTCF	CTCF and BORIS gene family, transcriptional regulators with 11 highly conserved zinc finger domains	V\$CTCF.02	202-228	(+)	0.702	cgaggggcgccgggAGCAgcccga
V\$PLAG	Pleomorphic adenoma gene	V\$PLAG1.01	203-223	(+)	0.929	GAGcgggcggggagcag
V\$ZNFP	Zinc finger proteins	V\$ZNF1.01	212-236	(+)	0.836	ggcGGGgagcagccgaccgcccaa
V\$ZBPF	Zinc binding protein factors	V\$ZBF9.01	217-239	(+)	0.911	ggagcagCCGCaccgccaact
V\$HESF	Vertebrate homologues of enhancer of split complex	V\$HES1.01	222-236	(-)	0.936	ttggcggGTGCggct
V\$E2FF	E2F-myc activator/cell cycle regulator	V\$E2F.02	225-241	(+)	0.896	egcaccgcCAAActtt
V\$MYT1	MYT1 C2HC zinc finger protein	V\$MYT1.02	231-243	(-)	0.982	ccaAAGTttggcg
V\$OAZF	Olfactory associated zinc finger protein	V\$ROAZ.01	233-249	(-)	0.752	cgGCACccaagtttgg
V\$NRF1	Nuclear respiratory factor 1	V\$NRF1.01	246-262	(-)	0.834	cgcGGCgcgctccggc
V\$HESF	Vertebrate homologues of enhancer of split complex	V\$HES1.01	247-261	(+)	0.932	ccggagcGGCGcgc
V\$NRF1	Nuclear respiratory factor 1	V\$NRF1.01	247-263	(+)	0.788	cgcGAGCgcgcgcgcc
V\$NRF1	Nuclear respiratory factor 1	V\$NRF1.01	248-264	(-)	0.942	ggcGGCgcgcgctccg
V\$NRF1	Nuclear respiratory factor 1	V\$NRF1.01	249-265	(+)	0.905	ggcGGCgcgcgcgccc
V\$ZF5F	ZF5 POZ domain zinc finger	V\$ZF5.01	249-259	(-)	0.962	ggcGGCtcc
V\$NRF1	Nuclear respiratory factor 1	V\$NRF1.01	250-266	(-)	0.882	eggGGCgcgcgctc
V\$ZF5F	ZF5 POZ domain zinc finger	V\$ZF5.01	250-260	(+)	0.958	gagcGGCgcg
V\$NRF1	Nuclear respiratory factor 1	V\$NRF1.01	251-267	(+)	0.942	agcGGCgcgcgccga
V\$ZF5F	ZF5 POZ domain zinc finger	V\$ZF5.01	251-261	(-)	0.968	ggcGGCgct
V\$E2FF	E2F-myc activator/cell cycle regulator	V\$E2F.03	252-268	(-)	0.860	ctcggGGCgcgcgcgcc
V\$HESF	Vertebrate homologues of enhancer of split complex	V\$HES1.01	252-266	(-)	0.936	cgggagcGGCGcgc
V\$NRF1	Nuclear respiratory factor 1	V\$NRF1.01	252-268	(-)	0.833	ctcGGCgcgcgcgcc
V\$ZF5F	ZF5 POZ domain zinc finger	V\$ZF5.01	252-262	(+)	0.968	ggcGGCgcg
V\$NRF1	Nuclear respiratory factor 1	V\$NRF1.01	253-269	(+)	0.833	cgcGGCgcgccccgagc
V\$ZF5F	ZF5 POZ domain zinc finger	V\$ZF5.01	253-263	(-)	0.968	ggcGGCgcg
V\$ZF5F	ZF5 POZ domain zinc finger	V\$ZF5.01	254-264	(+)	0.968	ggcGGCgccc
V\$ZF5F	ZF5 POZ domain zinc finger	V\$ZF5.01	255-265	(-)	0.968	ggcGGCgcg
V\$NRF1	Nuclear respiratory factor 1	V\$NRF1.01	256-272	(-)	0.792	ggcGGCgcgcgcgcc
V\$ZF5F	ZF5 POZ domain zinc finger	V\$ZF5.01	256-266	(+)	0.965	ggcGGCgccc
V\$NRF1	Nuclear respiratory factor 1	V\$NRF1.01	257-273	(+)	0.843	cgcGGCgccccgccc
V\$AP2F	Activator protein 2	V\$AP2.02	266-280	(-)	0.933	tgcGGCTcggggctc

V\$AP4R	AP4 and related proteins	V\$AP4.01	274-290	(+)	0.870	aggcgCAGCggccggcc
V\$ZFX	Zfx and Zfy - transcription factors implicated in mammalian sex determination	V\$ZFX.01	285-295	(+)	0.985	ccGGCCtggga
V\$ZBPF	Zinc binding protein factors	V\$ZNF219.01	286-308	(-)	0.917	cccgcagCCCcatcccaggccg
V\$GCMF	Chorion-specific transcription factors with a GCM DNA binding domain	V\$GCM1.01	293-303	(-)	0.856	agCCCCcatcc
V\$CTCF	CTCF and BORIS gene family, transcriptional regulators with 11 highly conserved zinc finger domains	V\$CTCF.01	308-334	(-)	0.835	tgcctggcggcccGGGctccctggc
V\$NFKB	Nuclear factor kappa B/c-rel	V\$NFKAPPAB50.01	309-321	(+)	0.849	ccaGGAGgcccc
V\$EGRF	EGR/nerve growth factor induced protein C & related factors	V\$WT1.01	336-352	(-)	0.922	ccggcGGGtggccggg
V\$EBOX	E-box binding factors	V\$ATF6.01	338-350	(+)	0.937	cggCCACccgcc
V\$KLFS	Kruppel like transcription factors	V\$EKLf.01	338-356	(-)	0.903	ccccccggcGGTggccg
V\$SPIF	GC-Box factors SPI/GC	V\$SPI.01	340-354	(-)	0.907	ccccGGGc'gggtggc
V\$DEAF	Homolog to deformed autoregulatory factor-1 from D. melanogaster	V\$NUDR.01	346-364	(+)	0.769	cgcCCGg'ggggctccgagc
V\$GLIF	GLI zinc finger family	V\$ZIC2.01	347-361	(-)	0.899	cggagccCCCgggc
V\$MTF1	Metal induced transcription factor	V\$MTF-1.01	368-382	(+)	0.891	ctctGCCcgcctcc
V\$WHNF	Winged helix binding sites	V\$WHN.01	372-382	(-)	0.952	gggACGCgggc
V\$KLFS	Kruppel like transcription factors	V\$KLF6.01	385-403	(-)	0.924	ggtggcGGGcctg'cggagc
V\$CTCF	CTCF and BORIS gene family, transcriptional regulators with 11 highly conserved zinc finger domains	V\$CTCF.02	391-417	(-)	0.701	gcaggcggc'cggggfGGCGgggctg
V\$SPIF	GC-Box factors SPI/GC	V\$GC.01	391-405	(-)	0.900	ggsgtGGCGgggctg
V\$ZBPF	Zinc binding protein factors	V\$ZNF202.01	392-414	(+)	0.766	agccccGCCAccccggc'ccg
V\$EGRF	EGR/nerve growth factor induced protein C & related factors	V\$EGR1.02	393-409	(-)	0.900	cggcgggTGGC'gsggc
V\$CTCF	CTCF and BORIS gene family, transcriptional regulators with 11 highly conserved zinc finger domains	V\$CTCF.01	394-420	(-)	0.823	ggcgcaggcgggc'CGGGgtggcgggg
V\$EBOX	E-box binding factors	V\$ATF6.01	396-408	(+)	0.944	ccGCCACcccggc
V\$NRF1	Nuclear respiratory factor 1	V\$NRF1.01	406-422	(-)	0.822	ctgGCCc'aggcggc'cc
V\$EGRF	EGR/nerve growth factor induced protein C & related factors	V\$NGFIC.01	407-423	(-)	0.822	gctgCGC'aggcggc'c
V\$NRF1	Nuclear respiratory factor 1	V\$NRF1.01	407-423	(+)	0.791	gcGCCc'ctgc'ccagc

V\$NRF1	Nuclear respiratory factor 1	V\$NRF1.01	412-428	(-)	0.884	eggGGCtggcgaggc
V\$NRF1	Nuclear respiratory factor 1	V\$NRF1.01	413-429	(+)	0.895	cctGGCagcgcccc
V\$ZF5F	ZF5 POZ domain zinc finger	V\$ZF5.01	419-429	(-)	0.951	gchgGGCtgg
V\$HAND	Twist subfamily of class B bHLH transcription factors	V\$HEN1.02	437-457	(-)	0.876	gchgctccaGCTGctccccggg
V\$HAND	Twist subfamily of class B bHLH transcription factors	V\$HEN1.02	438-458	(+)	0.880	ccgggagcaGCTGgagccgcc
V\$AP4R	AP4 and related proteins	V\$AP4.02	439-455	(-)	0.933	ggctccAGCTgctcccc
V\$MYOD	Myoblast determining factors	V\$MYF5.01	439-455	(+)	0.928	cgggagCAGCtggagcc
V\$AP4R	AP4 and related proteins	V\$AP4.01	440-456	(+)	0.888	gggagCAGCtggagccg
V\$MYOD	Myoblast determining factors	V\$MYOGENIN.02	440-456	(-)	0.959	cggtccCAGCtgcctccc
V\$ZFA	Zinc finger with interaction domain factors	V\$ZID.01	444-456	(-)	0.877	cgGCTCagctgc
O\$MTE	Core promoter motif ten elements	O\$HMT.01	459-479	(+)	0.902	ggAGCCctgcctggagccg
V\$MAZF	Myc associated zinc fingers	V\$MAZ.01	477-489	(-)	0.912	caagGAGGggcgc
V\$CTCF	CTCF and BORIS gene family, transcriptional regulators with 11 highly conserved zinc finger domains	V\$CTCF.01	484-510	(+)	0.814	tccttggccaccgGGGccactcttc
V\$HAND	Twist subfamily of class B bHLH transcription factors	V\$HAND2_E12.01	485-505	(-)	0.767	gtggccccggTGGCccaagg
V\$YBXF	Y-box binding transcription factors, multifunctional proteins involved in transcriptional and translational regulation, mRNA splicing, DNA replication and repair	V\$YB1.01	497-509	(-)	0.928	aagagTGGCcccc
V\$EBOX	E-box binding factors	V\$ATF6.01	499-511	(+)	0.945	gggCCAActcttcg
O\$MTE	Core promoter motif ten elements	O\$DMTE.01	500-520	(-)	0.830	ttaccgAGCGaagagtggcc
V\$FKHD	Fork head domain factors	V\$HNF3.01	512-528	(+)	0.986	ctcgggtAAACagggaaa
V\$ETSF	Human and murine ETS1 factors	V\$SPIB.01	516-536	(+)	0.897	ggtaaacagGAaggaaatac
V\$NFAT	Nuclear factor of activated T-cells	V\$NFAT.01	526-544	(+)	0.965	aaaGGAAtaccctctgtg
V\$NFKB	Nuclear factor kappa B/c-rel	V\$CREL.01	528-540	(-)	0.973	gggggtatTTCCt
V\$HMTB	Human muscle-specific Mt binding site	V\$MTBF.01	530-538	(-)	0.938	gggtATTc
V\$FAST	FAST-1 SMAD interacting proteins	V\$FAST1.02	536-552	(+)	0.888	ccccTGTGgattaaaa
V\$BCDF	Bicoid-like homeodomain transcription factors	V\$CRX.01	538-554	(-)	0.987	aatttTAATccacagg
V\$BRNF	Brn POU domain factors	V\$TST1.01	541-559	(+)	0.926	tgtggATTAAaatttaaaa
V\$MEF2	MEF2, myocyte-specific enhancer binding factor	V\$MEF2.01	547-569	(+)	0.822	ttaaaattTAAAAAAaattctgt
V\$RXRF	RXR heterodimer binding sites	V\$VDR_RXR.03	564-588	(+)	0.789	ttctgttgGGTcgaaggaggagg

V\$ZBNF	Zinc binding protein factors	V\$ZBNF202.01	576-598	(-)	0.730	gcaaacCCCACctccctcctteg
V\$EGRF	EGR/nerve growth factor induced protein C & related factors	V\$CKROX.01	579-595	(+)	0.900	aggaGGAGgtgsggtt
V\$HAML	Human acute myelogenous leukemia factors	V\$AML3.01	586-600	(+)	0.859	aggtGGGgtttgcct
V\$ZF5F	ZF5 POZ domain zinc finger	V\$ZF5.01	599-609	(+)	0.966	ctgcGGCGgtg
V\$CDEF	Cell cycle regulators: Cell cycle dependent element	V\$CDE.01	600-612	(+)	0.877	tgcgCGCGgtgtg
V\$NRF1	Nuclear respiratory factor 1	V\$NRF1.01	629-645	(-)	0.833	accGGCGgggtctctga
V\$CDEF	Cell cycle regulators: Cell cycle dependent element	V\$CDE.01	633-645	(-)	0.880	accgCGCGggctc
V\$CDEF	Cell cycle regulators: Cell cycle dependent element	V\$CDE.01	636-648	(+)	0.879	cccgCGCGgtcgt
V\$ZFX	Zfx and Zfy - transcription factors implicated in mammalian sex determination	V\$ZFX.01	655-665	(+)	0.992	ccGGCCtggcc
V\$STAF	Selenocysteine tRNA activating factor	V\$ZNF76_143.01	660-682	(-)	0.796	tcttCCCGccagtcctatggccag
V\$E2FF	E2F-myc activator/cell cycle regulator	V\$RB_E2F1_DP1.01	666-682	(-)	0.723	tcttcCCGCcagtcctat
V\$STAT	Signal transducer and activator of transcription	V\$STAT1.01	668-686	(+)	0.791	ggactggcgGGAAGagggga
V\$E2FF	E2F-myc activator/cell cycle regulator	V\$E2F1_DP1.01	669-685	(+)	0.916	gactGGCGggaagagg
V\$ETSF	Human and murine ETS1 factors	V\$GABP.01	669-689	(+)	0.933	gactggcgGGAAGagggagca
V\$ZF35	Zinc finger protein ZNF35	V\$ZNF35.01	673-685	(+)	0.981	ggcgggAAGAggg
O\$MTEN	Core promoter motif ten elements	O\$HMT.01	684-704	(+)	0.934	ggAGCAGggcgccgggctgc
V\$NRF1	Nuclear respiratory factor 1	V\$NRF1.01	689-705	(+)	0.788	aggGCGCccgggctgct
V\$HICF	Kruppel-like C2H2 zinc finger factors hypermethylated in cancer	V\$HIC1.01	697-709	(+)	0.942	cgggcTGC'Tgggg
O\$MTEN	Core promoter motif ten elements	O\$HMT.01	713-733	(+)	0.931	ctAGCCgggctcctcctcgc
V\$HESF	Vertebrate homologues of enhancer of split complex	V\$HES1.01	714-728	(+)	0.947	tagcggGCGCtccc
V\$ZF5F	ZF5 POZ domain zinc finger	V\$ZF5.01	718-728	(-)	0.956	gggaGCGCccg
V\$XBBF	X-box binding factors	V\$MIF1.01	720-738	(+)	0.771	ggcgtcctcGCCAaccgg
O\$XCPE	Activator-, mediator- and TBP-dependent core promoter element for RNA polymerase II transcription from TATA-less promoters	O\$XCPE1.01	722-732	(-)	0.847	gcGAGGgagcg
V\$ZBNF	Zinc binding protein factors	V\$ZBNF202.01	725-747	(+)	0.734	tcctcGCCAaccggccccctg
V\$PAX3	PAX-3 binding sites	V\$PAX3.01	728-746	(+)	0.767	cTCCGcaccggccccctg

V\$CTCF	CTCF and BORIS gene family, transcriptional regulators with 11 highly conserved zinc finger domains	V\$CTCF.03	732-758	(-)	0.819	cctagagcccccragcGGGGcgggtgg
V\$CTCF	CTCF and BORIS gene family, transcriptional regulators with 11 highly conserved zinc finger domains	V\$CTCF.04	732-758	(+)	0.854	ccaccggccccctgcGGCCctctagg
V\$PLAG	Pleomorphic adenoma gene	V\$PLAG1.01	734-754	(-)	0.922	GAGcccgcagcggggccgggt
V\$CTCF	CTCF and BORIS gene family, transcriptional regulators with 11 highly conserved zinc finger domains	V\$CTCF.01	743-769	(+)	0.823	gtcggggcctctaGGGactgagacg
V\$PAX5	PAX-5 B-cell-specific activator protein	V\$PAX5.03	744-772	(-)	0.838	gaccgTCTCagtcccttagagcccgcag
V\$MOKF	Mouse Krueppel like factor	V\$MOK2.01	752-772	(-)	0.789	gaccgtctcagtcCCCTagag
O\$INRE	Core promoter initiator elements	O\$DINR.01	757-767	(-)	0.954	tcTCAGtcccc
V\$NRSF	Neuron-restrictive silencer factor	V\$NRSF.01	777-807	(-)	0.692	tccctccgtcccCGGcgcctccaggcgaac
V\$KLFS	Krueppel like transcription factors	V\$KKLFF.01	786-804	(+)	0.916	gacgggcccGGGgagcga
V\$ETSF	Human and murine ETS1 factors	V\$PDEF.01	819-839	(+)	0.958	ggctccaGGATgtgcccgtc
V\$DMTF	Cyclin D binding myb-like transcription factor	V\$DMPI.01	822-834	(+)	0.855	ctccaGGATgtgc
V\$WHNF	Winged helix binding sites	V\$WHN.01	847-857	(+)	0.983	gggACGCtgtg
V\$HNF1	Hepatic Nuclear Factor 1	V\$HNF1.02	872-888	(+)	0.777	eggTACTcatcagcctg
V\$EV11	EV11-myeloid transforming protein	V\$MEL1.02	873-889	(-)	1.000	ccaggctGATGagtacc
V\$RU49	Zinc finger transcription factor RU49, zinc finger proliferation 1 - Zippro1	V\$RU49.01	873-879	(-)	0.990	gAGTacc
V\$NFAT	Nuclear factor of activated T-cells	V\$NFAT5.01	888-906	(-)	0.832	tttGGAaacagggggcc
V\$FKHD	Fork head domain factors	V\$ILF1.01	891-907	(-)	0.991	ctttggaaAACAgggcg
V\$WHNF	Winged helix binding sites	V\$WHN.01	911-921	(+)	0.953	aggACGCcggc

Table A.2.: **TFSEARCH** (<http://www.cbrc.jp/research/db/TFSEARCH.html>) results identifying potential transcription factor binding sites in the TMEM132D promoter.

Name	Detailed name	Position from-to	Strand	Score	Sequence
GATA-1	GATA-binding factor 1	88-97	(-)	86.9	catctggccc
MZF1	Myeloid zinc finger 1	104-110	(+)	96.5	agggggga
NF-kap	nuclear factor kappa light chain enhancer of activated B cells	108-125	(+)	90.7	ggggagcccc
NF-kap	nuclear factor kappa light chain enhancer of activated B cells	119-128	(-)	88.9	gagccccgcg
Sp1	Specificity Protein 1	188-196	(+)	86.3	ggggccgggc
MZF1	Myeloid zinc finger 1	212-219	(+)	85.2	gccgggga
E2F	E2F transcription factor 1	231-240	(-)	88.5	ttcaaaccg
GATA-2	GATA-binding factor 2	291-300	(+)	90.9	tgggatgggg
GATA-1	GATA-binding factor 1	291-300	(+)	90.6	tgggatgggg
GATA-3	GATA-binding factor 3	292-300	(+)	86.9	gggatgggg
Sp1	Specificity Protein 1	396-402	(-)	87.7	ccgccac
c-Rel	v-rel reticuloendotheliosis viral oncogene homolog (avian)	531-540	(-)	94.2	aaataccccc
NF-kap	nuclear factor kappa light chain enhancer of activated B cells	531-540	(-)	92.7	aaataccccc
NF-kap	nuclear factor kappa light chain enhancer of activated B cells	531-540	(-)	91.6	aaataccccc
c-Ets	v-ets erythroblastosis virus E26 oncogene homolog (avian)	524-536	(+)	86.6	ggaaaggaaatac
CdxA	caudal type homeobox 1	552-557	(+)	88.5	atttaaa
CdxA	caudal type homeobox 1	562-568	(+)	92.1	aattctg
AML-1a	Acute myeloid leukemia 1 protein	560-565	(+)	87.4	tggggt
AML-1a	Acute myeloid leukemia 1 protein	589-594	(+)	87.4	tggggt
Sp1	Specificity Protein 1	585-594	(+)	86.3	gaggtggggt
c-Rel	v-rel reticuloendotheliosis viral oncogene homolog (avian)	580-599	(+)	85.1	ggggtttgcc
MZF1	Myeloid zinc finger 1	792-799	(+)	85.2	gccgggga
GATA-3	GATA-binding factor 3	841-849	(+)	92.2	gagatgggg
MZF1	Myeloid zinc finger 1	843-850	(+)	92.2	gatgggga
GATA-1	GATA-binding factor 1	839-849	(+)	91.0	tgagatgggg
GATA-2	GATA-binding factor 2	839-849	(+)	88.9	tgagatgggg
c-Ets	v-ets erythroblastosis virus E26 oncogene homolog (avian)	824-833	(+)	87.3	ccaggatgtg
AML-1a	Acute myeloid leukemia 1 protein	862-868	(-)	85.4	cactggt
GATA-1	GATA-binding factor 1	879-888	(-)	89.0	catcagcctg
C/EBP	CCAAT-enhancer-binding proteins	899-908	(-)	86.2	tttccaaagg

References

- Abraham, W. C., Dragunow, M., and Tate, W. P. (1991). The role of immediate early genes in the stabilization of long-term potentiation. *Mol Neurobiol*, 5(2-4):297–314.
- Adamec, R., Hebert, M., Blundell, J., and Mervis, R. F. (2012). Dendritic morphology of amygdala and hippocampal neurons in more and less predator stress responsive rats and more and less spontaneously anxious handled controls. *Behav Brain Res*, 226(1):133–146.
- Adamec, R. E., Burton, P., Shallow, T., and Budgell, J. (1999). NMDA receptors mediate lasting increases in anxiety-like behavior produced by the stress of predator exposure—implications for anxiety associated with posttraumatic stress disorder. *Physiol. Behav.*, 65(4-5):723–737.
- Adlard, P. A., Engesser-Cesar, C., and Cotman, C. W. (2011). Mild stress facilitates learning and exercise improves retention in aged mice. *Exp. Gerontol.*, 46(1):53–59.
- Aerni, A., Traber, R., Hock, C., Roozendaal, B., Schelling, G., Papassotiropoulos, A., Nitsch, R. M., Schnyder, U., and de Quervain, D. J. (2004). Low-dose cortisol for symptoms of posttraumatic stress disorder. *Am. J. Psychiatry*, 161(8):1488–1490.
- Afadlal, S., Polaboon, N., Surakul, P., Govitrapong, P., and Jutapakdeegul, N. (2010). Prenatal stress alters presynaptic marker proteins in the hippocampus of rat pups. *Neurosci. Lett.*, 470(1):24–27.
- Affi, T. O., Asmundson, G. J. G., Taylor, S., and Jang, K. L. (2010). The role of genes and environment on trauma exposure and posttraumatic stress disorder symptoms: a review of twin studies. *Clin Psychol Rev*, 30(1):101–112.
- Aisa, B., Elizalde, N., Tordera, R., Lasheras, B., Del Río, J., and Ramírez, M. J. (2009). Effects of neonatal stress on markers of synaptic plasticity in the hippocampus: implications for spatial memory. *Hippocampus*, 19(12):1222–1231.
- Alfonso, J., Frick, L. R., Silberman, D. M., Palumbo, M. L., Genaro, A. M., and Frasch, A. C. (2006). Regulation of hippocampal gene expression is conserved in two species subjected to different stressors and antidepressant treatments. *Biol. Psychiatry*, 59(3):244–251.
- Altshuler, Y., Copeland, N. G., Gilbert, D. J., Jenkins, N. A., and Frohman, M. A. (1996). Gcm1, a mammalian homolog of drosophila glial cells missing. *FEBS Lett.*, 393(2-3):201–204.
- American Psychiatric Association (1980). *Diagnostic and Statistical Manual of Mental Disorders (3th ed.)*. Washington, DC : American Psychiatric Association, 1980.
- American Psychiatric Association (2000). *Diagnostic and Statistical Manual of Mental Disorders (Revised 4th ed.)*. Washington, DC: Author.

REFERENCES

- Amourette, C., Lamproglou, I., Barbier, L., Fauquette, W., Zoppe, A., Viret, R., and Diserbo, M. (2009). Gulf war illness: Effects of repeated stress and pyridostigmine treatment on blood-brain barrier permeability and cholinesterase activity in rat brain. *Behav Brain Res*, 203(2):207–214.
- Amstadter, A. B., Koenen, K. C., Ruggiero, K. J., Acierno, R., Galea, S., Kilpatrick, D. G., and Gelernter, J. (2009). Variant in RGS2 moderates posttraumatic stress symptoms following potentially traumatic event exposure. *J Anxiety Disord*, 23(3):369–373.
- Amstadter, A. B., Nugent, N. R., Yang, B., Miller, A., Siburian, R., Moorjani, P., Haddad, S., Basu, A., Fagerness, J., Saxe, G., Smoller, J. W., and Koenen, K. C. (2011). Corticotrophin-releasing hormone type 1 receptor gene (CRHR1) variants predict posttraumatic stress disorder onset and course in pediatric injury patients. *Dis. Markers*, 30(2-3):89–99.
- Anwyl, R. (2009). Metabotropic glutamate receptor-dependent long-term potentiation. *Neuropharmacology*, 56(4):735–740.
- Apfel, B. A., Ross, J., Hlavin, J., Meyerhoff, D. J., Metzler, T. J., Marmar, C. R., Weiner, M. W., Schuff, N., and Neylan, T. C. (2011). Hippocampal volume differences in gulf war veterans with current versus lifetime posttraumatic stress disorder symptoms. *Biol. Psychiatry*, 69(6):541–548.
- Armstrong, R. C., Kim, J. G., and Hudson, L. D. (1995). Expression of myelin transcription factor I (MyTI), a "zinc-finger" DNA-binding protein, in developing oligodendrocytes. *Glia*, 14(4):303–321.
- Ary, A. W., Aguilar, V. R., Szumlanski, K. K., and Kippin, T. E. (2007). Prenatal stress alters limbo-cortico-striatal homer protein expression. *Synapse*, 61(11):938–941.
- Atmaca, M., Kuloglu, M., Tezcan, E., Onal, S., and Ustundag, B. (2002). Neopterin levels and dexamethasone suppression test in posttraumatic stress disorder. *Eur Arch Psychiatry Clin Neurosci*, 252(4):161–165.
- Baker, D. G., Ekhtor, N. N., Kasckow, J. W., Hill, K. K., Zoumakis, E., Dashevsky, B. A., Chrousos, G. P., and Geraciotti, T D, J. (2001). Plasma and cerebrospinal fluid interleukin-6 concentrations in posttraumatic stress disorder. *NeuroImmunoModulation*, 9(4):209–217.
- Banerjee, D. and Nandagopal, K. (2007). Potential interaction between the GARS-AIRS-GART gene and CP2/LBP-1c/LSF transcription factor in down syndrome-related alzheimer disease. *Cell Mol Neurobiol*, 27(8):1117–1126.
- Barlow, D. H. (2000). Unraveling the mysteries of anxiety and its disorders from the perspective of emotion theory. *Am Psychol*, 55(11):1247–1263.
- Barnes, P. J. (2011). Glucocorticosteroids: current and future directions. *Br J Pharmacol*, 163(1):29–43.
- Bauer, M. E., Wieck, A., Lopes, R. P., Teixeira, A. L., and Grassi-Oliveira, R. (2010). Interplay between neuroimmunoendocrine systems during post-traumatic stress disorder: a minireview. *Neuroimmunomodulation*, 17(3):192–195.

- Baumann, M., Pontiller, J., and Ernst, W. (2010). Structure and basal transcription complex of RNA polymerase II core promoters in the mammalian genome: an overview. *Mol. Biotechnol.*, 45(3):241–247.
- Bayer, E. A., Belaich, J.-P., Shoham, Y., and Lamed, R. (2004). The cellulosomes: multienzyme machines for degradation of plant cell wall polysaccharides. *Annu. Rev. Microbiol.*, 58:521–554.
- Beasley, C. L., Honer, W. G., Bergmann, K., Falkai, P., Lütjohann, D., and Bayer, T. A. (2005). Reductions in cholesterol and synaptic markers in association cortex in mood disorders. *Bipolar Disord*, 7(5):449–455.
- Beattie, E. C., Stellwagen, D., Morishita, W., Bresnahan, J. C., Ha, B. K., Von Zastrow, M., Beattie, M. S., and Malenka, R. C. (2002). Control of synaptic strength by glial TNF α . *Science*, 295(5563):2282–2285.
- Bedi, U. S. and Arora, R. (2007). Cardiovascular manifestations of posttraumatic stress disorder. *J Natl Med Assoc*, 99(6):642–649.
- Berger, W., Mendlowicz, M. V., Marques-Portella, C., Kinrys, G., Fontenelle, L. F., Marmar, C. R., and Figueira, I. (2009). Pharmacologic alternatives to antidepressants in posttraumatic stress disorder: a systematic review. *Prog. Neuropsychopharmacol. Biol. Psychiatry*, 33(2):169–180.
- Binder, E. B., Bradley, R. G., Liu, W., Epstein, M. P., Deveau, T. C., Mercer, K. B., Tang, Y., Gillespie, C. F., Heim, C. M., Nemeroff, C. B., Schwartz, A. C., Cubells, J. F., and Ressler, K. J. (2008). Association of FKBP5 polymorphisms and childhood abuse with risk of posttraumatic stress disorder symptoms in adults. *JAMA*, 299(11):1291–1305.
- Binder, E. B., Salyakina, D., Lichtner, P., Wochnik, G. M., Ising, M., Pütz, B., Papiol, S., Seaman, S., Lucae, S., Kohli, M. A., Nickel, T., Künzel, H. E., Fuchs, B., Majer, M., Pfennig, A., Kern, N., Brunner, J., Modell, S., Baghai, T., Deiml, T., Zill, P., Bondy, B., Rupprecht, R., Messer, T., Köhnelein, O., Dabitz, H., Brückl, T., Müller, N., Pfister, H., Lieb, R., Mueller, J. C., Löhmußaar, E., Strom, T. M., Bettecken, T., Meitinger, T., Uhr, M., Rein, T., Holsboer, F., and Muller-Myhsok, B. (2004). Polymorphisms in FKBP5 are associated with increased recurrence of depressive episodes and rapid response to antidepressant treatment. *Nat Genet*, 36(12):1319–1325.
- Biomarkers Definitions Working Group (2001). Biomarkers and surrogate endpoints: preferred definitions and conceptual framework. *Clin. Pharmacol. Ther.*, 69(3):89–95.
- Blinzinger, K. and Kreutzberg, G. (1968). Displacement of synaptic terminals from regenerating motoneurons by microglial cells. *Z Zellforsch Mikrosk Anat*, 85(2):145–157.
- Blundell, J., Adamec, R., and Burton, P. (2005). Role of NMDA receptors in the syndrome of behavioral changes produced by predator stress. *Physiol. Behav.*, 86(1-2):233–243.
- Bock, J., Murmu, M. S., Biala, Y., Weinstock, M., and Braun, K. (2011). Prenatal stress and neonatal handling induce sex-specific changes in dendritic complexity and dendritic spine density in hippocampal subregions of prepubertal rats. *Neuroscience*, 193:34–43.

REFERENCES

- Boscarino, J. A. and Chang, J. (1999). Higher abnormal leukocyte and lymphocyte counts 20 years after exposure to severe stress: research and clinical implications. *Psychosom Med*, 61(3):378–386.
- Bowirrat, A., Chen, T. J. H., Blum, K., Madigan, M., Bailey, J. A., Chuan Chen, A. L., Downs, B. W., Braverman, E. R., Radi, S., Waite, R. L., Kerner, M., Giordano, J., Morse, S., Oscar-Berman, M., and Gold, M. (2010). Neuro-psychopharmacogenetics and neurological antecedents of posttraumatic stress disorder: Unlocking the mysteries of resilience and vulnerability. *Curr Neuropharmacol*, 8(4):335–358.
- Breslau, N. (2009). The epidemiology of trauma, ptsd, and other posttrauma disorders. *Trauma Violence Abuse*, 10(3):198–210.
- Brewin, C. R. (2011). The nature and significance of memory disturbance in posttraumatic stress disorder. *Annual Review of Clinical Psychology*, 7:203–227.
- Briones, A., Gagno, S., Martisova, E., Dobarro, M., Aisa, B., Solas, M., Tordera, R., and Ramírez, M. J. (2012). Stress-induced anhedonia is associated to increased alzheimer’s disease markers. *Br. J. Pharmacol.*, 165(4):897–907.
- Bronisch, T. (2010). Die Geschichte der Diagnose einer Posttraumatic stress disorder – Posttraumatische Belastungsstörung. *Psychotherapie*, 15:195–203.
- Buntinx, M., Vanderlocht, J., Hellings, N., Vandenabeele, F., Lambrechts, I., Raus, J., Ameloot, M., Stinissen, P., and Steels, P. (2003). Characterization of three human oligodendroglial cell lines as a model to study oligodendrocyte injury: morphology and oligodendrocyte-specific gene expression. *J. Neurocytol.*, 32(1):25–38.
- Burkhard, P., Stetefeld, J., and Strelkov, S. V. (2001). Coiled coils: a highly versatile protein folding motif. *Trends Cell Biol.*, 11(2):82–88.
- Carrasco, G. A. and Van de Kar, L. D. (2003). Neuroendocrine pharmacology of stress. *Eur. J. Pharmacol.*, 463(1-3):235–272.
- Cartharius, K., Frech, K., Grote, K., Klocke, B., Haltmeier, M., Klingenhoff, A., Frisch, M., Bayerlein, M., and Werner, T. (2005). MatInspector and beyond: promoter analysis based on transcription factor binding sites. *Bioinformatics*, 21(13):2933–2942.
- Cesca, F., Baldelli, P., Valtorta, F., and Benfenati, F. (2010). The synapsins: key actors of synapse function and plasticity. *Progress in Neurobiology*, 91(4):313–348.
- Chadman, K. K., Yang, M., and Crawley, J. N. (2009). Criteria for validating mouse models of psychiatric diseases. *Am. J. Med. Genet. B Neuropsychiatr. Genet.*, 150B(1):1–11.
- Chertkow-Deutsher, Y., Cohen, H., Klein, E., and Ben-Shachar, D. (2010). DNA methylation in vulnerability to post-traumatic stress in rats: evidence for the role of the post-synaptic density protein Dlgap2. *Int J Neuropsychopharmacol*, 13(3):347–359.
- Cohen, H., Kaplan, Z., Koresh, O., Matar, M. A., Geva, A. B., and Zohar, J. (2011). Early post-stressor intervention with propranolol is ineffective in preventing posttraumatic stress responses in an animal model for PTSD. *Eur Neuropsychopharmacol*, 21(3):230–240.

- Cohen, H., Liu, T., Kozlovsky, N., Kaplan, Z., Zohar, J., and Mathé, A. A. (2012). The neuropeptide y (NPY)-ergic system is associated with behavioral resilience to stress exposure in an animal model of post-traumatic stress disorder. *Neuropsychopharmacology*, 37(2):350–363.
- Cohen, H., Ziv, Y., Cardon, M., Kaplan, Z., Matar, M. A., Gidron, Y., Schwartz, M., and Kipnis, J. (2006). Maladaptation to mental stress mitigated by the adaptive immune system via depletion of naturally occurring regulatory CD4+CD25+ cells. *J Neurobiol*, 66(6):552–563.
- Cole, J., Costafreda, S. G., McGuffin, P., and Fu, C. H. Y. (2011). Hippocampal atrophy in first episode depression: a meta-analysis of magnetic resonance imaging studies. *J Affect Disord*, 134(1-3):483–487.
- Comings, D. E., Muhleman, D., and Gysin, R. (1996). Dopamine D2 receptor (DRD2) gene and susceptibility to posttraumatic stress disorder: a study and replication. *Biol. Psychiatry*, 40(5):368–372.
- Cornelis, M. C., Nugent, N. R., Amstadter, A. B., and Koenen, K. C. (2010). Genetics of post-traumatic stress disorder: review and recommendations for genome-wide association studies. *Current Psychiatry Reports*, 12(4):313–326.
- Corradi, A., Zanardi, A., Giacomini, C., Onofri, F., Valtorta, F., Zoli, M., and Benfenati, F. (2008). Synapsin-I- and synapsin-II-null mice display an increased age-dependent cognitive impairment. *J. Cell Sci.*, 121(Pt 18):3042–3051.
- Costa-Pinto, F. A. and Palermo-Neto, J. (2010). Neuroimmune interactions in stress. *Neuroimmunomodulation*, 17(3):196–199.
- Crooks, G. E., Hon, G., Chandonia, J.-M., and Brenner, S. E. (2004). Weblogo: a sequence logo generator. *Genome Res*, 14(6):1188–1190.
- Cui, H., Sakamoto, H., Higashi, S., and Kawata, M. (2008). Effects of single-prolonged stress on neurons and their afferent inputs in the amygdala. *Neuroscience*, 152(3):703–712.
- Cunha, G. M. A., Canas, P. M., Oliveira, C. R., and Cunha, R. A. (2006). Increased density and synapto-protective effect of adenosine A2A receptors upon sub-chronic restraint stress. *Neuroscience*, 141(4):1775–1781.
- Czeh, B. and Lucassen, P. J. (2007). What causes the hippocampal volume decrease in depression? Are neurogenesis, glial changes and apoptosis implicated? *Eur Arch Psychiatry Clin Neurosci*, 257(5):250–260.
- Czeh, B., Michaelis, T., Watanabe, T., Frahm, J., de Biurrun, G., van Kampen, M., Bartolomucci, A., and Fuchs, E. (2001). Stress-induced changes in cerebral metabolites, hippocampal volume, and cell proliferation are prevented by antidepressant treatment with tianeptine. *Proc. Natl. Acad. Sci. U.S.A.*, 98(22):12796–12801.
- Czeh, B., Simon, M., Schmelting, B., Hiemke, C., and Fuchs, E. (2006). Astroglial plasticity in the hippocampus is affected by chronic psychosocial stress and concomitant fluoxetine treatment. *Neuropsychopharmacology*, 31(8):1616–1626.

REFERENCES

- Dagyte, G., Luiten, P. G., De Jager, T., Gabriel, C., Mocaër, E., Den Boer, J. A., and Van der Zee, E. A. (2011). Chronic stress and antidepressant agomelatine induce region-specific changes in synapsin I expression in the rat brain. *J. Neurosci. Res.*, 89(10):1646–1657.
- Danbolt, N. C. (2001). Glutamate uptake. *Prog. Neurobiol.*, 65(1):1–105.
- De Kloet, C. S., Vermetten, E., Geuze, E., Kavelaars, A., Heijnen, C. J., and Westenberg, H. G. M. (2006). Assessment of HPA-axis function in posttraumatic stress disorder: pharmacological and non-pharmacological challenge tests, a review. *J Psychiatr Res*, 40(6):550–567.
- De Kloet, E. R., Joëls, M., and Holsboer, F. (2005). Stress and the brain: from adaptation to disease. *Nat. Rev. Neurosci.*, 6(6):463–475.
- DeCarolis, N. A. and Eisch, A. J. (2010). Hippocampal neurogenesis as a target for the treatment of mental illness: a critical evaluation. *Neuropharmacology*, 58(6):884–893.
- Dell’osso, L., Carmassi, C., Del Debbio, A., Dell’osso, M. C., Bianchi, C., da Pozzo, E., Origlia, N., Domenici, L., Massimetti, G., Marazziti, D., and Piccinni, A. (2009). Brain-derived neurotrophic factor plasma levels in patients suffering from post-traumatic stress disorder. *Prog. Neuropsychopharmacol. Biol. Psychiatry*, 33(5):899–902.
- Dereeper, A., Guignon, V., Blanc, G., Audic, S., Buffet, S., Chevenet, F., Dufayard, J., Guindon, S., Lefort, V., Lescot, M., Claverie, J., and Gascuel, O. (2008). Phylogeny.fr: robust phylogenetic analysis for the non-specialist. *Nucleic Acids Res.*, 36(Web Server issue):W465–469.
- Dickie, E. W., Brunet, A., Akerib, V., and Armony, J. L. (2011). Neural correlates of recovery from post-traumatic stress disorder: a longitudinal fMRI investigation of memory encoding. *Neuropsychologia*, 49(7):1771–1778.
- Dikanović, M., Demarin, V., Kadoji, D., Kadojić, M., Trkanjec, Z., Titlić, M., Bitunjac, M., and Soldo-Butković, S. (2011). Effect of elevated catecholamine levels on cerebral hemodynamics in patients with chronic post-traumatic stress disorder. *Coll Antropol*, 35(2):471–475.
- Ding, J., Han, F., and Shi, Y. (2010). Single-prolonged stress induces apoptosis in the amygdala in a rat model of post-traumatic stress disorder. *Journal of Psychiatric Research*, 44(1):48–55.
- Diz-Chaves, Y., Pernia, O., Carrero, P., and Garcia-Segura, L. M. (2012). Prenatal stress causes alterations in the morphology of microglia and the inflammatory response of the hippocampus of adult female mice. *J Neuroinflammation*, 9(1):71.
- Dong, X.-X., Wang, Y., and Qin, Z.-H. (2009). Molecular mechanisms of excitotoxicity and their relevance to pathogenesis of neurodegenerative diseases. *Acta Pharmacol. Sin.*, 30(4):379–387.
- Dragan, W. L. and Oniszczenko, W. (2009). The association between dopamine D4 receptor exon III polymorphism and intensity of PTSD symptoms among flood survivors. *Anxiety Stress Coping*, 22(5):483–495.

- Drury, S. S., Theall, K. P., Keats, B. J. B., and Scheeringa, M. (2009). The role of the dopamine transporter (DAT) in the development of PTSD in preschool children. *J Trauma Stress*, 22(6):534–539.
- Dugas, J. C. and Notterpek, L. (2011). MicroRNAs in oligodendrocyte and Schwann cell differentiation. *Dev. Neurosci.*, 33(1):14–20.
- Eastwood, S. L., Burnet, P. W., and Harrison, P. J. (1995). Altered synaptophysin expression as a marker of synaptic pathology in schizophrenia. *Neuroscience*, 66(2):309–319.
- Eastwood, S. L., Cairns, N. J., and Harrison, P. J. (2000). Synaptophysin gene expression in schizophrenia. investigation of synaptic pathology in the cerebral cortex. *Br J Psychiatry*, 176:236–242.
- Ehli, E. A., Hu, Y., Lengyel-Nelson, T., Hudziak, J. J., and Davies, G. E. (2012). Identification and functional characterization of three novel alleles for the serotonin transporter-linked polymorphic region. *Mol Psychiatry*, 17(2):185–192.
- Eiland, L. and McEwen, B. S. (2012). Early life stress followed by subsequent adult chronic stress potentiates anxiety and blunts hippocampal structural remodeling. *Hippocampus*, 22(1):82–91.
- Elenkov, I. J., Wilder, R. L., Chrousos, G. P., and Vizi, E. S. (2000). The sympathetic nerve—an integrative interface between two supersystems: the brain and the immune system. *Pharmacological Reviews*, 52(4):595–638.
- Elizalde, N., Pastor, P. M., Garcia-García, A. L., Serres, F., Venzala, E., Huarte, J., Ramírez, M. J., Del Rio, J., Sharp, T., and Tordera, R. M. (2010). Regulation of markers of synaptic function in mouse models of depression: chronic mild stress and decreased expression of VGLUT1. *J. Neurochem.*, 114(5):1302–1314.
- Elzinga, B. M. and Bremner, J. D. (2002). Are the neural substrates of memory the final common pathway in posttraumatic stress disorder (PTSD)? *J Affect Disord*, 70(1):1–17.
- Erhardt, A., Czibere, L., Roeske, D., Lucae, S., Unschuld, P. G., Ripke, S., Specht, M., Kohli, M. A., Kloiber, S., Ising, M., Heck, A., Pfister, H., Zimmermann, P., Lieb, R., Pütz, B., Uhr, M., Weber, P., Deussing, J. M., Gonik, M., Bunck, M., Kessler, M. S., Frank, E., Hohoff, C., Domschke, K., Krakowitzky, P., Maier, W., Bandelow, B., Jacob, C., Deckert, J., Schreiber, S., Strohmaier, J., Nöthen, M., Cichon, S., Rietschel, M., Bettecken, T., Keck, M. E., Landgraf, R., Müller-Myhsok, B., Holsboer, F., and Binder, E. B. (2011). TMEM132D, a new candidate for anxiety phenotypes: evidence from human and mouse studies. *Mol. Psychiatry*, 16(6):647–663.
- Erickson, K. I., Voss, M. W., Prakash, R. S., Basak, C., Szabo, A., Chaddock, L., Kim, J. S., Heo, S., Alves, H., White, S. M., Wojcicki, T. R., Mailey, E., Vieira, V. J., Martin, S. A., Pence, B. D., Woods, J. A., McAuley, E., and Kramer, A. F. (2011). Exercise training increases size of hippocampus and improves memory. *Proc. Natl. Acad. Sci. U. S. A.*, 108(7):3017–3022.
- Espinosa-Oliva, A. M., de Pablos, R. M., Villaran, R. F., Argüelles, S., Venero, J. L., Machado, A., and Cano, J. (2011). Stress is critical for lps-induced activation of microglia and damage in the rat hippocampus. *Neurobiol Aging*, 32(1):85–102.

REFERENCES

- Esposito, P., Chandler, N., Kandere, K., Basu, S., Jacobson, S., Connolly, R., Tutor, D., and Theoharides, T. C. (2002). Corticotropin-releasing hormone and brain mast cells regulate blood-brain-barrier permeability induced by acute stress. *J Pharmacol Exp Ther*, 303(3):1061–1066.
- Esposito, P., Gheorghe, D., Kandere, K., Pang, X., Connolly, R., Jacobson, S., and Theoharides, T. C. (2001). Acute stress increases permeability of the blood-brain-barrier through activation of brain mast cells. *Brain Res*, 888(1):117–127.
- Fasani, F., Bocquet, A., Robert, P., Peterson, A., and Eyer, J. (2004). The amount of neurofilaments aggregated in the cell body is controlled by their increased sensitivity to trypsin-like proteases. *J. Cell Sci.*, 117(Pt 6):861–869.
- Fdez, E. and Hilfiker, S. (2006). Vesicle pools and synapsins: new insights into old enigmas. *Brain Cell Biology*, 35(2-3):107–115.
- Felmingham, K., Williams, L. M., Whitford, T. J., Falconer, E., Kemp, A. H., Peduto, A., and Bryant, R. A. (2009). Duration of posttraumatic stress disorder predicts hippocampal grey matter loss. *Neuroreport*, 20(16):1402–1406.
- Ferreira, A., Kosik, K. S., Greengard, P., and Han, H. Q. (1994). Aberrant neurites and synaptic vesicle protein deficiency in synapsin II-depleted neurons. *Science*, 264(5161):977–979.
- Foa, E. B., Stein, D. J., and McFarlane, A. C. (2006). Symptomatology and psychopathology of mental health problems after disaster. *J Clin Psychiatry*, 67 Suppl 2:15–25.
- Forder, J. P. and Tymianski, M. (2009). Postsynaptic mechanisms of excitotoxicity: Involvement of postsynaptic density proteins, radicals, and oxidant molecules. *Neuroscience*, 158(1):293–300.
- Fourgeaud, L. and Boulanger, L. M. (2010). Role of immune molecules in the establishment and plasticity of glutamatergic synapses. *Eur. J. Neurosci.*, 32(2):207–217.
- Frank, M. G., Thompson, B. M., Watkins, L. R., and Maier, S. F. (2012). Glucocorticoids mediate stress-induced priming of microglial pro-inflammatory responses. *Brain Behav Immun*, 26(2):337–345.
- Funder, J. W. (2010). Minireview: Aldosterone and mineralocorticoid receptors: past, present, and future. *Endocrinology*, 151(11):5098–5102.
- Gamo, N. J. and Arnsten, A. F. T. (2011). Molecular modulation of prefrontal cortex: rational development of treatments for psychiatric disorders. *Behav. Neurosci.*, 125(3):282–296.
- Gao, Y., Bezchlibnyk, Y. B., Sun, X., Wang, J., McEwen, B. S., and Young, L. T. (2006). Effects of restraint stress on the expression of proteins involved in synaptic vesicle exocytosis in the hippocampus. *Neuroscience*, 141(3):1139–1148.
- García-Bueno, B., Caso, J. R., and Leza, J. C. (2008). Stress as a neuroinflammatory condition in brain: damaging and protective mechanisms. *Neurosci Biobehav Rev*, 32(6):1136–1151.

- García-Bueno, B., Caso, J. R., Pérez-Nievas, B. G., Lorenzo, P., and Leza, J. C. (2007). Effects of peroxisome proliferator-activated receptor gamma agonists on brain glucose and glutamate transporters after stress in rats. *Neuropsychopharmacology*, 32(6):1251–1260.
- García-Caceres, C., Lagunas, N., Calmarza-Font, I., Azcoitia, I., Diz-Chaves, Y., García-Segura, L. M., Baquedano, E., Frago, L. M., Argente, J., and Chowen, J. A. (2010). Gender differences in the long-term effects of chronic prenatal stress on the HPA axis and hypothalamic structure in rats. *Psychoneuroendocrinology*, 35(10):1525–1535.
- Gilbertson, M. W., Shenton, M. E., Ciszewski, A., Kasai, K., Lasko, N. B., Orr, S. P., and Pitman, R. K. (2002). Smaller hippocampal volume predicts pathologic vulnerability to psychological trauma. *Nat Neurosci*, 5(11):1242–1247.
- Gill, J. M., Saligan, L., Woods, S., and Page, G. (2009). PTSD is associated with an excess of inflammatory immune activities. *Perspect Psychiatr Care*, 45(4):262–277.
- Glover, D. A., Powers, M. B., Bergman, L., Smits, J. A. J., Telch, M. J., and Stuber, M. (2003). Urinary dopamine and turn bias in traumatized women with and without PTSD symptoms. *Behav. Brain Res.*, 144(1-2):137–141.
- Golub, Y., Kaltwasser, S. F., Mauch, C. P., Herrmann, L., Schmidt, U., Holsboer, F., Czisch, M., and Wotjak, C. T. (2011). Reduced hippocampus volume in the mouse model of posttraumatic stress disorder. *J Psychiatr Res*, 45(5):650–659.
- Gordon, S. L., Leube, R. E., and Cousin, M. A. (2011). Synaptophysin is required for synaptobrevin retrieval during synaptic vesicle endocytosis. *J Neurosci*, 31(39):14032–14036.
- Gotovac, K., Sabioncello, A., Rabatic, S., Berki, T., and Dekaris, D. (2003). Flow cytometric determination of glucocorticoid receptor (GCR) expression in lymphocyte subpopulations: lower quantity of GCR in patients with post-traumatic stress disorder (PTSD). *Clin. Exp. Immunol.*, 131(2):335–339.
- Gotovac, K., Vidović, A., Vukusić, H., Krcmar, T., Sabioncello, A., Rabatić, S., and Dekaris, D. (2010). Natural killer cell cytotoxicity and lymphocyte perforin expression in veterans with posttraumatic stress disorder. *Prog. Neuropsychopharmacol. Biol. Psychiatry*, 34(4):597–604.
- Gray, J. R., Braver, T. S., and Raichle, M. E. (2002). Integration of emotion and cognition in the lateral prefrontal cortex. *Proc Natl Acad Sci U S A*, 99(6):4115–4120.
- Grinevich, V., Fournier, A., and Pelletier, G. (1997). Effects of pituitary adenylate cyclase-activating polypeptide (PACAP) on corticotropin-releasing hormone (CRH) gene expression in the rat hypothalamic paraventricular nucleus. *Brain Res*, 773(1-2):190–196.
- Guest, K. A., Dyck, B. A., Shethwala, S., and Mishra, R. K. (2010). Atypical antipsychotic drugs upregulate synapsin II in the prefrontal cortex of post-mortem samples obtained from patients with schizophrenia. *Schizophr. Res.*, 120(1-3):229–231.
- Guo, L., Eviatar-Ribak, T., and Miskimins, R. (2010). Sp1 phosphorylation is involved in myelin basic protein gene transcription. *J. Neurosci. Res.*, 88(15):3233–3242.

REFERENCES

- Gurvits, T. V., Shenton, M. E., Hokama, H., Ohta, H., Lasko, N. B., Gilbertson, M. W., Orr, S. P., Kikinis, R., Jolesz, F. A., McCarley, R. W., and Pitman, R. K. (1996). Magnetic resonance imaging study of hippocampal volume in chronic, combat-related posttraumatic stress disorder. *Biol. Psychiatry*, 40(11):1091–1099.
- Guzowski, J. F. (2002). Insights into immediate-early gene function in hippocampal memory consolidation using antisense oligonucleotide and fluorescent imaging approaches. *Hippocampus*, 12(1):86–104.
- Haas, D. A. and George, S. R. (1989). Neuropeptide γ -induced effects on hypothalamic corticotropin-releasing factor content and release are dependent on noradrenergic/adrenergic neurotransmission. *Brain Res*, 498(2):333–338.
- Haddy, R. I. and Clover, R. D. (2001). The biological processes in psychological stress. *Fam Syst Health*, 19:291–302.
- Hampel, H., Frank, R., Broich, K., Teipel, S. J., Katz, R. G., Hardy, J., Herholz, K., Bokde, A. L. W., Jessen, F., Hoessler, Y. C., Sanhai, W. R., Zetterberg, H., Woodcock, J., and Blennow, K. (2010). Biomarkers for alzheimer’s disease: academic, industry and regulatory perspectives. *Nat Rev Drug Discov*, 9(7):560–574.
- Hayes, J. P., LaBar, K. S., McCarthy, G., Selgrade, E., Nasser, J., Dolcos, F., and Morey, R. A. (2011). Reduced hippocampal and amygdala activity predicts memory distortions for trauma reminders in combat-related PTSD. *J Psychiatr Res*, 45(5):660–669.
- Hazama, G.-I., Yasuhara, O., Morita, H., Aimi, Y., Tooyama, I., and Kimura, H. (2005). Mouse brain IgG-like immunoreactivity: strain-specific occurrence in microglia and biochemical identification of IgG. *J. Comp. Neurol.*, 492(2):234–249.
- Heim, C. and Nemeroff, C. B. (2009). Neurobiology of posttraumatic stress disorder. *CNS Spectr*, 14(1 Suppl 1):13–24.
- Heresco-Levy, U., Vass, A., Bloch, B., Wolosker, H., Dumin, E., Balan, L., Deutsch, L., and Kremer, I. (2009). Pilot controlled trial of d-serine for the treatment of post-traumatic stress disorder. *Int J Neuropsychopharmacol*, 12(9):1275–1282.
- Herman, J. P., Figueiredo, H., Mueller, N. K., Ulrich-Lai, Y., Ostrander, M. M., Choi, D. C., and Cullinan, W. E. (2003). Central mechanisms of stress integration: hierarchical circuitry controlling hypothalamo-pituitary-adrenocortical responsiveness. *Front Neuroendocrinol*, 24(3):151–180.
- Herman, J. P., Ostrander, M. M., Mueller, N. K., and Figueiredo, H. (2005). Limbic system mechanisms of stress regulation: hypothalamo-pituitary-adrenocortical axis. *Prog Neuropsychopharmacol Biol Psychiatry*, 29(8):1201–1213.
- Herrmann, L., Ionescu, I. A., Henes, K., Golub, Y., Wang, N. X. R., Buell, D. R., Holsboer, F., Wotjak, C. T., and Schmidt, U. (2012). Long-lasting hippocampal synaptic protein loss in a mouse model of posttraumatic stress disorder. *PLoS One*, 7(8):e42603.
- Hertzberg, M. A., Butterfield, M. I., Feldman, M. E., Beckham, J. C., Sutherland, S. M., Connor, K. M., and Davidson, J. R. (1999). A preliminary study of lamotrigine for the treatment of posttraumatic stress disorder. *Biol Psychiatry*, 45(9):1226–1229.

- Huang, J., Sun, X., Mao, Y., Zhu, X., Zhang, P., Zhang, L., Du, J., and Qiu, X. (2008). Expression of immunoglobulin gene with classical V-(D)-J rearrangement in mouse brain neurons. *Int. J. Biochem. Cell Biol.*, 40(8):1604–1615.
- Hughes, K. C. and Shin, L. M. (2011). Functional neuroimaging studies of post-traumatic stress disorder. *Expert Rev Neurother*, 11(2):275–285.
- Hulse, R. E., Swenson, W. G., Kunkler, P. E., White, D. M., and Kraig, R. P. (2008). Monomeric IgG is neuroprotective via enhancing microglial recycling endocytosis and TNF- α . *J Neurosci*, 28(47):12199–12211.
- Iwasaki, Y., Hosoya, T., Takebayashi, H., Ogawa, Y., Hotta, Y., and Ikenaka, K. (2003). The potential to induce glial differentiation is conserved between drosophila and mammalian glial cells missing genes. *Development*, 130(24):6027.
- Iwata, M., Shirayama, Y., Ishida, H., and Kawahara, R. (2006). Hippocampal synapsin I, growth-associated protein-43, and microtubule-associated protein-2 immunoreactivity in learned helplessness rats and antidepressant-treated rats. *Neuroscience*, 141(3):1301–1313.
- Jin, V. X., Singer, G. A. C., Agosto-Pérez, F. J., Liyanarachchi, S., and Davuluri, R. V. (2006). Genome-wide analysis of core promoter elements from conserved human and mouse orthologous pairs. *BMC Bioinformatics*, 7:114.
- Kammermeier, P. J. (2006). Surface clustering of metabotropic glutamate receptor 1 induced by long homer proteins. *BMC Neuroscience*, 7:1.
- Kamprath, K. and Wotjak, C. T. (2004). Nonassociative learning processes determine expression and extinction of conditioned fear in mice. *Learn. Mem.*, 11(6):770–786.
- Karl, A., Schaefer, M., Malta, L. S., Dörfel, D., Rohleder, N., and Werner, A. (2006). A meta-analysis of structural brain abnormalities in PTSD. *Neurosci Biobehav Rev*, 30(7):1004–1031.
- Kessler, M. S., Murgatroyd, C., Bunck, M., Czibere, L., Frank, E., Jacob, W., Horvath, C., Muigg, P., Holsboer, F., Singewald, N., Spengler, D., and Landgraf, R. (2007). Diabetes insipidus and, partially, low anxiety-related behaviour are linked to a SNP-associated vasopressin deficit in LAB mice. *Eur. J. Neurosci.*, 26(10):2857–2864.
- Kessler, R. C., Sonnega, A., Bromet, E., Hughes, M., and Nelson, C. B. (1995). Posttraumatic stress disorder in the national comorbidity survey. *Arch Gen Psychiatry*, 52(12):1048–1060.
- Khurana, R. C. and Devaud, L. L. (2007). Sex differences in neurotransmission parameters in response to repeated mild restraint stress exposures in intact male, female and ovariectomised female rats. *J. Neuroendocrinol.*, 19(7):511–520.
- Kilpatrick, D. G., Koenen, K. C., Ruggiero, K. J., Acierno, R., Galea, S., Resnick, H. S., Roitzsch, J., Boyle, J., and Gelernter, J. (2007). The serotonin transporter genotype and social support and moderation of posttraumatic stress disorder and depression in hurricane-exposed adults. *Am. J. Psychiatry*, 164(11):1693–1699.

REFERENCES

- Kim, J. G. and Hudson, L. D. (1992). Novel member of the zinc finger superfamily: A C2-HC finger that recognizes a glia-specific gene. *Mol. Cell. Biol.*, 12(12):5632–5639.
- Klempner, T. A., Sequeira, A., Canetti, L., Lalovic, A., Ernst, C., Ffrench-Mullen, J., and Turecki, G. (2009). Altered expression of genes involved in ATP biosynthesis and GABAergic neurotransmission in the ventral prefrontal cortex of suicides with and without major depression. *Mol. Psychiatry*, 14(2):175–189.
- Knoops, A. J. G., Gerritsen, L., van der Graaf, Y., Mali, W. P. T. M., and Geerlings, M. I. (2010). Basal hypothalamic pituitary adrenal axis activity and hippocampal volumes: the smart-medea study. *Biol Psychiatry*, 67(12):1191–1198.
- Knox, D., Perrine, S. A., George, S. A., Galloway, M. P., and Liberzon, I. (2010). Single prolonged stress decreases glutamate, glutamine, and creatine concentrations in the rat medial prefrontal cortex. *Neurosci Lett*, 480(1):16–20.
- Kodama, Y., Kikusui, T., Takeuchi, Y., and Mori, Y. (2008). Effects of early weaning on anxiety and prefrontal cortical and hippocampal myelination in male and female wistar rats. *Dev Psychobiol*, 50(4):332–342.
- Koenen, K. C., Aiello, A. E., Bakshis, E., Amstadter, A. B., Ruggiero, K. J., Acerno, R., Kilpatrick, D. G., Gelernter, J., and Galea, S. (2009). Modification of the association between serotonin transporter genotype and risk of posttraumatic stress disorder in adults by county-level social environment. *Am. J. Epidemiol.*, 169(6):704–711.
- Kohda, K., Harada, K., Kato, K., Hoshino, A., Motohashi, J., Yamaji, T., Morinobu, S., Matsuoka, N., and Kato, N. (2007). Glucocorticoid receptor activation is involved in producing abnormal phenotypes of single-prolonged stress rats: a putative post-traumatic stress disorder model. *Neuroscience*, 148(1):22–33.
- Kolassa, I., Ertl, V., Eckart, C., Glöckner, F., Kolassa, S., Papassotiropoulos, A., de Quervain, D. J., and Elbert, T. (2010a). Association study of trauma load and SLC6A4 promoter polymorphism in posttraumatic stress disorder: evidence from survivors of the rwandan genocide. *J Clin Psychiatry*, 71(5):543–547.
- Kolassa, I., Kolassa, S., Ertl, V., Papassotiropoulos, A., and De Quervain, D. J. (2010b). The risk of posttraumatic stress disorder after trauma depends on traumatic load and the catechol-o-methyltransferase Val(158)Met polymorphism. *Biol. Psychiatry*, 67(4):304–308.
- Kovacic, Z., Henigsberg, N., Pivac, N., Nedic, G., and Borovecki, A. (2008). Platelet serotonin concentration and suicidal behavior in combat related posttraumatic stress disorder. *Prog. Neuropsychopharmacol. Biol. Psychiatry*, 32(2):544–551.
- Kozlovsky, N., Matar, M. A., Kaplan, Z., Kotler, M., Zohar, J., and Cohen, H. (2007). Long-term down-regulation of BDNF mRNA in rat hippocampal CA1 subregion correlates with PTSD-like behavioural stress response. *Int. J. Neuropsychopharmacol.*, 10(6):741–758.
- Kozlovsky, N., Matar, M. A., Kaplan, Z., Kotler, M., Zohar, J., and Cohen, H. (2008). The immediate early gene arc is associated with behavioral resilience to stress exposure

- in an animal model of posttraumatic stress disorder. *Eur Neuropsychopharmacol*, 18(2):107–116.
- Kozlovsky, N., Matar, M. A., Kaplan, Z., Zohar, J., and Cohen, H. (2009). A distinct pattern of intracellular glucocorticoid-related responses is associated with extreme behavioral response to stress in an animal model of post-traumatic stress disorder. *Eur Neuropsychopharmacol*, 19(11):759–771.
- Krömer, S. A., Kessler, M. S., Milfay, D., Birg, I. N., Bunck, M., Czibere, L., Panhuysen, M., Pütz, B., Deussing, J. M., Holsboer, F., Landgraf, R., and Turck, C. W. (2005). Identification of glyoxalase-I as a protein marker in a mouse model of extremes in trait anxiety. *J Neurosci*, 25(17):4375–4384.
- Kuang, F., Wang, B., Zhang, P., Fei, L., Jia, Y., Duan, X., Wang, X., Xu, Z., Li, G., Jiao, X., and Ju, G. (2004). Extravasation of blood-borne immunoglobulin G through blood-brain barrier during adrenaline-induced transient hypertension in the rat. *Int. J. Neurosci.*, 114(6):575–591.
- Kugler, J., Reintjes, F., Tewes, V., and Schedlowski, M. (1996). Competition stress in soccer coaches increases salivary immunoglobulin a and salivary cortisol concentrations. *J Sports Med Phys Fitness*, 36(2):117–120.
- Landgraf, R., Kessler, M. S., Bunck, M., Murgatroyd, C., Spengler, D., Zimbelmann, M., Nussbaumer, M., Czibere, L., Turck, C. W., Singewald, N., Rujescu, D., and Frank, E. (2007). Candidate genes of anxiety-related behavior in HAB/LAB rats and mice: focus on vasopressin and glyoxalase-I. *Neurosci Biobehav Rev*, 31(1):89–102.
- Laursen, L. S. and Ffrench-Constant, C. (2007). Adhesion molecules in the regulation of CNS myelination. *Neuron Glia Biol.*, 3(4):367–375.
- Lee, H., Kwak, S., and Paik, J. (2007). Association between serotonin 2A receptor gene polymorphism and posttraumatic stress disorder. *Psychiatry Investig*, 4(2):104–8.
- Lee, H., Lee, M., Kang, R., Kim, H., Kim, S., Kee, B., Kim, Y. H., Kim, Y., Kim, J. B., Yeon, B. K., Oh, K. S., Oh, B., Yoon, J., Lee, C., Jung, H. Y., Chee, I., and Paik, I. H. (2005). Influence of the serotonin transporter promoter gene polymorphism on susceptibility to posttraumatic stress disorder. *Depress Anxiety*, 21(3):135–139.
- Lewitus, G. M., Cohen, H., and Schwartz, M. (2008). Reducing post-traumatic anxiety by immunization. *Brain Behav. Immun.*, 22(7):1108–1114.
- Li, Y., Lau, W., So, K., Tong, Y., and Shen, J. (2011). Caveolin-1 promote astroglial differentiation of neural stem/progenitor cells through modulating Notch1/NICD and Hes1 expressions. *Biochem. Biophys. Res. Commun.*, 407(3):517–524.
- Lightman, S. L. (2008). The neuroendocrinology of stress: a never ending story. *J Neuroendocrinol*, 20(6):880–884.
- Lim, C. Y., Santoso, B., Boulay, T., Dong, E., Ohler, U., and Kadonaga, J. T. (2004). The MTE, a new core promoter element for transcription by RNA polymerase II. *Genes Dev.*, 18(13):1606–1617.

REFERENCES

- Lindermayr, C., Palmeri, C. M., and Durner, J. (2008). In silico search for nitric oxide sensitive promoter elements in arabidopsis thaliana. *Plant Signal Behav*, 3(10):827–828.
- Liu, H., Wang, H.-T., Han, F., and Shi, Y.-X. (2011). Activity of 5-HT1A receptor is involved in neuronal apoptosis of the amygdala in a rat model of post-traumatic stress disorder. *Mol Med Report*, 4(2):291–295.
- Liu, J. and Casaccia, P. (2010). Epigenetic regulation of oligodendrocyte identity. *Trends Neurosci.*, 33(4):193–201.
- Llorente, R., Miguel-Blanco, C., Aisa, B., Lachize, S., Borcel, E., Meijer, O. C., Ramirez, M. J., De Kloet, E. R., and Viveros, M. P. (2011). Long term sex-dependent psychoneuroendocrine effects of maternal deprivation and juvenile unpredictable stress in rats. *J. Neuroendocrinol.*, 23(4):329–344.
- Loots, G. and Ovcharenko, I. (2007). ECRbase: database of evolutionary conserved regions, promoters, and transcription factor binding sites in vertebrate genomes. *Bioinformatics*, 23(1):122–124.
- Lu, A. T., Ogdie, M. N., Järvelin, M., Moilanen, I. K., Loo, S. K., McCracken, J. T., McGough, J. J., Yang, M. H., Peltonen, L., Nelson, S. F., Cantor, R. M., and Smalley, S. L. (2008). Association of the cannabinoid receptor gene (CNR1) with ADHD and post-traumatic stress disorder. *Am. J. Med. Genet. B Neuropsychiatr. Genet.*, 147B(8):1488–1494.
- Lucassen, P. J., Müller, M. B., Holsboer, F., Bauer, J., Holtrop, A., Wouda, J., Hoogendijk, W. J., De Kloet, E. R., and Swaab, D. F. (2001). Hippocampal apoptosis in major depression is a minor event and absent from subareas at risk for glucocorticoid overexposure. *Am. J. Pathol.*, 158(2):453–468.
- Lui, C. C., Wang, J., Tain, Y., Chen, Y., Chang, K., Lai, M., and Huang, L. (2011). Prenatal stress in rat causes long-term spatial memory deficit and hippocampus MRI abnormality: Differential effects of postweaning enriched environment. *Neurochem. Int.*, 58(3):434–441.
- Lunnon, K., Teeling, J. L., Tutt, A. L., Cragg, M. S., Glennie, M. J., and Perry, V. H. (2011). Systemic inflammation modulates fc receptor expression on microglia during chronic neurodegeneration. *J Immunol*, 186(12):7215–7224.
- Lupas, A., Van Dyke, M., and Stock, J. (1991). Predicting coiled coils from protein sequences. *Science*, 252(5009):1162–1164.
- Madrigal, J. L. M., Caso, J. R., de Cristobal, J., Cardenas, A., Leza, J. C., Lizasoain, I., Lorenzo, P., and Moro, M. A. (2003). Effect of subacute and chronic immobilisation stress on the outcome of permanent focal cerebral ischaemia in rats. *Brain Res.*, 979(1-2):137–145.
- Maes, M., Lin, A. H., Delmeire, L., Van Gastel, A., Kenis, G., De Jongh, R., and Bosmans, E. (1999). Elevated serum interleukin-6 (IL-6) and IL-6 receptor concentrations in posttraumatic stress disorder following accidental man-made traumatic events. *Biol. Psychiatry*, 45(7):833–839.
- Martins-de-Souza, D. (2010). Proteome and transcriptome analysis suggests oligodendrocyte dysfunction in schizophrenia. *J Psychiatr Res*, 44(3):149–156.

- Martisova, E., Solas, M., Horrillo, I., Ortega, J. E., Meana, J. J., Tordera, R. M., and Ramírez, M. J. (2012). Long lasting effects of early-life stress on glutamatergic/GABAergic circuitry in the rat hippocampus. *Neuropharmacology*, 62(5-6):1944–1953.
- McEwen, B. S. (1997). Possible mechanisms for atrophy of the human hippocampus. *Mol. Psychiatry*, 2(3):255–262.
- McEwen, B. S. (2007). Physiology and neurobiology of stress and adaptation: central role of the brain. *Physiol. Rev.*, 87(3):873–904.
- McEwen, B. S. (2010). Stress, sex, and neural adaptation to a changing environment: mechanisms of neuronal remodeling. *Annals of the New York Academy of Sciences*, 1204 Suppl:E38–59.
- McEwen, B. S. and Stellar, E. (1993). Stress and the individual. mechanisms leading to disease. *Arch. Intern. Med.*, 153(18):2093–2101.
- McGowan, P. O., Sasaki, A., D'Alessio, A. C., Dymov, S., Labonté, B., Szyf, M., Turecki, G., and Meaney, M. J. (2009). Epigenetic regulation of the glucocorticoid receptor in human brain associates with childhood abuse. *Nat Neurosci*, 12(3):342–348.
- Mück-Seler, D., Pivac, N., Jakovljević, M., Sagud, M., and Mihaljević-Peles, A. (2003). Platelet 5-HT concentration and comorbid depression in war veterans with and without posttraumatic stress disorder. *J Affect Disord*, 75(2):171–179.
- Mehta, D. and Binder, E. B. (2011). Gene x environment vulnerability factors for PTSD: the HPA-axis. *Neuropharmacology*.
- Melloni, R H, J., Hemmendinger, L. M., Hamos, J. E., and DeGennaro, L. J. (1993). Synapsin I gene expression in the adult rat brain with comparative analysis of mRNA and protein in the hippocampus. *J. Comp. Neurol.*, 327(4):507–520.
- Merino, J. J., Cordero, M. I., and Sandi, C. (2000). Regulation of hippocampal cell adhesion molecules ncam and l1 by contextual fear conditioning is dependent upon time and stressor intensity. *Eur J Neurosci*, 12(9):3283–3290.
- Mick, E., McGough, J., Loo, S., Doyle, A. E., Wozniak, J., Wilens, T. E., Smalley, S., McCracken, J., Biederman, J., and Faraone, S. V. (2011). Genome-wide association study of the child behavior checklist dysregulation profile. *J Am Acad Child Adolesc Psychiatry*, 50(8):807–817.e8.
- Miller, E. K., Freedman, D. J., and Wallis, J. D. (2002). The prefrontal cortex: categories, concepts and cognition. *Philos Trans R Soc Lond B Biol Sci*, 357(1424):1123–1136.
- Mishra, K. P., Yadav, A. P., Shweta, Chanda, S., Majumdar, D., and Ganju, L. (2011). Serum levels of immunoglobulins (IgG, IgA, IgM) in antarctic summer expeditioners and their relationship with seasickness. *Cell. Immunol.*, 271(1):29–35.
- Mitra, R., Jadhav, S., McEwen, B. S., Vyas, A., and Chattarji, S. (2005). Stress duration modulates the spatiotemporal patterns of spine formation in the basolateral amygdala. *Proc. Natl. Acad. Sci. U.S.A.*, 102(26):9371–9376.

REFERENCES

- Müller, H. K., Wegener, G., Popoli, M., and Elfving, B. (2011). Differential expression of synaptic proteins after chronic restraint stress in rat prefrontal cortex and hippocampus. *Brain Research*, 1385:26–37.
- Müller, M. B., Lucassen, P. J., Yassouridis, A., Hoogendijk, W. J., Holsboer, F., and Swaab, D. F. (2001). Neither major depression nor glucocorticoid treatment affects the cellular integrity of the human hippocampus. *Eur. J. Neurosci.*, 14(10):1603–1612.
- Mobley, P. and Greengard, P. (1985). Evidence for widespread effects of noradrenaline on axon terminals in the rat frontal cortex. *Proc. Natl. Acad. Sci. U.S.A.*, 82(3):945–947.
- Montoyo, H. P., Vaccaro, C., Hafner, M., Ober, R. J., Mueller, W., and Ward, E. S. (2009). Conditional deletion of the MHC class I-related receptor FcRn reveals the sites of IgG homeostasis in mice. *Proc Natl Acad Sci U S A*, 106(8):2788–2793.
- Murgatroyd, C., Patchev, A. V., Wu, Y., Micale, V., Bockmühl, Y., Fischer, D., Holsboer, F., Wotjak, C. T., Almeida, O. F. X., and Spengler, D. (2009). Dynamic DNA methylation programs persistent adverse effects of early-life stress. *Nature Neuroscience*, 12(12):1559–1566.
- Musazzi, L., Racagni, G., and Popoli, M. (2011). Stress, glucocorticoids and glutamate release: effects of antidepressant drugs. *Neurochem. Int.*, 59(2):138–149.
- Nagase, T., Kikuno, R., and Ohara, O. (2001). Prediction of the coding sequences of unidentified human genes. XXII. the complete sequences of 50 new cDNA clones which code for large proteins. *DNA Res.*, 8(6):319–327.
- Nair, J. and Singh Ajit, S. (2008). The role of the glutamatergic system in posttraumatic stress disorder. *CNS Spectr*, 13(7):585–591.
- Nelson, E. C., Agrawal, A., Pergadia, M. L., Lynskey, M. T., Todorov, A. A., Wang, J. C., Todd, R. D., Martin, N. G., Heath, A. C., Goate, A. M., Montgomery, G. W., and Madden, P. A. F. (2009). Association of childhood trauma exposure and GABRA2 polymorphisms with risk of posttraumatic stress disorder in adults. *Mol. Psychiatry*, 14(3):234–235.
- Nestler, E. J., Rainbow, T. C., McEwen, B. S., and Greengard, P. (1981). Corticosterone increases the amount of protein 1, a neuron-specific phosphoprotein, in rat hippocampus. *Science*, 212(4499):1162–1164.
- Nomoto, H., Yonezawa, T., Itoh, K., Ono, K., Yamamoto, K., Oohashi, T., Shiraga, F., Ohtsuki, H., and Ninomiya, Y. (2003). Molecular cloning of a novel transmembrane protein MOLT expressed by mature oligodendrocytes. *J. Biochem.*, 134(2):231–238.
- North, C. S., Suris, A. M., Davis, M., and Smith, R. P. (2009). Toward validation of the diagnosis of posttraumatic stress disorder. *Am J Psychiatry*, 166(1):34–41.
- Notredame, C., Higgins, D. G., and Heringa, J. (2000). T-coffee: A novel method for fast and accurate multiple sequence alignment. *J Mol Biol*, 302(1):205–217.

- Nowicka, D., Liguz-Leczmar, M., and Skangiel-Kramska, J. (2003). A surface antigen delineating a subset of neurons in the primary somatosensory cortex of the mouse. *Acta Neurobiol Exp (Wars)*, 63(3):185–195.
- Numakawa, T., Suzuki, S., Kumamaru, E., Adachi, N., Richards, M., and Kunugi, H. (2010). BDNF function and intracellular signaling in neurons. *Histol Histopathol*, 25(2):237–258.
- Oh-hashii, K., Hirata, Y., Koga, H., and Kiuchi, K. (2006). GRP78-binding protein regulates cAMP-induced glial fibrillary acidic protein expression in rat C6 glioblastoma cells. *FEBS Lett*, 580(16):3943–3947.
- Oh-hashii, K., Imai, K., Koga, H., Hirata, Y., and Kiuchi, K. (2010). Knockdown of transmembrane protein 132A by RNA interference facilitates serum starvation-induced cell death in Neuro2a cells. *Mol. Cell. Biochem.*, 342(1-2):117–123.
- Oh-hashii, K., Naruse, Y., Amaya, F., Shimosato, G., and Tanaka, M. (2003). Cloning and characterization of a novel GRP78-binding protein in the rat brain. *J Biol Chem*, 278(12):10531–10537.
- Ohtsuka, T., Ishibashi, M., Gradwohl, G., Nakanishi, S., Guillemot, F., and Kageyama, R. (1999). Hes1 and Hes5 as notch effectors in mammalian neuronal differentiation. *EMBO J.*, 18(8):2196–2207.
- O’Leary, O. F., Wu, X., and Castren, E. (2009). Chronic fluoxetine treatment increases expression of synaptic proteins in the hippocampus of the ovariectomized rat: role of BDNF signalling. *Psychoneuroendocrinology*, 34(3):367–381.
- Ono, M., Kikusui, T., Sasaki, N., Ichikawa, M., Mori, Y., and Murakami-Murofushi, K. (2008). Early weaning induces anxiety and precocious myelination in the anterior part of the basolateral amygdala of male balb/c mice. *Neuroscience*, 156(4):1103–1110.
- Pace, T. W. W. and Heim, C. M. (2011). A short review on the psychoneuroimmunology of posttraumatic stress disorder: from risk factors to medical comorbidities. *Brain Behav. Immun.*, 25(1):6–13.
- Palmieri, M. C., Sell, S., Huang, X., Scherf, M., Werner, T., Durner, J., and Lindermayr, C. (2008). Nitric oxide-responsive genes and promoters in arabidopsis thaliana: a bioinformatics approach. *J Exp Bot*, 59(2):177–186.
- Pamplona, F. A., Henes, K., Micale, V., Mauch, C. P., Takahashi, R. N., and Wotjak, C. T. (2011). Prolonged fear incubation leads to generalized avoidance behavior in mice. *Journal of Psychiatric Research*, 45(3):354–360.
- Papadimitriou, A. and Priftis, K. N. (2009). Regulation of the hypothalamic-pituitary-adrenal axis. *Neuroimmunomodulation*, 16(5):265–271.
- Parfitt, K. D., Hoffer, B. J., and Browning, M. D. (1991). Norepinephrine and isoproterenol increase the phosphorylation of synapsin I and synapsin II in dentate slices of young but not aged fisher 344 rats. *Proc. Natl. Acad. Sci. U. S. A.*, 88(6):2361–2365.

REFERENCES

- Park, D., Jeon, J. H., Shin, S., Jang, J. Y., Choi, B.-I., Nahm, S.-S., Kang, J.-K., Hwang, S.-Y., Kim, J.-C., and Kim, Y.-B. (2008). Debilitating stresses do not increase blood-brain barrier permeability: Lack of the involvement of corticosteroids. *Environ Toxicol Pharmacol*, 26(1):30–37.
- Parker, K. J., Schatzberg, A. F., and Lyons, D. M. (2003). Neuroendocrine aspects of hypercortisolism in major depression. *Horm Behav*, 43(1):60–66.
- Pasquini, L. A., Millet, V., Hoyos, H. C., Giannoni, J. P., Croci, D. O., Marder, M., Liu, F. T., Rabinovich, G. A., and Pasquini, J. M. (2011). Galectin-3 drives oligodendrocyte differentiation to control myelin integrity and function. *Cell Death Differ.*, 18(11):1746–1756.
- Perea, G., Navarrete, M., and Araque, A. (2009). Tripartite synapses: astrocytes process and control synaptic information. *Trends Neurosci.*, 32(8):421–431.
- Perisic, T., Zimmermann, N., Kirmeier, T., Asmus, M., Tuorto, F., Uhr, M., Holsboer, F., Rein, T., and Zschocke, J. (2009). Valproate and amitriptyline exert common and divergent influences on global and gene Promoter-Specific chromatin modifications in rat primary astrocytes. *Neuropsychopharmacology*, 35(3):792–805.
- Perkonig, A., Kessler, R. C., Storz, S., and Wittchen, H. U. (2000). Traumatic events and post-traumatic stress disorder in the community: prevalence, risk factors and comorbidity. *Acta Psychiatr Scand*, 101(1):46–59.
- Perry, V. H. and O'Connor, V. (2010). The role of microglia in synaptic stripping and synaptic degeneration: a revised perspective. *ASN Neuro*, 2(5):e00047.
- Pitman, R. K., Gilbertson, M. W., Gurvits, T. V., May, F. S., Lasko, N. B., Metzger, L. J., Shenton, M. E., Yehuda, R., Orr, S. P., and , H. A. P. T. S. D. T. S. I. (2006). Clarifying the origin of biological abnormalities in ptsd through the study of identical twins discordant for combat exposure. *Ann N Y Acad Sci*, 1071:242–254.
- Podojil, J. R. and Sanders, V. M. (2003). Selective regulation of mature IgG1 transcription by CD86 and β 2-adrenergic receptor stimulation. *J. Immunol.*, 170(10):5143–5151.
- Ponomarev, I., Rau, V., Eger, E. I., Harris, R. A., and Fanselow, M. S. (2010). Amygdala transcriptome and cellular mechanisms underlying stress-enhanced fear learning in a rat model of posttraumatic stress disorder. *Neuropsychopharmacology*, 35(6):1402–1411.
- Popoli, M., Yan, Z., McEwen, B. S., and Sanacora, G. (2012). The stressed synapse: the impact of stress and glucocorticoids on glutamate transmission. *Nat Rev Neurosci*, 13(1):22–37.
- Porton, B. and Wetsel, W. C. (2007). Reduction of synapsin III in the prefrontal cortex of individuals with schizophrenia. *Schizophr. Res.*, 94(1-3):366–370.
- Qi, C., Roseboom, P. H., Nanda, S. A., Lane, J. C., Speers, J. M., and Kalin, N. H. (2010). Anxiety-related behavioral inhibition in rats: a model to examine mechanisms underlying the risk to develop stress-related psychopathology. *Genes Brain Behav.*, 9(8):974–984.

- Quan, Y., Möller, T., and Weinstein, J. R. (2009). Regulation of fcgamma receptors and immunoglobulin g-mediated phagocytosis in mouse microglia. *Neurosci Lett*, 464(1):29–33.
- Quervain, D. J. d., Aerni, A., Schelling, G., and Roozendaal, B. (2009). Glucocorticoids and the regulation of memory in health and disease. *Front Neuroendocrinol*, 30(3):358–370.
- Radley, J. J., Sisti, H. M., Hao, J., Rocher, A. B., McCall, T., Hof, P. R., McEwen, B. S., and Morrison, J. H. (2004). Chronic behavioral stress induces apical dendritic reorganization in pyramidal neurons of the medial prefrontal cortex. *Neuroscience*, 125(1):1–6.
- Rasmusson, A. M., Hauger, R. L., Morgan, C. A., Bremner, J. D., Charney, D. S., and Southwick, S. M. (2000). Low baseline and yohimbine-stimulated plasma neuropeptide y (NPY) levels in combat-related PTSD. *Biol. Psychiatry*, 47(6):526–539.
- Rauch, S. L., Shin, L. M., and Phelps, E. A. (2006). Neurocircuitry models of posttraumatic stress disorder and extinction: human neuroimaging research—past, present, and future. *Biol. Psychiatry*, 60(4):376–382.
- Raudensky, J. and Yamamoto, B. K. (2007). Effects of chronic unpredictable stress and methamphetamine on hippocampal glutamate function. *Brain Res.*, 1135(1):129–135.
- Ravindran, L. N. and Stein, M. B. (2009). Pharmacotherapy of PTSD: premises, principles, and priorities. *Brain Res*, 1293:24–39.
- Reagan, L. P., Rosell, D. R., Wood, G. E., Spedding, M., Munoz, C., Rothstein, J., and McEwen, B. S. (2004). Chronic restraint stress up-regulates GLT-1 mRNA and protein expression in the rat hippocampus: reversal by tianeptine. *Proc. Natl. Acad. Sci. U.S.A.*, 101(7):2179–2184.
- Reinés, A., Cereseto, M., Ferrero, A., Sifonios, L., Podestá, M. F., and Wikinski, S. (2008). Maintenance treatment with fluoxetine is necessary to sustain normal levels of synaptic markers in an experimental model of depression: correlation with behavioral response. *Neuropsychopharmacology*, 33(8):1896–1908.
- Ressler, K. J., Mercer, K. B., Bradley, B., Jovanovic, T., Mahan, A., Kerley, K., Norrholm, S. D., Kilaru, V., Smith, A. K., Myers, A. J., Ramirez, M., Engel, A., Hammack, S. E., Toufexis, D., Braas, K. M., Binder, E. B., and May, V. (2011). Post-traumatic stress disorder is associated with PACAP and the PAC1 receptor. *Nature*, 470(7335):492–497.
- Revest, J., Kaouane, N., Mondin, M., Le Roux, A., Rougé-Pont, F., Vallée, M., Barik, J., Tronche, F., Desmedt, A., and Piazza, P. V. (2010). The enhancement of stress-related memory by glucocorticoids depends on synapsin-Ia/Ib. *Mol. Psychiatry*, 15(12):1125, 1140–1151.
- Riaza Bermudo-Soriano, C., Perez-Rodriguez, M. M., Vaquero-Lorenzo, C., and Baca-Garcia, E. (2012). New perspectives in glutamate and anxiety. *Pharmacol Biochem Behav*, 100(4):752–774.
- Rice, P., Longden, I., and Bleasby, A. (2000). Emboss: the european molecular biology open software suite. *Trends Genet*, 16(6):276–277.

REFERENCES

- Riethoven, J.-J. M. (2010). Regulatory regions in dna: promoters, enhancers, silencers, and insulators. *Methods Mol Biol*, 674:33–42.
- Rogers, M. A., Yamasue, H., Abe, O., Yamada, H., Ohtani, T., Iwanami, A., Aoki, S., Kato, N., and Kasai, K. (2009). Smaller amygdala volume and reduced anterior cingulate gray matter density associated with history of post-traumatic stress disorder. *Psychiatry Res*, 174(3):210–216.
- Roozendaal, B., McEwen, B. S., and Chattarji, S. (2009). Stress, memory and the amygdala. *Nat. Rev. Neurosci.*, 10(6):423–433.
- Rosahl, T. W., Spillane, D., Missler, M., Herz, J., Selig, D. K., Wolff, J. R., Hammer, R. E., Malenka, R. C., and Südhof, T. C. (1995). Essential functions of synapsins I and II in synaptic vesicle regulation. *Nature*, 375(6531):488–493.
- Roth, T. L., Zoladz, P. R., Sweatt, J. D., and Diamond, D. M. (2011). Epigenetic modification of hippocampal bdnf dna in adult rats in an animal model of post-traumatic stress disorder. *J Psychiatr Res*, 45(7):919–926.
- Sakai, T., Hino, K., Wada, S., and Maeda, H. (2003). Identification of the DNA binding specificity of the human ZNF219 protein and its function as a transcriptional repressor. *DNA Res.*, 10(4):155–165.
- Sanacora, G., Treccani, G., and Popoli, M. (2012). Towards a glutamate hypothesis of depression: an emerging frontier of neuropsychopharmacology for mood disorders. *Neuropharmacology*, 62(1):63–77.
- Sananbenesi, F., Fischer, A., Wang, X., Schrick, C., Neve, R., Radulovic, J., and Tsai, L. (2007). A hippocampal Cdk5 pathway regulates extinction of contextual fear. *Nat. Neurosci.*, 10(8):1012–1019.
- Schiraldi, G. R. (1999). *The post-traumatic stress disorder sourcebook: a guide to healing, recovery, and growth*. McGraw Hill, New York.
- Schmidt, U., Holsboer, F., and Rein, T. (2011). Epigenetic aspects of posttraumatic stress disorder. *Disease Markers*, 30(2-3):77–87.
- Schroeder, Jr, H. W. and Cavacini, L. (2010). Structure and function of immunoglobulins. *J Allergy Clin Immunol*, 125(2 Suppl 2):S41–S52.
- Schuff, N., Meyerhoff, D. J., Mueller, S., Chao, L., Sacrey, D. T., Laxer, K., and Weiner, M. W. (2006). N-acetylaspartate as a marker of neuronal injury in neurodegenerative disease. *Adv Exp Med Biol*, 576:241–62; discussion 361–3.
- Söding, J. (2005). Protein homology detection by HMM-HMM comparison. *Bioinformatics*, 21(7):951–960.
- Segman, R. H., Cooper-Kazaz, R., Macciardi, F., Goltser, T., Halfon, Y., Dobroborski, T., and Shalev, A. Y. (2002). Association between the dopamine transporter gene and posttraumatic stress disorder. *Mol. Psychiatry*, 7(8):903–907.

-
- Segman, R. H., Shefi, N., Goltser-Dubner, T., Friedman, N., Kaminski, N., and Shalev, A. Y. (2005). Peripheral blood mononuclear cell gene expression profiles identify emergent post-traumatic stress disorder among trauma survivors. *Mol. Psychiatry*, 10(5):500–513, 425.
- Selye, H. (1936). A syndrome produced by diverse nocuous agents. *Nature*, 138(3479):32.
- Semmler, A., Okulla, T., Sastre, M., Dumitrescu-Ozimek, L., and Heneka, M. T. (2005). Systemic inflammation induces apoptosis with variable vulnerability of different brain regions. *J. Chem. Neuroanat.*, 30(2-3):144–157.
- Shin, L. M. and Liberzon, I. (2010). The neurocircuitry of fear, stress, and anxiety disorders. *Neuropsychopharmacology*, 35(1):169–191.
- Shin, L. M., Rauch, S. L., and Pitman, R. K. (2006). Amygdala, medial prefrontal cortex, and hippocampal function in PTSD. *Ann. N. Y. Acad. Sci.*, 1071:67–79.
- Shirayama, Y., Muneoka, K. T., Iwata, M., Ishida, H., Hazama, G., and Kawahara, R. (2005). Pregnenolone and dehydroepiandrosterone administration in neonatal rats alters the immunoreactivity of hippocampal synapsin I, neuropeptide Y and glial fibrillary acidic protein at post-puberty. *Neuroscience*, 133(1):147–157.
- Shorter, E. (2005). *A historical dictionary of psychiatry*. Oxford University Press, Inc., New York, 1 edition.
- Siegmund, A., Kaltwasser, S. F., Holsboer, F., Czisch, M., and Wotjak, C. T. (2009). Hippocampal n-acetylaspartate levels before trauma predict the development of long-lasting posttraumatic stress disorder-like symptoms in mice. *Biol Psychiatry*, 65(3):258–262.
- Siegmund, A. and Wotjak, C. T. (2006). Toward an animal model of posttraumatic stress disorder. *Ann. N. Y. Acad. Sci.*, 1071:324–334.
- Siegmund, A. and Wotjak, C. T. (2007). A mouse model of posttraumatic stress disorder that distinguishes between conditioned and sensitised fear. *J Psychiatr Res*, 41(10):848–860.
- Silva, A. J., Rosahl, T. W., Chapman, P. F., Marowitz, Z., Friedman, E., Frankland, P. W., Cestari, V., Cioffi, D., Südhof, T. C., and Bourchouladze, R. (1996). Impaired learning in mice with abnormal short-lived plasticity. *Curr. Biol.*, 6(11):1509–1518.
- Skelton, K., Ressler, K. J., Norrholm, S. D., Jovanovic, T., and Bradley-Davino, B. (2012). PTSD and gene variants: New pathways and new thinking. *Neuropharmacology*, 62(2):628–637.
- Skultétyová, I., Tokarev, D., and Jezová, D. (1998). Stress-induced increase in blood-brain barrier permeability in control and monosodium glutamate-treated rats. *Brain Res Bull*, 45(2):175–178.
- Smale, S. T. (1997). Transcription initiation from TATA-less promoters within eukaryotic protein-coding genes. *Biochim Biophys Acta*, 1351(1-2):73–88.

REFERENCES

- Smale, S. T. and Kadonaga, J. T. (2003). The RNA polymerase II core promoter. *Annu Rev Biochem*, 72:449–479.
- Søndergaard, H. P., Hansson, L., and Theorell, T. (2004). The inflammatory markers c-reactive protein and serum amyloid a in refugees with and without posttraumatic stress disorder. *Clin. Chim. Acta*, 342(1-2):93–98.
- Soding, J., Biegert, A., and Lupas, A. N. (2005). The HHpred interactive server for protein homology detection and structure prediction. *Nucleic Acids Research*, 33(Web Server):W244–W248.
- Sommershof, A., Aichinger, H., Engler, H., Adenauer, H., Catani, C., Boneberg, E.-M., Elbert, T., Groettrup, M., and Kolassa, I.-T. (2009). Substantial reduction of naïve and regulatory T cells following traumatic stress. *Brain Behav. Immun.*, 23(8):1117–1124.
- Sondermann, P. and Oosthuizen, V. (2002). X-ray crystallographic studies of IgG-Fc gamma receptor interactions. *Biochem Soc Trans*, 30(4):481–486.
- Song, Y., Zhou, D., Guan, Z., and Wang, X. (2007). Disturbance of serum interleukin-2 and interleukin-8 levels in posttraumatic and non-posttraumatic stress disorder earthquake survivors in northern china. *Neuroimmunomodulation*, 14(5):248–254.
- Sorrells, S. F. and Sapolsky, R. M. (2007). An inflammatory review of glucocorticoid actions in the CNS. *Brain, Behavior, and Immunity*, 21(3):259–272.
- Sousa, N., Lukoyanov, N. V., Madeira, M. D., Almeida, O. F., and Paula-Barbosa, M. M. (2000). Reorganization of the morphology of hippocampal neurites and synapses after stress-induced damage correlates with behavioral improvement. *Neuroscience*, 97(2):253–266.
- Spivak, B., Shohat, B., Mester, R., Avraham, S., Gil-Ad, I., Bleich, A., Valevski, A., and Weizman, A. (1997). Elevated levels of serum interleukin-1 β in combat-related posttraumatic stress disorder. *Biol. Psychiatry*, 42(5):345–348.
- Spivak, B., Vered, Y., Graff, E., Blum, I., Mester, R., and Weizman, A. (1999). Low platelet-poor plasma concentrations of serotonin in patients with combat-related posttraumatic stress disorder. *Biol. Psychiatry*, 45(7):840–845.
- Steckler, T. and Risbrough, V. (2012). Pharmacological treatment of PTSD - established and new approaches. *Neuropharmacology*, 62(2):617–627.
- Sterlemann, V., Rammes, G., Wolf, M., Liebl, C., Ganea, K., Müller, M. B., and Schmidt, M. V. (2010). Chronic social stress during adolescence induces cognitive impairment in aged mice. *Hippocampus*, 20(4):540–549.
- Su, T., Zhang, L., Chung, M., Chen, Y., Bi, Y., Chou, Y., Barker, J. L., Barrett, J. E., Maric, D., Li, X. X., Li, H., Webster, M. J., Benedek, D., Carlton, J. R., and Ursano, R. (2009). Levels of the potential biomarker p11 in peripheral blood cells distinguish patients with PTSD from those with other major psychiatric disorders. *J Psychiatr Res*, 43(13):1078–1085.

- Tai, Y., Wang, Y., Wang, J., Tao, P., Tung, C., and Wong, C. (2006). Amitriptyline suppresses neuroinflammation and up-regulates glutamate transporters in morphine-tolerant rats. *Pain*, 124(1-2):77–86.
- Takahashi, N., Sakurai, T., Davis, K. L., and Buxbaum, J. D. (2011). Linking oligodendrocyte and myelin dysfunction to neurocircuitry abnormalities in schizophrenia. *Prog. Neurobiol.*, 93(1):13–24.
- Takai, T. (2002). Roles of Fc receptors in autoimmunity. *Nat. Rev. Immunol.*, 2(8):580–592.
- Takigawa, Y., Hata, K., Muramatsu, S., Amano, K., Ono, K., Wakabayashi, M., Matsuda, A., Takada, K., Nishimura, R., and Yoneda, T. (2010). The transcription factor Znf219 regulates chondrocyte differentiation by assembling a transcription factory with Sox9. *J. Cell. Sci.*, 123(Pt 21):3780–3788.
- Tata, D. A. and Anderson, B. J. (2010). The effects of chronic glucocorticoid exposure on dendritic length, synapse numbers and glial volume in animal models: implications for hippocampal volume reductions in depression. *Physiology & Behavior*, 99(2):186–193.
- Tessner, K. D., Walker, E. F., Dhruv, S. H., Hochman, K., and Hamann, S. (2007). The relation of cortisol levels with hippocampus volumes under baseline and challenge conditions. *Brain Res*, 1179:70–78.
- Thome, J., Pesold, B., Baader, M., Hu, M., Gewirtz, J. C., Duman, R. S., and Henn, F. A. (2001). Stress differentially regulates synaptophysin and synaptotagmin expression in hippocampus. *Biol. Psychiatry*, 50(10):809–812.
- Tokusumi, Y., Ma, Y., Song, X., Jacobson, R. H., and Takada, S. (2007). The new core promoter element XCPE1 (X core promoter element 1) directs activator-, mediator-, and TATA-binding protein-dependent but TFIID-independent RNA polymerase II transcription from TATA-less promoters. *Mol. Cell. Biol.*, 27(5):1844–1858.
- Touma, C., Gassen, N. C., Herrmann, L., Cheung-Flynn, J., Büll, D. R., Ionescu, I. A., Heinzmann, J., Knapman, A., Siebertz, A., Depping, A., Hartmann, J., Hausch, F., Schmidt, M. V., Holsboer, F., Ising, M., Cox, M. B., Schmidt, U., and Rein, T. (2011). FK506 binding protein 5 shapes stress responsiveness: modulation of neuroendocrine reactivity and coping behavior. *Biol. Psychiatry*, 70(10):928–936.
- Trapp, B. D., Wujek, J. R., Criste, G. A., Jalabi, W., Yin, X., Kidd, G. J., Stohlman, S., and Ransohoff, R. (2007). Evidence for synaptic stripping by cortical microglia. *Glia*, 55(4):360–368.
- Tremblay, M.-v., Lowery, R. L., and Majewska, A. K. (2010). Microglial interactions with synapses are modulated by visual experience. *PLoS Biol.*, 8(11):e1000527.
- Tremblay, M.-v. and Majewska, A. K. (2011). A role for microglia in synaptic plasticity? *Commun Integr Biol*, 4(2):220–222.
- Tronson, N. C., Guzman, Y. F., Guedea, A. L., Huh, K. H., Gao, C., Schwarz, M. K., and Radulovic, J. (2010). Metabotropic glutamate receptor 5/Homer interactions underlie stress effects on fear. *Biol. Psychiatry*, 68(11):1007–1015.

REFERENCES

- Tynan, R. J., Naicker, S., Hinwood, M., Nalivaiko, E., Buller, K. M., Pow, D. V., Day, T. A., and Walker, F. R. (2010). Chronic stress alters the density and morphology of microglia in a subset of stress-responsive brain regions. *Brain Behav Immun*, 24(7):1058–1068.
- Uddin, M., Aiello, A. E., Wildman, D. E., Koenen, K. C., Pawelec, G., de Los Santos, R., Goldmann, E., and Galea, S. (2010). Epigenetic and immune function profiles associated with posttraumatic stress disorder. *Proceedings of the National Academy of Sciences of the United States of America*, 107(20):9470–9475.
- Uddin, M., Galea, S., Chang, S., Aiello, A. E., Wildman, D. E., de los Santos, R., and Koenen, K. C. (2011). Gene expression and methylation signatures of MAN2C1 are associated with PTSD. *Dis. Markers*, 30(2-3):111–121.
- Uno, H., Eisele, S., Sakai, A., Shelton, S., Baker, E., DeJesus, O., and Holden, J. (1994). Neurotoxicity of glucocorticoids in the primate brain. *Horm Behav*, 28(4):336–348.
- Upender, M. B., Dunn, J. A., Wilson, S. M., and Naegele, J. R. (1997). Immunoglobulin molecules are present in early-generated neuronal populations in the rat cerebral cortex and retina. *J. Comp. Neurol.*, 384(2):271–282.
- Vaiva, G., Thomas, P., Ducrocq, F., Fontaine, M., Boss, V., Devos, P., Rasclé, C., Cottencin, O., Brunet, A., Laffargue, P., and Goudemand, M. (2004). Low posttrauma GABA plasma levels as a predictive factor in the development of acute posttraumatic stress disorder. *Biol. Psychiatry*, 55(3):250–254.
- Valente, N. L. M., Vallada, H., Cordeiro, Q., Migueta, K., Bressan, R. A., Andreoli, S. B., Mari, J. J., and Mello, M. F. (2011). Candidate-gene approach in posttraumatic stress disorder after urban violence: association analysis of the genes encoding serotonin transporter, dopamine transporter, and BDNF. *J. Mol. Neurosci.*, 44(1):59–67.
- Valentine, G. W. and Sanacora, G. (2009). Targeting glial physiology and glutamate cycling in the treatment of depression. *Biochem. Pharmacol.*, 78(5):431–439.
- Vallender, T. W. and Lahn, B. T. (2006). Localized methylation in the key regulator gene endothelin-1 is associated with cell type-specific transcriptional silencing. *FEBS Lett.*, 580(18):4560–4566.
- van der Hart, M. G. C., Czeh, B., de Biurrun, G., Michaelis, T., Watanabe, T., Natt, O., Frahm, J., and Fuchs, E. (2002). Substance P receptor antagonist and clomipramine prevent stress-induced alterations in cerebral metabolites, cytogenesis in the dentate gyrus and hippocampal volume. *Mol. Psychiatry*, 7(9):933–941.
- van Zuiden, M., Geuze, E., Willemen, H. L. D. M., Vermetten, E., Maas, M., Heijnen, C. J., and Kavelaars, A. (2011). Pre-existing high glucocorticoid receptor number predicting development of posttraumatic stress symptoms after military deployment. *Am. J. Psychiatry*, 168(1):89–96.
- Vawter, M. P., Thatcher, L., Usen, N., Hyde, T. M., Kleinman, J. E., and Freed, W. J. (2002). Reduction of synapsin in the hippocampus of patients with bipolar disorder and schizophrenia. *Mol. Psychiatry*, 7(6):571–578.

- Vaynman, S., Ying, Z., and Gomez-Pinilla, F. (2004). Exercise induces BDNF and synapsin I to specific hippocampal subfields. *J. Neurosci. Res.*, 76(3):356–362.
- Vidovic, A., Gotovac, K., Vilibic, M., Sabioncello, A., Jovanovic, T., Rabatic, S., Folnegovic-Smalc, V., and Dekaris, D. (2011). Repeated assessments of endocrine- and immune-related changes in posttraumatic stress disorder. *Neuroimmunomodulation*, 18(4):199–211.
- Voisey, J., Swagell, C. D., Hughes, I. P., Morris, C. P., van Daal, A., Noble, E. P., Kann, B., Heslop, K. A., Young, R. M., and Lawford, B. R. (2009). The DRD2 gene 957C>T polymorphism is associated with posttraumatic stress disorder in war veterans. *Depress Anxiety*, 26(1):28–33.
- von Känel, R., Begre, S., Abbas, C. C., Saner, H., Gander, M., and Schmid, J. (2010). Inflammatory biomarkers in patients with posttraumatic stress disorder caused by myocardial infarction and the role of depressive symptoms. *Neuroimmunomodulation*, 17(1):39–46.
- von Känel, R., Hepp, U., Kraemer, B., Traber, R., Keel, M., Mica, L., and Schnyder, U. (2007). Evidence for low-grade systemic proinflammatory activity in patients with posttraumatic stress disorder. *J Psychiatr Res*, 41(9):744–752.
- Wang, H.-N., Peng, Y., Tan, Q.-R., Chen, Y.-C., Zhang, R.-G., Qiao, Y.-T., Wang, H.-H., Liu, L., Kuang, F., Wang, B.-R., and Zhang, Z.-J. (2010a). Quetiapine ameliorates anxiety-like behavior and cognitive impairments in stressed rats: implications for the treatment of posttraumatic stress disorder. *Physiol Res*, 59(2):263–271.
- Wang, Y. and Qin, Z. (2010). Molecular and cellular mechanisms of excitotoxic neuronal death. *Apoptosis*, 15(11):1382–1402.
- Wang, Z., Neylan, T. C., Mueller, S. G., Lenoci, M., Truran, D., Marmar, C. R., Weiner, M. W., and Schuff, N. (2010b). Magnetic resonance imaging of hippocampal subfields in posttraumatic stress disorder. *Arch. Gen. Psychiatry*, 67(3):296–303.
- Wei, L., Simen, A., Mane, S., and Kaffman, A. (2012). Early life stress inhibits expression of a novel innate immune pathway in the developing hippocampus. *Neuropsychopharmacology*, 37(2):567–580.
- Weiner, J. A. and Chun, J. (1997). Maternally derived immunoglobulin light chain is present in the fetal mammalian CNS. *J. Neurosci.*, 17(9):3148–3156.
- Wessa, M. and Flor, H. (2007). Failure of extinction of fear responses in posttraumatic stress disorder: evidence from second-order conditioning. *Am J Psychiatry*, 164(11):1684–1692.
- Wiedenmann, B. and Franke, W. W. (1985). Identification and localization of synaptophysin, an integral membrane glycoprotein of mr 38,000 characteristic of presynaptic vesicles. *Cell*, 41(3):1017–1028.
- Wierstra, I. (2008). Sp1: emerging roles—beyond constitutive activation of TATA-less housekeeping genes. *Biochem. Biophys. Res. Commun.*, 372(1):1–13.

REFERENCES

- Wohleb, E. S., Hanke, M. L., Corona, A. W., Powell, N. D., Stiner, L. M., Bailey, M. T., Nelson, R. J., Godbout, J. P., and Sheridan, J. F. (2011). β -adrenergic receptor antagonism prevents anxiety-like behavior and microglial reactivity induced by repeated social defeat. *J Neurosci*, 31(17):6277–6288.
- Wong, D. L., Tai, T. C., Wong-Faull, D. C., Claycomb, R., Meloni, E. G., Myers, K. M., Carlezon, William A, J., and Kvetnansky, R. (2011). Epinephrine: A short- and Long-Term regulator of stress and development of illness : A potential new role for epinephrine in stress. *Cellular and Molecular Neurobiology*.
- Wood, G. E., Young, L. T., Reagan, L. P., Chen, B., and McEwen, B. S. (2004). Stress-induced structural remodeling in hippocampus: prevention by lithium treatment. *Proc. Natl. Acad. Sci. U. S. A.*, 101(11):3973–3978.
- Wu, L., Han, H., Wang, Q., Hou, H., Tong, H., Yan, X., and Zhou, J. (2007). Mifepristone repairs region-dependent alteration of synapsin i in hippocampus in rat model of depression. *Neuropsychopharmacology*, 32(12):2500–2510.
- Wu, Y., Liu, Y., Levine, E. M., and Rao, M. S. (2003). Hes1 but not Hes5 regulates an astrocyte versus oligodendrocyte fate choice in glial restricted precursors. *Dev. Dyn.*, 226(4):675–689.
- Wu, Y.-l., Peng, X.-e., Wang, D., Chen, W.-n., and Lin, X. (2012). Human liver fatty acid binding protein (hFABP1) gene is regulated by liver-enriched transcription factors HNF3 β and C/EBP α . *Biochimie*, 94(2):384–392.
- Xiao, B., Han, F., Wang, H., and Shi, Y. (2011a). Single-prolonged stress induces increased phosphorylation of extracellular signal-regulated kinase in a rat model of post-traumatic stress disorder. *Mol Med Report*, 4(3):445–449.
- Xiao, B., Yu, B., Wang, H.-t., Han, F., and Shi, Y.-x. (2011b). Single-prolonged stress induces apoptosis by activating cytochrome c/caspase-9 pathway in a rat model of post-traumatic stress disorder. *Cell Mol Neurobiol*, 31(1):37–43.
- Xie, P., Kranzler, H. R., Poling, J., Stein, M. B., Anton, R. F., Farrer, L. A., and Gelernter, J. (2010). Interaction of FKBP5 with childhood adversity on risk for post-traumatic stress disorder. *Neuropsychopharmacology*, 35(8):1684–1692.
- Xu, H., He, J., Richardson, J. S., and Li, X. (2004). The response of synaptophysin and microtubule-associated protein 1 to restraint stress in rat hippocampus and its modulation by venlafaxine. *J. Neurochem.*, 91(6):1380–1388.
- Yamamoto, S., Morinobu, S., Fuchikami, M., Kurata, A., Kozuru, T., and Yamawaki, S. (2008). Effects of single prolonged stress and D-cycloserine on contextual fear extinction and hippocampal nmda receptor expression in a rat model of ptsd. *Neuropsychopharmacology*, 33(9):2108–2116.
- Yamamoto, S., Morinobu, S., Iwamoto, Y., Ueda, Y., Takei, S., Fujita, Y., and Yamawaki, S. (2010). Alterations in the hippocampal glycinergic system in an animal model of posttraumatic stress disorder. *J Psychiatr Res*, 44(15):1069–1074.

- Yamashita, R., Suzuki, Y., Sugano, S., and Nakai, K. (2005). Genome-wide analysis reveals strong correlation between CpG islands with nearby transcription start sites of genes and their tissue specificity. *Gene*, 350(2):129–136.
- Yehuda, R. (2009). Status of glucocorticoid alterations in post-traumatic stress disorder. *Ann. N. Y. Acad. Sci.*, 1179:56–69.
- Yehuda, R., Bell, A., Bierer, L. M., and Schmeidler, J. (2008). Maternal, not paternal, PTSD is related to increased risk for PTSD in offspring of holocaust survivors. *J Psychiatr Res*, 42(13):1104–1111.
- Yehuda, R., Brand, S., and Yang, R. (2006). Plasma neuropeptide Y concentrations in combat exposed veterans: relationship to trauma exposure, recovery from PTSD, and coping. *Biol. Psychiatry*, 59(7):660–663.
- Yehuda, R., Cai, G., Golier, J. A., Sarapas, C., Galea, S., Ising, M., Rein, T., Schmeidler, J., Müller-Myhsok, B., Holsboer, F., and Buxbaum, J. D. (2009). Gene expression patterns associated with posttraumatic stress disorder following exposure to the world trade center attacks. *Biol. Psychiatry*, 66(7):708–711.
- Yehuda, R., Engel, S. M., Brand, S. R., Seckl, J., Marcus, S. M., and Berkowitz, G. S. (2005). Transgenerational effects of posttraumatic stress disorder in babies of mothers exposed to the world trade center attacks during pregnancy. *J Clin Endocrinol Metab*, 90(7):4115–4118.
- Yehuda, R., Koenen, K. C., Galea, S., and Flory, J. D. (2011). The role of genes in defining a molecular biology of PTSD. *Disease Markers*, 30(2-3):67–76.
- Ying, S., Futter, M., Rosenblum, K., Webber, M. J., Hunt, S. P., Bliss, T. V. P., and Bramham, C. R. (2002). Brain-derived neurotrophic factor induces long-term potentiation in intact adult hippocampus: requirement for ERK activation coupled to CREB and upregulation of Arc synthesis. *J. Neurosci.*, 22(5):1532–1540.
- Yoshimi, K., Woo, M., Son, Y., Baudry, M., and Thompson, R. F. (2002). IgG-immunostaining in the intact rabbit brain: variable but significant staining of hippocampal and cerebellar neurons with anti-IgG. *Brain Res.*, 956(1):53–66.
- You, J.-M., Yun, S.-J., Nam, K. N., Kang, C., Won, R., and Lee, E. H. (2009). Mechanism of glucocorticoid-induced oxidative stress in rat hippocampal slice cultures. *Can J Physiol Pharmacol*, 87(6):440–447.
- Young, R. M., Lawford, B. R., Noble, E. P., Kann, B., Wilkie, A., Ritchie, T., Arnold, L., and Shadforth, S. (2002). Harmful drinking in military veterans with post-traumatic stress disorder: association with the D2 dopamine receptor A1 allele. *Alcohol Alcohol.*, 37(5):451–456.
- Yu, Y., Casaccia, P., and Lu, Q. R. (2010). Shaping the oligodendrocyte identity by epigenetic control. *Epigenetics*, 5(2):124–128.
- Zhang, L., Li, H., Benedek, D., Li, X., and Ursano, R. (2009). A strategy for the development of biomarker tests for PTSD. *Med. Hypotheses*, 73(3):404–409.

REFERENCES

- Zink, M., Rapp, S., Donev, R., Gebicke-Haerter, P. J., and Thome, J. (2011). Fluoxetine treatment induces EAAT2 expression in rat brain. *J Neural Transm*, 118(6):849–855.
- Zink, M., Vollmayr, B., Gebicke-Haerter, P. J., and Henn, F. A. (2010). Reduced expression of glutamate transporters vGluT1, EAAT2 and EAAT4 in learned helpless rats, an animal model of depression. *Neuropharmacology*, 58(2):465–473.
- Zoppi, S., Pérez Nievas, B. G., Madrigal, J. L. M., Manzanares, J., Leza, J. C., and García-Bueno, B. (2011). Regulatory role of cannabinoid receptor 1 in stress-induced excitotoxicity and neuroinflammation. *Neuropsychopharmacology*, 36(4):805–818.

Acknowledgments

The work for this thesis was performed in the research group of Dr. Ulrike Schmidt at the Max Planck Institute of Psychiatry in Munich.

I would like to thank Prof. Dr. Dr. Dr. h.c. Florian Holsboer for giving me the opportunity to work at this highly interdisciplinary research institute and for supervising this thesis.

I am very grateful to Prof. Dr. Christoph W. Turck for taking over the supervision of this thesis at the Ludwigs-Maximilians-Universität (LMU) Munich.

I would like to extend special thanks to Dr. Ulrike Schmidt for the excellent supervision of the work for this thesis and for her extensive scientific and non-scientific support. It was highly motivating to work in this translational research group enabling the easy exchange of biomedical, psychiatric, and psychological knowledge.

I am furthermore grateful to all the members of the RG U. Schmidt contributing to the great working atmosphere, in particular Dominik Büll, Irina Ionescu, Božidar Novak, Christine Huber, Joanna Gutmann, and Julia Stich for lively discussions and assistance in performing the experiments for this thesis as well as Dominique Gall-Kleebach, Christine Schubert, and Monika for exiting lessons in psychology.

I would like to thank all the collaborators of the mouse experiments: Dr. Carsten Wotjak for valuable discussion and his assistance in designing the PTSD mouse model experiments; Dr. Kathrin Henes and Dr. Yulia Golub for performing the behavioral experiments with the PTSD mouse model. I would also like to thank Dr. Chadi Touma for designing and performing the combined restraint and forced swim stress experiments. Furthermore, I am grateful to Prof. Rainer Landgraf and Dr. Ludwig Czibere for providing the HAB and LAB mice for my experiments.

Thanks are due to D. Trümbach from the Institute for Developmental Genetics at the Helmholtz Zentrum München (German Research Center for Environmental Health) for his support in the *in silico* analysis of the TMEM132D promoter.

Finally, I would like to thank Dr. Theo Rein and all the members of the RG Rein, especially Tatjana Perisic, for discussion, helpful technical advice and supply of reagents.

Curriculum vitae

Name Leonie Herrmann, nee Christian
Date of birth 28/05/1985
Nationality German

Education

Since 03/2009 PhD student at the Max Planck Institute of Psychiatry in Munich
Research Group of Molecular Psychotraumatology, Dr. Ulrike Schmidt
Supervisor: Prof. Dr. Dr. Dr. h.c. F. Holsboer
Titel of PhD thesis: 'Identification and characterization of novel candidate molecules for PTSD'

02/2008-01/2009 Diploma thesis at the Department of Neurology, University of Bonn
Supervisor: Prof. Dr. J. Walter
Titel: 'Modulation of microglial A β degradation by insulin-degrading enzyme'

07/2006-08/2006 Internship at the Institute of Biomedicine, University of Bergen, Norway
Scholarship from the IFMSA (International Federation of Medical Students Association)

10/2004-01/2009 Diploma student in 'Molecular Biomedicine', University of Bonn

08/1995-07/2004 High School Carl-von-Ossietzky Gymnasium Bonn, Germany

Published Conference Abstracts

Herrmann, L., Henes, K., Büll, D., Ionescu, I.A., Holsboer, F., Rein, T., Touma, C., Wotjak, C.T., Schmidt, U. (2012). Immunoglobulin G as a potential biomarker for posttraumatic stress disorder (PTSD). *Eur Neuropsychopharmacol* 22(S1), S1-S108.
15-18/03/2012 ECNP Workshop for Young Scientists in Europe, Nice, France

Herrmann, L., Golub, Y., Henes, K., Ionescu, I., Büll, D., Holsboer, F., Wotjak, C.T., Schmidt, U. (2011). Decreased expression of synaptic proteins in a mouse model of posttraumatic stress disorder. *Pharmacopsychiatry* 06, 193-295.
05-08/10/2011 27th AGNP Symposium Munich, Germany

Christian, L., Golub, Y., Rein, T., Wotjak, C.T., Schmidt, U. (2009). Biomarkers in a mouse model of posttraumatic stress disorder. *Pharmacopsychiatry* 05, 169-208.
07-10/10/2009 26th AGNP Symposium Munich, Germany

Publications

Pietsch, M., **Christian, L.**, Inhester, T., Petzold, S., Gütschow, M., (2009). Kinetics of inhibition of acetylcholinesterase in the presence of acetonitrile. *FEBS J.* 276, 2292–2307.

Tamboli, I.Y., Barth, E., **Christian, L.**, Siepmann, M., Kumar, S., Singh, S., Tolksdorf, K., Heneka, M.T., Lütjohann, D., Wunderlich, P., Walter, J., (2010). Statins promote the degradation of extracellular amyloid β -peptide by microglia via stimulation of exosome-associated insulin-degrading enzyme (IDE) secretion. *J. Biol. Chem.* 285, 37405–37414.

Golub, Y., Kaltwasser, S.F., Mauch, C.P., **Herrmann, L.**, Schmidt, U., Holsboer, F., Czisch, M., Wotjak, C.T., (2011). Reduced hippocampus volume in the mouse model of Posttraumatic Stress Disorder. *J Psychiatr Res* 45, 650–659.

Touma, C., Gassen, N.C., **Herrmann, L.**, Cheung-Flynn, J., Büll, D.R., Ionescu, I.A., Heinzmann, J.-M., Knapman, A., Siebertz, A., Depping, A.-M., Hartmann, J., Hausch, F., Schmidt, M.V., Holsboer, F., Ising, M., Cox, M.B., Schmidt, U., Rein, T., (2011). FK506 binding protein 5 shapes stress responsiveness: modulation of neuroendocrine reactivity and coping behavior. *Biol. Psychiatry* 70, 928–936.

Ionescu, I.A., Dine, J., Yen, Y.-C., Buell, D.R., **Herrmann, L.**, Holsboer, F., Eder, M., Landgraf, R., Schmidt, U., (2012). Intranasally Administered Neuropeptide S (NPS) Exerts Anxiolytic Effects Following Internalization Into NPS Receptor-Expressing Neurons. *Neuropsychopharmacology* 37, 1323–1337.

Herrmann, L., Ionescu, I.A., Henes, K., Golub, Y., Wang, N.X.R., Buell, D.R., Holsboer, F., Wotjak, C.T., Schmidt, U., (2012). Long-Lasting Hippocampal Synaptic Protein Loss in a Mouse Model of Posttraumatic Stress Disorder. *PLoS ONE* 7, e42603 #

Schmidt, U., Buell, D.R., Ionescu, I.A., Holsboer, F., Touma, C., Rein, T., **Herrmann, L.** (2012). Stress-induced long-term alterations in synaptic protein expression does not differ in FKBP5 knockout and wildtype mice. *In preparation* #

Herrmann, L., Buell, D.R., Trümbach, D., Ionescu, I.A., Landgraf, R., Holsboer, F., Rein, T., Schmidt, U. (2012). Transcriptional regulation of the anxiety-associated gene transmembrane protein 132D (TMEM132D) in the context of oligodendrocyte differentiation. *In preparation* #

parts of this thesis were included in these articles